Dissertation

submitted to the

Combined Faculty of Natural Sciences and Mathematics

of

Heidelberg University, Germany

for the degree of

Doctor of Natural Sciences

Put forward by

Simone Blasi

Born in Arezzo, Italy

Oral examination: 7 July 2020

Hierarchies and New Symmetries:

from

Flavored Axions

to

Composite Higgs

Referees:

1st: Dr. Florian Goertz

2nd: Prof. Dr. Jörg Jäckel

Abstract: We investigate possible extensions of the Standard Model according to the either elementary or composite nature of the Higgs boson. In the former scenario, we present a model of flavored axion–Higgs unification in which electroweak symmetry breaking occurs dynamically and selects a small region for the axion decay constant that will be fully tested at forthcoming dark matter and flavor experiments. Moreover, if the Higgs is elementary, yukawa couplings are regarded as fundamental interactions: this relates to possible UV completions based on asymptotic safety for which we provide new insights by studying models containing a large multiplicity of fermion fields. Finally, we introduce a new realization of a composite Higgs that resolves the tension with null-signals of new physics at the LHC. It is based on a new symmetry structure that we call soft breaking, whose realization in the context of a warped extra dimension is particularly simple and straightforward. When combined with other possible symmetries this allows for a completely natural model to emerge predicting composite resonances above 2 TeV with fine-tuning at the minimum 10% already implied by LEP and thus restoring naturalness in the light of the LHC data.

Zusammenfassung: Wir untersuchen mögliche Erweiterungen des Standardmodells in Hinblick auf die Natur des Higgs Bosons als elementares oder zusammengesetztes Teilchen. Für das erste Szenario präsentieren wir ein Modell zur Axion–Higgs Vereinheitlichung mit Flavor-Struktur, in dem die elektroschwache Symmetrie dynamisch gebrochen und ein kleiner Bereich der Zerfallskonstante des Axions selektiert wird. Dieser wird vollständig durch zukünftige dunkle Materie- und Flavorexperimente getestet werden. Wenn das Higgs elementar ist, werden zudem die Yukawa-Kopplungen als fundamentale Wechselwirkung angesehen; dies stellt mittels des Konzepts von "asymptotic safety" eine Verbindung zu möglichen UV Komplementierungen her, für die wir neue Resultate, gewonnen durch die Untersuchung von Modellen mit einer Vielzahl fermionischer Felder, vorstellen. Schließlich führen wir eine neuartige Realisierung von Modellen zusammengesetzer Higgs Teilchen ein, die Diskrepanzen im Zusammenhang mit fehlenden Signalen neuer Physik am LHC auflöst. Diese basiert auf einer neuen Symmetriestruktur, die wir "soft breaking" nennen und die im Zusammenhang mit einer zusätzlichen, gefalteten Dimension besonders einfach und natürlich realisiert werden kann. Die Kombination mit möglichen zusätzlichen Symmetrien ermöglicht ein vollständig natürliches Modell, welches Resonanzen jenseits von 2 TeV bei einem minimalen "fine-tuning" von 10%, was bereits durch LEP Daten impliziert ist, vorhersagt und daher gut mit den LHC Daten übereinstimmt.

Da quel giorno in poi [...] volli, e volli sempre, e fortissimamente volli.

Vittorio Alfieri (1749 - 1803)

Contents

Publications

The work presented in this thesis is based on the following publications during author's PhD studies from September 2017 to April 2020 in collaboration with others:

I T. Alanne, S. Blasi and F. Goertz, *"Common source for scalars: Flavored axion-Higgs unification,"* Phys. Rev. D **99** (2019) no.1, 015028, [arXiv:1807.10156]

II T. Alanne and S. Blasi, *"The β-function for Yukawa theory at large N_f,"* JHEP **08** (2018), 081, [arXiv:1806.06954]

III T. Alanne and S. Blasi, *"Abelian gauge-Yukawa β-functions at large N_f,"* Phys. Rev. D **98** (2018) no.11, 116004, [arXiv:1808.03252]

IV T. Alanne, S. Blasi and N. A. Dondi, *"Bubble-resummation and critical-point methods for β-functions at large N,"* Eur. Phys. J. C **79** (2019) no.8, 689, [arXiv:1904.05751]

V T. Alanne, S. Blasi and N. A. Dondi, *"Critical look at β-function singularities at large N,"* Phys. Rev. Lett. **123** (2019) no.13, 131602, [arXiv:1905.08709]

VI S. Blasi and F. Goertz, *"Softened symmetry breaking in Composite Higgs models,"* Phys. Rev. Lett. **123** (2019) no.22, 221801, [arXiv:1903.06146]

VII S. Blasi, C. Csaki and F. Goertz, *"A natural Composite Higgs via universal boundary conditions,"* [arXiv:2004.06120]

In addition, Sec. 3.4.3 contains new results derived here by the author for the first time.

The following paper has been produced during author's PhD studies but is however not included in this thesis:

VIII S. Blasi, V. Brdar and K. Schmitz, *"Fingerprint of low-scale leptogenesis in the primordial gravitational-wave spectrum,"* [arXiv:2004.02889]

Chapter 1

Introduction

The Standard Model of particle physics (SM) contains 18 free parameters that are physical: their actual values are not predicted within the theory and can only be determined by comparison with the experiments. When accounting for massive neutrinos this number increases either to 25 or 27 depending on their Dirac or Majorana nature, and one more parameter is found when considering the topological terms for the gauge fields. Since the origin behind all these free parameters is unknown, each of them represents an opportunity for learning something more about Nature at the fundamental level.

When seeking for new physics, however, one should not forget the huge theoretical breakthrough that has lead to the formulation of the SM itself. Probably the most formidable aspect of it is the common understanding of the fundamental forces in the language of gauge theories, and it is interesting to notice that this already brings several hints for possible extensions. The first of them is related to the semi-simple nature of the SM gauge symmetry,

$$SU(3)_c \times SU(2)_L \times U(1)_Y, \tag{1.1}$$

and the fact that the electric charges of the proton and the electron cancel each other at the level of one part out of 10^{21} without a rigid structure to ensure it. This fact is known as "charge quantization" and is intimately related to the presence of the abelian factor $U(1)_Y$. This, together with the intriguing convergence of all the gauge couplings at energies as high as $\sim 10^{16}\,\text{GeV}$ with $\sim 20\%$ accuracy, is in fact one of the best motivations for the existence of a Grand Unified Theory (GUT) [1,2] based on a larger gauge group in which the SM symmetry is embedded. Thus, the three parameters corresponding to the strong and electroweak gauge couplings, g_S, g and g', respectively, could be reconciled in a single force at high energies.

In this respect, it is worth mentioning that the gauge symmetry in (1.1) can be straightforwardly extended if three right-handed neutrinos (RHNs) are included in the theory. In this case, the baryon (B) and lepton (L) numbers which are accidental global symmetries of the SM can be used to form an anomaly-free combination, $U(1)_{\text{B-L}}$, that can be gauged [3]. The RHNs naturally explain the tiny masses of the active neutrinos via the seesaw mechanism if they are as heavy as $\sim 10^{13}\,\text{GeV}$ which in turn sets the natural scale for the spontaneous breaking of $U(1)_{\text{B-L}}$. As this is not too far from the naive GUT scale, the gauging of this symmetry can also be seen as a preliminary step towards unification.

There is however another mystery that follows from the gauge symmetry of the SM and is related to the inclusion of a topological term for each of the group factors in (1.1).

As we shall see in Chapter 2, these terms are total derivates and do not contribute to the equations of motion; nonetheless they are relevant as for instance they induce CP violation. One can show that including the topological terms brings three free parameters that are defined in the interval $[0, 2\pi)$ and thus correspond to angular variables. However, not all of them are physical: the topological term for $U(1)_Y$ vanishes upon integration at the space-time boundaries and can be neglected. The story is more subtle for the non-abelian factors: the $SU(2)_L$ topological term turns out to be unphysical as well because of baryon and lepton numbers which are global symmetries and can be used to rotate it away. However, there is no symmetry of the SM that can remove the topological term for the $SU(3)_c$ color group, and its consequences must be dealt with. In particular, the astonishing conservation of CP in the strong interactions implies that the actual size of the QCD θ-angle needs to be as small as $\theta < 10^{-10}$. This apparent fine-tuning is interpreted as a severe lack of understanding of the high-energy completion of the SM and is referred to as the strong CP problem.

Of course, our original counting for the free parameters in the SM was implicitly assuming that we stick to renormalizable operators $\mathcal{O}$ with mass dimension $[\mathcal{O}] \leqslant 4$. Once all these parameters are fixed by low-energy observables, renormalizability ensures that the model remains predictive up to extremely high scales as the first internal inconsistency is truly set by the hypercharge Landau pole at $\sim 10^{40}$ GeV. However, there are many reasons to regard the SM as an effective theory, and it makes sense to look at what happens if we start considering higher-dimensional operators. At dimension five, the only invariant that is allowed by gauge symmetry is remarkably the one by Weinberg [4] which violates lepton number by two units and thus induces a Majorana mass for the neutrinos. This may actually explain why massive neutrinos are indeed the first sign of physics beyond the SM (BSM), as for comparison proton decay is generated only at dimension six. The natural cutoff suppressing the Weinberg operator can be related to the mass of the RHNs discussed above, and points again to energies as high as the GUT scale. The surprise comes when realizing that the only term in the SM with mass dimension $[\mathcal{O}] = 2$, whose natural value within this effective-theory approach should correspond to these high-energy scales, is the electroweak mass of the Higgs boson!

Probably the most puzzling sector of the SM is in fact the one responsible for the spontaneous breaking of the electroweak symmetry, $SU(2)_L \times U(1)_Y$, down to the electromagnetic group, $U(1)_{\rm em}$. This is realized through a mexican-hat potential for the Higgs doublet, h, which is given by

$$V(h) = \frac{1}{2}\mu^2(h^\dagger h) + \frac{1}{4}\lambda(h^\dagger h)^2 \tag{1.2}$$

and is in fact minimized by configurations with $h^\dagger h = v^2/2$, where $v = 246$ GeV corresponds to the Fermi scale of the weak interactions. This is possible because the coefficient μ^2 is negative, and the origin, $h^\dagger h = 0$, corresponds to a local maximum. On the other hand, the quartic coupling, λ, needs to be positive to ensure that the electroweak-breaking vacuum is a minimum and the potential is bounded from below. The Higgs mass, m_h^2, according to (1.2) is given as $m_h^2 = -\mu^2 = \lambda v^2/2$. The electroweak gauge bosons, W and Z, become massive due to the Higgs mechanism, and similarly for the SM fermions thus solving the issue of mass generation in chiral gauge theories.

From a structural point of view, the potential in (1.2) is the simplest effective theory that can describe a second-order phase transition. This was first introduced by Landau as a Taylor expansion of the free energy for the order parameter, m^2, acquiring different

values in the broken ($m^2 \neq 0$) and unbroken phase ($m^2 = 0$). This directly relates to (1.2) with the identification $m^2 = h^\dagger h$. Clearly, the theory by Landau was never meant to be fundamental, and the origin of the coefficients parameterizing the phase transition can be understood only within a microscopic description of the system. In a similar way, the quantities describing the Higgs potential are supposed to become calculable once the underlying theory beyond the SM will be unconvered.

On the other hand, the necessity for a deeper understanding of electroweak symmetry breaking emerges when trying to extrapolate the potential in (1.2) to energies much above the electroweak scale. In fact, regarding the SM as an effective theory valid up to a certain cutoff $\Lambda \gg v$, the quantum corrections to the Higgs mass set its natural value to be anyway $\sim \Lambda^2$ which is in tension with the light Higgs boson discovered at the Large Hadron Collider (LHC). This statement is independent of the way the theory is regularized, as physical thresholds will still contribute quadratically also in dimensional regularization, see e.g. [5]. In the absence of an underlying mechanism to cancel this quadratic sensitivity, a large fine-tuning is needed to keep the Higgs light: this is referred to as the hierarchy problem.

In addition to the (in)stability of the Higgs mass, the scalar quartic, λ, introduces a puzzle as well. As mentioned above, the scalar quartic needs to be positive to ensure that the symmetry-breaking vacuum is in fact a minimum. However, even if this is the case at the electroweak scale, the value of λ can be seen as effectively changing with the energy according to its renormalization-group evolution and is predicted to turn negative within the SM at energies $\sim 10^{11}$ GeV [6]. This means that our vacuum is actually a *local* minimum, as there exist configurations at much larger field values that are more favorable energetically. Nevertheless, the vacuum that we observe turns out to be long-lived enough to be compatible with the cosmological evolution of our Universe, so that this cannot be considered as a real inconsistency of the theory. Nevertheless, the fact that the SM remarkably sits in a small metastability region can be seen as a further hint for the theory to be extended with new particles and new interactions to ensure that λ remains positive at least up to the Planck scale.

Let us now move to discuss the last sector of the SM describing the yukawa interactions between the Higgs and the elementary fermions. After performing all possible field redefinitions, one there finds 13 (!) free parameters that are physical: three masess for the leptons, e, μ, τ, six masses for the up quarks, u, c, t, and down quarks, d, s, b, three mixing angles and a CP violating phase, δ, contained in the Cabibbo-Kobayashi-Maskawa (CKM) matrix. The occurrence of these parameters is intimately linked to the SM being redundant in the fermion content, as all gauge eigenstates appear in exact three replicas "without no one ordering it". In fact, while we could motivate the existence of leptons as a fix to the chiral anomalies of the quarks, there is absolutely no need for repeating this three times. In this sense, it is quite remarkable that the large flavor symmetry related to the SM families, $[U(3)]^5$, is actually broken only by the interaction with the Higgs, whereas gauge forces are flavor universal. When considering BSM scenarios with a relatively low new-physics scale, this property is so important that one usually needs to assume that these yukawas in fact remain the only source of flavor violation [7]. Moreover, the actual size of the SM fermion masses is found to span several orders of magnitude, from $\sim 1\,\text{MeV}$ to $\sim 170\,\text{GeV}$. On the other hand, the way the quarks are mixing is far from being random: the CKM matrix shows a clear structure with dominant diagonal entries and sizeable mixing among the two light

flavors, while third-generation mass and gauge eigenstates mostly coincide. Since the origin of the hierarchical fermion masses and mixings cannot be understood in the SM, this introduces what is called a "flavor puzzle".

When compared to the SM of particle physics, the Standard Model of Cosmology (ΛCDM) contains less free parameters but is certainly not less mysterious. In fact, the initial conditions for the standard cosmological evolution describe a Universe that is remarkably flat and also homogeneous on scales that are too large for these regions to have ever been in causal contact. Explaining these initial conditions is indeed one of the best motivations for cosmic inflation. Moreover, 70% of the energy budget of the Universe comes in a form of energy density that is not diluted during the expansion [8] and is in fact compatible with a cosmological constant. In a sense, it is surprising that we were even able to know about this as the Universe needs to have expanded enough for the vacuum energy to become relevant, and this has happened only recently giving rise to a "coincidence problem" [1]. The next-to-leading component amounting to the 25% of the energy budget consists of a form of non-relativistic matter that has no electromagnetic charge and is therefore "dark". Only the remaining 5% appears as ordinary baryon matter, whereas relativistic degrees of freedom contribute today with 0.01 %. Moreover, it is also apparent that our Universe is favoring a population of baryons with respect to anti-baryons: since these two species are equivalent from a relativistic point of view, this suggests the presence of a mechanism responsible for this asymmetry.

It is reasonable to expect the microscopic theory of Nature to account for (at least some of) the puzzles emerging from the ΛCDM. When trying to do so with the SM, one encounters the soundest arguments for claiming that its description is necessarily incomplete. In fact, even forgetting about inflation and vacuum energy, whose resolution may actually arise from a better understanding of the gravity side, the nature of dark matter and the origin of baryon asymmetry should both be possibly addressed within a particle physics framework. This is particularly motivated given that there is no clear way of accounting for these facts with the help of astrophysical objects such as primordial black holes. However, it turns out that no particle in the SM can be considered as a candidate for dark matter, as none of them can meet the essential requirements of being dark, cold, and stable. Moreover, although baryon number can be violated in the SM at the non-perturbative level, the baryon asymmetry cannot be generated both because of a too little amount of CP violation due to the specific flavor structure, and because of the lack of non-equilibrium processes that could have ever been triggered in the early Universe according to SM physics only.

We conclude that despite being very successful in reproducing an incredible amount of data at the terrestrial level, and also crucial processes in the early Universe such as big bang nucleosynthesis, the SM can only be regarded as an effective description, whereas a more fundamental theory will provide an explanation for (at least some of) the quantities that are currently paremeterizing our ignorance.

In this thesis, we will investigate possible solutions to the shortcomings of the SM from the perspective of the Higgs boson. In fact, the fragile nature of electroweak symmetry breaking and the yukawa couplings being the core of the flavor puzzle allow the Higgs to play a relevant role in many extensions of the SM. In doing so, we will consider two distinct scenarios. In the first one, the Higgs is an elementary particle

[1] The concept of "recently" is questionable, as it depends on the way time is measured. Still, the actual value of the vacuum energy turns out to be rather special, see e.g. [9].

and the hierarchy problem may or may not be solved in this framework. As a matter of fact, the reason for a light Higgs could rely on something completely different than what has been traditionally thought, such as the selection of our vacuum due to some early-Universe dynamics [10], or even on mere anthropic reasons. Bearing this in mind, we will explore the consequences of having a fundamental scalar in the theory when discussing its interplay with the open questions of the SM that are not directly related to the hierarchy problem. For the second scenario we will instead reverse this point of view: we will in fact follow the idea that uncovering the mechanism behind a natural electroweak symmetry breaking will also provide new insights for the other puzzles in the SM. We will then turn to discuss composite Higgs models with the aim of resolving the present tension with the continued absence of new physics at the LHC, which is in fact endangering the idea of a natural electroweak scale.

When considering an elementary Higgs, we will first focus on the flavor puzzle and the strong CP problem. As mentioned above, the latter is related to the unnatural value of the QCD topological term, $\theta < 10^{-10}$. One of the most attractive solutions consists of making the θ-angle, which in the SM is just a free parameter, a dynamical field by introducing a new spontaneously broken Peccei-Quinn symmetry, $U(1)_{\rm PQ}$, and a new pseudoscalar particle, the axion [11, 12]. The apparent conservation of CP in the strong interactions then follows simply from the fact that the configuration with $\theta \ll 1$ is energetically more favorable. The couplings of the axion with the SM particles need however to be tiny in order to pass present constraints, thus requiring the spontaneous breaking of $U(1)_{\rm PQ}$ to occur much above the Fermi scale. Besides solving the fine-tuning issue related to the strong CP problem, it was soon realized that axions produced non-thermally can account for all the dark matter in our Universe. This is particularly relevant in present times since one of the primary candidates for dark matter, namely a weakly-interacting massive particle with a mass in the GeV–TeV range, has not been found in direct-detection experiments which already cut deeply in the parameter space [13]. Conversely, the natural region for the QCD axion to be dark matter remains basically unconstrained.

The simplest solution to the flavor puzzle is probably the one based on the Froggatt-Nielsen mechanism [14], namely the existence of a new global symmetry, $U(1)_{\rm H}$, under which the SM fermions are chirally charged. This symmetry controls the generation of fermion masses such that the large hierarchies that we observe are accounted for starting with $\mathcal{O}(1)$ couplings to a new scalar particle, the flavon, that realizes the spontaneous breaking of $U(1)_{\rm H}$. In a similar way, this simple mechanism can naturally explain the mixings between the different quark families as described by the CKM matrix.

Recently, it has been shown that these two distinct solutions to the strong CP problem and flavor puzzle, respectively, can actually be realized in a unified framework in which the Peccei-Quinn symmetry itself is a flavor symmetry, thereby identifying the $U(1)_{\rm PQ}$ as the Froggatt-Nielsen flavor charge, $U(1)_{\rm H}$. Thus, the axion and the flavon are identified as the axial and radial components, respectively, of the same complex scalar field that we will refer to as the axiflavon [15, 16]. A very interesting feature of this model is that the axion couplings to matter are now predicted by the SM fermion masses and mixings and feature a flavor violation that is sizeable enough to be possibly detected in forthcoming experiments.

In this unified solution to several puzzles in the SM, the Higgs and the axiflavon have been considered as two independent objects. In Chapter 2, we will discuss a possi-

ble scenario in which all the scalars in the theory are crucially unified within the same multiplet of an enlarged global symmetry at high energies [I]. In this setup, the Higgs will be realized as an elementary pseudo-Nambu-Goldstone boson in order to provide a rationale for it being lighter than the other states. However, since the generic scale of new physics is tied to the Peccei–Quinn scale, the hierarchy problem becomes explicit. Nevertheless, the hypothesis of scalar unification will generate correlations in the radiatively-generated Higgs potential such that, once the Higgs mass is phenomenologically set to the experimental value, only a small range of the axion decay constant is selected. This range is close to the natural window for axion dark matter and entirely within the reach of forthcoming flavor and dark matter experiments, thus making this minimal solution to the SM puzzles with scalar unification fully testable in the near future.

Regarding the Higgs as an elementary particle also allows us to explore different perspectives for the UV completion of the SM. One possibility is to assume that the quantum field theory in which the SM is embedded features an interacting ultraviolet (UV) fixed point for its renormalization-group flow which in turn defines a fundamental theory valid up to arbitrarily short distances. The occurrence of this scenario is called asymptotic safety [17], and has many relevant implications. First of all, asymptotic safety can offer an alternative point of view on quantum gravity. In fact, it is well known that general relativity (GR) is perturbatively non-renormalizable and is supposed to lose its predictive power for energies above the Planck scale. However, if the renormalization-group flow for GR is connected to a UV fixed point this would automatically define a consistent theory of quantum gravity. Examples where this is actually the case are known from condensed-matter systems such as the Gross-Neveu model in three dimensions, in which the existence of such an interacting UV fixed point can be proved rigorously despite the characteristic interaction being power-counting non-renormalizable, see e.g. [18]. This also means that asymptotic safety can be interpreted as a common framework in which the SM quantum field theory and gravity can be married, see e.g. [19]. In addition, it has been shown that the presence of yukawa interactions is a fundamental requirement for asymptotic safety to emerge in the perturbative regime [20], thus providing a completely different motivation for the existence of elementary scalars like possibly the Higgs boson. Moreover, asymptotic safety may also have a saying on the hierarchy problem: in fact, even if the UV fixed point is reached at a very high scale this does not represent a hard cutoff and the masses of the scalar fields will be insensitive to it [21].

One class of theories in which asymptotic safety has been proven rigorously are those containing a large number of flavor degrees of freedom, N_f, together with a large number of colors for the gauge interactions, N_c [22]. Following this first result and motivated by the search of asymptotically safe extensions of the SM, there has been some interest in investigating the complementary case in which N_f is large but N_c is small. Our contribution to this research is presented in Chapter 3, where we will enlarge the tools for the investigation of gauge–yukawa theories at high energies by considering the novel setup in which a yukawa coupling features a large-N_f enchancement as is the case in Froggatt-Nielsen-inspired models [II, III]. Moreover, we will analyze the connection between the large-N_f formalism and condensed-matter theory by working out the relations between β-functions and critical exponents correspoding to Wilson-Fisher-type of fixed points [IV]. This new perspective will also have relevant implications for asymptotic safety and large N_f [V].

The search of alternative paradigms for the UV completion of the SM is certainly motivated by the null signals of new physics at the LHC, which are in fact threatening natural models of electroweak symmetry breaking. Nevertheless, extensions of the SM that provide a structural solution to the hierarchy problem still represent one of the most appealing scenarios for new physics. A renown example of this is given by composite Higgs models [23–25]. Here, the Higgs boson is no longer a fundamental scalar but rather a bound state of a new strong dynamics, resolvable only at short distances. Thus, quantum corrections are cut off at the compositeness scale, and the Higgs mass is saturated in the IR, screening it from large corrections.

In order to reduce the mass of the Higgs boson with respect to the other composite resonances which generically have to be in the multi-TeV range, the Higgs also needs to be a pseudo Nambu-Goldstone boson of a spontaneously broken global symmetry of the new strong sector. This has the added benefit that the Higgs potential becomes calculable since it is radiatively generated by the couplings of the composite sector to the SM, which generically break the global symmetry. Moreover, the presence of a light Higgs boson in the spectrum allows this class of models to be more easily compatible with the electroweak observables that have been precisely measured by LEP. From these measurements one is already able to tell that some fine-tuning $\sim 10\%$ is at least needed in order to realize a viable composite Higgs. This degree of accidental cancellation would however be considered as a fair price for making the Higgs mass insensitive to any other thresholds up to the Planck scale.

Besides solving the hierarchy problem, Higgs compositeness provides a very elegant solution to the flavor puzzle called partial compositeness. In fact, the spread of the SM fermion masses is easily obtained as a renormalization-group effect in presence of strong dynamics starting from small differences in the anomalous dimensions of the operators that couple to the different families. Other shortcomings of the SM such as dark matter and electroweak baryogenesis can also be addressed in this framework, see e.g. [26].

However, while consistency with the electroweak precision tests does not require much fine-tuning, the situation is in practice much worse when considering the constraints coming from the LHC. In fact, minimal realizations generically predict a Higgs mass that is still too heavy due to the large yukawa coupling associated to the top quark. This requires anomalously light colored states, called top partners, below the generic scale of new physics to keep the Higgs light. However, the LHC data by now exclude the presence of top partners with mass $\lesssim 1.3\,\text{TeV}$, thus posing a serious threat to a natural composite Higgs. In fact, the only way in which minimal models can comply with the LHC bounds is to make the Higgs more elementary, thus decoupling all the effects associated with the composite sector. This implies that concrete realizations become less natural and the overall tuning is pushed towards the percent level.

In Chapter 4 we will present a new idea in composite Higgs models that we call "soft breaking" and is based on a structural change in the way the Higgs potential is generated. As we shall see, this corresponds to a simple modification of partial compositeness that will help mitigating the effect of the top yukawa and allow for a light Higgs while avoiding the prediction of light top partners [VI]. This new resolution of the tension does not rely on making the Higgs more elementary and thus is not necessarily increasing the tuning. In fact, we will show that when implementing soft breaking with other possible symmetries of the strong dynamics, a natural spectrum of composite resonances above the LHC bounds becomes now compatible with the minimal tuning from LEP [VII].

Our concrete realization shows that the non-observation of new physics at the LHC can be reconciled with natural electroweak symmetry breaking, as this model becomes practically testable only now, at the High-Luminosity phase (HL-LHC) or at the Future Circular Collider (FCC).

Chapter 2

The Higgs and the flavored axion

Two major issues of the SM are certainly the lack of a candidate to explain dark matter in our Universe and the astonishing conservation of CP in the strong interactions. It has been known for a long time that these issues can be simultaneously solved by introducing a new, spontaneously broken Peccei-Quinn global symmetry, $U(1)_{\rm PQ}$, together with a new light particle, the axion [11, 12]. The axion solution to the strong CP problem has therefore drawn a lot of interest in the community and several efforts are ongoing on the experimental side aiming for a discovery. Indeed, axion physics can be constrained in many different ways by means of both terrestrial experiments and astrophysical observations. Moreover, the possibility of axion dark matter motivates the developement of tailored direct-detection experiments. On the other hand, the scale at which the Peccei-Quinn symmetry is broken is generically much above the electroweak scale thus making the axion a very light and feebly interacting particle.

A powerful strategy for discovering the axion is to investigate rare processes in the SM as those related to flavor-violating neutral currents. In fact, axions can feature sizeable off-diagonal couplings in flavor-space to the SM fermions and can mediate flavor transitions such as $d \to s$ or $\mu \to e$, which are already severely constrained by current measurements and will be further investigated in future searches. A possible issue with this strategy is that axion couplings to matter considerably depend on the way the SM particles feel the $U(1)_{\rm PQ}$ global symmetry, and this introduces a certain degree of model dependence. It is therefore important to construct well-motivated models to be used as benchmarks for this kind of searches.

An interesting way to do this is by connecting the axion solution to the strong CP problem to other issues in the SM. A prime candidate for this is the "flavor puzzle", namely the observation that the fermion masses in the SM span several orders of magnitude without a mechanism that can explain it. Also, the structure of the CKM matrix is far from being random, and this reinforces the idea of an underlying symmetry. Probably the simplest way of addressing the flavor puzzle is to implement the Froggatt-Nielsen mechanism [14]. This is based on a new, spontaneously broken, $U(1)_{\rm H}$ global symmetry under which the SM fermions are chirally charged, together with a new heavy scalar field, the flavon. The breaking of this $U(1)_{\rm H}$ controls the fermion mass generation and reproduces the observed pattern in the CKM matrix as well as the mass hierarchies in a natural way. It has been recently pointed out in Refs. [15, 16] that the solution to the strong CP problem and the flavor puzzle can actually be combined by identifying the Peccei-Quinn symmetry with the $U(1)_{\rm H}$ symmetry of the Froggatt-Nielsen mechanism,

thereby providing a unified solution to all these open questions. As a consequence, the axion couplings are now dictated by the observed pattern of masses and mixings of the SM fermions, making the model extremely predictive. In particular, these couplings inherit the flavor structure of the SM, and $d \to s$ transitions are sizeable, as they are only suppressed by the Cabibbo angle.

This setup was realized in Refs [15, 16] by employing an effective-field-theory approach motivated by the large separation between the axion decay constant and the electroweak scale. In particular, the Higgs was considered there as an independent field with respect to the axion and the flavon that have instead been crucially unified in a single complex scalar— the axiflavon. In Ref. [I] we took a further step in this direction and provided a model that is based on a non-trivial interplay between the scalar fields in the game. In particular, we have analyzed the possibility that all the scalars actually have a common origin, thereby linking the Higgs to the axiflavon. In this setup, it is natural to assume that both the Higgs and the axion are realized as pseudo Nambu-Goldstone bosons of an enlarged global symmetry group as a means to explain their lightness when compared to the flavon. This provides a concrete example of axion-Higgs unification [27] (see also Ref. [28]) in a renormalizable context. A major consequence is that electroweak symmetry breaking occurs dynamically and is controlled by the microscopic parameters of the model via the Coleman-Weinberg potential for the Goldstone Higgs. Reproducing the correct electroweak vacuum provides then a powerful requirement on the system that in turn will select a very small region of the axiflavon parameter space increasing the predictivity of the model.

This chapter is organized as follows. In Sec. 2.1 we will review the strong CP problem and its connection to the vacuum structure of QCD as well as the picture in the SM. In Sec. 2.2 we will discuss the axion solution to the strong CP problem by looking at the effective field theory below the Peccei-Quinn and electroweak-symmetry-breaking scale. The status of axion searches is discussed in Sec. 2.3, with particular emphasis on the constraints coming from flavor experiments. The idea of interpreting the Peccei-Quinn as a flavor symmetry is presented in Sec. 2.4. Finally, Sec. 2.5 is devoted to our model that combines the Higgs with the axiflavon and is mainly based on Ref. [I]. A summary of our findings is given in Sec. 2.6.

2.1 Strong CP problem, θ-vacua and the SM

The strong CP problem concerns the so-called QCD θ-term, a dimension-four topological operator built with the gluon field strength G and the Levi-Civita symbol ϵ,

$$\mathcal{L}_\theta = \theta \frac{\alpha_S}{8\pi} \frac{1}{2} \epsilon^{\mu\nu\alpha\beta} \operatorname{Tr} G_{\mu\nu} G_{\alpha\beta}, \tag{2.1}$$

where the trace runs over $SU(3)_c$ indices. An equivalent way of writing the θ-term is to introduce the dual field strength $\tilde{G}$ as $\tilde{G}^{\mu\nu} \equiv \frac{1}{2}\epsilon^{\mu\nu\alpha\beta} G_{\alpha\beta}$,

$$\mathcal{L}_\theta = \theta \frac{\alpha_S}{8\pi} \operatorname{Tr} G_{\mu\nu} \tilde{G}^{\mu\nu}. \tag{2.2}$$

This operator is called topological as it is independent of the space-time metric: the Lorentz indices are in fact simply contracted by anti-symmetrization with the ϵ symbol. One can also check that the θ-term is in fact a total derivative, $G\tilde{G} \equiv \partial_\mu K^\mu$, and thus

only concerns the information at the boundary. As a consequence, it does not contribute to the classical equation of motion, and no effect can be found in perturbation theory. Nevertheless, the contribution from this operator cannot be neglected as important physical observables crucially dependend on it, as we shall see.

The existence of the θ-term is connected with the non-trivial vacuum structure of QCD [29] that we will briefly review (see e.g. [30,31]). In the temporal gauge, $A_0(x) = 0$, the vacuum condition at the space-time boundary, $|\mathbf{x}| \to \infty$, is $F_{\mu\nu} = 0$ and is solved by time-independent field configurations,

$$A_i(x) = g^{-1}(\mathbf{x})\partial_i\, g(\mathbf{x}) \tag{2.3}$$

that are obtained acting on the simplest configuration, $A_i(x) = 0$, via the gauge transformation $g(\mathbf{x})$. The relation above defines a mapping between the physical space at the boundary and the QCD group, $SU(3)_c$. Each gauge configuration as in (2.3) can then be labelled according to the winding number $n \in \mathbb{Z}$ of the corresponding class in the $\Pi_{d-1}(SU(3)_c)$ homotopy group, where $d = 4$ is the dimension of space time:

$$n = \frac{ig_S^3}{24\pi^2}\int d^3\mathbf{x}\,\mathrm{Tr}\,\epsilon_{ijk}\,A_i^n(\mathbf{x})A_j^n(\mathbf{x})A_k^n(\mathbf{x}), \tag{2.4}$$

where A^n is related to the gauge transformation g_n as in (2.3). One thus realizes that there exists a *plethora* of vacuum states that can be labelled by $|n\rangle$, and are actually connected by gauge transformations as

$$g_1|n\rangle = |n+1\rangle. \tag{2.5}$$

Standard perturbation theory assumes the vacuum to be $A_i(x) = 0$ corresponding to $|0\rangle$ in this notation. The crucial question is then: do the $|n \neq 0\rangle$ vacua actually have an impact on the path-integral? Remarkably, the answer is yes [29], and the transition probability gets instanton contributions:

$$\langle n|n+1\rangle \propto \exp(-2\pi/\alpha_S). \tag{2.6}$$

As we can see, the transition probability among vacua is non-zero and non-analytical at $\alpha_S = 0$, and therefore this effect cannot be captured in perturbation theory!

This also shows that $|0\rangle$ cannot be considered the true vacuum of the theory, nor can any of the other $|n\rangle$ states. A step towards the resolution of this ambiguity is to construct gauge invariant vacua. This is possible by taking a coherent superposition of the $|n\rangle$ states as

$$|\theta\rangle = \sum_n e^{-in\theta}|n\rangle, \tag{2.7}$$

where θ is a real number in the interval $\theta \in [0, 2\pi)$. Under a gauge transformation, g_n, one has

$$g_n|\theta\rangle = e^{in\theta}|\theta\rangle, \tag{2.8}$$

showing that $|\theta\rangle$ is in fact stable under gauge transformations. The crucial property of the θ-states is that

$$\langle\theta|\theta'\rangle = 0 \quad \text{for} \quad \theta \neq \theta', \tag{2.9}$$

meaning that transition among θ-vacua are forbidden. Moreover, the path integral formulation of the theory based on the θ-vacuum is given by

$$\langle\theta|\theta\rangle = \int \mathcal{D}A \; e^{iS_{\text{eff}}}, \tag{2.10}$$

where S_{eff} contains the θ-term in (2.1),

$$S_{\text{eff}} = S_0 + \theta\frac{\alpha_S}{8\pi}\int \mathrm{d}^4x \,\mathrm{Tr}\, G_{\mu\nu}\tilde{G}^{\mu\nu}, \tag{2.11}$$

and S_0 is the standard Yang-Mills action containing the kinetic terms and gauge interactions. Therefore, we can see that the effects of topologically different field configurations in the path integral can be accounted for as a new θ-term in the effective action of the standard path integral. As transitions between different θ-vacua are forbidden, θ should be regarded as a new free parameter of the theory.

The presence of the θ-term affects the energy of the QCD vacuum and acts as a source of C and CP violation. As for the vacuum energy, $E(\theta)$, one has [32]

$$E(\theta) \simeq -e^{-2\pi/\alpha_S}\cos\theta. \tag{2.12}$$

As we can see, the energy has a minimum at $\theta = 0$; however, as transitions between θ-vacua are forbidden, the system cannot relax to it. Moreover, the θ-term induces a CP-violating electric dipole moment for the neutron, d_N, of the order

$$d_N \simeq e\frac{m_q}{m_N^2}\theta, \tag{2.13}$$

where e is the electric charge, m_N is the mass of the neutron and m_q is the mass scale of the light up and down quarks. Experimentally, constraints on the size of d_N imply that $\theta \lesssim 10^{-10}$ [33]. As θ cannot relax to its minimum, this gives rise to the strong CP problem in QCD, namely the question why in our Universe the free parameter θ, that could be any number in the range $[0, 2\pi)$, was set so close to zero without any dynamical explanation.

This fine-tuning becomes even worse when discussing the strong CP problem in the full SM. In fact, the fermion masses in the SM originate from yukawa interactions with the Higgs field: these yukawa matrices contain off-diagonal terms and complex entries. By implementing a bi-unitary transformation acting on the left- and right-handed fermions, U_L and U_R, it is always possible to obtain a mass matrix, M_{diag}, that is real and diagonal:

$$M_{\text{diag}} = U_L^\dagger M_q U_R, \tag{2.14}$$

where M_q is the (block diagonal) mass matrix collecting up and down quarks prior rotations. The unitary transformations can be decomposed with respect to $U(1)\times SU(N)$ as

$$U_{L,R} = e^{i\phi_{L,R}}S_{L,R}. \tag{2.15}$$

The presence of these two phases signals that a chiral rotation is needed in the process of diagonalization. However, the $U(1)_A$ group of chiral rotations is anomalous under QCD [1]: the corresponding axial current made of quarks,

$$J_5^\mu = \bar{q}\gamma^\mu\gamma_5\, q, \tag{2.16}$$

[1] This axial anomaly is indeed the reason why no additional light pseudo scalar is observed in the hadron spectrum besides the pion triplet.

is not conserved, $\partial_\mu J_5^\mu \neq 0$. This non conservation is relevant for the θ-term discussed above; in particular, one has

$$\partial_\mu J_5^\mu = n_f \frac{\alpha_S}{2\pi} \mathrm{Tr}\, G_{\mu\nu}\tilde{G}^{\mu\nu} \tag{2.17}$$

where $n_f = 6$ is the number of quarks. Hence, the chiral rotations in (2.15) actually introduce an independent contribution to the operator in (2.1), thus shifting θ by an amount that is determined by $\phi_{L,R}$:

$$\theta \to \bar{\theta} = \theta + \arg\det M_q = \theta + \arg\det U_R^\dagger U_L = \theta + n_f(\phi_L - \phi_R), \tag{2.18}$$

where we have used that $M_{\rm diag}$ is real, and $\det S_{L,R} = 1$. The actual value of these phases is unknown within the SM, as they only contribute through the topological term. However, we do know that the SM yukawa matrices have complex entries, and one of them, δ, is responsible for CP violation in the weak interactions [34]. As this phase is $\delta \sim \mathcal{O}(1)$, see e.g. [35], one naturally expects the same order of magnitude for $\phi_{L,R}$. Thus, the strong CP problem in the SM is somehow worse than what discussed in the previous section, as the question is now why the combination of the two independent contributions from the QCD θ-term and from the electroweak sector cancel to $\mathcal{O}(10^{-10})$ accuracy.

Before discussing possible solutions to this fine-tuning problem, let us mention that similar topological terms can be written also for the electroweak group $SU(2)_L \times U(1)_Y$. Similarly to QCD, these terms are total derivatives; this turns out to be sufficient to make the $U(1)_Y$ topological term vanish upon integration at the boundaries (in the absence of monopoles) [36]. As for $SU(2)_L$, it is possible to use the baryon plus lepton number, $B+L$, which is an accidental global symmetry of the SM Lagrangian with non-zero anomaly, to rotate the topological term away [37]. However, there is no symmetry in the SM that can absorb the QCD θ-term.

In general, there exist three classes of solutions to the strong CP problem. The first one builds on the fact that if any of the bare quark masses, say the up mass m_u, was zero, $\bar{\theta}$ would be unphysical, as it could be always rotated away by anomalous transformations acting on the up quark [2]. The bare up mass could instead be generated by non-perturbative QCD dynamics in order to comply with lattice results that solidly exclude the possibility of massless quarks [38]— see [39] for a recent revival of this idea.

The second class of solutions was first presented in the works of A. E. Nelson [40] and S. M. Barr [41, 42]. The main idea is to forbid the bare θ-term by imposing CP as a true symmetry of the theory. CP is then broken spontaneously in order to account for its apparent violation by the weak interactions due to the CKM phase, δ. The main challenge is then to construct the theory such that $\arg\det M_q \ll 1$ while $\delta \sim \mathcal{O}(1)$ after spontaneous CP breaking. A characteristic of the Nelson-Barr solution is that, unlike the $m_u = 0$ case and the axion solution, it leaves the low-energy QCD unchanged, and the strong CP problem is solved at the scale at which the SM yukawas are generated.

The third class of solution was proposed by R. Peccei and H. Quinn in 1977 [11, 12]. It relies on the existence of a spontaneously broken $U(1)_{\rm PQ}$ symmetry that is anomalous under QCD. The most important prediction that comes along with this is the presence of a light, feebly-coupled pseudoscalar in the low energy theory, the axion. This will be the focus of the next sections.

[2] Notice that the case of massless quarks is indeed special, as $\det M_q = 0$, and its argument in (2.18) is not defined.

2.2 The axion solution

We have seen that the CP-converving vacuum with $\theta = 0$ is actually the one favoured by energy consideration; see (2.12). However, the θ-angle cannot relax to zero, as it is just a static parameter, and transitions among different vacua are forbidden. The essence of the axion solution to the strong CP problem relies on making θ a dynamical quantity. This is done by identifying θ with the axion vacuum expectation value (vev), $\langle a \rangle$, whose smallness follows from the fact that the axion potential is minimized at $\langle a \rangle = 0$, as we shall see [3].

Let us discuss the Peccei-Quinn (PQ) solution to the strong CP problem in a model-independent way. The crucial ingredient is a new chiral $U(1)_{\rm PQ}$ symmetry with a non-zero QCD anomaly. This requires the existence of colored fermions with non-zero PQ charge. If $U(1)_{\rm PQ}$ were unbroken, the strong CP problem would be solved similarly to the case of a massless quark, as this extra symmetry could be used directly to rotate the θ-term away. However, the strong CP problem can also be solved in case $U(1)_{\rm PQ}$ is spontaneously broken. In this case, by the Goldstone theorem, a light scalar, the axion, appears in the spectrum.

Below the scales of Peccei-Quinn and electroweak symmetry breaking, the effective axion Lagrangian reads [43, 44]:

$$\mathcal{L}_a = \frac{1}{2}\left(\partial_\mu a\right)^2 + \frac{1}{2f_a}\left(\partial_\mu a\right) J^\mu + \frac{\alpha_S}{8\pi}\left(\theta + \frac{a}{f_a}\right) G_{\mu\nu}\tilde{G}^{\mu\nu} + \frac{\alpha_{\rm em}}{8\pi}\frac{a}{f_a}\frac{E}{N} F_{\mu\nu}\tilde{F}^{\mu\nu}, \qquad (2.19)$$

where J^μ is a model-dependent current involving the SM fermions, E and N are the electromagnetic and strong-interaction anomaly coefficients of the PQ current, respectively. The PQ symmetry is non-linearly realized in (2.19) as a shift symmetry on the axion field,

$$a(x) \to a(x) + \alpha f_a, \qquad (2.20)$$

whereas the fermions do not transform [4]. The fact that the PQ symmetry is actually broken by anomalies is ensured by the last two terms involving non-derivative couplings between the axion and the topological terms. The axion shift symmetry makes the θ angle in (2.19) a spurious quantity, as it can always be eliminated by an appropriate transformation (2.20) with $\alpha = -\theta$ with no other effect [5]. The θ-angle in (2.19) is then fully replaced by the axion field.

In passing, let us mention that the use of the axion shift symmetry to eliminate the bare θ-angle relies on the fact that $U(1)_{\rm PQ}$ is supposed to be an exact global symmetry of the classical Lagrangian which is only broken by anomalies. However, global symmetries are usually understood as accidental symmetries arising at the renormalizable level (as, for instance, baryon and lepton number in the SM) and are believed to be broken by higher dimensional operators. By taking the cutoff to be the Planck scale and $f_a \simeq 10^{11}\,\text{GeV}$ [6], it turns out that one can tolerate only operators $\mathcal{O}$ with dimensionality

[3] The actual minimum is slightly shifted from $\langle a \rangle = 0$ due to the CP violation in the yukawa sector of the SM. This effect is nevertheless far below the current bound on θ, and does not spoil the solution to the strong CP problem.

[4] This is consistent also in case SM fermions are charged under PQ; see [43].

[5] The induced constant topological term $-\theta\frac{\alpha_{\rm em}}{8\pi}\frac{E}{N}F\tilde{F}$ can be safely neglected [36].

[6] Lower values of f_a help reducing this issue but they are more severely constrained experimentally, as we shall see.

$[\mathcal{O}] > 13$ not to spoil the solution to the strong CP problem, see e.g. [36]. Despite this being possible, the question of how a global symmetry can exhibit such a spectacular degree of conservation is still an open question and is usually referred to as the "axion quality problem".

Going back to our discussion, eliminating the bare θ-term is still not enough to solve the strong CP problem as one needs to ensure that the axion vev is actually driven to zero. Yet, we already know that this has to be the case as (2.12) implies that the CP-conserving vacuum is energetically favourable. As the axion shift symmetry is explicitly broken by the QCD anomaly, a potential for the axion will be generated at the non-perturbative level. In order to evaluate it, one can employ chiral perturbation theory. The strategy is to get rid of the $aG\tilde{G}$ term in (2.19) by performing a chiral rotation on the light u and d quarks. This reults in a "dressed" axion-dependent mass matrix for the quarks that eventually enters the pion Lagrangian to keep track of the explicit chiral symmetry breaking. This procedure allows to take into account the mixing between the axion and the other QCD mesons, as the neutral pion π_0, that affects axion physics, as for instance its effective coupling to photons. After integrating out all the hadrons, one finds the following potential for the physical axion [44]:

$$V(a) = -m_\pi^2 f_\pi^2 \sqrt{1 - \frac{4 m_u m_d}{(m_u + m_d)^2} \sin^2\left(\frac{a}{2 f_a}\right)}, \tag{2.21}$$

which implies a mass m_a given by

$$m_a = \sqrt{\frac{m_u m_d}{(m_u + m_d)^2}} \frac{m_\pi f_\pi}{f_a} \simeq 6 \times 10^{-4}\,\text{eV} \left(\frac{10^{10}\,\text{GeV}}{f_a}\right), \tag{2.22}$$

where $f_\pi \simeq 92\,\text{MeV}$ is the pion decay constant. As we can see, the minimum is at $a = 0$, thus solving the strong CP problem.

Eqs (2.19) and (2.22) show two very important phenomenological properties of the axion: all its interactions as well as its mass become extremely small if the PQ breaking scale, f_a, becomes large. Axions of this type are thus referred to as "invisible" and are broadly classified into DFSZ [45, 46] and KSVZ [47, 48] models, depending on whether or not the SM fermions are charged under PQ. Visible axions with $f_a \approx v$, including the original PQWW model [11, 49, 50], are by now excluded experimentally. Axion physics can indeed be constrained in many different ways exploiting for instance the axion coupling to photons, nucleons, leptons, and also gravity.

Before moving to the different strategies that can be used to detect the axion, let us discuss a very important property of the axion solution to the strong CP problem, namely that it can simultaneously account for the total abundance of dark matter in the Universe [51–53]. Despite being extremely light, typically far below the eV scale, axions can still behave as cold dark matter if the axion population is produced non-thermally. Assuming that the Peccei-Quinn symmetry is broken during inflation, our Universe started with a constant value of the axion field everywhere, parametrized by $\theta_0 = a(t_0)/f_a \in (-\pi, \pi)$ [7]. The axion field then evolves in the Friedmann-Lemaître-Robertson-Walker metric according to the equation of motion

$$\ddot{a}(t) + 3H(t)\dot{a}(t) + m_a^2 a(t) = 0, \tag{2.23}$$

[7] The occurrence of inflation after PQ symmetry breaking solves the issue related to dangerous topological relics of the $U(1)_{\text{PQ}}$ breaking, such as domain walls, that are always produced whenever the color anomaly N is $N > 1$. However, isocurvature-perturbation bounds apply [54].

where $H(t) = \dot{\tilde{a}}(t)/\tilde{a}(t)$ is the Hubble rate, and $\tilde{a}(t)$ is the scale factor. As long as $H \gtrsim m_a$, the axion field is frozen to its initial value. However, for $H \lesssim m_a$, the axion starts oscillating with a frequency that is dicated by its mass. During these coherent oscillations around the $a = 0$ minimum, the axion energy density ρ_a,

$$\rho_a = \frac{1}{2}\dot{a}(t)^2 + \frac{1}{2}m_a^2 a(t)^2, \tag{2.24}$$

actually red-shifts like dust, $\rho_a \sim \tilde{a}^{-3}$. As a result, axions are good dark matter candidates, and the relic abundance is fixed by the angle θ_0 corresponding to the initial misalignment. For this reason, this mechanism is referred to as the "misalignment mechanism". According to the energy density in (2.24) for the simple harmonic potential, the relic abundance of axions, $\Omega_a h^2$, is given by [31]

$$\Omega_a h^2 \simeq 2 \times 10^{-3} \left(\frac{f_a}{10^{10}\,\mathrm{GeV}}\right)^{7/6} \theta_0^2. \tag{2.25}$$

Through (2.22) we can rewrite the expression above in terms of m_a:

$$\Omega_a h^2 \simeq 3.5 \left(\frac{\mu\mathrm{eV}}{m_a}\right)^{7/6} \theta_0^2. \tag{2.26}$$

Since $\theta^2 < \pi^2$, Eq. (2.26) sets an upper bound on the axion mass when requiring that all dark matter, $\Omega_c h^2 \simeq 0.12$ [8], is accounted by axions produced by misalignment:

$$m_a \lesssim 130\,\mu\mathrm{eV}. \tag{2.27}$$

For larger masses, the axion can still be a subdominant component. Assuming that axions are a relevant fraction of dark matter, one could detect them directly via interactions with the dark matter halo of our galaxy. Experiments of this type are ADMX [55] and its future upgrade [56], CAsPEr [57], MADMAX [58], and ABRACADABRA [59].

In the next section, we will discuss the axion searches according to the exploited physical mechanism. As we shall see, these constraints apply regardless of the axion being dark matter or not.

2.3 Axion searches

Even though the axion has no electromagnetic charge, it couples to photons due to a generically non-zero contribution from the electromagnetic anomaly and from its couplings to QCD. This interaction can be described by a single parameter $g_{a\gamma\gamma}$:

$$\mathcal{L}_{a\gamma\gamma} = g_{a\gamma\gamma} \frac{\alpha_{\mathrm{em}}}{8\pi} \frac{a}{f_a} F\tilde{F}, \tag{2.28}$$

where

$$g_{a\gamma\gamma} = |E/N - 1.92|. \tag{2.29}$$

The first term, E/N, comes directly from (2.19) and reflects the fact that the PQ symmetry can have a non-zero electromagnetic anomaly. This depends on the particular UV completion of (2.19) and is therefore model-dependent. Conversely, the second term arises from the axion couplings to QCD and is model independent.

Whenever the fermions charged under PQ fill complete $SU(5)$ representations such as in the original DFSZ models, one has $E/N = 8/3$, see e.g. [60]. However, it could also be that the fermions responsible for the PQ color anomaly are electroweak singlet, as in the KSVZ type of models, and thus $E/N = 0$. Taking into account this model dependence, there have been various attempts to identify the possible window for $g_{a\gamma\gamma}$. The "standard" axion window is obtained by looking at different variants of the DFSZ and KSVZ models and reads [61]

$$g_{a\gamma\gamma} \in (0.07, 7). \tag{2.30}$$

Recently, this has been revisited in [62], finding that the axion coupling to photons could be as big as $g_{a\gamma\gamma} \approx 60$ compatibly with cosmology and internal consistency of the theory.

As for the axion couplings to matter, let us refer to the effective Lagrangian in (2.19) and write down the fermion current J^μ more explicitly:

$$\frac{1}{2f_a}\partial_\mu a(x)\, J^\mu(x) = \frac{1}{2f_a}\partial_\mu a(x)\, \bar{\Psi}(x)\gamma^\mu \left(C_V + C_A\gamma_5\right) \Psi(x), \tag{2.31}$$

where Ψ collects the SM fermions in their mass eigenstates:

$$\mathcal{L}_{\rm kin} = \bar{\Psi}(i\partial\!\!\!/ - m_{\rm diag})\Psi. \tag{2.32}$$

The $C_{V,A}$ matrices contain couplings in the flavor space. Also note that below the QCD condensation scale the couplings to quarks induce axion couplings to nucleons, C^{nn}, where n refers to protons or neutrons. Notice that only the off-diagonal entries of the matrix C_V matter, as the diagonal terms, C_V^{ii}, can always be eliminated by vector transformations

$$\Psi_i \to \exp\left(i\frac{1}{2f_a}\, C_V^{ii}\, a(x)\right) \Psi_i \tag{2.33}$$

that are not anomalous and induce a new contribution from the kinetic term,

$$\mathcal{L}_{\rm kin} \to \mathcal{L}_{\rm kin} - \frac{1}{2f_a}(\partial_\mu a)\bar{\Psi}_i\, C_V^{ii}\, \Psi_i, \tag{2.34}$$

that exactly cancels against the one from (2.31). This is relevant when discussing possible long-range force constraints on the axion parameter space which are in fact automatically evaded as for instance the vector coupling to electrons, C_V^{ee}, is unphysical, and its axial counterpart, C_A^{ee}, can only induce spin-dependent interactions that are suppressed for macroscopic bodies (unless they are polarized), see e.g. [31].

Constraints on the axion parameter space can be divided according to the physical effect that is exploited. We will discuss energy loss due to axion production, conversion to photons via Primakoff effect, and flavor violation, as detailed below.

Energy loss

If the axion mass allows for efficient thermal production, the consequent axion flux represents an additional source of energy loss for astrophysical objects. This is because the axion, similarly to neutrinos, interacts feebly with matter and can easily stream away. From the analysis of the evolution of globular clusters, one can set a bound on the rate of axion-photon conversion inside the stars for masses $m_a \lesssim 0.1\,\text{MeV}$ [63]:

$$g_{a\gamma\gamma} < 0.6\, \frac{f_a}{10^7\,\text{GeV}}. \tag{2.35}$$

An order of magnitude weaker bound on $g_{a\gamma\gamma}$, but valid for axion masses $m_a \lesssim 50$ MeV, can be placed by the supernova event SN1987a [64].

As for couplings to matter, the white-dwarf luminosity function can place a constraint on the axion coupling to electrons when the energy loss due to the axion flux is compared to the neutrino flux. This provides the following limit [65]:

$$C_A^{ee} < 0.5 \, \frac{f_a}{10^9 \, \text{GeV}}. \tag{2.36}$$

On similar grounds, the SN1987a event can place a bound on the average axion coupling to nucleons [66]:

$$C_A^{nn} < 0.7 \, \frac{f_a}{10^9 \, \text{GeV}}. \tag{2.37}$$

Primakoff effect

In the presence of a magnetic field, an axion can be converted to a photon (and vice versa) due to the Primakoff effect [67] sourced by the $g_{a\gamma\gamma}$ coupling. Taking this into account, the SN1987a can set an upper limit on $g_{a\gamma\gamma}$ from the non-observation of gamma rays resulting from axion conversion mediated by the magnetic field of our galaxy [68]:

$$g_{a\gamma\gamma} < 0.5 \, \frac{f_a}{10^8 \, \text{GeV}} \tag{2.38}$$

for $m_a \lesssim 4 \times 10^{-10} \, \text{eV}$. Moreover, axions can be emitted by stars like our Sun and travel to Earth where they can be converted to photons in regions where a strong magnetic field is applied. This strategy has been employed at the CERN Axion Solar Telescope (CAST), setting a bound that is similar to (2.35) [69]:

$$g_{a\gamma\gamma} < 0.6 \, \frac{f_a}{10^7 \, \text{GeV}} \tag{2.39}$$

for $m_a \lesssim 10^{-2} \, \text{eV}$. This bound will likely be improved by the new generation of "helioscopes" such as IAXO [70] by one order of magnitude. The same concept is used in the Light-Shining-Through-a-Wall experiments, where the astrophysical source is replaced by a laser. The idea is to let the light pass through a barrier by converting it into axions with the help of a strong magnetic field, and convert it back to photons on the other side of the barrier in order to detect it. Currently, the strongest bound is given by the Any Light Particle Search (ALPS) experiment at DESY [71]:

$$g_{a\gamma\gamma} < 0.6 \frac{f_a}{10^4 \, \text{GeV}}. \tag{2.40}$$

This limit is expected to be further improved by ALPS II by three orders of magnitude [72].

Flavor violation

Axions can mediate flavor-changing neutral currents whenever the $C_{V,A}$ matrices in (2.31) have non-zero off-diagonal elements. Two couplings that are particularly relevant

for current and future experiments are C^{ds} in the quark sector and $C^{e\mu}$ in the lepton sector [8].

The $d \to s$ transition can be looked for in heavy meson decays. The strongest bound is found for $K^+ \to \pi^+ a$, for which the main SM background is given by the $K^+ \to \pi^+ \nu\bar{\nu}$ rare decay. The current best limit on this branching ratio is [74]:

$$\mathcal{B}(K^+ \to \pi^+ a) < 0.73 \times 10^{-10}. \tag{2.41}$$

This bound is expected to be improved by the NA62 experiment at CERN by one order of magnitude [75]. The theoretical calculation for $K^+ \to \pi^+ a$ depends on C^{ds} as [73]

$$\mathcal{B}(K^+ \to \pi^+ a) \simeq \frac{1}{64\pi\Gamma_K} \frac{|C_V^{ds}|^2}{f_a^2} m_K^3 \left(1 - \frac{m_\pi^2}{m_K^2}\right)^3. \tag{2.42}$$

Notice that only the vector component contributes, as the decaying particle has no spin. From (2.41) one finds

$$f_a > 3.5 \times 10^{11} |C_V^{ds}| \,\text{GeV} \quad \Leftrightarrow \quad m_a < \frac{2 \times 10^{-5}}{C_V^{ds}} \,\text{eV}. \tag{2.43}$$

The $C^{e\mu}$ coupling mediates a process that violates charged-lepton flavor. It can be searched for directly as a rare muon decay, $\mu \to ea$ or in combination with a photon, $\mu \to ea\gamma$. The main SM background for $\mu^+ \to e^+ a$ is the β decay $\mu^+ \to e^+ \nu\bar{\nu}$. The strongest limit is obtained if one assumes isotropic decays, namely either fully vectorial or axial, and is given by [76]

$$\mathcal{B}(\mu^+ \to e^+ a) < 2.6 \times 10^{-6}, \tag{2.44}$$

whereas bounds on anisotropic decays can be one order of magnitude weaker [77]. These limits are going to be largely improved by future experiments, as Mu3e [78] and MEG II [79]. The theoretical calculation for this branching ratio follows (2.42) with the kaon mass and width replaced by the analogous for the muon, and the pion mass replaced by the electron mass. The effective coupling entering the width is now $|C^{e\mu}|^2 = |C_V^{e\mu}|^2 + |C_A^{e\mu}|^2$. Considering the case of isotropic decays, namely either a purely vectorial or axial coupling, one obtains a bound on f_a given by

$$f_a > 2.8 \times 10^9 \, |C^{e\mu}| \,\text{GeV} \quad \Leftrightarrow \quad m_a < \frac{2 \times 10^{-3}}{|C^{e\mu}|} \,\text{eV}, \tag{2.45}$$

and similarly for anisotropic decays. By looking at (2.43) and (2.45), we see that precision flavor observables are very relevant in constraining the QCD axion parameter space and new experiments have the potential of discovering an axion independently of the other searches. However, axion couplings to SM fermions are model-dependent quantities and are ultimately related to their PQ charges. For instance, $C_{V,A} = 0$ in the KSVZ model, and $C_V = 0, C_A \propto \mathbb{1}$ in the simplest DFSZ model, so that no flavor-violating effect is found. On the other hand, non-vanishing off-diagonal couplings such as C^{ds} or $C^{\mu e}$ are generic predictions of PQ charges that are flavor non-universal.

[8] Although the axion field in (2.19) is not the physical one, its off-diagonal couplings are unchanged after the axion-pion system is diagonalized [73], as the QCD anomaly is insensitive to flavor.

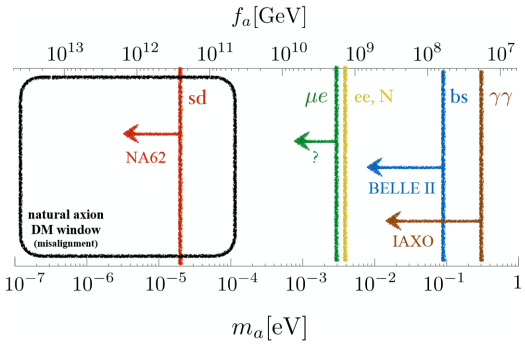

Figure 2.1: Constraints on the axion parameter space by setting all the relevant $C_{V,A}$ couplings and $g_{a\gamma\gamma}$ to 1. Arrows indicate the sensitivity of future experiments. Graphics taken from Ref. [80].

To see how this works, let us consider the charged-lepton sector before electroweak symmetry breaking. Indicating by

$$X_L^{\rm e} = \text{diag}(x_{e_L}, x_{\mu_L}, x_{\tau_L}), \quad X_R^{\rm e} = \text{diag}(x_{e_R}, x_{\mu_R}, x_{\tau_R}) \tag{2.46}$$

the flavor-diagonal, but not universal, matrices collecting the PQ charges for the left- and right-handed charged leptons as gauge eigenstates, one has that the current $J^\mu_{\rm ch.lep.}(x)$ coupled derivatively to the axion is:

$$\frac{\partial_\mu a(x)}{f_a} J^\mu_{\rm ch.lep.}(x) = \frac{\partial_\mu a(x)}{f_a}\left[\frac{1}{N}\bar{l}_L(x)\gamma^\mu X_L^{\rm e} l_L(x) + \frac{1}{N}\bar{l}_R(x)\gamma^\mu X_R^{\rm e} l_R(x)\right], \tag{2.47}$$

where $l = (e, \mu, \tau)$ and N is the color anomaly. The current above can be thought as originating from the lepton kinetic terms after a chiral rotation at high energies of angle $iX_{L,R}\, a(x)/(f_a N)$. After electroweak symmetry breaking, charged leptons obtain their masses from the yukawa interaction with the Higgs. Flavor and mass eigenstates are thus not aligned, but rather connected via a bi-unitary transformation, $l_L = U_L l'_L$ and $l_R = U_R l'_R$. Rewriting (2.47) in the mass basis, one finds:

$$J^\mu_{\rm ch.lep.}(x) = \frac{1}{N}\bar{l}'_L(x)\gamma^\mu\, U_L^\dagger X_L^{\rm e} U_L\, l'_L(x) + \frac{1}{N}\bar{l}'_R(x)\gamma^\mu\, U_R^\dagger X_R^{\rm e} U_R\, l'_R(x), \tag{2.48}$$

so that when comparing with (2.31) one sees that the coupling matrices $C_{V,A}$ are related to the charges $X_{L,R}$ as

$$C_V = \frac{1}{N}\left(U_R^\dagger X_R U_R + U_L^\dagger X_L U_L\right), \quad C_A = \frac{1}{N}\left(U_R^\dagger X_R U_R - U_L^\dagger X_L U_L\right). \tag{2.49}$$

Analogous structure holds for the SM quarks. Thus, whenever the PQ charges X do not commute with the yukawa matrices, flavor-diagonal couplings arise. This is in fact the case whenever the charges are not flavor-universal. Conversely, when the PQ charges are flavor universal, $X \propto \mathbb{1}$, one trivially finds $U^\dagger X U = \mathbb{1}$ with no flavor violation.

To summarize, flavor-violating axion couplings are potentially sizable and offer an excellent probe of the axion parameter space. However, this statement crucially depends on the PQ charges of the SM fermions that are model-dependent quantities. In the

next section we will discuss a particularly predictive scenario which interpretes the PQ symmetry as a flavor symmetry. The PQ charges are then no longer arbitrary but rather fixed by the observed pattern of fermion masses and mixings in the SM. As we shall see, this model offers interesting predictions for flavor observables such as $K \to \pi a$.

2.4 Peccei-Quinn as flavor symmetry

The idea that the PQ symmetry and flavor symmetries may be related actually goes back to Wilczek [81]. Before investigating this possibility in a new concrete realization, let us recall that a "flavor puzzle" can be identified as the observation that:

1. the yukawa couplings between the Higgs and the SM fermions span several orders of magnitude, from $\mathcal{O}(1)$ to $\mathcal{O}(10^{-5})$ (not considering neutrinos), reflected in a large mass hierarchy;

2. the CKM matrix shows a clear pattern with $\mathcal{O}(1)$ diagonal couplings and approximate $U(2)$ symmetry for the first two quark generations:

$$\text{CKM} \approx \begin{pmatrix} 1 & \lambda & \lambda^3 \\ \lambda & 1 & \lambda^2 \\ \lambda^3 & \lambda^2 & 1 \end{pmatrix}, \tag{2.50}$$

   where $\lambda = \sin\theta_{\text{C}} \simeq 0.2$ is the sine of the Cabibbo angle.

Perhaps the simplest flavor symmetry one can advocate to explain these observations is the Froggatt-Nielsen (FN) mechanism [14]. The idea is to chirally charge the SM fermions under a new horizontal (namely, flavor non-universal) $U(1)_{\text{H}}$ symmetry. Similarly to what happens with the electroweak symmetry and the Higgs, the masses and mixings of the SM fermions are now controlled by the breaking of $U(1)_{\text{H}}$. This can be achieved by introducing a new scalar field Φ, charged under $U(1)_{\text{H}}$, that acquires a vev. Because of its role in addressing the flavor puzzle, the radial component of Φ is referred to as the flavon.

In addition to the new scalar, Φ, the SM field content needs to be augmented by new vector-like fermions, ξ_j, dubbed the FN messengers, which connect the different SM-fermion chiralities, bridging their $U(1)_{\text{H}}$ charge difference via a chain of Φ insertions. Taking the FN messengers to reside much above the electroweak scale, they can be integrated out in favor of an IR effective description. Once the $U(1)_{\text{H}}$ is spontaneously broken by the flavon vev $\langle\Phi\rangle \equiv f/\sqrt{2}$, the SM yukawa couplings are effectively reproduced starting with $\mathcal{O}(1)$ couplings in the UV theory.

To show this, consider an up-type quark u chirally charged under $U(1)_{\text{H}}$ such that $\text{H}(q_L) = l$ and $\text{H}(u_R) = r$. Taking Φ to carry unitary PQ charge, SM gauge symmetry and $U(1)_{\text{H}}$ together imply that the up mass, m_u, comes from the following operator:

$$\mathcal{O}_u = \frac{1}{\Lambda^{l-r}} \lambda_u \, \bar{q_L} \, \tilde{h} \, \Phi^{l-r} \, u_R, \tag{2.51}$$

where h is the Higgs doublet and $\tilde{h} = i\sigma_2 h^*$. This operator can be visualized as the result of integrating out the FN chain shown in Fig. 2.2, where wiggly lines are the FN messengers, simple crosses stand for insertions of Φ, and the circled cross represents the Higgs. The main difference with respect to the standard yukawa coupling in the SM is

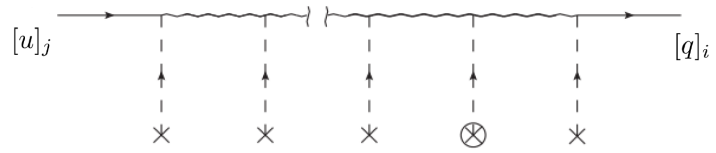

Figure 2.2: Froggatt-Nielsen chain made of the vector-like fermions ξ_j (wiggly lines) to bridge the charge difference of the two fermion chiralities. Simple crosses represent insertions of the Φ vev, and the circled cross stands for the Higgs vev. Graphics adapted from [14].

that $\mathcal{O}_u$ is higher dimensional and suppressed by the large scale Λ. After $U(1)_{\rm H}$ and electroweak symmetry breaking, the mass m_u is given by

$$m_u = \frac{1}{\sqrt{2}}\lambda_u v \left(\frac{f}{\sqrt{2}\Lambda}\right)^{l-r} \equiv \frac{1}{\sqrt{2}} y_u v. \tag{2.52}$$

Therefore, the effective yukawa y_u can actually be very small starting from $\lambda_u \sim \mathcal{O}(1)$ as a consequence of integrating out the FN chain. The scale Λ is here related to the mass scale of the FN messengers, which needs to be parametrically larger than f. Lighter fermions are then resulting from a larger separation of chiral charges $l - r$, whereas the top quark features $l = r$ so that $y_t \simeq \lambda_t = \mathcal{O}(1)$.

In order to see what structure is predicted for the CKM matrix, let us write down the analogous of (2.51) including down quarks and considering all the three flavors:

$$\mathcal{L}_{\rm yukawa} = \bar{q}_L^i \, \lambda_u^{ij} \left(\frac{\Phi}{\Lambda}\right)^{l_i - r_j^u} \tilde{h} \, u_R^j + \bar{q}_L^i \, \lambda_d^{ij} \left(\frac{\Phi}{\Lambda}\right)^{l_i - r_j^d} h \, d_R^j, \tag{2.53}$$

where l stands for the H charge of the left-handed quark doublets and $r^{u,d}$ is the H charge of the right-handed up and down quarks, respectively. The i, j indices run over the three families. Setting Φ and h to their vev, one finds the following mass matrices:

$$\mathcal{L}_{\rm mass} = \bar{u}_L^i \, M_{ij}^u u_R^j + \bar{d}_L^i \, M_{ij}^d d_R^j, \tag{2.54}$$

where

$$M_{ij}^u = \frac{1}{\sqrt{2}}\lambda_u^{ij} v \left(\frac{f}{\sqrt{2}\Lambda}\right)^{l_i - r_j^u}, \quad M_{ij}^d = \frac{1}{\sqrt{2}}\lambda_d^{ij} v \left(\frac{f}{\sqrt{2}\Lambda}\right)^{l_i - r_j^d}. \tag{2.55}$$

These mass matrices can be diagonalized by the usual bi-unitary transformations,

$$u_{L,R} \to U_{L,R} \, u_{L,R}, \quad d_{L,R} \to V_{L,R} \, d_{L,R}, \tag{2.56}$$

such that

$$U_L^\dagger M^u U_R = \text{ diag}(m_u, m_c, m_t) \quad V_L^\dagger M^d V_R = \text{ diag}(m_d, m_s, m_b). \tag{2.57}$$

Because of the peculiar structure of $M^{u,d}$ in (2.55), the CKM matrix is predicted to be:

$$\text{CKM} \equiv U_L^\dagger V_L \approx \begin{pmatrix} 1 & \epsilon^{l_1 - l_2} & \epsilon^{l_1 - l_3} \\ \epsilon^{l_1 - l_2} & 1 & \epsilon^{l_2 - l_3} \\ \epsilon^{l_1 - l_3} & \epsilon^{l_2 - l_3} & 1 \end{pmatrix}, \tag{2.58}$$

where we have defined $\epsilon \equiv f/(\sqrt{2}\Lambda)$. One can see that this exactly matches (2.50) by identifying ϵ with λ and choosing the following charges for the left-handed quark doublets, see e.g. [16]:

$$\epsilon = \lambda \simeq 0.2 \quad \text{and} \quad (l_1, l_2, l_3) = (3 + l_3, 2 + l_3, l_3). \tag{2.59}$$

So far we have focussed only on the mass matrix arising from (2.53) by setting Φ to its vev. However, the complex scalar field carries another dynamical degree of freedom, $a(x)$, that enters as a phase:

$$\Phi = \frac{1}{\sqrt{2}}(\sigma(x) + f)e^{ia(x)/f}, \tag{2.60}$$

where $\sigma(x)$ is flavon excitation around the vev f. From (2.53) we see that even though it plays no role in the derivation of the flavor structure the field $a(x)$ does couple to SM fermions. Actually, one could decide to make a chiral transformation,

$$q_L^i \to e^{i\frac{a(x)}{f}l_i} q_L^i, \quad u_R^i \to e^{i\frac{a(x)}{f}r_i^u} u_R^i, \quad d_R^i \to e^{i\frac{a(x)}{f}r_i^d} d_R^i, \tag{2.61}$$

with the effect of introducing derivative interactions between $a(x)$ and a current made of SM fermions, together with a new contribution to the θ-term of QCD given by

$$\mathcal{L}_\theta = \left(\theta + \frac{N}{f}a(x)\right)\frac{\alpha_S}{8\pi}G\tilde{G}, \tag{2.62}$$

where the color anomaly, N, is here explicitly given by

$$N = \sum_i 2l_i - r_i^u - r_i^d. \tag{2.63}$$

The $U(1)_{\rm H}$ charges of the SM fermions are clearly flavor non-universal, as they reflect the flavor hierarchies in the SM. From what we have concluded in the previous section, off-diagonal couplings between $a(x)$ and the SM flavors will be generated. It is thus clear that $a(x)$ behaves exactly as a flavored axion with decay constant $f_a = f/N$, and $N \simeq 30$ for typical charge assignments. There is however one caveat: since the aim of the FN mechanism is not to solve the strong CP problem, one does not need to assume that $U(1)_{\rm H}$ is exact at the classical level. Consequently, $a(x)$ can receive a large mass by sources of explicit $U(1)_{\rm H}$ breaking other than the QCD anomaly. By making $a(x)$ heavy, the constrains of the previous section can be automatically avoided.

However, as first realized in [15,16], there is nothing preventing one to *identify* $U(1)_{\rm H}$ with $U(1)_{\rm PQ}$, thus solving several puzzles of the SM at the same time. We can also see that the PQ and the FN mechanism actually complement each other, as the angular degree of freedom that plays no role in the FN mechanism is now the axion that solves the strong CP problem, and the radial component of the PQ field that is usually simply ignored is now responsible for the flavor structure of the SM. We will thus refer to the complex field Φ in (2.60) as the "axiflavon".

An immediate implication of this is that $a(x)$ can obtain a non-vanishing mass through the QCD anomaly only, and axion constraints immediately apply. Therefore, the $U(1)_{\rm H}$ breaking scale f needs to be large enough for the axion to be "invisible", whereas the FN mechanism can be viable already for f in the multi-TeV region.

The identification of $U(1)_{\rm H}$ as the PQ symmetry allows to fix the axion couplings to the fermion current in (2.31). This prediction is accurate up to $\mathcal{O}(1)$ factors, as the FN charges for the SM fermions are not unique due to the $\mathcal{O}(1)$ arbitrariness of the λ_{ij} coefficients in (2.55). Choosing the charges as specified in [16] (implying $N = 26$), one finds that the coefficients controlling the relevant processes $K \to \pi a$ and $\mu \to e a$ are given by:

$$C_V^{ds} = \frac{1}{N} 5\,\epsilon \simeq 0.04 \tag{2.64}$$

and

$$C_V^{e\mu} = C_A^{e\mu} = \frac{\epsilon}{N} \simeq 0.008, \tag{2.65}$$

with ϵ fixed due to the Cabibbo angle, see below (2.58). As we can see, flavor-violating effects are only suppressed by the Cabibbo angle and are therefore sizable. Referring to (2.43) and (2.45), one finds

$$f_a|_{K\to\pi a} \gtrsim 1.4 \times 10^{10}\,\text{GeV}, \quad f_a|_{\mu\to e a} \gtrsim 2.2 \times 10^{7}\,\text{GeV}. \tag{2.66}$$

The strongest bound comes from kaon decay and translates to the following axion mass:

$$m_a < 500\ \mu\text{eV}, \tag{2.67}$$

which is not far from the natural window for the axion to constitute all the dark matter, see (2.27) and below.

The identification of the PQ with the FN charge also fixes the possible values of E/N. The electromagnetic anomaly is given in terms of the charges as

$$E = \sum_i \frac{4}{3}(l_i - r_i^u) + \frac{1}{3}(l_i - r_i^d) + L_i - e_i, \tag{2.68}$$

where L and e refer to the charges of left- and right-handed leptons, respectively. The charges can be related to the fermion masses up to $\mathcal{O}(1)$ factors as in (2.55). This leads to [15]:

$$\frac{E}{N} = \frac{8}{3} - 2\frac{\log\frac{\det m_d}{\det m_e} - \log\alpha_{de}}{\log\frac{\det m_u \det m_d}{v^6} - \log\alpha_{ud}}, \tag{2.69}$$

where α_{de} and α_{ud} contain the $\mathcal{O}(1)$ number uncertainties. Taking a flat distribution around $(1/3, 3)$ for α_{de} and α_{ud} one finds from (2.29) the 99.9% range

$$\frac{E}{N} \in (2.4, 3.0) \Rightarrow g_{a\gamma\gamma} \in (0.5, 1.1). \tag{2.70}$$

Therefore, we see that the axiflavon setup predicts a narrow band within the KSVZ/DSFZ standard window $(0.07, 7)$ in (2.30). The summary of the constraints and the predicted sensitivity of future experiments that can test the axiflavon setup is shown in Fig. 2.3. As we can see, the tightest constrain for $10^{-10}\,\text{eV} < m_a < 10^{-2}\,\text{eV}$ is given by flavor violation in the $K \to \pi a$ decay.

Let us conclude this section by noting that up to this point the Higgs and the axiflavon have been treated as independent objects. In the following, we will move to discuss a scenario in which all the scalar degrees of freedom are unified at high energies. As we shall see, this hypothesis bears relevant implications for the viable axiflavon parameter space.

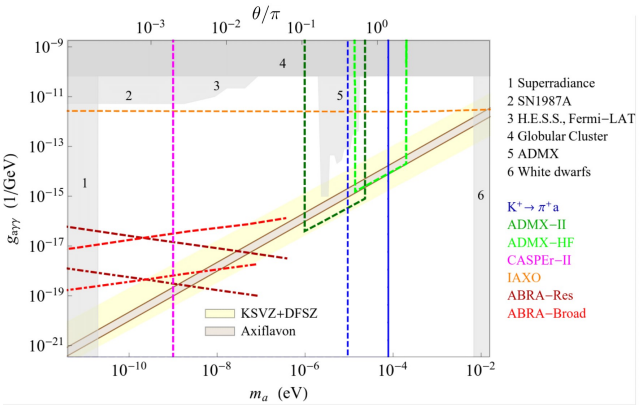

Figure 2.3: Summary of the constrains on the axiflavon parameter space. The axiflavon gray band lies within the KSVZ/DSFZ standard window. The flavor constraint from $K^+ \to \pi^+ a$ is found to be the most relevant for the range $m_a \in \left(10^{-10}, 10^{-2}\right)$ eV. Plot taken from [15].

2.5 Axiflavon-Higgs unification

We will present here a possible completion of the axiflavon effective theory in (2.53) which focusses on the non-trivial interplay between the scalar fields. In particular, we will entertain the possibility that the axiflavon and the Higgs share a common origin. This section is based on Ref. [I].

Let us recall that, because of the identification of the PQ symmetry with the $U(1)_{\rm H}$ charge, the $U(1)_{\rm H}$ symmetry breaking scale, f, needs to be well above the electroweak scale for the axiflavon model to be viable and solve the strong CP problem. Moreover, the FN mechanism requires the presence of new fermionic states (the FN messengers, ξ) to connect the opposite chiralities of the SM fermions as in Fig. 2.2, and the mass scale of the messengers has to be identified with the cutoff scale Λ in (2.53). Furthermore, for the effective theory to be consistent (and reproduce the CKM structure) the messengers need to be even heavier than f.

Driven by these considerations, we can ask ourselves what is the size of the corrections to the Higgs mass within this setup. Generically, we identify two possible sources: *(i)* tree-level corrections due to a portal interaction between the axiflavon field and the Higgs, $\lambda_{\rm P}\,(\Phi^*\Phi)(h^\dagger h)$; *(ii)* loop corrections due to the yukawa coupling of a FN messenger ξ to a SM fermion q via the Higgs, $y\,\bar{\xi}\,h\,q$. This gives the following estimante for $\delta\, m_h^2$:

$$\delta m_h^2 \simeq \lambda_{\rm P} f^2 + N_c \frac{y^2}{16\pi^2} m_\xi^2 \tag{2.71}$$

where the first contribution to δm_h^2 comes from the portal term after setting the flavon to its vev, and the second one is a simple one-loop diagram with q and ξ as internal lines. Note also that, as the purpose of the FN mechanism is to eliminate hierarchies among the fundamental parameters of the theory, the yukawa coupling y is $\mathcal{O}(1)$. Thus, by looking at (2.71), it is fair to say that whenever the FN mechanism is realized at a scale $f \gtrsim 10\,\text{TeV}$, the Higgs mass receives large corrections that need to be fine-tuned to reproduce its observed value. What we have just seen is a particular example of the Higgs hierarchy problem, namely the high sensitivity of the Higgs mass to UV scales in

the theory. Of course, fine-tuning does not represent an inconsistency of the theory, and one can take different approaches about it: for instance, the corrections to the Higgs mass discussed above can in fact be ignored as they can always be subtracted away with an adequate choice of the bare Higgs mass.

In this section, we will take a different perspective and concentrate on whether we can learn something from requiring the Higgs to remain light. The first observation is that after the $U(1)_{\rm H}$ symmetry breaking the radial component σ (the flavon) obtains a mass $m_\sigma \propto f$, whereas the axion mass behaves in the opposite way: $m_a \propto 1/f$. The reason for this is simply that the axion is a pseudo Nambu-Goldstone boson (pNGB): its mass is protected by a shift symmetry, $a \to a + \alpha f$, and must be proportional to the explicit breaking of such symmetry. In this case, this is given by non-perturbative QCD effects, and thus $m_a \sim m_\pi f_\pi / f_a$ making the axion naturally much lighter.

Following the same reasoning, one could then try realize the Higgs as pNGB as well in order to explain its apparent hierarchy with the flavon mass. This has the immediate advantage of removing all tree-level contributions to its potential thus setting the tree-level $\lambda_{\rm P}$ term in (2.71) equal to zero. However, the loop correction $\propto m_\xi^2$ in (2.71) is generically present, and its precise form depends on how the Higgs shift symmetry is broken. These loop contributions are actually needed in order to generate a non-vanishing Higgs potential in the first place. As its parameters are no longer free inputs but rather calculable quantities starting from the microscopic theory, one needs to make sure that the overall contribution to the potential can successfully trigger electroweak symmetry breaking. Of course, the natural size of the Higgs mass will still be $m_h^2 \propto f^2 \gg v^2$ so that fine-tuning is needed to generate the electroweak scale. However, the condition of reproducing the correct Higgs mass will narrow down the possible values of the Higgs quartic coupling and in turn the value of the scale f itself, as we shall see in Sec. 2.5.2. In this sense, we can say that the fine-tuning in this model will be traded for increased predictivity.

Before discussing our setup in detail, let us outline the relevant model-building steps that will be employed. According to the previous discussion, we will assume that the Higgs and the axiflavon field, Φ, containing the axion a and the flavon σ, actually originate from the same source, namely a common multiplet Σ. The axion and the Higgs are much lighter than σ because of their pNGB nature. In particular, the axion and the Higgs need to share the same decay constant f_a providing an explicit example of axion-Higgs unification [27]. Indeed, the vanishing of the Higgs quartic coupling in the SM around $\mu \sim 10^{11}\,\text{GeV}$ [6] can already hint for a pNGB nature of the Higgs. Moreover, the vicinity of this scale to the natural scale for the axion to be dark matter can be taken as a further clue for the unification.

As for the symmetry of the model, $\mathcal{G}$, the axion solution to the strong CP problem requires at least the presence of a $U(1)_{\rm H}$ global symmetry, whereas the pNGB Higgs requires $\mathcal{G}$ to contain also the full electroweak group:

$$G \supset U(1)_H \times SU(2)_L \times U(1)_Y. \tag{2.72}$$

The simplest choice for G is to keep the flavor symmetry $U(1)_{\rm H}$ as an abelian factor with respect to the electroweak group. Thus, we shall take $G = G' \times U(1)_{\rm H}$. The minimal choice for G' would be $SU(3) \times U(1)_X$ and the next-to-minimal $SO(5) \times U(1)_X$ [9], which is often employed in Composite Higgs models, as we shall see. The difference between

[9] The $U(1)_X$ factor is necessary to accommodate the hypercharge of up and down quarks.

these two constructions is that the former provides no custodial protection making it generically less favourable. However, this would not be a problem if the Higgs decay constant is much larger than the electroweak scale, as we are envisaging here. In any case, both groups result in a similar structure, and in the following we shall focus on $SO(5)$. This is also motivated by the attempt of lowering f_a by adopting a non-standard axion model, as we shall see in Sec. 2.5.3.

In practice, we will formulate the theory at the scale f as a linear σ-model for the field Σ realizing the global symmetry breaking pattern

$$[SO(5) \times U(1)_{\rm H}] \times U(1)_X \to SO(4) \times U(1)_X, \tag{2.73}$$

and the SM hypercharge, Y, is related to $SU(2)_R$ and $U(1)_X$ as $Y = T_R^3 + X$. The coset structure implies that there are five Nambu-Goldstone bosons, θ_i, in the spectrum that transform as

$$\theta_i \sim (\mathbf{2}, \mathbf{2}) \oplus \mathbf{1} \tag{2.74}$$

under $SO(4) \sim SU(2)_L \times SU(2)_R$. The bi-doublet in fact has the right quantum numbers to be identified with the Higgs, and the singlet is the axion. To generate a non-zero Higgs potential, the global $SO(5)$ has to be broken explicitly. This is realized by electroweak gauging and by yukawa interactions between the SM fermions, the FN messengers, and Σ that are introduced as a microscopic realization of the FN mechanism. In particular, the FN messengers are defined as full representations of $SO(5)$, and the actual breaking originates due to the presence of the SM fermions only. On the other hand, $U(1)_H$ needs to be exact at the classical level and only broken through anomalies to solve the strong CP problem.

Before moving to our model setup, let us note that this construction can also be seen as adding a flavor story to the recently proposed elementary-Goldstone-Higgs scenario [82, 83]. Including the axiflavon can in fact address fermion masses and mixings while providing a solution to the strong CP problem. This is a compelling renormalizable alternative to partial compositeness generating flavor hierarchies in composite-Higgs models that will be discussed in Chapter 4.

2.5.1 Model setup

We present here the explicit model setup. The symmetry-breaking pattern that leads to the unified realization of the Higgs doublet and the axion as pNGBs is the one in (2.73). This is obtained within a linear σ-model for the field Σ living in the fundamental representation **5** of $SO(5)$ with flavor charge $\mathrm{H}(\Sigma) = 1$ and null X charge. The renormalizable tree-level potential for Σ is

$$V(\Sigma) = \lambda_1 (\Sigma^\dagger \Sigma)^2 - \lambda_2 \, (\Sigma^T \Sigma) \, (\Sigma^\dagger \Sigma^*) - \mu^2 \Sigma^\dagger \Sigma \, . \tag{2.75}$$

The electroweak gauge group is embedded in $SO(5)$ by defining the $SU(2)_L \times SU(2)_R \cong SO(4)$ generators as detailed in Appendix A. The $SO(4)$-preserving minimum is given by

$$\langle \Sigma \rangle = (0, 0, 0, 0, f/\sqrt{2})^T, \tag{2.76}$$

with $\mu^2 = (\lambda_1 - \lambda_2) f^2$, and after the breaking, (2.73), the scalar degrees of freedom can be parametrized by angular and radial fields:

$$\Sigma = \, \exp[i(\sqrt{2} T^{\hat{a}} h^{\hat{a}} + a)/f] \begin{pmatrix} \widetilde{H} \\ \frac{1}{\sqrt{2}}(f + \sigma) \end{pmatrix} , \tag{2.77}$$

where $T^{\hat{a}}$ are the $SO(5)$ broken generators in the fundamental representation, $\hat{T}^{\hat{a}}\langle\Sigma\rangle \neq 0$, given in (A.2). As for the physical states, one finds a heavy Higgs doublet, $\widetilde{H}$, with mass $m^2_{\widetilde{H}} = 2\lambda_2 f^2$, and a heavy flavon, σ, with mass $m^2_\sigma = 2(\lambda_1 - \lambda_2)f^2$, while the SM-like Higgs doublet, $h^{\hat{a}}$, and the axion, a, are instead pNGBs and their masses vanish at the classical level [10]. The potential is bounded from below for $\lambda_1 > \lambda_2 \geq 0$.

Let us now move to the fermion sector. The FN messengers are denoted by ξ_j, where the subscript refers to the $U(1)_{\rm H}$ charge, $\mathrm{H}(\xi_j) = j$. As mentioned above, we will assume that all the ξ_j fields come as complete $SO(5)$ representations. Among the possible choices, we will commit to the spinorial representation $\mathbf{4}$, of $SO(5)$, because it turns out to be the best option in constructing the FN chain as in Fig. 2.2 [11]. Moreover, we shall take $X = 1/6$ for all the messengers, such that they can interact with the SM fermions, as we shall see. The ξ_j components read (suppressing the subscript j):

$$\xi = (\xi_+^{1/6},\, \xi_-^{1/6},\, \xi_0^{2/3},\, \xi_0^{-1/3})^T, \tag{2.78}$$

where $\pm$ refers to the $\pm\frac{1}{2}$ eigenvalues with respect to T^3_L, and zero means that those components are singlets under $SU(2)_L$. The superscripts instead indicate the weak hypercharge obtained as $Y = X + T^3_R$. The generators $T_{L,R}$ are given explicitly in (A.3) for the spinorial representation. Moreover, the ξs need to be vector-like under the full global symmetry G (namely, left- and right-handed components are in the same G representation) as their mass should not come from the flavon vev, but rather be slightly larger ($f/\sqrt{2}m_\xi \simeq 0.2$). Because of their vector-like nature, the FN messengers do not contribute to the $U(1)_{\rm H}$ anomaly which thus entirely depends on the chiral charges of the SM fermions.

The SM quarks, q^i_L, u^i_R, and d^i_R (with $i = 1, 2, 3$ a flavor index), in general do not fill complete $SO(5)$ representations, and their couplings to the FN messengers are a source of explicit $SO(5)$ breaking. The interactions between them are more easily written if the SM fermions are embedded as spurious Ψ^i_f multiplets in the spinorial representation with $X = 1/6$:

$$\Psi^i_{q_L} \equiv \Delta_L^T q^i_L = \begin{pmatrix} u^i_L \\ d^i_L \\ 0 \\ 0 \end{pmatrix}, \quad \Psi^i_{u_R} \equiv \Delta_u^T u^i_R = \begin{pmatrix} 0 \\ 0 \\ u^i_R \\ 0 \end{pmatrix}, \quad \Psi^i_{d_R} \equiv \Delta_d^T d^i_R = \begin{pmatrix} 0 \\ 0 \\ 0 \\ d^i_R \end{pmatrix}, \tag{2.79}$$

where

$$\Delta_L = \begin{pmatrix} 1 & 0 & 0 & 0 \\ 0 & 1 & 0 & 0 \end{pmatrix}, \quad \Delta_u = (0,0,1,0)\,, \quad \Delta_d = (0,0,0,1)\,. \tag{2.80}$$

Comparing with the quantum numbers of the components in (2.78), one can see that this choice reproduces the correct quark quantum numbers. The matrices $\Delta_{L,u,d}$ have mixed indices, namely the columns represent $SU(2)_L$ indices (doublet and singlet representation for Δ_L and $\Delta_{u,d}$, respectively), whereas the rows correspond to $SO(5)$ indices in the spinorial representation $\mathbf{4}$. The fact that the SM fermions come as incomplete $SO(5)$ representation is now clearly signaled by the null entries in (2.79).

[10] Notice that the point with $\lambda_2 = 0$ corresponds to a larger $SO(10)$ symmetry that is broken to $SO(9)$. In that case, the $\widetilde{H}$ doublet becomes a pNGB as well.

[11] The other possibility would be a mixture of fundamental and singlet representations.

The $U(1)_{\rm H}$ charge of each Ψ_f^i is chosen such that the correct pattern of masses and mixings is reproduced. The larger the charge difference between the left- and right-handed components of a given fermion, the more suppressed is the resulting mass. Notice that the Ψ-fields have to be considered only as $SO(5)$ spurions, while the $U(1)_{\rm H}$ needs to be exact at the Lagrangian level to solve the strong CP problem. For both the SM fermions and the FN messengers, the $U(1)_X$ charge is chosen to match the correct hypercharge, $Y = T_R^3 + X$, and will be omitted in the following.

We now have all the ingredients to write down the classical Lagrangian $\mathcal{L}$ of the system. It contains all the renormalizable interactions between Ψ_f^i, ξ_j, and Σ allowed by symmetries:

$$\begin{aligned} -\mathcal{L} =& V(\Sigma) + \sum_j m_j\, \bar{\xi}_j\, \xi_j + \left(a_j \bar{\xi}_{j+1}\, \Gamma^\alpha\, \Sigma_\alpha\, \xi_j + \text{h.c.}\right) \\ &+ \sum_{i,f} z_i^f\, \bar{\Psi}_f^i\, \Gamma^\alpha\, \Sigma_\alpha\, \xi_j + \tilde{z}_i^f\, \bar{\xi}_{j+2}\, \Gamma^\alpha\, \Sigma_\alpha\, \Psi_f^i + \text{h.c.} \\ &+ x\, \bar{\Psi}_{q_L}^3\, \Gamma^\alpha\, \Sigma_\alpha\, \Psi_{u_R}^3 + \text{h.c.} \end{aligned} \tag{2.81}$$

The first line in (2.81) describes the SO(5)-symmetric sector, namely the scalar potential in (2.75), the vector-like masses for the FN messengers m_j, and yukawa couplings between the latter and Σ which represent the inner links of the FN chain in Fig. 2.2. The matrices Γ^α connect the spinorial representation with the fundamental representation and are given explicitly in (A.5). They are defined such that the combination $\bar{\xi}_{j+1}\, \Gamma^\alpha \xi_j$ transforms as the fundamental **5** that is eventually contracted with Σ_α to make an $SO(5)$ invariant.

The second line in (2.81) consists of yukawa couplings involving the SM fermions and the FN messengers, where $f = q_L, u_R, d_R$, and the index j selects the ξ field that makes each term $U(1)_{\rm H}$ invariant, $j \equiv j(f,i) = H(f^i) - 1$. Notice that the use of the spinorial representation is particularly suitable for the purpose of building the FN chain, as both ξ-fields appear symmetrically in the yukawa coupling, and thus only a single species of FN messengers is needed, see footnote 11.

Finally, the third line accounts for the fact that the top mass features no FN suppression— namely, the top yukawa is already $\mathcal{O}(1)$— and thus a direct coupling of t_L and t_R via the Σ-field must be allowed.

Due to the presence of the spurions Ψ_f, the last two lines of (2.81) break the $SO(5)$ symmetry explicitly, and a potential for the Higgs is generated at the loop level. Before presenting the computation of the Higgs potential, let us discuss a simple example to show how the FN mechanism is explicitly realized in our setup.

Mass hierarchies from broken $U(1)_{\rm H}$

To see how the FN mechanism works in our setup, let us consider the mixing between the (left-handed) top t_L and the (right-handed) charm quark c_R. This mixing will eventually contribute to the CKM matrix. In our notation, t_L and c_R are found in the $\Psi_{q_L}^3$ and $\Psi_{u_R}^2$ multiplets, respectively, as given in (2.79). Their flavor charges are fixed in order to reproduce the observed flavor structure as

$$\text{H}(q_L^3) = 1 \quad \text{and} \quad \text{H}(u_R^2) = 4. \tag{2.82}$$

For these fields to communicate, we need to include at least two messengers with H charge 2 and 3, $\xi_{2,3}$. We can then pick the relevant terms coming from the first and second line of (2.81):

$$-\mathcal{L} \supset \left(a_2\,\bar{\xi}_3\,\Sigma'\,\xi_2 + z\,\bar{\Psi}^2_{u_R}\Sigma'\,\xi_3 + \tilde{z}\,\bar{\xi}_2\,\Sigma'\,\Psi^3_{q_L} + \text{h.c.}\right) + m\left(\bar{\xi}_2\xi_2 + \bar{\xi}_3\xi_3\right), \tag{2.83}$$

where we have defined Σ' to include the Γ^α matrices, $\Sigma' \equiv \Gamma^\alpha\,\Sigma_\alpha$. The dimensionless couplings z and $\tilde{z}$ are assumed to be $\mathcal{O}(1)$. Moreover, we have taken the masses for ξ_2 and ξ_3 to be the same for simplicity, $m_2 = m_3 = m$. By integrating out ξ_2 and ξ_3 on the classical equations of motion, one finds an effective Lagrangian, $\mathcal{L}_{\text{eff}}$, which at the leading order in $1/m$ reads

$$\mathcal{L}_{\text{eff}} = -z\,\tilde{z}\,a_2\,\frac{1}{m^2}\bar{\Psi}^2_{u_R}\Sigma'\Sigma'\Sigma'\Psi^3_{q_L} + \text{h.c.} \tag{2.84}$$

As we can see, the effective operator shows three powers of Σ', which is in fact the $4-1$ flavor-charge difference corresponding to (2.82). Notice that for the more minimal chain between two light fermions that differ only by $\Delta H = 2$ units of flavor charge, the corresponding effective Lagrangian would be

$$\mathcal{L}_{\text{eff}} \propto \bar{\Psi}^3_{q_L}\Sigma'\Sigma'\Psi^2_{u_R} = \bar{q}^3_L\Delta_L\Sigma'\Sigma'\Delta_u^T\,u^2_R \equiv 0 \tag{2.85}$$

due to $\Sigma_\alpha\Sigma_\beta\Gamma^\alpha\Gamma^\beta = \Sigma^\alpha\Sigma_\alpha\,\mathbb{1}$, and $\Delta_L\Delta_u^T = 0$.

Below the symmetry-breaking scale, one can also integrate out the flavon and the second Higgs doublet, as their mass is $\propto f$. Thus, the Σ-field can be written as

$$\Sigma = \frac{f}{\sqrt{2}}\,e^{ia/f}\left(0,\,0,\,\sin\frac{h}{f},\,0,\,\cos\frac{h}{f}\right)^T, \tag{2.86}$$

where we have chosen the unitary gauge to get rid of the NG modes that will be eaten by the W and the Z bosons, so that h represents the physical Higgs field, and a is the axion. Using (2.86), we can single out the contribution to the mass matrix in (2.84):

$$\mathcal{L}_{\text{eff}} \supset -\frac{1}{\sqrt{2}}m_{32}\,\bar{c}_R\,t_L + \text{h.c.}, \quad m_{32} = z\,\tilde{z}\,a_2\frac{f^2}{2m^2}f\sin(\langle h\rangle/f) + \ldots \tag{2.87}$$

where $f\,\sin(\langle h\rangle/f) \equiv v = 246\,\text{GeV}$ is to be identified with the electroweak scale and the dots stand for higher orders in $f^2/2m^2$. Defining $\delta_{ij} \equiv \text{H}(q^i_L) - \text{H}(q^j_R)$, we see that the suppression with respect to the top mass is

$$\frac{m_{32}}{m_t} \simeq \left(\frac{f}{\sqrt{2}m}\right)^{|\delta_{32}|-1}, \tag{2.88}$$

with $\delta_{32} = 3$ in the present case. The addtional -1 in the exponent, which is not present in the usual FN setup, compensates for the Higgs carrying one unit of flavor charge, since it is unified in the Σ-field. One can show that this result holds in general for odd $|\delta_{ij}|$, while for even $|\delta_{ij}|$ the corresponding term vanishes due to the properties of the Γ matrices, see (2.85). We thus conclude that a general entry in the fermion mass matrix, m_{ij}, corresponding to a charge difference of $|\delta_{ij}|$ is suppressed with respect to the top mass by

$$\frac{m_{ij}}{m_t} \simeq \left(\frac{f^2}{2m^2}\right)^{\frac{|\delta_{ij}|-1}{2}}, \quad |\delta_{ij}|\ \text{odd}\,. \tag{2.89}$$

Eq. (2.89) shows that $f^2/(2m^2) \equiv \epsilon$ is the smallest building block we can use to reproduce the flavor hierarchies, and therefore we identify $\epsilon \simeq 0.2$ with the sine of the Cabibbo angle.

2.5.2 Successful matching

We compute here the Higgs potential generated by the interaction with the top quark and the FN messengers which directly couple to it and can be used to connect its opposite chiralities, t_L and t_R. Subleading contributions will be discussed at the end of this section. A charge assignment that is compatible with the top mass must satisfy $|\delta_{33}| \equiv |\mathrm{H}(q_L^3) - \mathrm{H}(u_R^3)| = 1$ [12], and we take $\mathrm{H}(q_\mathrm{L}^3) = 1$ and $\mathrm{H}(u_\mathrm{R}^3) = 2$. Referring to (2.81), this corresponds to the following terms

$$\begin{aligned} -\mathcal{L} \supset & \left(a_0 e^{i\alpha} \bar{\xi}_1 \Sigma' \xi_0 + \text{h.c.}\right) + m(\bar{\xi}_0 \xi_0 + \bar{\xi}_1 \xi_1) \\ & + \left(x e^{i\zeta} \bar{\Psi}^3_{q_L} \Sigma' \Psi^3_{u_R} + z_\mathrm{L} e^{i\zeta_\mathrm{L}} \bar{\Psi}^3_{q_L} \Sigma' \xi_0 + z_\mathrm{R} e^{i\zeta_\mathrm{R}} \bar{\Psi}^3_{u_R} \Sigma' \xi_1 + \text{h.c.}\right) , \end{aligned} \tag{2.90}$$

where we have defined $z_\mathrm{L} \equiv z_3^{q_\mathrm{L}}$, $z_\mathrm{R} \equiv z_3^{u_\mathrm{R}}$, and potential phases have been pulled out into $\zeta_{\mathrm{L,R}}$. Note that we are here assuming mass degeneracy for the messenger fields, $m_0 = m_1 = m$ and we are neglecting interactions involving other FN messengers, as for instance ξ_2 and ξ_3 in (2.83), which will give a subleading contribution.

Let us first compute the top mass according to (2.90) in the background of h. This can be done by solving the characteristic polynomial for the fermion mass matrix, or alternatively by integrating out the heavy fields at tree level. The expression for m_t is obtained as an expansion in $f^2/2m^2 = \epsilon$ and h/f as

$$m_t^2(h) = \frac{1}{2}\left(\alpha_0 - \alpha_1\epsilon - \alpha_2\epsilon^2\right) f^2 \sin^2(h/f) - \frac{1}{2}\beta\,\epsilon^2 f^2 \sin^4(h/f) + \text{h.o.}, \tag{2.91}$$

where h.o. stands for higher-order terms in $f^2/2m^2$ and $(h/f)^n$ terms with $n \geq 6$, and

$$\begin{aligned} \alpha_0 &= x^2, \\ \alpha_1 &= x^2\left(z_\mathrm{L}^2 + z_\mathrm{R}^2\right) - 2\,x\,z_\mathrm{L}\,z_\mathrm{R}\,a_0 \cos\Omega, \\ \alpha_2 &= -x^2\left(z_\mathrm{L}^4 + z_\mathrm{L}^2 z_\mathrm{R}^2 + z_\mathrm{R}^4\right) + a_0^2\left(3x^2 z_\mathrm{L}^2 + z_\mathrm{R}^2(3x^2 - z_\mathrm{L}^2)\right) \\ &\quad - 2a_0 x z_\mathrm{L} z_\mathrm{R}\left(a_0^2 - z_\mathrm{L}^2 - z_\mathrm{R}^2\right)\cos\Omega, \\ \beta &= x^4\left(z_\mathrm{L}^2 + z_\mathrm{R}^2\right) - 6x^3\,z_\mathrm{L}\,z_\mathrm{R}\,a_0\cos\Omega, \end{aligned} \tag{2.92}$$

with $\Omega \equiv \alpha - \zeta_\mathrm{L} + \zeta - \zeta_\mathrm{R}$. The expression of Eq. (2.91) needs to coincide with the SM result, $m_t^2 = \frac{1}{2}y_t^2 v^2$ implying $x \simeq y_t$ and $f^2 \sin^2(\langle h\rangle^2/f^2) = v^2$ at the leading order.

Our strategy for the Higgs potential is to calculate it in the UV theory specified by (2.81), whose leading contribution is given by (2.90), and match it with the Higgs potential in the SM extrapolated at the scale $m \gtrsim f$ where the new particles appear. By doing so, we shall keep m as a free parameter, which will in fact be fixed by the condition of a successful matching.

In the axiflavon-Higgs (AFH) picture, the Higgs potential arises at one-loop and it is given in terms of the field-dependent masses of the physical eigenstates, namely the

[12] This differs from the usual FN mechanism, where $\delta_{33} = 0$, as the Higgs carries here unit flavor charge.

SM particles and the FN messengers. Considering the top sector in (2.90), the standard Coleman-Weinberg formula [84] yields at one-loop:

$$V^{(1)}_{\rm AFH} = -\frac{N_c}{16\pi^2}\left\{ m_t^4(h)\left(\log\frac{m_t^2(h)}{m^2}-\frac{3}{2}\right)+\sum_j m^4_{\xi_j}(h)\left(\log\frac{m^2_{\xi_j}(h)}{m^2}-\frac{3}{2}\right)\right\}. \quad (2.93)$$

Notice that the sum over j involves all the components included in ξ_0 and ξ_1, see (2.78), namely eight states in total.

In the SM alone, the effective potential for the Higgs includes tree-level plus radiative corrections. Keeping only the contribution from the top quark, the potential reads:

$$V^{(1)}_{\rm SM} = \frac{1}{4}\lambda(m)h^4-\frac{1}{2}\mu^2(m)h^2-\frac{N_c}{16\pi^2}m_t^4(h)\left(\log\frac{m_t^2(h)}{m^2}-\frac{3}{2}\right). \quad (2.94)$$

Notice that both effective potentials are evaluated at the scale $m\approx f$ corresponding to the threshold of the new states. Then, by requiring

$$V^{(1)}_{\rm SM} = V^{(1)}_{\rm AFH}, \quad (2.95)$$

we obtain

$$V\equiv\frac{1}{4}\lambda(m)h^4-\frac{1}{2}\mu^2(m)h^2=-\frac{N_c}{16\pi^2}\sum_j m^4_{\xi_j}(h)\left(\log\frac{m^2_{\xi_j}(h)}{m^2}-\frac{3}{2}\right). \quad (2.96)$$

Notice that the contribution from the top eigenstate appears on both side of Eq. (2.95), and therefore it cancels. Such cancellation takes care of the large logarithm arising from the hierarchy between the electroweak and the flavon scale. We expect this behavior to persist beyond the one-loop level, given that the pure SM contribution always appears on both sides, so that Eq. (2.96) gives the leading-order matching condition.

The RHS of (2.96) can be computed as an expansion in $f^2/2m^2=\epsilon$. To this end, we parametrize the field-dependent FN masses as

$$m^2_{\xi_j}(h) = m^2+f_j(h), \quad (2.97)$$

where $f_j(h)\sim f\times m$. By expanding the logarithm, we find that

$$V=-\frac{N_c}{16\pi^2}\sum_j\left[-2f_j(h)m^2+\frac{f_j^3(h)}{3m^2}-\frac{f_j^4(h)}{12m^4}+\frac{f_j^5(h)}{30m^6}-\frac{f_j^6(h)}{60m^8}+\text{h.o.}\right], \quad (2.98)$$

where we dropped a constant term. The computation of $F_n=\sum_j f_j^n(h)$, $n=1,\dots,6$, can be done recursively as

$$\begin{aligned} F_1 &= \sum_j f_j(h) = \mathrm{Tr}\left[m^\dagger(h)m(h)\right]-m_t^2(h),\\ F_2 &= \sum_j f_j^2(h) = \mathrm{Tr}\left[\left(m^\dagger(h)m(h)\right)^2\right]-2F_1m^2-m_t^4(h), \end{aligned} \quad (2.99)$$

and so on. By $m(h)$, we indicate the field dependent mass matrix for the fermionic fields. By direct inspection, the terms F_5 and F_6 turn out to be higher order. We eventually find for the RHS of (2.96):

$$V=\frac{N_c}{32\pi^2}f^4\left[(\gamma_0+\gamma_1\epsilon)\,\sin^2(h/f)+\delta\,\epsilon\sin^4(h/f)\right] \quad (2.100)$$

where it turns out that γ_0 and δ are related to α_1 and β in (2.92) as $\gamma_0 = \alpha_1$, $\delta = \beta$, and

$$\gamma_1 = \frac{1}{3}\left(-3x^2\left(z_{\rm L}^4 + z_{\rm L}^2 z_{\rm R}^2 + z_{\rm R}^4\right) + a_0^2\left(3x^2 z_{\rm L}^2 + z_{\rm R}^2\left(3x^2 - z_{\rm L}^2\right)\right) + 2a_0^3 z_{\rm L} x z_{\rm R}\cos\Omega\right). \tag{2.101}$$

Expanding the trigonometric functions and focussing on the term $\propto h^2$, we see that the matching requires

$$-\frac{1}{2}\mu^2(m)h^2 \stackrel{!}{=} \frac{N_c}{32\pi^2} f^2\left(\gamma_0 + \gamma_1\epsilon\right)h^2\,. \tag{2.102}$$

The relation above makes the tuning in the model explicit: the natural value of μ^2 is not much below the scale f^2. However, the Higgs mass turned out to be at the electroweak scale and we here remain agnostic about the actual reason behind the cancellation on the RHS of (2.102) that makes it $\ll f^2$. Rather, we investigate the physical implications of this fact regarding the consequent possible values of the Higgs quartic coupling. According to our expansion in ϵ, reproducing the correct value of the Higgs mass requires γ_0 and γ_1 to be both $\gamma_{0,1} \ll 1$. The matching for h^4 is then driven only by the $\sin^4(h/f)$ term in (2.100), which implies

$$\frac{1}{4}\lambda(m)h^4 \stackrel{!}{=} \frac{N_c}{32\pi^2}\delta\,\epsilon\,h^4. \tag{2.103}$$

Moreover, the condition $\gamma_0 = \alpha_1 \ll 1$ gives, with reference to (2.92),

$$x^2(z_{\rm L}^2 + z_{\rm R}^2) \simeq 2x z_{\rm L} z_{\rm R} a_0\cos\Omega \quad \Rightarrow \quad \delta \simeq -2x^4(z_{\rm L}^2 + z_{\rm R}^2), \tag{2.104}$$

which finally yields for $\lambda(m)$:

$$\lambda(m) = -\frac{N_c}{4\pi^2}x^4(z_{\rm L}^2 + z_{\rm R}^2)\,\epsilon < 0. \tag{2.105}$$

Now, since the running Higgs quartic coupling $\lambda(m)$ is entirely predicted in the SM below the threshold of the new states, the relation above can be used to determine the scale m at which a successful matching is achieved. What is interesting about (2.105) is that the sign on λ is predicted to be negative. Interestingly, this happens in the SM at around the scale $\mu \simeq 10^{11}$ GeV [6], which is indeed the right order of magnitude for the axion decay constant to make the axion dark matter. This observation was already made in Ref. [27] in the context of realizing the Higgs and the axion as composite pNGBs. Here, we find it arising again in a concrete incarnation of axion-Higgs unification in the context of a renormalizable model.

In order to quantitatively tell at which scale the matching is possible, we recall that the goal of the FN mechanism is to construct a model where there is no hierarchy among the fundamental parameters. Since we know from (2.91) that $x \simeq y_t(m)$, the top yukawa at the scale m fixes the overall magnitude of the other couplings. Thus, Eq. (2.105) can be rewritten as ($N_c = 3$)

$$\lambda(m) = -\frac{3}{2\pi^2}y_t^6(m)(1+\bar{\delta})^6\,\epsilon, \tag{2.106}$$

where we have parametrized an average yukawa coupling as $y_t(m)(1+\bar{\delta})$. In Fig. 2.4 we show the SM running of $\lambda(m)$ in red (the band takes into account the uncertainty in

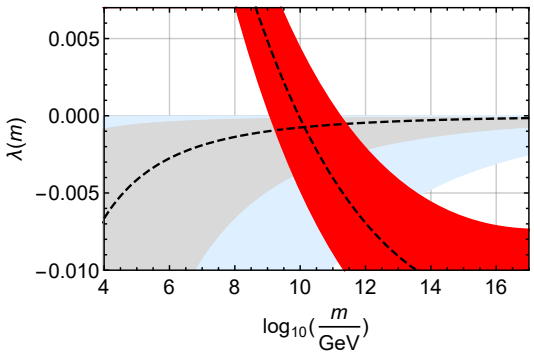

Figure 2.4: Matching of the Higgs quartic coupling at the scale m in the SM (red band) with the prediction of (2.106), considering a yukawa coupling spread of $\bar{\delta} = \pm 0.6$ (light blue band), $\bar{\delta} = \pm 0.3$ (light gray band), and $\bar{\delta} = 0$ (dashed black line). The intersection corresponds to the allowed range for m. See text for details.

the initial conditions) and the RHS of (2.106) for $\bar{\delta} = \pm 0.6$ (light blue band), $\bar{\delta} = \pm 0.3$ (light gray band), and $\bar{\delta} = 0$ (dashed black line). The matching is possible only for negative values of $\lambda(m)$, which selects $10^9\,\text{GeV} \lesssim m \lesssim 10^{14}\,\text{GeV}$. By recalling $\epsilon \simeq 0.2$, we conclude that

$$7 \times 10^8\,\text{GeV} \lesssim f \lesssim 7 \times 10^{13}\,\text{GeV}. \tag{2.107}$$

Since the flavon expectation value, f, is related to the axion decay constant by $f_a = f/N$,

$$N = \sum_{i=1}^{3} 2\text{H}(\Psi^i_{q_L}) - \text{H}(\Psi^i_{u_R}) - \text{H}(\Psi^i_{d_R}) \approx 50, \tag{2.108}$$

the previous bound yields

$$10^7\,\text{GeV} \lesssim f_a \lesssim 10^{12}\,\text{GeV}. \tag{2.109}$$

Notice that the color anomaly N is double the one used above (2.64) because of the peculiarity of our setup discussed in (2.89), which generically requires double charge differences.

It is useful to confront this region with constraints following from the flavor-violating couplings of the axiflavon. Taking into account the bound from the kaon decay $K^+ \to \pi^+ a$ as in Ref. [15], one finds a relatively thin stripe [13] of

$$f_a \approx (10^{11} - 10^{12})\,\text{GeV}. \tag{2.110}$$

Interestingly, this range will almost entirely be tested by the NA62 experiment, as discussed below (2.41).

Before moving to the next section, let us discuss the contribution from states other than the ones from the "top sector" in (2.90). As for the SM gauge bosons, their contribution equally appears on both sides of Eq. (2.95) and thus do not alter the one-loop matching condition; the same reasoning applies to the other SM eigenstates. However,

[13] Note that the axion couplings to fermions differ by approximately a factor of two with respect to the axiflavon case of [15], which is however cancelled to good approximation by a similar factor entering Eq. (2.108).

an additional contribution is expected when the FN messengers mixing with the light fermions are included. We have calculated this for the FN messengers related to the charm quark as in (2.83). Their contribution to the Higgs potential is found to be $\mathcal{O}(\epsilon)$ for the $\sin^2(h/f)$ and $\mathcal{O}(\epsilon^2)$ for the $\sin^4(h/f)$ term, which is subleading compared to the top sector contribution, $\mathcal{O}(\epsilon^0)$ and $\mathcal{O}(\epsilon^1)$, respectively. This confirms the intuitition that lighter quarks give a subdominant contribution to the Higgs potential.

In the SM, this easily follows from the fact that lighter quarks have a smaller direct yukawa to the Higgs, and thus contribute less to the effective potential. In the axiflavon-Higgs setup, however, all fundamental yukawas are actually $\mathcal{O}(1)$. Nonetheless, the top quark is still the only one featuring a direct coupling to the Higgs, see the last line of (2.81), and this term is also the only one where two spurions appear at the same time. Hence, interacting with the top is more efficient in transmitting the $SO(5)$ explicit breaking, explaining why the leading contribution is found from (2.90).

2.5.3 Including right-handed neutrinos

So far we have mainly focussed on the quark sector, as the leading contribution to the Higgs potential arises from it as long as the particle content of the SM is concerned. However, the picture can actually change if right-handed neutrinos (RHNs) are included in the game. In fact, the FN mechanism is quite efficient in explaining the hierarchies in the quark sector in terms of an ϵ^n suppression, where n is the difference of flavor charges. For neutrinos, however, much larger charge differences would be needed to explain sub-eV states. Thus, a more natural option is to combine the FN mechanism with the standard Type I seesaw [85–90]:

$$M = \begin{pmatrix} 0 & m_D \\ m_D & M \end{pmatrix}, \tag{2.111}$$

where m_D is the Dirac mass connecting lefth-handed and right-handed neutrinos, that will feature the usual FN suppression, and M is the Majorana mass for the RHNs. Such Majorana mass is usually associated with some heavy new-physics scale; it is then natural to connect it to the scale f in our setup, as we shall see shortly.

Starting with a single-family example, we shall consider the left-handed lepton doublet l_L and the RHN N_R coming as $SO(5)$ spurions in the spinorial $\mathbf{4}$ of SO(5), similarly to what we have assumed for the quarks in (2.79):

$$\Psi_L = \Delta_{\rm L}^T l_L, \quad \Psi_N = \Delta_u^T N_R. \tag{2.112}$$

The Type I seesaw explains the lightness of the left-handed neutrino due to a large mass scale associated with the right-handed counterpart. In our model, such mass scale can be naturally interpreted as the flavon vev f. We will then assume that the RHNs have charge $\mathrm{H}(\Psi_N) = 1/2$, so that their mass is generated dynamically from Σ through the following term:

$$-\mathcal{L}_N = \frac{1}{\sqrt{2}} y_N \bar{\Psi}_N \Sigma' \mathcal{C} \bar{\Psi}_N^T + \text{h.c.} = -\frac{1}{2} y_N f \cos(h/f) \bar{N}_{\rm R} \mathcal{C} \bar{N}_{\rm R}^T e^{ia/f} + \text{h.c.}, \tag{2.113}$$

which yields a Majorana mass

$$m_{N_{\rm R}}^2(h) = y_N^2 f^2 \cos^2(h/f). \tag{2.114}$$

The Dirac mass term, m_D, is obtained by integrating out the FN chain as usual. The actual size of m_D thus depends on the charge difference of right- and left-handed neutrinos, $\delta_\nu = \mathrm{H}(l_L) - \mathrm{H}(N_R)$:

$$m_{\mathrm{D}} \sim m_t \epsilon^{\frac{|\delta_\nu|-1}{2}}. \tag{2.115}$$

The light neutrino mass, m_ν, is then given by

$$m_\nu \sim m_t \frac{m_t}{m_{N_{\mathrm{R}}}} \epsilon^{|\delta_\nu|-1}, \tag{2.116}$$

which shows a double suppresion originating from the type-I seesaw and from the FN mechanism, as mentioned above.

Let us now discuss the impact of (2.113) to the Higgs potential. First, the term in (2.113) features a similarity with the yukawa interaction between the top quark and Σ— third line of (2.81)— as two spurions (Ψ_N in this case) are directly connected with the Higgs. This already tells us that the RH neutrinos will contribute sizeably to the Higgs potential. Moreover, RHNs are absent in the SM, and therefore their contribution will not cancel in the matching condition (2.95).

Let us then rederive the matching condition in case RHNs are included. The strategy is the same of the previous section: calculating the effective potential in the AFH setup and investigate at which scale it can be matched with the SM effective potential. The contribution from the top sector is unchanged by the presence of RHNs. We thus focus on the additional part due to the RHNs, $\Delta V^{(1)}_{\mathrm{AFH}}$, given by:

$$\begin{aligned}
\Delta V^{(1)}_{\mathrm{AFH}} &= -\frac{2}{64\pi^2} m^4_{N_R}(h) \left(\log \frac{m^2_{N_R}(h)}{m^2} - \frac{3}{2} \right) \\
&= -\frac{1}{32\pi^2} y_N^4 f^4 \cos^4(h/f) \left[\log\left(y_N^2 \frac{f^2}{m^2} \right) + \log\left(1 - \sin(h/f)^2\right) - \frac{3}{2} \right] \\
&\simeq -\frac{1}{32\pi^2} y_N^4 f^4 \left[2\left(1 + \log\frac{1}{\tilde{\epsilon}}\right) \sin^2(h/f) - \log\frac{1}{\tilde{\epsilon}} \sin^4(h/f) \right],
\end{aligned} \tag{2.117}$$

where we have defined $\tilde{\epsilon} \equiv (y_N f/m)^2$. The matching conditions in (2.102) and (2.103) are modified as:

$$-\frac{1}{2}\mu^2(m)h^2 \stackrel{!}{=} -\frac{f^2}{32\pi^2}\left[2y_N^4 \left(1 + \log\frac{1}{\tilde{\epsilon}}\right) - N_c\gamma_0 - N_c\gamma_1\epsilon \right] h^2, \tag{2.118}$$

and

$$\frac{1}{4}\lambda(m)h^4 \stackrel{!}{=} \frac{1}{32\pi^2}\left[\log\frac{1}{\tilde{\epsilon}}\, y_N^4 + N_c\,\delta\,\epsilon \right] h^4. \tag{2.119}$$

At the leading order in ϵ, the new condition for $\mu^2(m)$ gives

$$2y_N^4(1 + \log 1/\tilde{\epsilon}) - N_c\gamma_0 \ll 1, \tag{2.120}$$

which implies that a cancellation between the lepton and quark sector must occur to keep the Higgs light.

As for the quartic $\lambda(m)$, we see that the leading order is now driven by the contribution from the RHNs. This is because the direct contribution from the top quark

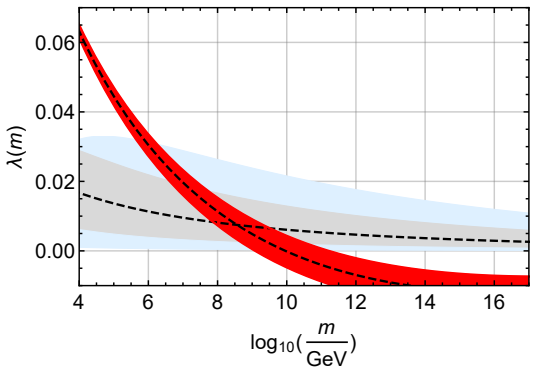

Figure 2.5: Matching of the Higgs quartic coupling at the scale m in the SM (red band) with the prediction of (2.121), considering a yukawa spread of $\bar{\delta} = \pm 0.6$ (light blue band), $\bar{\delta} = \pm 0.3$ (light gray band), and $\bar{\delta} = 0$ (dashed black line). The intersection corresponds to the allowed range for m. See text for details.

cancels in the matching condition, whereas this is not the case for RH neutrinos. Assuming three almost degenerate RH neutrinos, with a typical coupling y_N parametrized as $y_N = (1+\bar{\delta})y_t$, Eq. (2.119) becomes

$$\lambda(m) = \frac{3}{8\pi^2} \log\left(\frac{1}{2y_t^2(m)(1+\bar{\delta})^2\epsilon}\right)(1+\bar{\delta})^4 y_t^4(m) > 0. \tag{2.121}$$

In Fig. 2.5 we show the SM running of $\lambda(m)$ in red and the RHS of (2.121) for $\bar{\delta} = \pm 0.6$ (light blue band), $\bar{\delta} = \pm 0.3$ (light gray band) and $\bar{\delta} = 0$ (dashed black line). The matching is now possible for smaller values of m with respect to the case without RH neutrinos, because the RHS of (2.121) is positive. The allowed region for f is:

$$3 \times 10^5\,\text{GeV} \lesssim f \lesssim 10^{11}\text{GeV}. \tag{2.122}$$

Furthermore, since $m_{N_R} \simeq y_N f$ with $y_N \approx 1$, Eq. (2.122) also sets the range of the RH neutrino masses. Eventually, we find:

$$6 \times 10^3\,\text{GeV} \lesssim f_a \lesssim 2 \times 10^9\,\text{GeV}\,. \tag{2.123}$$

One can immediately see that, when comparing with the limits coming from the non-observation of $K \to \pi a$, such low values of f_a as in (2.123) are already excluded. This is then a good opportunity to revisit the assumptions behind these flavor bounds. For the QCD axion, the mass is in one-to-one correspondence with f_a, yielding meV mass for $f_a \approx 10^{10}\,\text{GeV}$. Thus, the kaon decay proceeds on-shell as $m_K > m_\pi$ and the axion is practically massless. However, if the axion mass and the decay constant could be disentangled, low-f_a models could become viable by pushing the axion mass at the GeV or even TeV scale, in order to kinematically forbid the kaon decay. In this case, astrophysical bounds are also automatically evaded (recall that the bounds in Sec. 2.3 could apply only for a light axion) and the axion becomes visible at the LHC, as for instance $a \to \gamma\gamma$ decays could be detectable. Concrete examples of this have been recently presented in Refs [91, 92]. As a drawback, the axion can no longer be dark matter because it is not stable on cosmological scales; nevertheless, it still solves the strong CP problem.

Although we are not attempting to construct a concrete model, it is worth mentioning that a heavy axion would be compatible with the AFH setup including right-handed neutrinos with f_a as low as $f_a \sim 5\,\text{TeV}$. This would provide an axion that is potentially detectable at the LHC, and largely reduce the fine-tuning related to the Higgs mass.

2.6 Summary

In this chapter, we have discussed the strong CP problem as a serious fine-tuning issue of the SM, as the topological term from the QCD θ-vacuum and the electroweak sector need to cancel at $\mathcal{O}\left(10^{-10}\right)$ accuracy to comply with current bounds on CP violation. Among the possible solutions to this puzzle, the axion is certainly one of the most intriguing possibilities as it can simultaneously explain dark matter and provide several interesting signatures one can look for.

When considering the ways the axion can communicate with the SM particles, it turns out that flavor-violating couplings are generically possible, and can be constrained (or discovered) very efficiently by future experiments. Flavored axions, however, contain a certain degree of model dependence. A very predicted and motivated scenario is found by identifying the $U(1)_{\text{PQ}}$ as the simplest flavor symmetry that addresses the flavor puzzle in the SM, namely the $U(1)_{\text{H}}$ of the Froggatt-Nielsen mechanism. These two approaches interestingly complement each other by giving a purpose to both the degrees of freedom, a (the axion) and σ (the flavon), within the complex field Φ, which is referred to as the axiflavon— see (2.60) and below. The axion couplings to the SM fermions are fixed by the observed pattern of masses and mixings in the SM: the model thus predicts a sizable contribution to flavor-violating axion couplings, in particular for the $d \to s$ transition that is only suppressed by the sine of the Cabibbo angle, $\sin\theta_C \simeq 0.2$.

In Sec. 2.5 we took a further step and analyzed a scenario in which the axiflavon and the Higgs, which were previously considered as independent fields, are unified at high energies within a common multiplet Σ [I]. Both the Higgs and the axion are then realized as pseudo Nambu-Goldstone bosons to explain their lightness with respect to the flavon. The main consequence is that the Higgs potential is generated dynamically by loops involving the SM fermions and the Froggatt-Nielsen messengers, that are explicitly introduced as a microscopic realization of the Froggatt-Nielsen mechanism. Electroweak symmetry breaking is thereby connected with the origin of the SM-fermion mass hierarchies. Taking this into account narrows down the possible values that the axion/Higgs decay constant can take, leaving only a small strip after flavor constrains are applied, $f_a \approx (10^{11}, 10^{12})$ GeV, which is visualized in Fig. 2.6. Interestingly, this region is a prime target of future axion searches by NA62 and ADMX [93, 94].

Such sharp prediction for f_a could actually be avoided introducing RHNs in our setup. This would account for the smallness of the active-neutrino masses through a combined Froggatt-Nielsen/Type I seesaw suppresion. This new ingredient can make low-scale f_a models viable, with f_a as low as $f_a \sim 5$ TeV, but requires additional model-building to disentangle the axion mass from its decay constant, see e.g. [91, 92]. This gives up the axion as dark matter but still solves the strong CP problem. Moreover, the resulting axion can now be visible at the LHC, for instance through the decay $a \to \gamma\gamma$, and the fine-tuning in order to reproduce the correct Higgs mass in our unified scenario would be largely cut-down.

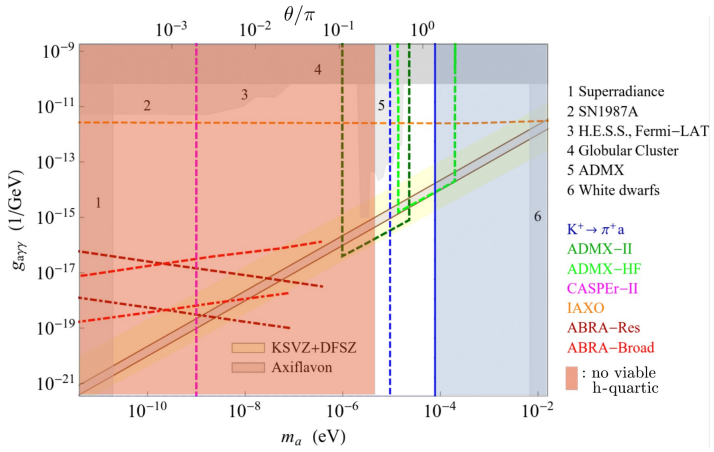

Figure 2.6: The Axiflavon-Higgs parameter space. The red region is exluced as it does not lead to a successful electroweak symmetry breaking, whereas the blue region is constrained by flavor. The remaining strip corresponding $f_a \approx (10^{11}, 10^{12})$ GeV will be almost fully tested by future searches. The model-variant with RHNs and low-scale axion is not displayed. Plot taken from [95].

Chapter 3

Gauge–Yukawa β–functions at large N_f

In Sec. 2.5, we have presented a concrete UV completion of the Froggatt-Nielsen mechanism to explain the hierarchies in the SM fermion masses and the structure of the CKM matrix. The model consists of a potentially large number of vector-like fermions, the FN messengers ξ, coupled to the flavon field via yukawa interactions (considering $\mathcal{O}(10)$ messengers in the spinorial **4** of $SO(5)$ already gives $\mathcal{O}(40)$ states, not including color). These are the key ingredients to construct the chain in Fig. 2.2, which is the microscopic realization of the low-energy operators suppressing the mass of the light SM fermions. Besides our concrete model, the existence of many fermionic degrees of freedom seems to be a necessary ingredient for the FN mechanism to work. This poses some questions about the UV behavior of the model itself, as for instance the messengers will generically have a strong impact in the renormalization-group (RG) evolution of the system. This is encoded in the β-functions for the couplings that define the UV theory, including the SM gauge interactions. However, it is not obvious how the β-functions for such models with many degrees of freedom should be calculated in the first place, as the presence of large multiplicities may interfer with the standard perturbation theory.

In this chapter, we will investigate the RG evolution for gauge–yukawa theories that contain a large number of matter fields, N_f, of which the FN setup discussed above can be seen as a possible example. As we shall see shortly, this study finds several applications both in high-energy physics and condensed-matter theory.

Our analysis will employ resummation techniques for the calculation of the β-functions that are alternative to the conventional loop expansion. This is particularly suitable to keep track of the all-order contribution stemming from the N_f multiplicity. We will thus reorganize the perturbative series by replacing the conventional loop expansion in a generic coupling α

$$\frac{1}{\alpha^2}\,\beta(\alpha) = a_{1\text{-L}} + a_{2\text{-L}}\,\alpha + a_{3\text{-L}}\,\alpha^2 \ldots \tag{3.1}$$

with inverse powers of N_f:

$$\frac{1}{(\alpha N_f)^2}\,\beta(\alpha N_f) = F^{(0)}(\alpha N_f) + \frac{1}{N_f}F^{(1)}(\alpha N_f) + \frac{1}{N_f^2}F^{(2)}(\alpha N_f) + \ldots \tag{3.2}$$

where $\beta(\alpha N_f) = N_f\beta(\alpha)$. As we can see, the $1/N_f$ expansion is actually established by defining a 't Hooft coupling $K \equiv \alpha N_f$ which ideally remains constant in the limit

Figure 3.1: Dressing of a gauge propagator with n fermion bubbles.

of $N_f \to \infty$. The quantities $F^{(n)}$ are then non-trivial functions of the rescaled coupling that one needs to calculate. In most cases of interest, the function $F^{(0)}$ is completely determined at one-loop. Conversely, the higher order functions, $F^{(n\geq 1)}$, get contributions from (infinite) Feynman diagrams with an increasing number of loops corresponding to well defined classes. Thus, resummation techniques are needed and calculations can be successfully carried out only for the first few orders, $F^{(1)}$ and $F^{(2)}$.

To get a feeling of how this works, consider the case of a $U(1)$ gauge symmetry with N_f fermion flavors. Let us focus on a generic loop diagram that contains an internal gauge line. The main observation is that dressing this line with n fermion loops does not change the order in the $1/N_f$ expansion (although it does change the loop order of the diagram), see Fig. 3.1. The reason is that any fermion loop brings an additional power of α that gets compensated by a factor of N_f due to the fact that all flavors circulate in the loop. This amounts to correct the original gauge propagator as

$$\frac{1}{q^2} \to \frac{(\alpha N_f)^n (\Pi^{(1)})^n}{(q^2)^{1+n(4-d)/2}}, \tag{3.3}$$

where $\Pi^{(1)}$ is the one-loop bubble and $d = 4-\epsilon$ according to dimensional regularization. Dealing with large-N_f β-functions thus requires to resum expressions like the one in (3.3) within a given Feynman diagram, whose basic topology can be one-loop, two-loop etc., as we shall see in detail. Remarkably, the contribution from n bubbles as in (3.3) is regular enough to make it possible to resum the whole series in a closed form, at least for the very first orders in the $1/N_f$ expansion.

In the following, we will engage in the calculation of the first non-trivial functions in (3.2) for models that contain an arbitrary number of degrees of freedom, N_f, and also exhibit a large flavor symmetry such as $SU(N_f)$. The presence of this symmetry ensures that all these degrees of freedom contribute in the same way, thus making it possible to account for their multiplicity in a general way.

These models turn out to be relevant also for condensed-matter theory, where β-functions of this type are used to investigate the existence of quantum phase transitions corresponding to the fixed points of the RG flow, and to calculate the corresponding critical exponents. In particular, our calculation will be relevant for the QED_3-Gross-Neveu-Yukawa model that has recently attracted some interest because of its critical behavior in $d = 3$. As the fixed point there turns out to be strongly-coupled, one possibility to extract information about the phase transition is to perform the analysis in $d = 4 - \epsilon$, where the theory is weakly coupled for $\epsilon \to 0$, and extrapolate to $d = 3$ through the "ϵ-expansion" [96, 97]. In this respect, we will be able to complement the information about the critical exponents coming from standard perturbation theory by providing the large-N_f counterpart. This is presented for the first time in Sec. 3.4.3.

On the other hand, the RG flow of gauge-yukawa theories is certainly important for high-energy physics in $d = 4$, as it provides information on the UV behavior of possible extensions of the SM. This is particularly relevant for scenarios in which the Higgs

is an elementary scalar, as the requirement of a UV fixed point for the SM quantum field theory could be used as a guiding principle for new physics (alternatively to compositeness and also to supersymmetry). Intriguingly, the very existence of the Higgs boson can be actually linked to the requirement of having yukawa interactions in the theory, which have been shown to be crucial in generating interacting fixed points in perturbation theory [20]. (The occurrence of a UV interacting fixed point is referred to as "asymptotic safety" as opposed to asymptotic freedom, where the fixed point is simply the non-interacting Gaussian one as in QCD.) In this respect, large-N techniques are useful for investigating asymptotic safety in a complementary way with respect to standard perturbation theory. In fact, the result of Ref. [22] proves the existence of interacting UV fixed points in a theory with a large number of colors of the gauge dynamics, N_c, and fermion flavors, N_f, in the Veneziano limit (namely, $N_c/N_f \to$ constant when $N_{c,f} \to \infty$). After that, there has been a lot of activity in considering the complementary scenario in which N_c is fixed while N_f is taken large, such as large-N_f QED ($N_c = 1$) and large-N_f QCD ($N_c = 3$). In particular, by using the properties of the resummed large-N_f β-functions, some attempts to construct asymptotically-safe extensions of the SM have been carried out, see [98–100] [1].

The necessary ingredient for all these studies is of course the explicit form of the $F^{(n)}$ functions in (3.2). The first direct calculation ever performed in this context involves the $U(1)$ gauge β-function with N_f flavors [101,102] (large-N_f QED), where the authors managed to obtain $F^{(1)}$ in a closed form. This result was later extended to non-abelian gauge theories due to the work in [103], see also Refs [104,105] [2]. Recently, the leading $1/N_f$ contribution from the gauge sector to a single yukawa coupling was calculated in Ref. [106], whereas an extension to semi-simple gauge groups can be found in Ref. [107].

Nonetheless, the case in which a scalar field couples to several fermion flavors through yukawa interactions (as in Froggatt-Nielsen-inspired UV models) was not yet studied. In the following, we will bridge this gap in the literature and compute the β-function for the pure yukawa interaction up to $\mathcal{O}(1/N_f)$ [II] and also extend this result to include gauge interactions [III]. We will also discuss the connection between resummation and critical-point method, thereby making contact with condensed matter theory [IV]. Driven by this new perspective, we will finally present an alternative approach to large-N and asymptotic safety [V].

This chapter is organized as follows: the framework we will be using is specified in Sec. 3.1 whereas the actual calculation is presented in Sec. 3.2 for the pure yukawa case [II] and in Sec. 3.3 for the gauge contribution [III], respectively. Sec. 3.4 is devoted to the critical-point method and contains the connections with condensed-matter systems [IV]. A new way of dealing with large-N_f singularities [V] is finally discussed in Sec. 3.5.

3.1 The framework

Let us here introduce the model we will be dealing with in this chapter. It consists of a $U(1)$ gauge theory in $d = 4$ with N_f fermion flavors and a gauge-singlet real scalar field

[1] These results make use of singularities of the $F^{(1)}$ function at physical values of the couplings to enforce the UV fixed point. An alternative way of dealing with such singularities will be discussed in Sec. 3.5.

[2] The non-abelian gauge β-function at $\mathcal{O}(1/N_f)$ was actually not obtained through resummation but rather via the critical-point method; more on this in Sec. 3.4

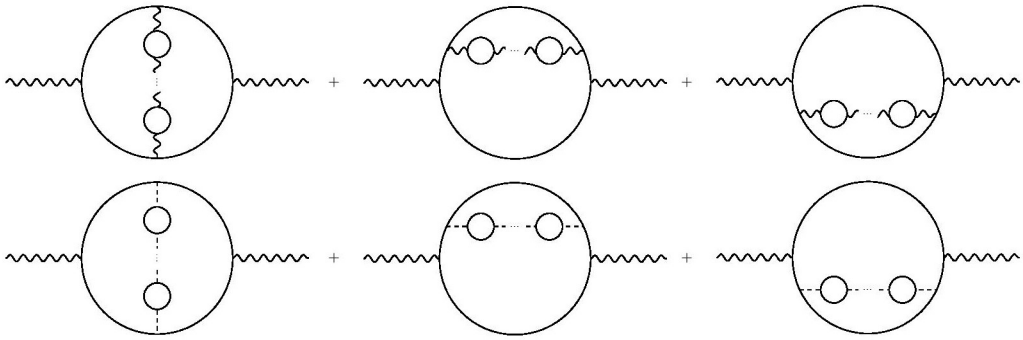

Figure 3.2: Photon self-energy corrections.

coupling to the fermionic multiplet, ψ, via yukawa interaction:

$$\mathcal{L} = -\frac{1}{4}F_{\mu\nu}F^{\mu\nu} + \frac{1}{2}\partial_\mu\phi\partial^\mu\phi - \frac{1}{2}m_\phi^2\phi^2 + \bar{\psi}(i\partial\!\!\!/ - m_\psi)\psi + y\bar{\psi}\psi\phi - igA_\mu\,\bar{\psi}\gamma^\mu\psi - \lambda\phi^4. \quad (3.4)$$

This model is known as the QED$_3$-Gross-Neveu-Yukawa model in condensed matter language, but it can also mimic the system responsible for the FN mechanism, where ϕ is the flavon and ψ corresponds to the FN messengers, that are vector-like under the SM gauge symmetry mimicked here by the gauged $U(1)$. The common yukawa coupling y would correspond to the couplings a_j in (2.81), although the latter exhibit a nearest-neighbour type of structure that needs diagonalization to be properly compared with (3.4). The masses for ψ and ϕ will be neglected in the following, as they do not contribute to the β-functions. As for the scalar quartic coupling, λ, we will set it to zero at tree-level, as it considerably complicates the calculation. The impact of a non-zero tree-level λ will be discussed in Sec. 3.4.2; for the moment, we just notice that setting $\lambda = 0$ at tree-level is consistent given that the loop-induced quartic will be higher-order in the $1/N_f$ expansion. As mentioned below (3.2), we define the rescaled gauge and yukawa 't Hooft couplings E and K as

$$E \equiv \frac{e^2}{4\pi^2}N_f, \text{ and } K \equiv \frac{y^2}{4\pi^2}N_f, \quad (3.5)$$

which are kept constant in the limit $N_f \to \infty$.

Our purpose is to derive the coupled system of β-functions for E and K at the $1/N_f$ level

$$\beta_K \equiv K^2\left[F^{(0)} + \frac{1}{N_f}F_1^{(1)}(K) + \frac{1}{N_f}F_2^{(1)}(K,E) + \mathcal{O}\left(1/N_f^2\right)\right], \quad (3.6)$$

$$\beta_E \equiv E^2\left[\tilde{F}^{(0)} + \frac{1}{N_f}F_3^{(1)}(E) + \frac{1}{N_f}F_4^{(1)}(K) + \mathcal{O}\left(1/N_f^2\right)\right]. \quad (3.7)$$

The first coefficients $F^{(0)} = 1$ and $\tilde{F}^{(0)} = 2/3$ simply correspond to the one-loop β-function, whereas the pure-gauge contribution to the gauge β-function, $F_3^{(1)}(E)$, has been computed in Ref. [102]. Our task is thus to provide a closed formula for $F_1^{(1)}(K)$, $F_2^{(1)}(K,E)$ and $F_4^{(1)}(K)$.

In the following, we will use dimensional regularization in $d = 4 - \epsilon$ dimensions and minimal subtraction (MS) scheme for determining the divergences for $\epsilon \to 0$ (in any case,

the $\mathcal{O}(1/N_f)$ β-functions are scheme independent [105]). The β-functions can then be extracted from:

$$\beta_E \equiv \frac{\mathrm{d}E}{\mathrm{d}\ln\mu} = E\left(K\frac{\partial}{\partial K} + E\frac{\partial}{\partial E}\right)G_1(K,E), \tag{3.8}$$

$$\beta_K \equiv \frac{\mathrm{d}K}{\mathrm{d}\ln\mu} = K\left(K\frac{\partial}{\partial K} + E\frac{\partial}{\partial E}\right)H_1(K,E), \tag{3.9}$$

where G_1 and H_1 are defined by

$$\log Z_E \equiv \log Z_3^{-1} = \sum_{n=1}^{\infty}\frac{G_n(K,E)}{\epsilon^n}, \tag{3.10}$$

$$\log Z_K \equiv \log(Z_S^{-1}Z_f^{-2}Z_V^2) = \sum_{n=1}^{\infty}\frac{H_n(K,E)}{\epsilon^n}, \tag{3.11}$$

and Z_3, Z_S, Z_f, and Z_V are the renormalization constants for the photon, the scalar, and the fermion wave function, and the 1PI vertex, respectively. In the following, we will give explicit formulas for the structure of the various counterterms up to $\mathcal{O}(1/N_f)$ as this is preparatory for the actual calculation of the β-functions:

- The **photon wave-function** renormalization constant, Z_3, is given by

$$Z_3 = 1 - \mathrm{div}\left\{Z_3\Pi_0(p^2, Z_K K, Z_E E, \epsilon)\right\}, \tag{3.12}$$

  where Π_0 is the photon self-energy divided by the external momentum squared, p^2, and we denote the poles of X in ϵ by div$X$. At $\mathcal{O}(1/N_f)$, the self-energy can be rewritten as

$$\Pi_0(p^2, K_0, E_0, \epsilon) = E_0\,\Pi_E^{(1)}(p^2,\epsilon) + \frac{1}{N_f}\sum_{n=2}^{\infty}\left(E_0^n\Pi_E^{(n)}(p^2,\epsilon) + E_0K_0^{n-1}\Pi_K^{(n)}(p^2,\epsilon)\right), \tag{3.13}$$

  where $\Pi_E^{(1)}$ is the simple one-loop fermion bubble (Fig. 3.1 with $n=1$) and $\Pi_E^{(n)}$ and $\Pi_K^{(n)}$ contain the n-loop part consisting of $n-2$ fermion bubbles in the gauge and yukawa chains summing over the topologies given in Fig. 3.2. Hereafter the subscripts for K_0 and E_0 indicate the bare couplings before renormalization.

- The **scalar wave-function** renormalization constant, Z_S, is determined via

$$Z_S = 1 - \mathrm{div}\left\{Z_S S_0(p^2, Z_K K, Z_E E, \epsilon)\right\}, \tag{3.14}$$

  with the scalar self-energy S_0 given by

$$S_0(p^2, K_0, E_0, \epsilon) = K_0 S_K^{(1)}(p^2,\epsilon) + \frac{1}{N_f}\sum_{n=2}^{\infty}\left(K_0^n S_K^{(n)}(p^2,\epsilon) + K_0E_0^{n-1}S_E^{(n)}(p^2,\epsilon)\right), \tag{3.15}$$

  where $S_K^{(1)}$ is the one-loop result, and $S_K^{(n)}$ and $S_E^{(n)}$ the n-loop terms consisting of $n-2$ fermion bubbles in the yukawa and gauge chains summing over the topologies shown in Fig. 3.3.

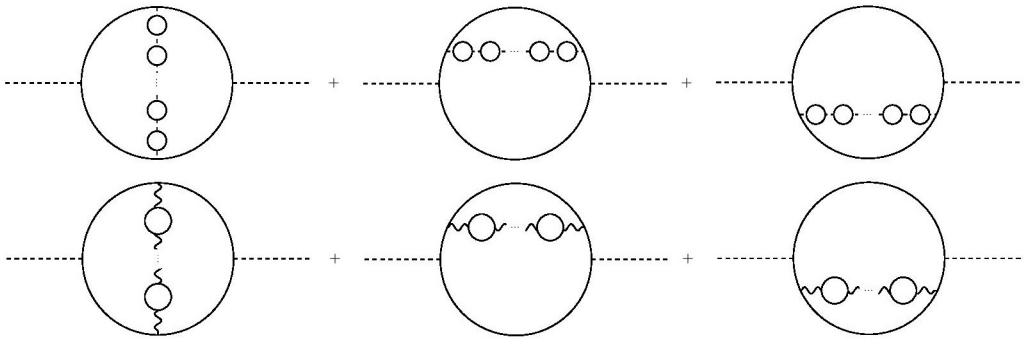

Figure 3.3: Scalar self-energy corrections.

- For the **fermion self-energy** and **vertex** renormalization constants Z_f and Z_V, respectively, the lowest non-trivial contributions are already $\mathcal{O}(1/N_f)$, and we have

$$Z_f = 1 - \mathrm{div}\left\{\Sigma_0(p^2, Z_K K, Z_E E, \epsilon)\right\}, \tag{3.16}$$

$$\Sigma_0(p^2, K_0, E_0, \epsilon) = 1 + \frac{1}{N_f}\sum_{n=1}^{\infty}\left(K_0^n \Sigma_K^{(n)}(p^2,\epsilon) + E_0^n \Sigma_E^{(n)}(p^2,\epsilon)\right), \tag{3.17}$$

  where $\Sigma_K^{(n)}$ and $\Sigma_E^{(n)}$ are depicted in Fig. 3.4 (a) with $n-1$ fermion bubbles. Similarly, one has for the vertex

$$Z_V = 1 - \mathrm{div}\left\{V_0(p^2, Z_K K, Z_E E, \epsilon)\right\}, \tag{3.18}$$

$$V_0(p^2, K_0, E_0, \epsilon) = 1 + \frac{1}{N_f}\sum_{n=1}^{\infty}\left(K_0^n V_K^{(n)}(p^2,\epsilon) + E_0^n V_E^{(n)}(p^2,\epsilon)\right), \tag{3.19}$$

  where $V_K^{(n)}$ and $V_E^{(n)}$ contain $n-1$ fermion bubbles and are shown diagrammatically in Fig. 3.4 (b).

The task of determining the coupled system in (3.6) and (3.7) can actually be splitted in two parts. In Sec. 3.2, we will first calculate the β-function for the yukawa coupling by switching off the gauge interactions, thus determining $F_1^{(1)}(K)$. The remaining mixed contributions, $F_2^{(1)}(K,E)$ and $F_4^{(1)}(K)$, are tackled in Sec. 3.3.

3.2 Pure yukawa

In this section, we will set $E = 0$ and work out the contribution from the pure yukawa interaction. This allows to eavaluate $F_1^{(1)}(K)$ in (3.6) in a closed form. The starting point is the calculation of the counterterms Z_S, Z_f and Z_V as a series in the number of fermion bubbles. The series for each counterterm needs to be resummed in order to extract the $1/\epsilon$ pole (the knowledge of these counterterms will be very useful also when evaluating the mixed contributions in Sec. 3.3). The β-function is then simply obtained by taking derivatives as in (3.8) and (3.9). This section is based on Ref. [II].

(a) Fermion self-energy corrections.

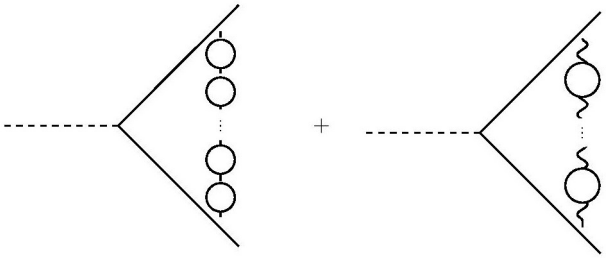

(b) Vertex corrections.

Figure 3.4: Gauge and yukawa contributions to fermion self-energy and the vertex corrections due to a chain of fermion bubbles.

3.2.1 Renormalization constants

Let us start by evaluating the counterterm for the **scalar self-energy**, Z_S. Our starting point is (3.14). The contributions we are considering are the pure-yukawa diagrams depicted in the first row of Fig. 3.3. Using the expansion of the scalar self-energy in (3.15) we obtain

$$Z_S = 1 - \mathrm{div}\left\{ Z_S Z_K K S_K^{(1)}(p^2,\epsilon) + \frac{1}{N_f}\sum_{n=2}^{\infty} Z_S (Z_K K)^n S_K^{(n)}(p^2,\epsilon) \right\}. \tag{3.20}$$

Recalling that $Z_K \equiv Z_S^{-1} Z_f^{-2} Z_V^2$ and substituting (3.16) and (3.18), the first term between brackets can be written as

$$\begin{aligned} &\mathrm{div}\left\{ Z_S Z_K S_K^{(1)}(p^2,\epsilon) K \right\} \\ &\quad = K\,\mathrm{div}\left\{ S_K^{(1)} \right\} + \frac{1}{N_f}\mathrm{div}\left\{ 2K\,\mathrm{div}\left\{ \Sigma_0(p^2, Z_K K, \epsilon) - V_0(p^2, Z_K K, \epsilon) \right\} S_K^{(1)}(p^2,\epsilon) \right\}. \end{aligned} \tag{3.21}$$

The $S_K^{(1)}$ part corresponds to the one-loop diagram and is given by

$$S_K^{(1)}(p^2,\epsilon) \equiv \underbrace{\mathrm{div}\left\{ S_K^{(1)} \right\}}_{=1/\epsilon} + S_{\mathrm{F}}^{(1)}(p^2,\epsilon) = \frac{1}{(4\pi)^{d/2-2}} \frac{G(1,1)}{2} (-p^2)^{d/2-2} \tag{3.22}$$

where $d = 4 - \epsilon$, the loop function, $G(1,1)$, is given in (B.2) in Appendix B, and we have introduced the notation $S_{\rm F}^{(1)}$ to indicate the finite part of $S_K^{(1)}$. Then,

$$\begin{aligned}
&\mathrm{div}\left\{Z_S Z_K S_K^{(1)}(p^2,\epsilon)K\right\} \\
&\quad = \frac{K}{\epsilon} + \frac{1}{N_f}\mathrm{div}\Big\{2K\,\mathrm{div}\left\{\Sigma_0(p^2, Z_K K, \epsilon) - V_0(p^2, Z_K K, \epsilon)\right\} \\
&\qquad\qquad \times \left(\mathrm{div}\left\{S_K^{(1)}\right\} + S_{\rm F}^{(1)}(p^2,\epsilon)\right)\Big\} \\
&\quad = \frac{K}{\epsilon} + \frac{1}{N_f}\mathrm{div}\left\{2K S_{\rm F}^{(1)}(p^2,\epsilon)\left[\Sigma_0(p^2, Z_K K, \epsilon) - V_0(p^2, Z_K K, \epsilon)\right]\right\} + \text{ higher poles},
\end{aligned} \tag{3.23}$$

where the higher poles, i.e., higher than $1/\epsilon$, arise from the product of two divergent parts and will be omitted because they play no role in what follows. Then, at the lowest order in $1/N_f$,

$$Z_S = 1 - \frac{K}{\epsilon} + \mathcal{O}\left(1/N_f\right). \tag{3.24}$$

Therefore, every time $Z_K K$ appears in the argument of Σ_0 and V_0, it can be replaced by $K\left(1-\frac{K}{\epsilon}\right)^{-1}$; the additional contributions are higher order in $1/N_f$. By using (3.17) and (3.19), we can rewrite Eq. (3.23) as

$$\begin{aligned}
&\mathrm{div}\left\{Z_S Z_K S_K^{(1)}(p^2,\epsilon)K\right\} \\
&\quad = \frac{K}{\epsilon} + \sum_{n=1}^{\infty} K^{n+1}\mathrm{div}\left\{2S_{\rm F}^{(1)}(p^2,\epsilon)\left(1-\frac{K}{\epsilon}\right)^{-n}\left[\Sigma_K^{(n)}(p^2,\epsilon) - V_K^{(n)}(p^2,\epsilon)\right]\right\}.
\end{aligned} \tag{3.25}$$

Similarly, the second term of (3.20) reads

$$\frac{1}{N_f}\mathrm{div}\left\{\sum_{n=2}^{\infty} Z_S (Z_S^{-1}K)^n S_K^{(n)}(p^2,\epsilon)\right\} = \frac{1}{N_f}\sum_{n=2}^{\infty} K^n \mathrm{div}\left\{\left(1-\frac{K}{\epsilon}\right)^{1-n} S_K^{(n)}(p^2,\epsilon)\right\}. \tag{3.26}$$

Altogether, we can write Z_S as

$$Z_S = 1 - \frac{K}{\epsilon} - \frac{1}{N_f}\sum_{n=2}^{\infty} K^n \left\{\left(1-\frac{K}{\epsilon}\right)^{1-n}\left(2S_{\rm F}^{(1)}\left[\Sigma_K^{(n-1)} - V_K^{(n-1)}\right] + S_K^{(n)}\right)\right\}, \tag{3.27}$$

where the explicit functional dependence on (p^2,ϵ) has been omitted to lighten the notation. Using the negative-binomial expansion,

$$\left(1-\frac{K}{\epsilon}\right)^{1-n} = \sum_{i=0}^{\infty}\binom{n+i-2}{i}\frac{K^i}{\epsilon^i} \tag{3.28}$$

and performing a shift in the summation, $n \to n-i$, we find our final expression for Z_S:

$$Z_S = 1 - \frac{K}{\epsilon} - \frac{1}{N_f}\sum_{n=2}^{\infty} K^n \mathrm{div}\left\{\sum_{i=0}^{n-2}\binom{n-2}{i}\frac{1}{\epsilon^i}\left(2S_{\rm F}^{(1)}\left(\Sigma_K^{(n-i-1)} - V_K^{(n-i-1)}\right) + S_K^{(n-i)}\right)\right\}. \tag{3.29}$$

We notice that Eq. (3.29) differs essentially from its counterpart in the $U(1)$ gauge theory (QED) in Ref. [102] because of the contribution from the fermion self-energy and the vertex, which exactly cancel in QED because of the Ward identity. As we shall see, they are instead fundamental for a yukawa theory as they will ensure that the counterterms are momentum independent.

Let us now move to evaluate the **fermion self-energy** and **vertex** counterterms Z_f and Z_V, respectively. As for the former, the expression for Z_f involves the pure-yukawa diagrams in Fig. 3.4 (a) and can be derived from (3.16) similarly to Z_S:

$$\begin{aligned} Z_f &= 1 - \frac{1}{N_f}\sum_{n=1}^{\infty} K^n \mathrm{div}\left\{\left(1-\frac{K}{\epsilon}\right)^{-n}\Sigma_K^{(n)}(p^2,\epsilon)\right\} \\ &= 1 - \frac{1}{N_f}\sum_{n=1}^{\infty} K^n \mathrm{div}\left\{\sum_{i=0}^{n-1}\binom{n-1}{i}\frac{1}{\epsilon^i}\Sigma_K^{(n-i)}(p^2,\epsilon)\right\}, \end{aligned} \tag{3.30}$$

where we have again used the negative-binomial expansion and performed the same shift $n \to n-i$ in the last line. The derivation of Z_V is completely analogous, and we can readily write

$$Z_V = 1 - \frac{1}{N_f}\sum_{n=1}^{\infty} K^n \mathrm{div}\left\{\sum_{i=0}^{n-1}\binom{n-1}{i}\frac{1}{\epsilon^i}V_K^{(n-i)}(p^2,\epsilon)\right\}. \tag{3.31}$$

3.2.2 Resummation

In the previous section, the expressions for Z_V, Z_f and Z_S were given as a series in the number of fermion bubbles, n. We will here perform an explicit resummation and provide closed formulas for all these renormalization constants.

Let us start with the **vertex** counterterm Z_V in (3.31). In order to resum this series, we need to investigate the explicit form of $V_K^{(n)}$. According to the left diagram in Fig. 3.4 (b) we find the n-loop contribution to be

$$\begin{aligned} V_K^{(n)}(p^2,\epsilon) =& \frac{(-1)^n}{4}\left(\frac{1}{(4\pi)^{d/2-2}}\right)^n\left(\frac{G(1,1)}{2}\right)^{n-1}(-p^2)^{n(d/2-2)} \\ &\times G\left(1, 1-(n-1)(d/2-2)\right), \end{aligned} \tag{3.32}$$

where $G(n_1,n_2)$ is the loop-function defined in (B.2). Since the calculation of the β-function requires to obtain the $1/\epsilon$ pole of the various counterterms, it is useful to rewrite $V_K^{(n)}$ by extracting the highest degree of divergence in $1/\epsilon$. This is done by noticing that, as in Ref. [102], Eq. (3.32) allows for the following expansion:

$$V_K^{(n)}(p^2,\epsilon) = (-1)^n \frac{1}{n\epsilon^n}\frac{v_K(p^2,\epsilon,n)}{2}, \tag{3.33}$$

where

$$v_K(p^2,\epsilon,n) = \sum_{j=0}^{\infty} v_K^{(j)}(p^2,\epsilon)(n\epsilon)^j, \tag{3.34}$$

and $v_K^{(j)}(p^2,\epsilon)$ are regular in the limit $\epsilon \to 0$ for all j. In particular, $v_K^{(0)}(\epsilon)$ is independent of p^2 and is explicitly given by

$$v_K^{(0)}(\epsilon) = \frac{2\Gamma(2-\epsilon)}{\Gamma\left(1-\frac{\epsilon}{2}\right)^2\Gamma\left(2-\frac{\epsilon}{2}\right)\Gamma\left(\frac{\epsilon}{2}\right)\epsilon}. \tag{3.35}$$

Substituting (3.32) and (3.33) in (3.31), we find:

$$Z_V = 1 - \frac{1}{N_f}\sum_{n=1}^{\infty}(-K)^n \mathrm{div}\left\{\sum_{j=0}^{n-1}\frac{1}{\epsilon^{n-j}}\sum_{i=0}^{n-1}\binom{n-1}{i}(-1)^i(n-i)^{j-1}\frac{v_K^{(j)}(p^2,\epsilon)}{2}\right\}. \tag{3.36}$$

The advante of using the expressions in (3.33) and (3.34) is that the sum over j in (3.36) is cut off at $j = n-1$ as higher terms will be finite in ϵ and therefore irrelevant for the β-function [3]. This leads to a dramatic simplification of (3.36) that follows from the binomial properties. In fact, as noticed in Ref. [102], one has:

$$\sum_{i=0}^{n-1}\binom{n-1}{i}(-1)^i(n-i)^{j-1} = -\delta_{j,0}\frac{(-1)^n}{n},\ j = 0,\dots,n-1, \tag{3.37}$$

and Eq. (3.36) gets simplified to

$$Z_V = 1 + \frac{1}{2N_f}\sum_{n=1}^{\infty}\frac{K^n}{\epsilon^n}\frac{v_K^{(0)}(\epsilon)}{n}. \tag{3.38}$$

where we can see that only the function $v_K^{(0)}$ given in (3.35) actually matters, justifying the expansion in (3.34). Notice also that (3.37) crucially holds only for $j < n$, namely for the divergent part only: larger values of j correspoding to finite terms will instead give contributions $\sim n!$ that would need a special treatment such as Borel transform.

The simple form in (3.38) for the divergent part in ϵ allows for a straightforward resummation. In particular, since only the $1/\epsilon$ pole contributes to the β-function, one can simply Taylor-expand $v_K^{(0)}(\epsilon)$ around $\epsilon = 0$, isolate the $1/\epsilon$ contribution in (3.38), and reconstruct $v_K^{(0)}$ back. In practice, one has

$$v_K^{(0)}(\epsilon) = \sum_{j=0}^{\infty} v_j^{(0)}\epsilon^j, \tag{3.39}$$

and keeping only the $1/\epsilon$ pole of (3.38) we find the closed formula for Z_V:

$$Z_V = 1 + \frac{1}{2\epsilon N_f}\sum_{n=1}^{\infty}\frac{K^n}{n}v_{n-1}^{(0)} = 1 + \frac{1}{2\epsilon N_f}\int_0^K v_K^{(0)}(t)\mathrm{d}t, \tag{3.40}$$

which is our first achievement in this section and the prototype for the next calculations.

For future comparison, it is worth noticing that the ultimate product of this resummation, (3.40), is to replace the quantity ϵ, that originally appeared as the argument of $v_K^{(0)}(\epsilon)$ in (3.38) and corresponds to the space-time dimension as $d = 4-\epsilon$, with an integral function in (3.40) that depends only on the coupling K. The reason for this can be understood when considering the Wilson-Fisher fixed for this theory in $d = 4-\epsilon$ dimensions and will be further discussed in Sec. 3.4.

[3] However, these terms should be taken into account if one is interested in resumming the finite parts of these diagrams.

Similar resummation strategy can be employed to treat the **fermion self-energy** in (3.30). The n-loop contribution shown in the left panel of Fig. 3.4 (a) is found by direct calcuation to be

$$\begin{aligned}\Sigma_K^{(n)}(p^2,\epsilon) = &-\frac{(-1)^n}{8}\left(\frac{1}{(4\pi)^{d/2-2}}\right)^n\left(\frac{G(1,1)}{2}\right)^{n-1}(-p^2)^{n(d/2-2)}\\ &\times\left[G(1,1-(n-1)(d/2-2))-G(1,-(n-1)(d/2-2))\right],\end{aligned} \tag{3.41}$$

where $G(n_1,n_2)$ is again the loop-function given in (B.2). Similarly to Eq. (3.32), Eq. (3.41) can be expanded as

$$\Sigma_K^{(n)}(p^2,\epsilon) = -(-1)^n\frac{1}{n\epsilon^n}\frac{\sigma_K(p^2,\epsilon,n)}{4}, \tag{3.42}$$

where

$$\sigma_K(p^2,\epsilon,n) = \sum_{j=0}^{\infty}\sigma_K^{(j)}(p^2,\epsilon)(n\epsilon)^j, \tag{3.43}$$

and $\sigma_K^{(j)}(p^2,\epsilon)$ are regular for $\epsilon\to 0$. Again, $\sigma_K^{(0)}(\epsilon)$ is independent of p^2, and it is given by

$$\sigma_K^{(0)}(\epsilon) = -\frac{2^{5-\epsilon}\Gamma\left(\frac{3}{2}-\frac{\epsilon}{2}\right)}{\sqrt{\pi}(4-\epsilon)\Gamma\left(-\frac{\epsilon}{2}\right)\epsilon}\frac{\sin\left(\frac{\pi\epsilon}{2}\right)}{\pi\epsilon}. \tag{3.44}$$

Using the same procedure shown for the vertex counterterm Z_V, we find that only $\sigma_K^{(0)}(\epsilon)$ eventually contributes to Z_f. Keeping only the $1/\epsilon$ pole, the closed formula for Z_f is

$$Z_f = 1-\frac{1}{4\epsilon N_f}\int_0^K\sigma_K^{(0)}(t)\mathrm{d}t, \tag{3.45}$$

which is fully analogous to (3.40).

Finally, let us tackle the **scalar self-energy** expression in (3.29). Evaluating the bubble diagrams in the upper row of Fig. 3.3 is quite cumbersome and the formula is given in (B.3). Here, we just notice that the expression for $S_K^{(n)}(p^2,\epsilon)$, $n\geq 2$, allows for the following expansion:

$$S_K^{(n)} = -\frac{3}{2}\frac{(-1)^n}{n(n-1)\epsilon^n}\pi_K(p^2,\epsilon,n), \tag{3.46}$$

where

$$\pi_K(p^2,\epsilon,n) = \sum_{j=0}^{\infty}\pi_K^{(j)}(p^2,\epsilon)(n\epsilon)^j, \tag{3.47}$$

and $\pi_K^{(j)}(p^2,\epsilon)$ are regular for $\epsilon\to 0$. Similarly to the previous cases, $\pi_K^{(0)}(\epsilon)$ is independent of p^2. In view of Eq. (3.29), we define

$$2S_{\mathrm{F}}^{(1)}(p^2,\epsilon)\left(\Sigma_K^{(n-1)}(p^2,\epsilon)-V_K^{(n-1)}(p^2,\epsilon)\right)+S_K^{(n)}(p^2,\epsilon)\equiv\frac{(-1)^n}{n(n-1)\epsilon^n}\xi_K(p^2,\epsilon,n), \tag{3.48}$$

where

$$\xi_K(p^2,\epsilon,n)\equiv n\epsilon\, S_{\mathrm{F}}^{(1)}\left(\frac{\sigma_K(p^2,\epsilon,n-1)}{2}+v_K(p^2,\epsilon,n-1)\right)-\frac{3}{2}\pi_K(p^2,\epsilon,n), \tag{3.49}$$

and

$$\xi_K(p^2,\epsilon,n)=\sum_{j=0}^{\infty}\xi_K^{(j)}(p^2,\epsilon)(n\epsilon)^j, \tag{3.50}$$

with $\xi_K^{(j)}(p^2,\epsilon)$ regular for $\epsilon\to 0$ for all j. Notice that (3.49) is defined for $n>1$. In particular, $\xi_K^{(0)}(\epsilon)$ is independent of p^2 and is explicitly given by

$$\xi_K^{(0)}(\epsilon)=-\frac{(1-\epsilon)\Gamma(4-\epsilon)}{\Gamma\left(2-\frac{\epsilon}{2}\right)\Gamma\left(3-\frac{\epsilon}{2}\right)\pi\epsilon}\sin\left(\frac{\pi\epsilon}{2}\right) \tag{3.51}$$

Then, using the above definitions, (3.29) can be written as

$$\begin{aligned}Z_S&=1-\frac{K}{\epsilon}-\frac{1}{N_f}\sum_{n=2}^{\infty}K^n\mathrm{div}\left\{\sum_{i=0}^{n-2}\binom{n-2}{i}\frac{1}{\epsilon^i}\frac{(-1)^{n-i}}{(n-i)(n-i-1)\epsilon^{n-i}}\xi_K(p^2,\epsilon,n-i)\right\}\\&=1-\frac{K}{\epsilon}-\frac{1}{N_f}\sum_{n=2}^{\infty}(-K)^n\mathrm{div}\left\{\sum_{j=0}^{n-1}\frac{1}{\epsilon^{n-j}}\xi_K^{(j)}(p^2,\epsilon)\sum_{i=0}^{n-2}\binom{n-2}{i}(-1)^i\frac{(n-i)^{j-1}}{(n-i-1)}\right\}.\end{aligned} \tag{3.52}$$

The expression above can now be reduced by using the properties of the binomials. We in fact find a new formula which resembles the original one in (3.37):

$$\sum_{i=0}^{n-2}\binom{n-2}{i}(-1)^i\frac{(n-i)^{j-1}}{(n-i-1)}=\begin{cases}\frac{(-1)^n}{n} & j=0\\ \frac{(-1)^n}{n-1} & j=1,\dots,n-1\end{cases}, \tag{3.53}$$

and therefore the expression for Z_S can be significantly simplified:

$$\begin{aligned}Z_S&=1-\frac{K}{\epsilon}-\frac{1}{N_f}\sum_{n=2}^{\infty}K^n\,\mathrm{div}\left\{\frac{\xi_K^{(0)}(\epsilon)}{n\epsilon^n}+\frac{1}{(n-1)\epsilon^n}\sum_{j=1}^{\infty}\xi_K^{(j)}(p^2,\epsilon)\epsilon^j\right\}\\&=1-\frac{K}{\epsilon}-\frac{1}{N_f}\sum_{n=2}^{\infty}K^n\,\mathrm{div}\left\{\frac{\xi_K^{(0)}(\epsilon)}{n\epsilon^n}+\frac{\xi_K(p^2,\epsilon,1)-\xi_K^{(0)}(\epsilon)}{(n-1)\epsilon^n}\right\},\end{aligned} \tag{3.54}$$

where in the first line we extended the sum over j up to ∞ without affecting the result, since all the terms for $j>n-1$ are finite. The function $\xi(p^2,\epsilon,1)$, corresponding to

$$\xi_K(p^2,\epsilon,1)\equiv\sum_{j=0}^{\infty}\xi_K^{(j)}(p^2,\epsilon)\epsilon^j, \tag{3.55}$$

can be actually evaluated by taking in (3.49) the limit $n\to 1$, although the latter is formally defined for $n>1$. We find the following expression:

$$\xi_K(p^2,\epsilon,1)=-\frac{\Gamma(4-\epsilon)}{\Gamma\left(2-\frac{\epsilon}{2}\right)\Gamma\left(3-\frac{\epsilon}{2}\right)\pi\epsilon}\sin\left(\frac{\pi\epsilon}{2}\right)\equiv\xi_K(\epsilon), \tag{3.56}$$

where $\xi_K(\epsilon)$ is actually related to $\xi_K^{(0)}(\epsilon)$ in (3.51) as

$$\xi_K(\epsilon)=\frac{\xi_K^{(0)}(\epsilon)}{1-\epsilon}. \tag{3.57}$$

Few comments are in order: Eq. (3.56) ensures that Z_S is independent of the external momentum p^2, as it should due to renormalizability. This result comes from an exact cancellation among all the different contributions of the scalar self-energy, the fermion self-energy, and the vertex in (3.49). In particular, we find that

$$\pi_K(p^2,\epsilon,1) = \frac{2}{3}\left(\frac{\sigma_K^{(0)}(\epsilon)}{2} + v_K^{(0)}(\epsilon)\right)\left[1+\epsilon\, S_{\rm F}^{(1)}(p^2,\epsilon)\right], \tag{3.58}$$

and therefore

$$\xi_K(\epsilon) = -\frac{\sigma_K^{(0)}(\epsilon)}{2} - v_K^{(0)}(\epsilon), \tag{3.59}$$

which is equivalent to (3.56). All in all, the p^2 independence of Eq. (3.56) provides a non-trivial check for our computation.

We are now ready to resum the series in (3.54). By expanding $\xi_K^{(0)}(\epsilon)$ as

$$\xi_K^{(0)}(\epsilon) = \sum_{j=0}^{\infty} \xi_j^{(0)} \epsilon^j, \tag{3.60}$$

the $1/n$ term in (3.54) is given by

$$\sum_{n=2}^{\infty} \frac{K^n}{\epsilon^n}\frac{\xi_K^{(0)}(\epsilon)}{n} = \frac{1}{\epsilon}\left(\sum_{n=0}^{\infty} K^{n+1}\frac{\xi_n^{(0)}}{n+1} - K\xi_0^{(0)}\right) = \frac{1}{\epsilon}\int_0^K \left[\xi_K^{(0)}(t) - \xi_K^{(0)}(0)\right] {\rm d}t, \tag{3.61}$$

where we have neglected higher poles in $1/\epsilon$. As for the $1/(n-1)$ term in (3.54), using $\xi_K^{(0)}(\epsilon) = (1-\epsilon)\xi_K(\epsilon)$ and expanding $\xi_K(\epsilon)$ as

$$\xi_K(\epsilon) = \sum_{j=0}^{\infty} \tilde{\xi}_j \epsilon^j, \tag{3.62}$$

we find

$$\sum_{n=2}^{\infty} \frac{K^n}{\epsilon^n}\frac{\xi_K(\epsilon) - (1-\epsilon)\xi_K(\epsilon)}{n-1} = \frac{K}{\epsilon}\int_0^K \xi_K(t){\rm d}t + \text{higher poles}. \tag{3.63}$$

Finally, putting together (3.63) and (3.61), the closed formula for Z_S reads

$$Z_S = 1 - \frac{K}{\epsilon} - \frac{1}{\epsilon N_f}\int_0^K \left[\xi_K^{(0)}(t) - \xi_K^{(0)}(0) + \xi_K(t)K\right] {\rm d}t. \tag{3.64}$$

3.2.3 The β-function

Using the results derived for Z_S, Z_f and Z_V, we can finally proceed to evaluating the pure-yukawa contribution to the β-function. First, we find that $H_1(K)$ in (3.11) reads:

$$H_1(K) = K + \frac{1}{N_f}\int_0^K \left(\xi_K^{(0)}(t) - \xi_K^{(0)}(0) + \xi_K(t)K + \frac{\sigma_K^{(0)}(t)}{2} + v_K^{(0)}(t)\right) {\rm d}t, \tag{3.65}$$

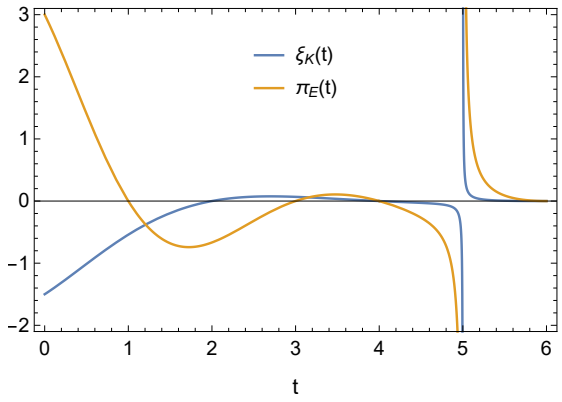

Figure 3.5: The function $\xi_K(t)$ given in (3.68) and $\pi_E(t)$ given in (3.72).

and straightforwardly for the β_K:

$$\beta_K = K^2 + \frac{K^2}{N_f}\left\{3/2 + \xi_K(K) + \frac{\sigma_K^{(0)}(K)}{2} + v_K^{(0)}(K) + \int_0^K \xi_K(t)\mathrm{d}t\right\}, \tag{3.66}$$

where we have used $\xi_K^{(0)}(0) = -3/2$. Recalling (3.59), Eq. (3.66) can be further simplified to

$$\frac{\beta(K)}{K^2} = 1 + \frac{1}{N_f}\left\{\frac{3}{2} + \int_0^K \xi_K(t)\mathrm{d}t\right\}, \tag{3.67}$$

where $\xi_K(t)$ is explicitly given by

$$\xi_K(t) = -\frac{\Gamma(4-t)}{\Gamma(2-\frac{t}{2})\Gamma(3-\frac{t}{2})\pi t}\sin\left(\frac{\pi t}{2}\right) \tag{3.68}$$

Finally, by comparison with (3.6), we see that $F^{(0)} = 1$ and

$$\boxed{F_1^{(1)}(K) = \frac{3}{2} + \int_0^K \xi_K(t)\mathrm{d}t.} \tag{3.69}$$

We plot the integrand, $\xi_K(t)$, in Fig. 3.5. We have checked that our β-function agrees at the leading order in N_f up to four-loop level by comparing with the result of Ref. [108], and, as we shall see in Sec. 3.4, with the result extracted from the critical exponents in Gross–Neveu–Yukawa model computed using a different technique [109]. Finally, let us comment on the pole structure: the integrand, $\xi_K(t)$, has the first pole occuring at $t = 5$, which results in a logarithmic singularity for $F_1^{(1)}(K)$ around $K = 5$. Due to the sign of $\xi_K(t)$, we see that $F_1^{(1)}(K)$ approaches large negative values for $K \to 5^-$.

3.3 Gauge-yukawa

Let us summarize the findings of the previous section by rewriting (3.6) amd (3.7) including (3.69) and the known result for $F_3^{(1)}$ from Ref. [102]:

$$\beta_K = K^2\left[1+\frac{1}{N_f}\left(\frac{3}{2}+\int_0^K \xi_K(t)\mathrm{d}t\right)+\frac{1}{N_f}F_2^{(1)}(K,E)\right]+\mathcal{O}(1/N_f^2), \tag{3.70}$$

$$\beta_E = E^2\left[\frac{2}{3}+\frac{1}{4N_f}\int_0^{2/3E}\pi_E(t)\mathrm{d}t+\frac{1}{N_f}F_4^{(1)}(K)\right]+\mathcal{O}(1/N_f^2), \tag{3.71}$$

where

$$\pi_E(t)=\frac{\Gamma(4-t)(1-t)\left(1-\frac{t}{3}\right)\left(1+\frac{t}{2}\right)}{\Gamma\left(2-\frac{t}{2}\right)^2\Gamma\left(3-\frac{t}{2}\right)\Gamma\left(1+\frac{t}{2}\right)}, \tag{3.72}$$

and ξ_K is given in (3.68). The function $\pi_E(t)$ is shown in Fig. 3.5.

In this section, we will mainly follow Ref. [III] and provide closed formulas for the remaining two unknowns, $F_2^{(1)}$ and $F_4^{(1)}$, corresponding to the mixed contributions. In doing so, one can take advantage from the results of the pure-yukawa case, such as the knowledge of Z_S, Z_f and Z_V. In particular, the crucial point is that a bubble-chain constructed with yukawa interactions differ from the same chain with gauge interactions just by an overall factor. In fact, analogously to (3.3), a yukawa chain with n bubbles correspond to a modified propagator

$$\frac{i}{k^2}\to\frac{i}{k^2}\left(\frac{iS^{(1)}(k^2)}{k^2}\right)^n \tag{3.73}$$

where each bubble evaluates to

$$S^{(1)}(p^2)=i\pi\frac{p^2}{(4\pi)^{d/2-1}}K_0 2N_c(-p^2)^{d/2-2}G(1,1), \tag{3.74}$$

where K_0 is the bare coupling before renormalization. As for the gauge chain, the dressed propagator is

$$\frac{-i}{k^2}\left(g_{\mu\nu}-\frac{k_\mu k_\nu}{k^2}\right)\left(-\Pi_\gamma^{(1)}(k^2)\right)^n \tag{3.75}$$

where the 1-loop bubble evaluates to

$$\Pi_\gamma^{(1)}(p^2)=\frac{2(d-2)}{d-1}E_0\frac{\pi}{(4\pi)^{d/2-1}}(-p^2)^{d/2-2}G(1,1), \tag{3.76}$$

with E_0 being the bare coupling before renormalization. The correspondence is then:

$$\frac{-ig_{\mu\nu}}{k^2}\left(-\Pi_\gamma^{(1)}\right)^n\Big/\frac{i}{k^2}\left(\frac{iS^{(1)}(k^2)}{k^2}\right)^n=-g_{\mu\nu}\left(\frac{d-2}{d-1}\right)^n\left(\frac{E_0}{K_0}\right)^n \tag{3.77}$$

(Notice that $g_{\mu\nu}$ is the only relevant Lorentz structure in the photon propagator, since the $k_\mu k_\nu$ term does not contribute to the β-function.) Thanks to (3.77), some of the results of the pure-yukawa case can be used to evaluate the mixed contributions. Rather than detailing all the steps, we will thus highlight the similarities with the previous calculation.

3.3.1 Mixed contribution

We present here the calculation for the mixed contributions in (3.70) and (3.71), namely $F_2^{(1)}(K,E)$ and $F_4^{(1)}(K)$. Let us start with the **yukawa contribution** to the $U(1)$ β-function.

The yukawa contribution to the photon self-energy, depicted in the lower row of Fig. 3.2, is obtained by substituting (3.13) in (3.12). We get:

$$Z_3(K) = -\frac{E}{N_f}\mathrm{div}\left\{\sum_{n=1}^{\infty}(Z_K K)^n \Pi_K^{(n+1)}(p^2,\epsilon)\right\}. \tag{3.78}$$

The calculation of Π_K is mainly carried out by referring to S_K in (3.46) and using (3.77). However, one also needs to carefully take into account the difference due to the algebra of the γ-matrices. We find:

$$\Pi_K^{(n)}(p^2,\epsilon) = (-1)^{n-1}\frac{3}{4(d-1)n\epsilon^{n-1}}\pi_K(p^2,\epsilon,n), \tag{3.79}$$

where $\pi_K(p^2,\epsilon,n)$ can be expanded as

$$\pi_K(p^2,\epsilon,n) = \sum_{j=0}^{\infty}\pi_K^{(j)}(p^2,\epsilon)(n\epsilon)^j, \tag{3.80}$$

with $\pi_K^{(j)}(p^2,\epsilon)$ regular for $\epsilon\to 0$. Recalling that $Z_K = \left(1-\frac{1}{\epsilon}K\right)^{-1} + \mathcal{O}(1/N_f)$, we can evaluate $Z_3(K)$ from (3.78):

$$\begin{aligned} Z_3(K) &= -\frac{E}{N_f}\mathrm{div}\left\{\sum_{n=1}^{\infty}K^n\sum_{i=0}^{n-1}\binom{n-1}{i}\frac{1}{\epsilon^i}\Pi_K^{(n-i+1)}(p^2,\epsilon)\right\} \\ &= -\frac{3E}{4N_f}\frac{1}{\epsilon}\int_0^K\frac{\pi_K^{(0)}(t)}{t-3}\left(1-\frac{t}{K}\right)\mathrm{d}t + \text{higher poles}. \end{aligned} \tag{3.81}$$

The function $\pi_K^{(0)}$ is independent of p^2, as it should and reads

$$\pi_K^{(0)}(t) = \frac{(t-2)(t-1)\Gamma(5-t)}{6\Gamma(3-\frac{t}{2})^2\pi t}\sin\left(\frac{\pi t}{2}\right). \tag{3.82}$$

The contribution of $Z_3(K)$ to β_E, Eq. (3.8), is encoded in $F_4^{(1)}(K)$ and after some simplification is found to be

$$\boxed{F_4^{(1)}(K) = \frac{3}{4}\int_0^K\frac{\pi_K^{(0)}(t)}{t-3}\mathrm{d}t \equiv \frac{3}{4}\int_0^K\pi_K(t)\mathrm{d}t.} \tag{3.83}$$

We show the function $\pi_K(t)\equiv\pi_K^{(0)}(t)/(t-3)$ in Fig. 3.6. Since $\pi_K(t)$ has a first order pole at $t=3$, the first singularity of β_E occurs at $K=3$ and is a logarithmic one.

Let us now consider the **gauge contribution** to the yukawa β-function. The $U(1)$ contributions to the fermion self-energy and to the yukawa vertex, correspoding to right diagrams of Fig. 3.4 (a-b), are closely related to the pure-yukawa case. The crucial point

here is again that the gauge chain is equivalent to the yukawa chain besides an overall factor, (3.77). In fact, $\Sigma_E^{(n)}$ and $V_E^{(n)}$ are related to $\Sigma_K^{(n)}$ and $V_K^{(n)}$ as

$$\Sigma_E^{(n)}(\not{p}) = (d-2)\left(\frac{d-2}{d-1}\right)^{n-1}\Sigma_K^{(n)}(\not{p}), \tag{3.84}$$

$$V_E^{(n)}(p^2) = -d\left(\frac{d-2}{d-1}\right)^{n-1}V_K^{(n)}(p^2), \tag{3.85}$$

where the factors $(d-2)$ and $-d$ come from the algebra of the γ-matrices. We thus find something very similar to (3.45) and (3.40):

$$Z_f(E) = -\frac{1}{N_f}\sum_{n=1}^{\infty}\mathrm{div}\left\{(Z_E E)^n \Sigma_E^{(n)}(p^2,\epsilon)\right\} = -\frac{1}{N_f}\frac{3}{4\epsilon}\int_0^{\frac{2}{3}E}\sigma_E^{(0)}(t)\mathrm{d}t, \tag{3.86}$$

$$Z_V(E) = -\frac{1}{N_f}\sum_{n=1}^{\infty}\mathrm{div}\left\{(Z_E E)^n V_E^{(n)}(p^2,\epsilon)\right\} = -\frac{1}{N_f}\frac{3}{\epsilon}\int_0^{\frac{2}{3}E}v_E^{(0)}(t)\mathrm{d}t, \tag{3.87}$$

where we kept only the $1/\epsilon$ pole. The functions $\sigma_E^{(0)}$ and $v_E^{(0)}$ are independent of p^2, and are given by

$$\sigma_E^{(0)}(t) = \frac{2\Gamma(4-t)}{3\pi\Gamma\left(1-\frac{t}{2}\right)\Gamma\left(3-\frac{t}{2}\right)t}\sin\left(\frac{\pi t}{2}\right), \tag{3.88}$$

$$v_E^{(0)}(t) = \left(\frac{1-\frac{t}{4}}{1-\frac{t}{2}}\right)^2\sigma_E^{(0)}(t). \tag{3.89}$$

The $U(1)$ contribution to the scalar self-energy is shown in the lower row of Fig. 3.3. The calculation and resummation is analogous to the one performed for S_K starting from (3.46). Jumping to the result, we find for Z_S:

$$Z_S(E) = \frac{3K}{\epsilon\, N_f}\left\{\frac{3}{2E}\int_0^{\frac{2}{3}E}\left(\xi_E^{(0)}(t)-\xi_E^{(0)}(0)\right)\mathrm{d}t + \int_0^{\frac{2}{3}E}\frac{\xi_E(t)-\xi_E^{(0)}(t)}{t}\mathrm{d}t\right\}. \tag{3.90}$$

The analog of (3.59) is

$$\xi_E(p^2,t,0) = -2v_E^{(0)}(t) + \frac{1}{2}\sigma_E^{(0)}(t) \equiv \xi_E(t). \tag{3.91}$$

Defining $\tilde{\xi}_E(t) \equiv (\xi_E(t) - \xi_E^{(0)}(t))/t$, the functions $\xi_E(t)$ and $\tilde{\xi}_E(t)$ are explicitly given by

$$\xi_E(t) = -\frac{2(t-3)^2\Gamma(2-t)}{3\Gamma\left(2-\frac{t}{2}\right)\Gamma\left(3-\frac{t}{2}\right)\pi t}\sin\left(\frac{\pi t}{2}\right), \tag{3.92}$$

$$\tilde{\xi}_E(t) = \frac{1}{6}(5+2t-t^2)\xi_E(t). \tag{3.93}$$

With Eqs (3.86), (3.87) and (3.90) at hand, we can compute the $U(1)$ contribution to the yukawa β-function. This results in $F_2^{(1)}(K,E)$ given by:

$$\boxed{F_2^{(1)}(K,E) = -3\left\{\int_0^{\frac{2}{3}E}\tilde{\xi}_E(t)\mathrm{d}t + \frac{3}{2} + \left(1-\frac{2E}{3K}\right)\xi_E\left(\frac{2}{3}E\right)\right\}.} \tag{3.94}$$

We plot the function $\xi_E(t)$ in Fig. 3.6, whereas $\tilde{\xi}_E(t)$ is related to it as in (3.93).

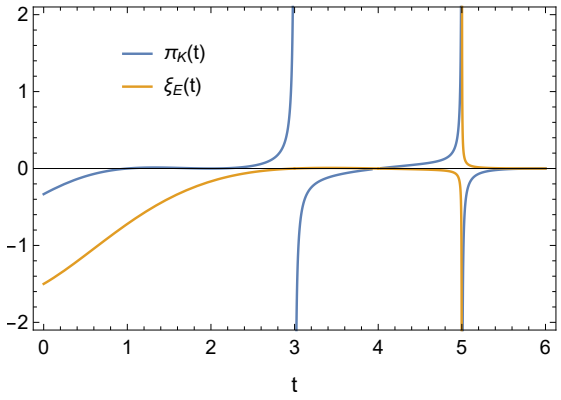

Figure 3.6: The function $\pi_K(t) \equiv \pi_K^{(0)}(t)/(t-3)$ as in (3.82) and $\xi_E(t)$ given in (3.92).

3.3.2 Coupled system

Here we summarize and discuss our results for the coupled system. Combining Eqs (3.70) and (3.71) with the results in Eqs (3.83) and (3.94), we obtain the full system at $\mathcal{O}(1/N_f)$:

$$\frac{\beta_K}{K^2} = 1 - \frac{3}{N_f}\left\{1 - \frac{1}{3}\int_0^K \xi_K(t)\mathrm{d}t + \int_0^{\frac{2}{3}E} \tilde{\xi}_E(t)\mathrm{d}t + \left(1 - \frac{2E}{3K}\right)\xi_E\left(\frac{2}{3}E\right)\right\}, \tag{3.95}$$

$$\frac{\beta_E}{E^2} = \frac{2}{3} + \frac{1}{4N_f}\left\{\int_0^{\frac{2}{3}E} \pi_E(t)\mathrm{d}t + 3\int_0^K \pi_K(t)\mathrm{d}t\right\}. \tag{3.96}$$

The functions $\xi_K(t)$ and $\pi_E(t)$ are given in (3.68) and (3.72), respectively, whereas $\pi_K(t) \equiv \pi_K^{(0)}(t)/(t-3)$, $\xi_E(t)$, $\tilde{\xi}_E(t)$ are given in (3.82), (3.92) and (3.93), respectively.

It is possible to make connection between our system of large-N_f β-functions and standard perturbation theory by simply expanding the closed forms of β_K and β_E around the Gaussian fixed point $(K = 0, E = 0)$ that corresponds to the free theory. By doing so, one can obtain the leading-N_f coefficients of the standard perturbative series. The explicit formulas can be found in Sec. B.2.1 up to five-loop. These expansions allow us to compare our findings with known results in standard perturbation theory and also to predict new coefficients that may serve themselves as a crosscheck for future perturbative calculations.

We have made sure that our expansions agree with the four-loop results [97,110–113] in the leading order in N_f. Furthermore, the $-\frac{2E}{3K}\xi_E\left(\frac{2}{3}E\right)$ part in the last term of (3.95) corresponds to the result of Refs [106,107], and we have checked that our result agrees with those. Going beyond four-loop, it is of course impossible for us to predict the full five-loop β-function, as our calculation captures only the leading $1/N_f$ terms. Nonetheless, we provide the leading new coefficients at five-loop in the last line of (B.7) and (B.8); higher orders can be obtained just by further expanding the closed forms of the β-functions above.

Let us now comment on the radius of convergence for β_K and β_E. This is simply defined as the maximum value of the coupling that one can reach without running into singularities. The first singularity of the pure-$U(1)$ β-function is located at $E = 15/2$, whereas for the pure-yukawa case it occurs at $K = 5$. These singularities are now accompanied by the ones from the mixed contributions that arise at $K = 3$ for β_E and at

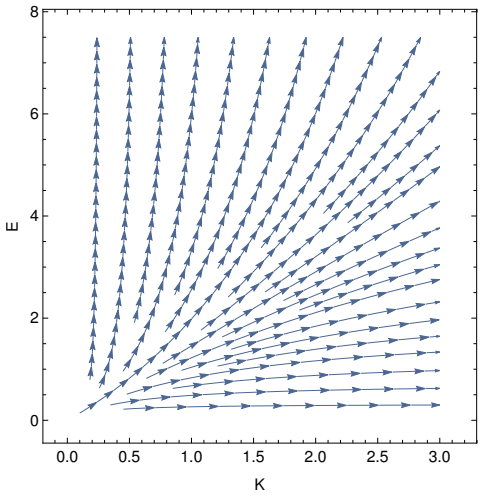

Figure 3.7: The flow diagram for the coupled system with $N_f = 30$ in $d = 4$. The arrows point towards UV.

$E = 15/2$ for β_K. The RG flow is shown in Fig. 3.7. The boundaries are dictated by the radius of convergence. As we can see, both couplings increase towards the UV, suggesting the presence of a Landau pole. Actually, if the singularities near the boundaries were to be taken seriously, the β functions would approach a fixed point exponentially close to the boundaries of our flow at $(K^*, E^*) = (0, 15/2)$, which is the only point in which both β-functions vanish due to the effect of the singularities. However, this possibility will turn out to be disfavored by our analysis in Sec. 3.5, where a more careful way of dealing with these large-N_f singularities is presented.

3.4 Relation to critical exponents

From the high-energy physics point of view, our original motivation to look into the large-N_f β-functions was being able to treat systems with many fermionic degrees of freedom, as those inspired by UV completions of Froggatt-Nielsen-like models. This was also motivated as part of a larger program aiming to investigate the UV fate of gauge-yukawa theories, with the goal of discovering more examples of asymptotic safety in four dimensions.

In this section, which is mainly based on Ref. [IV], we will instead discuss how all of this is actually intimately related to the infrared (IR) properties of the theory and relevant for condensed matter physics. To do so, one needs to move slightly away from $d = 4$ (and not only for the purpose of dimensional regularization). In fact, alternatively to explicit bubble resummation, the large-N_f β-functions can be calculated by evaluating the critical exponents at the Wilson–Fisher (WF) fixed point in arbitrary dimension for theories in the same universality class— see e.g. Refs [103, 109, 114–126] and Ref. [127] for a recent review.

To sketch how this works, let us consider a theory with only one relevant coupling, $g > 0$ (for QED, $g \sim \alpha$). The β-function in d dimensions is given by

$$\beta(g) = (d - d_c)g + a_1 g^2 + a_2 g^3 + \dots, \tag{3.97}$$

where d_c is the critical dimension (for QED, $d_c = 4$). Let us assume $a_1 > 0$, corresponding to a theory for which asymptotic freedom is lost. Perturbing around d_c, $d = d_c - \epsilon$, one obtains the WF fixed-point by balancing the first term against the others (as opposed to Banks-Zaks fixed points, where one-loop is balanced against two-loop). Requiring $\beta(g_c) = 0$, one can obtain g_c within the ϵ-expansion:

$$g_c = \frac{\epsilon}{a_1} + \mathcal{O}(\epsilon^2). \tag{3.98}$$

Fixed points in a quantum field theory define universality classes and often describe phase transitions in the real world. During a phase transition, the correlation length diverges and all physical quantities show a power-law behavior. The system can thus be described by the corresponding critical exponents, containing information about the classical scaling plus quantum corrections. Particularly relevant for us is the exponent ω that is related to the β-function as

$$\omega(d) = \beta'(g_c). \tag{3.99}$$

Physically, the exponent ω represents the leading correction to the scaling exponent ν that controls the correlation length ξ,

$$\xi \sim |x|^{-\nu}(1 + C|x|^{\omega} + \dots), \tag{3.100}$$

where $x = (\chi - \chi_c)/\chi_c$ measures how close the system is to criticality. It is worth mentioning that, at the WF fixed point, the only variable is indeed the dimension d as the coupling g_c has been traded for the dimensionality in (3.98) (recall that $d = d_c - \epsilon$). This is clearly reminescent of our resummation procedure, where the parameter ϵ in the various loop functions was eventually traded for the coupling— see discussion below (3.40)!

Working out the QFT at the WF fixed point has its advantages, as for instance all propagators have power-law behavior. In particular, the large-N_f critical-point method developed by Vasiliev et al. and Gracey (see references above) exploits the conformal properties of the theory at the WF fixed point and allows to calculate $\omega(d)$ as an expansion in $1/N_f$,

$$\omega(d) \equiv \sum_{n=0}^{\infty} \frac{\omega^{(n)}(d)}{N_f^n}. \tag{3.101}$$

The connection among these results and the large-N_f β-functions we are interested in is simply contained in (3.99). This has been actually known for long time, and the QCD β-function was indeed obtained in Ref. [104] by using the exponent ω from Ref. [103]. In fact, direct resummation becomes infeasible already at $\mathcal{O}(1/N_f)$ for non-abelian gauge theories due to diagrams with the simultaneous presence of two distinct bubble chains which do not allow for explicit resummation. This is the actual reason why higher orders in the $1/N$ expansions are in general difficult to obtain, and the few known results are in fact based on the corresponding critical exponents which are more powerful in this respect. Notice also that the calculation in Ref. [103] is not performed for QCD directly, but rather within the non-abelian Thirring model, which is in the same universality class of QCD in the large-N_f limit.

However, a systematic and general analysis of how to connect critical exponents and β-functions was missing, and most of the high-energy community was not aware of this.

Moreover, it was unclear whether this connection could be used in the same way as Ref. [104] to calculate the system of β-functions for multi-coupling systems (the answer will be negative, as we shall see shortly). In the following, we will systematically state the interplay between the critical-point method and bubble resummation in one-coupling models and extend these considerations to multi-coupling theories. By doing so, we will also go back to the system in (3.4) and include the missing $\lambda\phi^4$ term in Sec. 3.4.2. What follows is mainly taken from [IV], whereas some results in Sec. 3.4.3 are new.

3.4.1 One-coupling model

In this section, we discuss the general ansatz for the β-function in the large-N_f expansion for any system with one coupling, g. Our goal is to derive a general form for the β-function once the critical exponent $\omega = \beta'(g_c)$ is known. The ansatz for the β-function is:

$$\beta(g) \equiv (d - d_c)g + g^2 \left(bN_f + c + \sum_{n=1}^{\infty} \frac{F^{(n)}(gN_f)}{N_f^{n-1}} \right), \tag{3.102}$$

where d is the space-time dimension, d_c the critical dimension, b and c are model-dependent one-loop coefficients, and $F^{(n)}$ are the resummed functions we are interested in, all satisfying $F^{(n)}(0) = 0$ by definition.

This ansatz is conceptually the same as (3.2) but this new definition is more convenient for our purpose here. First, we need to find the position of the WF fixed point: setting $\beta(g_c) = 0$, we find an implicit expression for the critical coupling

$$g_c = -\frac{d - d_c}{bN_f + c + \sum_{n=1}^{\infty} \frac{F^{(n)}(g_c N_f)}{N_f^{n-1}}}. \tag{3.103}$$

The slope of the β-function at criticality can then be expanded in $1/N_f$ to yield

$$\begin{aligned} \beta'(g_c) = &-(d - d_c) + \frac{(d - d_c)^2}{b^2} \sum_{m=1}^{\infty} \frac{F^{(n)\prime}(g_c N_f)}{N_f^m} \\ &\times \sum_{k=0}^{\infty} (-b)^{-k}(k+1) \left(\frac{c}{N_f} + \sum_{n=1}^{\infty} \frac{F^{(n)}(g_c N_f)}{N_f^n} \right)^k \overset{!}{=} \sum_{n=0}^{\infty} \frac{\omega^{(n)}(d)}{N_f^n}, \end{aligned} \tag{3.104}$$

where we have used (3.99) for the last equality and the primed functions are understood as derivatives. Thus, by using Eqs (3.104) and (3.103), we can relate the functions $F^{(n)}$ to $\omega^{(n)}$. To obtain the result in a closed form, it is necessary to compute g_c order by order in $1/N_f$ according to (3.103). This, in turn, enters the argument of the functions $F^{(n)}$, which then need to be Taylor-expanded to include all the relevant contributions.

This analysis makes clear that the various $F^{(n)}$ functions for one-coupling models can be fully reconstructed if the critical exponent $\omega^{(n)}$ as a function of d is known at the same order in the $1/N_f$ expansion, the dictionary being provided by (3.103) and (3.104). In the following, we will give explicitly the first two orders. At $\mathcal{O}(1/N_f)$, we obtain

$$\frac{(d - d_c)^2}{b^2} F^{(1)\prime}\left(\frac{d_c - d}{b} \right) = \omega^{(1)}(d), \tag{3.105}$$

which, defining $t \equiv (d_c - d)/b$, results in ($x = gN_f$)

$$F^{(1)}(x) = \int_0^x \mathrm{d}t \frac{\omega^{(1)}\,(d_c - bt)}{t^2}. \tag{3.106}$$

At $\mathcal{O}(1/N_f^2)$, the expansion of (3.104) gives

$$F^{(2)}(x) = \int_0^x \mathrm{d}t \left(\frac{c + F^{(1)}(t)}{b} (tF^{(1)\prime\prime}(t) + 2F^{(1)\prime}(t)) + \frac{\omega^{(2)}\,(d_c - bt)}{t^2} \right). \tag{3.107}$$

Note that the critical exponent $\omega^{(1)}$ contributes to the β-function also beyond $\mathcal{O}(1/N_f)$ through $F^{(1)}$ and its derivatives, as can be seen explicitly in (3.107). The same structure is found at higher orders: $F^{(n)}$ receives contributions from $\omega^{(n-1)}, \ldots, \omega^{(1)}$—or, equivalently, from $F^{(n-1)}, \ldots, F^{(1)}$—and their derivatives, together with a pure $\omega^{(n)}$-term as in (3.107). Therefore, if $F^{(1)}$ has a singularity say at $x = x_s$, it will propagate to $F^{(n)}$ with a stronger degree of divergence up to the n-th derivative of $F^{(1)}$. However, the very fact that this illustrative singularity at $x = x_s$ would appear at any order in the $1/N_f$-expansion at the same coupling value suggests that a resummation could exist such that the β-function is regular at x_s, as we shall see in Sec. 3.5.

In what follows, we apply our findings for $F^{(1)}$ and $F^{(2)}$ to the Gross-Neveu model, extending previous studies on the possible appearance of an IR fixed point.

Gross–Neveu model in $d = 2$

As a prime example, we consider the Gross–Neveu (GN) model [128]. This is a benchmark model for studying asymptotic freedom and chiral-symmetry breaking in a simpler environment with respect to QCD. It has only one relevant coupling and the Lagrangian is given by

$$\mathcal{L}_{\mathrm{GN}} = i\bar{\psi}\partial\!\!\!/\psi + \frac{g}{2}(\bar{\psi}\psi)^2, \tag{3.108}$$

where ψ is a fermion multiplet containing N_f flavors. Usually, the Lagrangian above is rewritten with help of an auxiliary field ϕ that is non dynamical and only acts as a Lagrange multiplier:

$$\mathcal{L}_{\mathrm{GN}} = i\bar{\psi}\partial\!\!\!/\psi + \phi\bar{\psi}\psi + \frac{1}{2g}\phi^2. \tag{3.109}$$

Integrating out ϕ gives back (3.108). The advantage is that the four-fermion interaction has now been turned into a yukawa coupling. The form in (3.109) is useful to make contact with the next section. The critical exponents for this model have been extensively studied; see e.g. Refs [119, 122, 124, 125].

Recently, the possibility of an IR fixed point in the GN model at $d = 2$ was studied in Ref. [129] using the perturbative four-loop result [130] with Padé approximants. On the other hand, the presence of an IR fixed point in the large-N_f limit has already been excluded taking the $\mathcal{O}(1/N_f)$ contributions into account [131].

Here, we extend the analysis to $\mathcal{O}(1/N_f^2)$ by using the results of the previous section and the known results for $\omega(d)$ which is currently available up to $\mathcal{O}(1/N_f^2)$ [124]. By doing so, we will also predict new coefficients for the perturbative expansion that can be used as crosschecks for future calculations. The $\mathcal{O}(1/N_f)$ exponent, $\omega^{(1)}$, is explicitly given by

$$\omega^{(1)}(t) = \frac{4t\Gamma(t+2)\sin(\pi t/2)}{\pi(t+2)\Gamma(t/2+1)^2}, \tag{3.110}$$

while the expression for $\omega^{(2)}(t)$ is relatively lengthy and can be explicitly found in Ref. [124] (where it is called λ). Referring to (3.102), the GN model is characterized by $d_c = 2$, $b = -1$ and $c = 2$. For $N_f = 2$, the GN model turns out to be equivalent to the abelian Thirring model [132], and thus the β-function identically vanishes [133,134]; we can therefore implement this additional information already at the ansatz level, and improve our original form in (3.102) as:

$$\beta(g) = (d-2)g + (N_f - 2)g^2 \left(-1 + \frac{\tilde{F}^{(1)}(gN_f)}{N_f} + \frac{\tilde{F}^{(2)}(gN_f)}{N_f^2} + \dots \right), \tag{3.111}$$

where

$$\tilde{F}^{(1)}(x) = \int_0^x \frac{\omega^{(1)}(t)}{t^2} \mathrm{d}t \tag{3.112}$$

and

$$\tilde{F}^{(2)}(x) = \int_0^x \left\{ \frac{-2\omega^{(2)}(t) + 4\omega^{(1)}(t) + 4\omega^{(1)}(t)F^{(1)}(t)}{t^2} - t[2 + F^{(1)}(t)]F^{(1)\prime\prime}(t) \right\} \mathrm{d}t. \tag{3.113}$$

The functions $\tilde{F}^{(1),(2)}$ are related to $F^{(1),(2)}$ of the standard ansatz as $\tilde{F}^{(1)} = F^{(1)}$ and $\tilde{F}^{(2)} = F^{(2)} + 2F^{(1)}$, so that the two ansätze only differ at $\mathcal{O}(1/N_f^3)$. On the other hand, the β-function for the GN model is known perturbatively up to four-loop level [130]:

$$\begin{aligned} \beta_{4\mathrm{L}}(g) =& (d-2)g - (N_f - 2)g^2 + (N_f - 2)g^3 \\ &+ \frac{1}{4}(N_f - 2)(N_f - 7)g^4 \\ &- \frac{1}{12}(N_f - 2)\left[N_f^2 + (66\zeta_3 + 19)N_f - 204\zeta_3 - 48\right] g^5. \end{aligned} \tag{3.114}$$

We find that the improved ansatz, (3.111), additionally reproduces the first subleading $1/N_f^3$ terms, in particular providing the correct three-loop coefficient [4]. Furthermore, the prediction for the leading orders in N_f for the five-loop β-function based on (3.112) and (3.113) is

$$\beta_{5\mathrm{L}}(g) = \frac{1}{96}(N_f - 2)\left[(3 - 6\zeta_3)N_f^3 + (297\zeta_4 + 120\zeta_3 + 1)N_f^2 + \dots\right] g^6. \tag{3.115}$$

We show the β-function of (3.111) truncated to $\mathcal{O}(1/N_f)$, $\beta_{1/N}$, and to $\mathcal{O}(1/N_f^2)$, β_{1/N^2}, along with the four-loop perturbative result in Fig. 3.8 as a function of the rescaled coupling $x = gN_f$ for $N_f = 10$ (left) and $N_f = 15$ (right). We conclude that there is no clear hint for the IR fixed point at intermediate N_f in the region where the $1/N_f$ expansion is under control.

[4] Notice that while the leading N_f coefficient is scheme independent [105], the subleading ones are not. The result obtained with the critical exponent method should be compared with perturbation theory where $\overline{\mathrm{MS}}$ dimensional regularisation is employed.

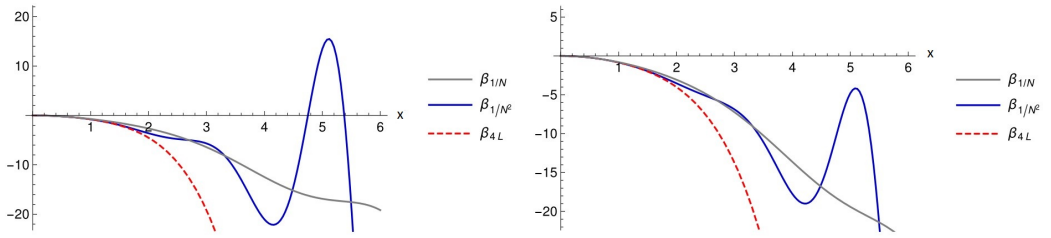

Figure 3.8: The β-function of (3.111) truncated to $\mathcal{O}(1/N_f)$, $\beta_{1/N}$, and to $\mathcal{O}(1/N_f^2)$, β_{1/N^2} along with the four-loop perturbative result, $\beta_{4\mathrm{L}}$, as a function of the rescaled coupling $x = gN_f$ for $N_f = 10$ (left) and $N_f = 15$ (right).

3.4.2 Two-coupling model: Gross–Neveu–Yukawa

We will consider here a two-coupling model, the Gross–Neveu–Yukawa (GNY) model [135] in $d = 4$, that will be defined shortly. The main message of this section is that, conversely to the one-coupling case, the knowledge of the critical exponent ω is not sufficient to reconstruct the β-function of the system for models with two or more couplings. In order to obtain the β-functions we will have to rely again on explicit bubble-resummation.

The GNY model is the bosonised GN model in (3.109) with the auxiliary scalar field ϕ promoted to a dynamical degree of freedom. It thus describes N massless fermion flavors, ψ, coupling to a massless real scalar, ϕ, via yukawa interaction

$$\mathcal{L}_{\mathrm{GNY}} = \bar{\psi}\mathrm{i}\partial\!\!\!/\psi + \frac{1}{2}\partial_\mu\phi\partial^\mu\phi + g_1\phi\bar{\psi}\psi + g_2\phi^4. \tag{3.116}$$

It is a good moment to compare the GNY model above with our prototype in (3.4). In fact, the system in (3.4) is well known in condensed matter theory and it is referred to as the QED$_3$-GNY model. The reason is simply that it differs from GNY for the fermions being charged under a gauged $U(1)$. For the QED$_3$-GNY model the critical exponents have not yet been determined at $\mathcal{O}(1/N_f)$. Actually, the closest attempt turns out to be our result for the system of β-functions in Sec. 3.3, as in fact one could obtain the critical exponents just by reversing the logic in the relation $\beta'(g_c) = \omega(d)$. However, the quartic coupling has been neglected in our analysis in Sec. 3.3, meaning that our knowledge of the system of β-functions is still incomplete. In the following, we will focus on the GNY model, restoring a non-zero quartic coupling in (3.4), but neglecting the gauge interactions. Although more missing pieces will be uncovered at the end of this section, the results presented here are still not enough to calculate the system of β-functions for QED$_3$-GNY [5]. Completing this task is desirable and left for future work.

Going back to the GNY in (3.116), the critical exponents were recently computed up to $1/N_f^2$ [109,126], and on the other hand, they are known perturbatively up to four-loop level [108, 136]. This is thus the right model to carry on our discussion about the relation between critical exponents and β-functions beyond one-coupling. We follow the notations of Refs [108,136] in order to provide for a straight-forward comparison with the perturbative result and define rescaled couplings

$$y \equiv \frac{g_1^2\mu^\epsilon}{8\pi^2}, \quad K \equiv 2yN_f, \quad \text{and} \quad \lambda \equiv \frac{g_2\mu^\epsilon}{8\pi^2}. \tag{3.117}$$

[5] We will nevertheless comment on the possibility of extracting the QED$_3$-GNY critical exponents later on.

The critical dimension is $d_c = 4$ and we will work in $d = 4 - \epsilon$ dimensions. The yukawa β-function at $\mathcal{O}(1/N_f)$ depends only on the yukawa coupling, y:

$$\beta_y = (d - d_c)y + y^2(2N_f + 3 + \varphi_1^{(1)}(yN_f)). \tag{3.118}$$

Notice that $\varphi_1^{(1)}$ corresponds to the pure yukawa contribution to the yukawa β-function, and we have already calculated it in Sec. 3.2. As we shall see, $\varphi_1^{(1)}$ can be determined independently with the help of the GNY critical exponents, thus providing a non-trivial crosscheck of our calculation.

Conversely, the β-function for the quartic coupling, λ, at $\mathcal{O}(1/N_f)$ is

$$\beta_\lambda = (d - d_c)\lambda + y^2(-N_f + \varphi_2^{(1)}(yN_f)) + \lambda^2(36 + \varphi_3^{(1)}(yN_f)) + y\lambda(4N_f + \varphi_4^{(1)}(yN_f)). \tag{3.119}$$

According to Eqs (3.118) and (3.119), the coupled system of β-functions at $\mathcal{O}(1/N_f)$ contains four unknown functions, namely $\varphi_1^{(1)}$, $\varphi_2^{(1)}$, $\varphi_3^{(1)}$ and $\varphi_4^{(1)}$. Note that $\varphi_{1-4}^{(1)}$ are functions of the rescaled yukawa coupling only due to the $1/N_f$ counting. Diagrammatically this corresponds to chain of fermion bubbles. Similar diagrams of scalar bubbles lack the N_f enhancement, and these chains are subleading.

Because of the two-coupling system, the GNY critical exponents $\omega_\pm$ are the eigenvalues of the Jacobian of the β-functions evaluated at the WF fixed point:

$$J_{(y,\lambda)}(\beta_y, \beta_\lambda) = \left(\begin{array}{cc} \partial_y\beta_y & \partial_y\beta_\lambda \\ \partial_\lambda\beta_y & \partial_\lambda\beta_\lambda \end{array} \right)\Big|_{\mathrm{WF}} = \left(\begin{array}{cc} \partial_y\beta_y & \partial_y\beta_\lambda \\ 0 & \partial_\lambda\beta_\lambda \end{array} \right)\Big|_{\mathrm{WF}}, \tag{3.120}$$

where we have noticed that β_y in (3.118) does not depend on λ at $\mathcal{O}(1/N)$. This means that at the WF fixed point one simply has

$$\partial_y\beta_y = \omega_-, \quad \partial_\lambda\beta_\lambda = \omega_+. \tag{3.121}$$

In order to gain information on $\varphi_{1-4}^{(1)}$ exploiting the knowledge of $\omega_\pm$ we need to determine the couplings at the WF fixed point, namely we have to solve $\beta_{y,\lambda} = 0$. Using $d - d_c = -\epsilon$, we find

$$y^c = \frac{\epsilon}{2N_f + 3 + \varphi_1^{(1)}(y^cN_f)}, \quad \lambda^c = \frac{\epsilon - y^c\left(4N_f + \varphi_4^{(1)}(y^cN_f)\right) + \sqrt{\Delta^c}}{2\left(36 + \varphi_3^{(1)}(y^cN_f)\right)}, \tag{3.122}$$

where we have taken the positive solution for λ^c and defined

$$\Delta^c \equiv \left[-\epsilon + y^c(4N_f + \varphi_4^{(1)}(y^cN_f))\right]^2 - 4\left(36 + \varphi_3^{(1)}(y^cN_f)\right)(y^c)^2\left(-N_f + \varphi_2^{(1)}(y^cN_f)\right). \tag{3.123}$$

Up to leading order in $1/N_f$, we have

$$y^c = \frac{\epsilon}{2N_f} + \mathcal{O}(1/N_f^2), \quad \lambda^c = \frac{\epsilon}{4N_f} + \mathcal{O}(1/N_f^2). \tag{3.124}$$

Now we are ready to evaluate (3.121) at criticality by using (3.122) (notice that using (3.124) is not enough):

$$\frac{\partial\beta_y}{\partial y} = \epsilon + \frac{1}{4N_f}\epsilon^2\varphi_1^{(1)\prime}(\epsilon/2) \stackrel{!}{=} \epsilon + \frac{1}{N_f}\tilde{\omega}_-^{(1)}(\epsilon), \tag{3.125}$$

$$\frac{\partial\beta_\lambda}{\partial\lambda} = \epsilon + \frac{\epsilon}{2N_f}\left(30 - 2\varphi_1^{(1)}(\epsilon/2) + \varphi_3^{(1)}(\epsilon/2) + \varphi_4^{(1)}(\epsilon/2)\right) \stackrel{!}{=} \epsilon + \frac{1}{N_f}\tilde{\omega}_+^{(1)}(\epsilon). \tag{3.126}$$

where we have defined $\tilde{\omega}_\pm^{(1)}(\epsilon) \equiv \omega_\pm^{(1)}(4-\epsilon)$ for simplicity. As we can see, (3.125) completely fixes $\varphi_1^{(1)}(t)$ which is readily found to be

$$\varphi_1^{(1)}(t) = \int_0^t \frac{\tilde{\omega}_-^{(1)}(2\epsilon)}{\epsilon^2}\mathrm{d}\epsilon. \tag{3.127}$$

The explicit form of $\tilde{\omega}_\pm$ is [109, 126]

$$\tilde{\omega}_-^{(1)}(t) = -\frac{t\Gamma(4-t)}{\pi\Gamma\left(2-\frac{t}{2}\right)\Gamma\left(3-\frac{t}{2}\right)}\sin\left(\frac{\pi t}{2}\right), \tag{3.128}$$

$$\tilde{\omega}_+^{(1)}(t) = \frac{3t-10}{t}\tilde{\omega}_-^{(1)}(t). \tag{3.129}$$

As mentioned above, $\varphi_1^{(1)}(t)$ in (3.125) is closely related to $F_1^{(1)}(K)$ in (3.69). We have checked that our result achieved with direct bubble resummation matches the one following from the critical point method. In particular, with respect to (3.69) one simply has

$$\xi_K(x) = \frac{\tilde{\omega}_-^{(1)}(x)}{x^2}. \tag{3.130}$$

Actually, we could have obtained $F_1^{(1)}$ directly this way rather than going through the calculation in Sec. 3.2. However, the direct resummation provided us with the necessary ingredients (namely, the renormalization constants) to tackle the mixed gauge contributions in Sec. 3.3, for which there is no critical exponent available. The same counterterms will be crucial also for the calculation at the end of this section, as we shall see.

Considering (3.126), one finds

$$30 - 2\varphi_1^{(1)}(\epsilon/2) + \varphi_3^{(1)}(\epsilon/2) + \varphi_4^{(1)}(\epsilon/2) = 2\frac{\tilde{\omega}_+^{(1)}(\epsilon)}{\epsilon}. \tag{3.131}$$

As we can see, β_λ cannot be computed with the knowledge of $\omega_\pm$, since only the combination $\varphi_3^{(1)} + \varphi_4^{(1)}$ can be accessed. In particular, $\varphi_2^{(1)}$ is fully unconstrained.

This shows that the critical exponents encoding the slope of the β-function can fully determine the β-function only for single-coupling theory, while for multi-coupling theory they are sensitive only to certain combinations. Notice that the problem is not the discrepancy between the number of the eigenvalues (two) and the entries of the Jacobian (four), but rather that, for multi-coupling models, the number of the possible coupling structures proliferates too fast (there are already three of them in (3.119): y^2, λ^2 and $y\lambda$). Therefore, either more information is input or one needs to rely on a direct resummation to get β_λ in a closed form. Nevertheless, the knowledge of $\omega_\pm$ can be used to obtain independent cross-checks and gain information regarding the radius of

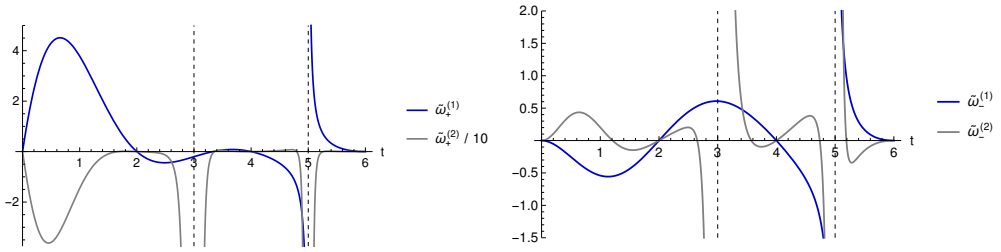

Figure 3.9: The first two coefficients of the $1/N_f$ expansion of the critical exponents $\tilde{\omega}_\pm = \sum_{n=1}^{\infty} \tilde{\omega}_\pm^{(n)}/N_f^n$. The explicit formulae for the $\mathcal{O}(1/N_f^2)$ coeffiecients can be found in Ref. [126].

convergence of the $1/N_f$ expansion. We show the critical exponents $\tilde{\omega}_\pm^{(1)}(t)$ along with the $\mathcal{O}(1/N_f^2)$ results [126], $\tilde{\omega}_\pm^{(2)}(t)$, in Fig. 3.9. The $\mathcal{O}(1/N_f^2)$ results indicate that there is a new singularity not present at $\mathcal{O}(1/N_f)$ occurring at $t = 3$. Correspondingly, this would suggest a shrinking in the radius of convergence for the β-functions when higher orders are included. However, as we will see shortly, this singularity is actually already present at $\mathcal{O}(1/N_f)$, namely in the functions $\varphi_{2,3,4}^{(1)}$, but it exactly cancels in $\tilde{\omega}_+^{(1)}$, (3.131)!

Going beyond $\mathcal{O}(1/N_f)$ the sitution gets worse as the system of β-functions at $\mathcal{O}(1/N_f^2)$ contains seven more unknowns. The knowledge of $\omega_\pm$ at $\mathcal{O}(1/N_f^2)$, $\omega_\pm^{(2)}$, can only constrain two linear combinations of them, similarly to (3.131)— see Appendix A in Ref. [IV] for the explicit formulas.

Bubble resummation

The knowledge of the critical exponent ω_- at $\mathcal{O}(1/N_f)$ is enough to obtain the explicit form of β_y in (3.118) at the same order in $1/N_f$. This is not the case for β_λ in (3.119), as the information contained in ω_+ can only constrain a linear combination of $\varphi_1^{(1)}$, $\varphi_3^{(1)}$ and $\varphi_4^{(1)}$, see (3.131). In order to obtain β_λ at the order $1/N_f$, we have thus to rely on explicit bubble resummation.

The β-function for λ is obtained by acting with derivatives on the 1PI vertex counterterm, Z_λ, and on the scalar self-energy counterterm, Z_S. The bare coupling, λ_0, and the renormalized coupling, λ, are related via

$$\lambda_0 = Z_\lambda Z_S^{-2} \lambda, \tag{3.132}$$

and the β-function is

$$\beta_\lambda = \lambda \left(\lambda \frac{\partial}{\partial \lambda} + K \frac{\partial}{\partial K} \right) \ln \left(Z_\lambda Z_S^{-2} \right)_{1/\epsilon}. \tag{3.133}$$

The self-energy renormalization constant due to the yukawa interaction, Z_S, has been computed in Sec. 3.2 up to $\mathcal{O}(1/N_f)$, see (3.64), and needs no further calculation. However, Z_λ needs to be computed. It is obtained by solving

$$Z_\lambda = 1 - \mathrm{div}\{ Z_\lambda \Lambda_0(\lambda_0, K_0, p^2, \epsilon) \}, \tag{3.134}$$

where K_0 is the rescaled yukawa coupling, and Λ_0 contains the 1PI contributions to the four-point function. At the order $\mathcal{O}(1/N)$, we have

$$\begin{aligned}\Lambda_0 =&\lambda_0 \sum_{n=0}^{\infty} K_0^n \Lambda_\lambda^{(n+1)}(p^2,\epsilon) + \frac{1}{\lambda_0 N_f} K_0^2 \Lambda_K^{(1)}(p^2,\epsilon) + \frac{1}{\lambda_0 N_f^2} K_0^3 \sum_{n=0}^{\infty} K_0^n \Lambda_K^{(n+2)}(p^2,\epsilon) \\ &+ \frac{1}{N_f} K_0^2 \sum_{n=0}^{\infty} K_0^n L^{(n+2)}(p^2,\epsilon) + \frac{1}{\lambda_0 N_f^2} K_0^4 \sum_{n=0}^{\infty} K_0^n {\Lambda'_K}^{(n+3)}(p^2,\epsilon).\end{aligned} \tag{3.135}$$

These terms are defined via the corresponding Feynman diagrams, as explained in the following. The first term corresponds to a basic candy diagram where the yukawa couplings only enters through the chain of fermion bubbles and is depicted in Fig. 3.10. The second and third terms correspond to the basic one-loop box diagram and a box diagram with an additional internal scalar propagator, respectively, shown in Fig. 3.12. The fourth term is a candy with two different vertices, namely one λ and one effective quartic made of a fermion loop represented in Fig. 3.11. The last term is a three-loop candy diagram with two fermion loops as effective quartics, which is given in Fig. 3.13. Since we assume that λN_f is a 't Hoof coupling, we will consider $\lambda \sim 1/N_f$ to catch all possible contributions. The p^2 in the arguments refers generically to the IR regulator. We use two IR regulation strategies depending on the subclass of diagrams: For fermion-box type diagrams, we use a convenient choice of non-zero external momenta, and for the scalar-candy-type diagrams we give a non-zero regulating mass for the propagating scalars. The sum of the contributions in each of these subclasses is IR finite, justifying the different regularisations.

Notice that the candy diagrams in Figs 3.10, 3.11 and 3.13 contain double chains. This is usually a no-go for performing a direct resummation as mentioned below (3.101). Nevertheless, in case a suitable choice of external momenta allows to have the same loop momentum flowing in both chains, it is possible to treat them as to be effectively one and perform the resummation successfully, as shown in Ref. [107]. This is the main reason for choosing the IR regulator for the candy diagrams as mentioned above.

After trading the bare couplings with the renormalized couplings,

$$\lambda_0 = Z_\lambda Z_S^{-2} \lambda, \quad K_0 = Z_S^{-1} (Z_V Z_f^{-1})^2 K, \tag{3.136}$$

where $Z_{V,f} = 1 + \mathcal{O}(1/N_f)$ are the renormalisation constants for the 1PI yukawa vertex and fermion self-energy that were already calculated in (3.40) and (3.45), resp., and keeping only term that contribute up to $\mathcal{O}(1/N_f)$, we eventually find for Z_λ:

$$\begin{aligned}Z_\lambda = 1 - \mathrm{div}\Bigg\{ &\lambda Z_S^{-2} \sum_{n=0}^{\infty} (Z_S^{-1}K)^n \Lambda_\lambda^{(n+1)} + \frac{1}{N_f} K^2 Z_S^{-2} \sum_{n=0}^{\infty} (Z_S^{-1}K)^n \left(L^{(n+2)} - 2D\Lambda_\lambda^{(n+1)} \right) \\ &+ \frac{1}{\lambda N_f} K^2 (Z_V Z_F^{-1})^4 \Lambda_K^{(1)} + \frac{1}{\lambda N_f^2} K^3 Z_S^{-1} \sum_{n=0}^{\infty} (Z_S^{-1}K)^n \Lambda_K^{(n+2)} \\ &+ \frac{1}{\lambda N_f^2} K^4 Z_S^{-2} \sum_{n=0}^{\infty} (Z_S^{-1}K)^n \left(D^2 {\Lambda_\lambda}^{(n+1)} - D L^{(n+2)} + {\Lambda'_K}^{(n+3)} \right) \Bigg\},\end{aligned} \tag{3.137}$$

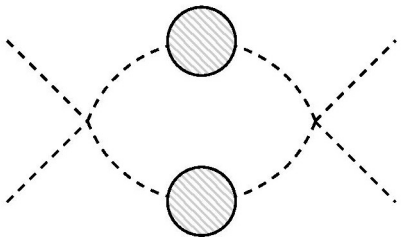

Figure 3.10: Diagram for $\varphi_3^{(1)}(yN_f)$. The gray blob represents a bubble chain.

where we have iterated (3.134) to include all the contributions up to $\mathcal{O}(1/N_f)$, and we have defined D as

$$D = \mathrm{div}\{\Lambda_K^{(1)}\}. \tag{3.138}$$

Notice that, despite the explicit $1/N_f^2$ dependence, the $1/\lambda N_f^2$ contributions are actually $\mathcal{O}(1/N_f)$ when interpreted in terms of the rescaled quartic. After taking derivatives according to (3.133), the first non-trivial term in (3.137) will give the λ^2-contribution in (3.119), namely the function $\varphi_3^{(1)}$, and the second term will give $\varphi_4^{(1)}$. All the other terms in the second and third line of (3.137) behave like $1/\lambda$ and will correspond to the pure yukawa contribution, $\varphi_2^{(1)}$.

$\varphi_3^{(1)}$, $\varphi_4^{(1)}$ and cross-check

In principle, it would be enough for us to calculate either $\varphi_3^{(1)}$ or $\varphi_4^{(1)}$, and obtain the remaining one with the help of (3.131). However, we will rather calculate both $\varphi_3^{(1)}$ and $\varphi_4^{(1)}$ and use (3.131) as a cross-check.

Diagrammatically, $\varphi_3^{(1)}$ corresponds to Fig. 3.10, where the internal scalar lines are dressed with fermion bubbles. To obtain its expression, we refer to the first non-trivial term of (3.137) and compute:

$$\begin{aligned} T_3 &\equiv -\,\mathrm{div}\left\{\lambda Z_S^{-2}\sum_{n=0}^{\infty}(Z_S^{-1}K)^n\Lambda_\lambda^{(n+1)}\right\} \\ &= -\,\mathrm{div}\left\{\lambda\sum_{n=0}^{\infty}K^n\sum_{i=0}^{n}\binom{n+1}{i}\frac{(-1)^i}{\epsilon^i}\Lambda_\lambda^{(n-i+1)}\right\} \end{aligned} \tag{3.139}$$

The function $\Lambda_\lambda^{(m)}$ is found to be

$$\Lambda_\lambda^{(m)} = \frac{1}{\epsilon^m}l(\epsilon,m) = \frac{1}{\epsilon^m}\sum_{j=0}^{\infty}(m\epsilon)^j l_j(\epsilon). \tag{3.140}$$

After resummation, and keeping only the $1/\epsilon$ pole of T_3, we find

$$T_3 = -\frac{1}{\epsilon}\lambda\, l_0(K)\ + \dots\,, \tag{3.141}$$

where

$$l_0(t) = \frac{9\cdot 2^{4-t}\Gamma\left(\frac{3}{2}-\frac{t}{2}\right)\sin\left(\frac{\pi t}{2}\right)}{\pi^{3/2}t\Gamma\left(2-\frac{t}{2}\right)}. \tag{3.142}$$

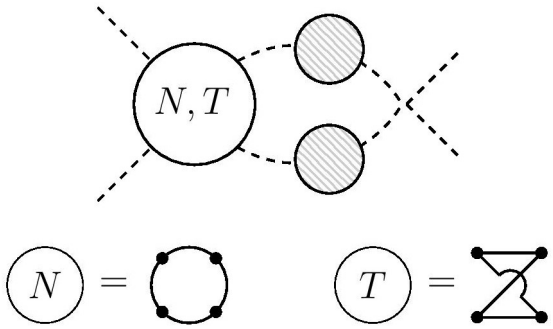

Figure 3.11: Diagram for $\varphi_4^{(1)}(yN_f)$. The gray blob represents a chain of fermion bubbles. The labels N and T correspond to non-twisted and twisted fermion bubbles, respectively, and are pictorially represented below the $\varphi_4^{(1)}$ diagram.

With our rescaled-coupling convention, the function F_3 is

$$\boxed{\varphi_3^{(1)}(t) = l_0(2t) + 2tl_0'(2t) - 36} \tag{3.143}$$

where -36 removes the one-loop contribution.

To compute $\varphi_4^{(1)}$, we start from the second term in the first line of (3.137), which diagrammatically corresponds to Fig. 3.11:

$$\begin{aligned} T_4 &\equiv -\frac{K^2}{N_f}\mathrm{div}\left\{Z_S^{-2}\sum_{n=0}^{\infty}(Z_S^{-1}K)^n\left(L^{(n+2)} - 2D\Lambda_\lambda^{(n+1)}\right)\right\} \\ &= -\frac{K^2}{N_f}\mathrm{div}\left\{\sum_{n=0}^{\infty}K^n\sum_{i=0}^{n}\binom{n+1}{i}\frac{(-1)^i}{\epsilon^i}\Gamma(n+2-i,\epsilon)\right\} \end{aligned} \tag{3.144}$$

where we have introduced

$$\Gamma(m,\epsilon) \equiv L^{(m)} - 2D\Lambda_\lambda^{(m-1)} = \frac{1}{m\epsilon^m}(-1)^m\gamma(\epsilon,m), \tag{3.145}$$

with

$$\gamma(\epsilon,m) = \sum_{j=0}^{\infty}(m\epsilon)^j\gamma_j(\epsilon). \tag{3.146}$$

After resummation, and keeping only the $1/\epsilon$ pole of T_4, we find

$$T_4 = \frac{1}{\epsilon N_f}\left(K\gamma(K,1) - \int_0^K \gamma_0(t)\mathrm{d}t\right) + \dots, \tag{3.147}$$

where

$$\gamma_0(t) = \frac{3\cdot 2^{3-t}(t-3)\Gamma\left(\frac{3}{2}-\frac{t}{2}\right)}{\pi^{3/2}t\Gamma(2-t/2)}\sin\left(\frac{\pi t}{2}\right), \tag{3.148}$$

and

$$\gamma(t,1) = \frac{1}{1-t/3}\gamma_0(t). \tag{3.149}$$

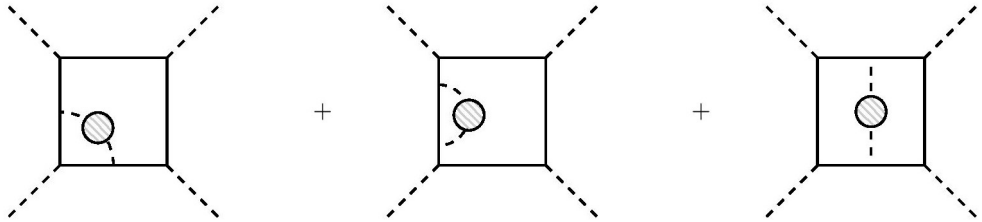

Figure 3.12: Different types of box diagrams for $F_2(yN_f)$. The gray blob represents a chain of fermion bubbles.

Besides T_4, the function $\varphi_4^{(1)}$ gets contribution from Z_S in (3.64). Altogether, it is given by

$$\boxed{\varphi_4^{(1)}(t) = 2\gamma(2t,1) - 2\gamma_0(2t) + 4t\gamma'(2t,1) + 4\xi_K^{(0)}(2t) + 8t\xi_K(2t) + 6 + 4\int_0^{2t}\xi_K(x)\mathrm{d}x.} \tag{3.150}$$

With the results of (3.143) and (3.150) together with (3.127), one can check that (3.131) is fulfilled. This provides a powerful cross-check for our computation.

The function $\varphi_2^{(1)}$

The function $\varphi_2^{(1)}$ can be computed evaluating the $1/\lambda$ terms in the last two lines of (3.137), corresponding to the one-loop box diagram, the box diagrams with additional internal scalar propagator in Fig. 3.12 and the candy diagrams in Fig. 3.13.

Let us start with the box contribution, $\varphi_{2\,\mathrm{box}}^{(1)}$. The counterterms Z_V and Z_f have been computed up to $\mathcal{O}(1/N_f)$ in the Sec. 3.2. Notice that we need to use the full expression for $Z_{V,f}$ and not only the $1/\epsilon$ pole:

$$Z_V = 1 + \frac{1}{2N_f}\sum_{n=1}^{\infty}\frac{K^n}{\epsilon^n}\frac{v_K^{(0)}(\epsilon)}{n}, \quad Z_f = 1 - \frac{1}{4N_f}\sum_{n=1}^{\infty}\frac{K^n}{\epsilon^n}\frac{\sigma_K^{(0)}(\epsilon)}{n}. \tag{3.151}$$

The first term in the second line of (3.137) gives a divergent part

$$T_{b_1} \equiv \frac{4K^2}{\lambda N_f}\left[\frac{D}{4} + \mathrm{div}\left\{(\tilde{Z}_f - \tilde{Z}_V)\Lambda_F^{(1)}(p^2,\epsilon)\right\}\right], \tag{3.152}$$

where $\tilde{Z}_{f,V} \equiv Z_{f,V} - 1$, and we have defined the finite part of the one-loop box diagram as

$$\Lambda_F^{(1)} = \Lambda_K^{(1)} - D. \tag{3.153}$$

The first term in (3.152) gives the basic one-loop contribution of the box diagram and will be omitted in the following. Using (3.151) and keeping only the $1/\epsilon$ pole of T_{b_1}, we have:

$$T_{b_1} = \frac{K^2}{\epsilon\lambda N_f^2}\int_0^K \Lambda_F^{(1)}(p^2,t)(\sigma_K^{(0)}(t) + 2v_K^{(0)}(t))\mathrm{d}t \ + \ldots \tag{3.154}$$

As for the second term in the second line in (3.137), we have

$$T_{b_2} \equiv \frac{K^3}{\lambda N_f^2} \sum_{n=0}^{\infty} K^n \mathrm{div} \sum_{i=0}^{n} \left\{ \begin{pmatrix} n \\ i \end{pmatrix} \frac{1}{\epsilon^i} \Lambda_K^{(n+2-i)}(p^2, \epsilon) \right\}. \tag{3.155}$$

The quantity $\Lambda_K^{(m)}$ allows for the following expansion:

$$\Lambda_K^{(m)}(p^2, \epsilon) = \frac{1}{\epsilon^m m(m-1)} \lambda(p^2, \epsilon, m), \tag{3.156}$$

where $\lambda(p^2, \epsilon, m)$ is regular for $\epsilon \to 0$ and can be written as

$$\lambda(\epsilon, m) = \sum_{j=0}^{\infty} (m\epsilon)^j \lambda_j(p^2, \epsilon). \tag{3.157}$$

Plugging (3.156) and (3.157) in (3.155) and using the usual summation formulas, we find for the $1/\epsilon$ pole:

$$T_{b_2} = \frac{K}{\epsilon \lambda N_f^2} \int_0^K \left(\lambda_0(t) - \lambda_0(0) + K \frac{\lambda(p^2, t, 1) - \lambda_0(t)}{t} \right) \mathrm{d}t \, + \ldots \tag{3.158}$$

When the $1/\epsilon$ poles of T_{b_1} and T_{b_2} are put together, the p^2 dependence of $\lambda(p^2, t, 1)$ cancels. We find the $1/\epsilon$ pole of Z_λ^{box} to be

$$Z_\lambda^{\mathrm{box}} = -(T_{b_1} + T_{b_2}) = -\frac{K}{\epsilon \lambda N_f^2} \int_0^K \left(\lambda_0(t) - \lambda_0(0) + K \frac{5-t}{4 - 5t + t^2} \lambda_0(t) \right) \mathrm{d}t, \tag{3.159}$$

where the function $\lambda_0(t)$ is given by

$$\lambda_0(t) = (t-1) \frac{\Gamma(4-t) \sin\left(\frac{\pi t}{2}\right)}{\pi t \Gamma\left(2 - \frac{t}{2}\right)^2}. \tag{3.160}$$

In the coupling convention of (3.119), $\varphi_{2\,\mathrm{box}}^{(1)}$ reads

$$\boxed{\varphi_{2\,\mathrm{box}}^{(1)}(t) = \int_0^{2t} \frac{x-5}{x^2 - 5x + 4} \lambda_0(x) \mathrm{d}x + \lambda_0(0) - \frac{4}{4 - 10t + 4t^2} \lambda_0(2t).} \tag{3.161}$$

Let us now compute the contribution of the candy diagrams in Fig. 3.13, $Z_\lambda^{\mathrm{candy}}$, arising from the last line of (3.137). This will lead to the calculation of our last ingredient, $\varphi_{2\,\mathrm{candy}}^{(1)}$, and corresponds to the first large-N_f resummation that is performed on a three-loop basic diagram. To this end, it is convenient to define

$$T_c \equiv \frac{K^4}{\lambda N_f^2} \mathrm{div} \left\{ \sum_{n=0}^{\infty} K^n \sum_{i=0}^{n} \begin{pmatrix} n+1 \\ i \end{pmatrix} \frac{1}{\epsilon^i} C^{(n+1-i)} \right\}, \tag{3.162}$$

where

$$C^{(n+1-i)} \equiv D^2 {\Lambda_\lambda}^{(n+1-i)} - D L^{(n+2-i)} + \Lambda_K'^{(n+3-i)}. \tag{3.163}$$

The structure of $C^{(m)}$ is:

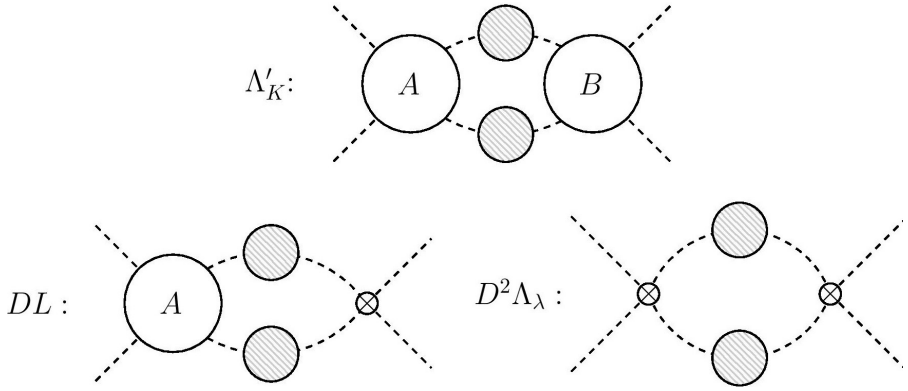

Figure 3.13: Candy diagrams for $\varphi_2^{(1)}(yN_f)$. The basic diagram is the three-loop diagram Λ'_K. The fermion loops A, B are either of the form N (non-twisted) or T (twisted), cf. Fig. 3.11. The diagrams DL and $D^2\Lambda_\lambda$ come from Λ'_K when A or B are shrunk to a counterterm vertex D, which is the same for N and T.

$$C^{(m)} = \frac{1}{\epsilon^{m+2}} \frac{1}{(m+1)(m+2)} c(p^2, \epsilon, m), \tag{3.164}$$

where the function $c(p^2, \epsilon, m)$ is regular for $\epsilon \to 0$ and can be expanded as

$$c(p^2, \epsilon, m) = \sum_{j=0}^{\infty} (m\epsilon)^j c_j(p^2, \epsilon). \tag{3.165}$$

The IR regulator, p^2, stands here for a soft mass for the scalar field. Plugging Eqs (3.164) and (3.165) in (3.162) yields

$$T_c = \frac{K^4}{\lambda N_f^2} \mathrm{div} \left\{ \sum_{n=0}^{\infty} \frac{K^n}{\epsilon^{n+3}} \sum_{j=0}^{n+2} \epsilon^j c_j(p^2, \epsilon) S(n, j) \right\}, \tag{3.166}$$

where

$$S(n, j) = \sum_{i=0}^{n} \left(\begin{array}{c} n+1 \\ i \end{array} \right) (-1)^i \frac{(n+2-i)^{j-1}}{n+3-i}. \tag{3.167}$$

We find

$$S(n, j) = \begin{cases} (-1)^n \frac{n+1}{2(n+3)} & j = 0, \\ (-1)^n \frac{(n+1)(n+4)}{2(n+2)(n+3)} & j \text{ odd}, \\ (-1)^n \frac{8+n(n+5)}{2(n+2)(n+3)} & j \text{ even}. \end{cases} \tag{3.168}$$

Equation (3.168) tells that three functions are relevant: $c_0(\epsilon)$, $c_e(\epsilon)$, and $c_o(\epsilon)$,

$$\begin{aligned} c_e(\epsilon) &\equiv \sum_{j \text{ even}}^{\infty} \epsilon^j c_j(\epsilon) = \frac{c(p^2, \epsilon, 1) + c(p^2, \epsilon, -1)}{2} - c_0(\epsilon), \\ c_o(\epsilon) &\equiv \sum_{j \text{ odd}}^{\infty} \epsilon^j c_j(\epsilon) = \frac{c(p^2, \epsilon, 1) - c(p^2, \epsilon, -1)}{2}, \end{aligned} \tag{3.169}$$

where the summation over j has been extended to infinity without affecting the result (namely, finite terms in the $\epsilon \to 0$ limit), and all the resulting functions are found to be independent of the IR regulator. They read

$$c_0(t) = -3\frac{2^{4-t}\,\Gamma\left(\frac{5}{2}-\frac{t}{2}\right)\sin\left(\frac{\pi t}{2}\right)}{\pi^{3/2}t\Gamma\left(2-\frac{t}{2}\right)},\; c_e(t) = \frac{t^2}{6(3-t)}c_0(t),\; c_o(t) = \frac{t(6-t)}{6(3-t)}c_0(t). \quad (3.170)$$

After performing the sum over n using Eqs (3.168), and retaining only the $1/\epsilon$ pole, we arrive at

$$T_c = \frac{1}{\epsilon\lambda N_f^2}\left(\frac{1}{2}K^2\left(c_0(K)+c_0(0)\right) + \frac{K^3}{6-2K}c_0(K) + \frac{1}{3}K\int_0^K (t-3-K)c_0(t)\mathrm{d}t\right) + \dots \quad (3.171)$$

In the convention of (3.119), we find

$$\boxed{\varphi^{(1)}_{2\,\mathrm{candy}}(t) = \frac{9-24t+8t^2}{2(2t-3)^2}c_0(2t) + \frac{3t}{2t-3}c_0'(2t) - \frac{1}{6}\left(3c_0(0) - 2\int_0^{2t} c_0(x)\mathrm{d}x\right).} \quad (3.172)$$

Combining Eqs (3.161) and (3.172), we obtain the final form of $\varphi_2^{(1)}(t)$

$$\boxed{\varphi_2^{(1)}(t) = \varphi^{(1)}_{2\,\mathrm{box}}(t) + \varphi^{(1)}_{2\,\mathrm{candy}}(t)} \quad (3.173)$$

which completes our calcuation of the $\mathcal{O}(1/N_f)$ system of β-functions in (3.118) and (3.119).

3.4.3 QED$_3$–Gross–Neveu–Yukawa critical exponents (new)

Let us summarize here our findings in this section and also present a new result for the QED$_3$-GNY critical exponents at $\mathcal{O}(1/N_f)$ that can be actually deduced from them with small additional information.

Our first observation was that for one-coupling systems the knowledge of the critical exponent ω is always enough to reconstruct the β-function at the same order in the $1/N_f$ expansion. We have therefore stated the general procedure to relate β and ω and shown explicit formulas up to $\mathcal{O}(1/N_f^2)$.

The picture changes when considering multi-coupling systems. To investigate this we have focussed on the GNY model that contains two relevant interactions. We in fact showed that the critical exponents $\omega_\pm^{(1)}$ could not provide the full system of β-functions, (3.118) and (3.119), but rather constrain some combinations of $\varphi^{(1)}_{1-4}$ as in (3.127) and (3.131). We hence had to rely on explicit bubble resummation to obtain the β-functions in a closed form [6]. The functions $\varphi^{(1)}_{1-4}$ are shown together in Fig. 3.14. We notice that $\varphi^{(1)}_{2-4}$ feature the first singularity at $t = 3/2$. This singularity is actually not signaled by $\omega_\pm^{(1)}$, as it gets exactly cancelled in the combination $\varphi_3^{(1)}+\varphi_4^{(1)}$ entering (3.131), but does

[6] However, we envisage that it might be possible to reconstruct the full system of RG functions in a multiple-coupling theory within the critical-point formalism through extraction of the operator-product-expansion coefficients. This is in line with the recent analyses carried out in [137–140].

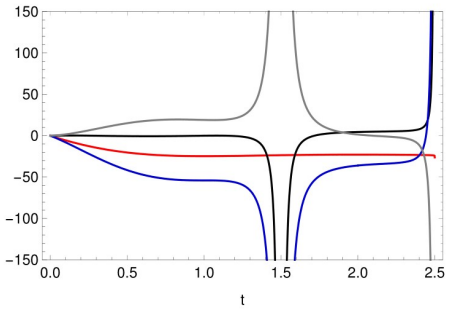

Figure 3.14: The functions $10 \times \varphi_1^{(1)}(t)$ (red), $\varphi_2^{(1)}(t)$ (black), $\varphi_3^{(1)}(t)$ (blue) and $\varphi_4^{(1)}(t)$ (grey) given in Eqs (3.127), (3.173), (3.143), (3.150), respectively. We notice that $\varphi_1^{(1)}$ has the first singularity at $t = 5/2$, whereas $\varphi_{2-4}^{(1)}$ show a second-order pole at $t = 3/2$.

show up in $\omega_\pm^{(2)}$ at $\mathcal{O}(1/N_f^2)$. We thus conclude that the radius of convergence for the GNY β-function does not necessarily shrink when moving from $\mathcal{O}(1/N_f)$ to $\mathcal{O}(1/N_f^2)$ as one would have naively guessed just by looking at the critical exponents, because the "new" singularity for ω is already present in the $\mathcal{O}(1/N_f)$ β-functions.

With the closed form of $\varphi_{1-4}^{(1)}$ at hand we can expand around $(y = 0, \lambda = 0)$, thus comparing our results with standard perturbation theory and predicting new coefficients. We have checked that our expansions agree with the known leading-N_f four-loop perturbative result [108]. This, together with our predictions for the five- and six-loop leading-N_f terms is shown in Sec. B.2.2.

Finally, let us comment on the possibility of combining the results in this section with the ones in Sec. 3.3 which include gauge interactions. As mentioned below (3.116), this could lead to the set of the $\mathcal{O}(1/N_f)$ β-functions for the QED$_3$-GNY model that contains gauge, yukawa and scalar quartic couplings at the same time. However, the calculation in Sec. 3.3 was lacking the inclusion of the quartic λ, and uncovering the $\varphi_{1-4}^{(1)}$ functions is still not enough to complete the system. To make this statement more precise and discuss which ingredients are still missing, let us write down the ansatz for the QED$_3$-GNY β-functions at $\mathcal{O}(1/N_f)$ (in doing so, we will follow the coupling convention of [97] to have a straightforward comparison with the perturbative results):

$$\begin{aligned}
\beta_y &= (d-d_c)y + y^2\left[4N_f + 6 + \varphi_1^{(1)}(2yN_f) + \tilde{F}_1^{(1)}(\alpha N_f)\right] + y\,\alpha\,\left[-12 + \tilde{F}_2^{(1)}(\alpha N_f)\right], \\
\beta_\lambda &= (d-d_c)\lambda + y^2\left[-2N_f + \varphi_2^{(1)}(2yN_f) + \mathbf{X_1^{(1)}}(\alpha N_f)\right] + \lambda^2(72 + \varphi_3^{(1)}(2yN_f)) \\
&\qquad + y\lambda\left[8N_f + \varphi_4^{(1)}(2yN_f) + \mathbf{X_2^{(1)}}(\alpha N_f)\right], \\
\beta_\alpha &= (d-d_c)\alpha + \alpha^2\left[8/3N_f + \tilde{F}_3^{(1)}(\alpha N_f) + \tilde{F}_4^{(1)}(yN_f)\right],
\end{aligned} \tag{3.174}$$

where we have noticed that the quartic coupling λ does not affect the β-function for the QED coupling, β_α. The functions $\varphi_{1-4}^{(1)}$ have been calculated in this section. Also, the functions $\tilde{F}_{1-4}^{(1)}$ can all be obtained from a comparison with the explicit results in (3.95) and (3.96). Thus, the only remaining unknowns are $X_1^{(1)}$ and $X_2^{(1)}$.

Actually, we notice that determining $X_2^{(1)}$ does not involve any new ingredient, as this term $\propto y\lambda$ comes from the gauge contribution to the scalar self-energy, Z_S, that has been already resummed in (3.90). Hence, $X_2^{(1)}$ can be obtained by simply acting with derivatives upon Z_S. Conversely, $X_1^{(1)}$ requires to perform a calculation similar to the one for $\varphi_2^{(1)}$, namely replacing the internal scalar chains in Fig. 3.12 and Fig. 3.13 with gauge chains. This does not introduce any new technical difficulties, and the relations in (3.77) can still be used to translate the known result for $\varphi_2^{(1)}$. The task of completing the full system of β-functions for QED$_3$-GNY is certainly interesting and left for future work.

If all the terms in (3.174) were known, the critical exponents ω could be evaluated by computing the $\mathcal{O}(1/N_f)$ eigenvalues of the Jacobian at criticality:

$$J_{(y,\lambda,\alpha)}(\beta_y,\beta_\lambda,\beta_\alpha)=\begin{pmatrix}\partial_y\beta_y & \partial_y\beta_\lambda & \partial_y\beta_\alpha\\ 0 & \partial_\lambda\beta_\lambda & 0\\ \partial_\alpha\beta_y & \partial_\alpha\beta_\lambda & \partial_\alpha\beta_\alpha\end{pmatrix}. \tag{3.175}$$

Nevertheless, it turns out by direct inspection that $X_1^{(1)}$ does not enter the critical exponents ω at $\mathcal{O}(1/N_f)$, and therefore these are calculable by simply combining the results of this chapter. The procedure is analogous to what discussed in (3.120) and below: one needs to calculate the position of the QED$_3$-GNY fixed point at $\mathcal{O}(1/N_f)$ and substitute it in (3.175), which is evaluated with the help of (3.174). The diagonalization of the Jacobian provides then the critical epxonents. Explicitly, we find:

$$\omega_0(\epsilon)=\epsilon+\frac{1}{N_f}\frac{(8-3\epsilon)\Gamma(5-\epsilon)}{(2-\epsilon)\Gamma\left(2-\frac{\epsilon}{2}\right)\Gamma\left(3-\frac{\epsilon}{2}\right)\pi}\sin\left(\frac{\pi\epsilon}{2}\right)+\mathcal{O}(1/N_f^2), \tag{3.176}$$

$$\omega_\pm(\epsilon)=\epsilon+\frac{1}{N_f}\frac{\left[(2-\epsilon)(12+\epsilon-\epsilon^3)\pm\sqrt{\Delta(\epsilon)}\right]\Gamma(4-\epsilon)}{4(4-\epsilon)(2-\epsilon)\Gamma\left(2-\frac{\epsilon}{2}\right)^2\pi}\sin\left(\frac{\pi\epsilon}{2}\right)+\mathcal{O}(1/N_f^2), \tag{3.177}$$

where

$$\Delta(\epsilon)=576-864\epsilon+372\epsilon^2+196\epsilon^3-143\epsilon^4-24\epsilon^5+42\epsilon^6-12\epsilon^7+\epsilon^8. \tag{3.178}$$

The smallest eigenvalue turns out to be ω_- and is to be identified with the leading correction in (3.100) (this is also referred to as "stability exponent"). Expanding around $\epsilon=0$, we can check with known perturbative results:

$$\omega_-(\epsilon)=\epsilon+\frac{3}{4N_f}\epsilon^2-\frac{1}{4N_f}\epsilon^3-\frac{53}{64N_f}\epsilon^4+\underbrace{\left(\frac{3}{16N_f}\zeta_3-\frac{7}{192N_f}\right)}_{\text{five-loop prediction}}\epsilon^5+\ldots, \tag{3.179}$$

where the first four terms coincide with the leading-N_f four-loop result of [97], and the last term is our prediction for the five-loop leading-N_f coefficient.

It is worth mentioning that the most interesting application related to the QED$_3$-GNY model is actually found in $d=2+1$ where it can describe quantum phase transitions occuring for fermionic systems on the lattice [96]. However, the underlying quantum field theory turns out the be strongly coupled at the fixed point in $d=3$, and therefore one

needs to rely on alternative methods in order to extract the correspoding critical exponents. One possibility is in fact to investigate the theory between the lower- and upper-critical dimension, $2 < d < 4$, and then extrapolate to the desired dimensionality. The case of $d = 4-\epsilon$ is particularly suitable as all the couplings are marginal and within perturbative control at the fixed point for $\epsilon \ll 1$. The idea is then to calculate the critical exponents as precisely as possible (namely, including higher orders in perturbation theory) and then extrapolate the results to $d = 3$ employing other methods such as Padé approximants [97]. In this respect, our results in (3.176) and (3.177) stemming from the large-N_f expansion provide complementary information with respect to standard perturbation theory, and can help improving the extrapolation to $d = 3$. Moreover, we envisage that the calculation of the various renormalization constants accomplished throughout this chapter can be used to access other critical exponents besides ω characterizing the fixed point at large-N_f in $d = 4 - \epsilon$. We leave this analysis for future investigation.

3.5 Treatment of the singularities

As noticed throughout this chapter, the large-N_f resummed functions show a finite radius of convergence, namely they feature singularities at finite, physical values of the coupling. This is a consequence of the large-N_f results arising from the resummation of a power series in the rescaled coupling. As a matter of fact, such singularities can dramatically affect the RG evolution and, if the singularity has the right sign, enforce a zero in the β-function. This turns out to be the case in very familiar examples of quantum field theories, such as gauged $U(1)$ and $SU(3)$, namely large-N_f QED and QCD. The presence of such a zero would then suggest that these theories may actually feature a UV interacting fixed-point, thus providing an example of asymptotic safety in four dimension. This has been exploited in several works to obtain asymptotically safe extensions of the SM, see [98–100, 141–144].

However, some shadow on the existence of the fixed point as a consistent conformal field theory (CFT) is cast already by studying anomalous dimensions of other operators in the vicinity of the β-function singularity: in the case of large-N_f QED, the $\mathcal{O}(1/N)$ anomalous dimension of the fermion mass diverges at the putative fixed point [101, 102] (which is enough to rule out this possibility), and it was recently pointed out that in the large-N QCD the anomalous dimension of the glueball operator breaks the unitarity bound near the singularity [145] (which could however be reconciled by saying that this operator is decoupled at the fixed point).

In this section based on Ref. [V], we will provide further evidence against the interpretation of these singularities as fixed-points by employing the results of Sec. 3.4 regarding the connection of ω and β-function for one-coupling models, where the latter is given in (3.102).

The main idea is that, as a singularity in the β-function at $\mathcal{O}(1/N_f)$ was actually found to propagate to all higher-order functions at the same value of the coupling— see discussion below (3.107)— these singularities can actually be resummed away when fully exploiting the knowledge of the critical exponent ω. In fact, we have seen that the critical exponent $\omega^{(1)}$ contributes to the β-function also beyond $\mathcal{O}(1/N_f)$. Same holds for each $\omega^{(j)}$: it contributes to all $F^{(n)}$ with $n \geq j$. In the following, we denote the contribution of $\omega^{(1)}, \ldots, \omega^{(j)}$ to $F^{(n)}$, $n \geq j$, by $F^{(j,n)}$. It is worth to stress that these

contributions are necessary in order to obtain the correct perturbative result from the critical point formalism.

Since $\omega^{(1)}$, or equivalently $F^{(1)}$, is known, all the $F^{(1,n)}$ can be computed from (3.104) and (3.106). We find these induced terms in closed form as ($x = gN_f$)

$$F^{(1,1)}(x) \equiv F^{(1)}(x) = \int_0^x \frac{\mathrm{d}t}{t^2}\omega^{(1)}(d_c - bt) \tag{3.180}$$

$$F^{(1,n>1)}(x) = \int_0^x \frac{\mathrm{d}t}{t^2}\sum_{\ell=1}^{n-1}\frac{1}{\ell!}c^{(\ell)}_{n-\ell-1}\left(\frac{t}{b}\right)^{\ell}\frac{\mathrm{d}^{\ell}}{\mathrm{d}t^{\ell}}\left[t^2 F^{(1)\prime}(t)\right], \tag{3.181}$$

where the $c^{(k)}_m$ are defined iteratively:

$$c^{(k)}_0 = (F^{(1)} + c)^k \tag{3.182}$$

$$c^{(k)}_n = \frac{1}{n(F^{(1)}+c)}\sum_{q=1}^{n}(qk + q - n)F^{(q+1)}c^{(k)}_{n-q}. \tag{3.183}$$

One can check that this is consistent at $1/N_f^2$ with (3.107). It follows from (3.181) that if $F^{(1)}$ features a negative singularity (as it is the case for (non)-abelian gauge theories) at a given x, this results into sequence of singularities of alternating signs in $F^{(1,n)}$ at the same point x with increasingly high divergent power. This means that the putative fixed point in the β-function driven by the singularity of $F^{(1)}$ alone is not guaranteed to persist when all the $F^{(1,n)}$ are taken into account. As we shall see, all the $F^{(1,n)}$ can be actually resummed, and the final result features no singularity.

A direct resummation of the $F^{(1,n)}$ terms as presented in (3.181) is not straightforward, and we therefore employ a different approach. Denoting

$$\mathcal{F}(x, N_f) \equiv \sum_{n=1}^{\infty}\frac{F^{(n)}(x)}{N_f^{n-1}}, \tag{3.184}$$

the relation $\beta'(g_c) = \omega(d)$ is rewritten as

$$-(d - d_c) + \frac{x_c^2}{N_f}\,\partial_x\mathcal{F}(x_c, N_f) = \omega(d), \tag{3.185}$$

where we have used that $\beta(g_c) = 0$, and the dimension d and the critical coupling are related via

$$d = d_c - x_c\left(b + \frac{c + \mathcal{F}(x_c, N_f)}{N_f}\right). \tag{3.186}$$

Equation (3.185) would provide an exact solution, if ω were known to all orders. However, in practice this is not the case, but rather we have access to the contributions induced by $\omega^{(1)}, \ldots, \omega^{(j)}$ only. Nonetheless, a consistent solution to (3.185) incorporating all known coefficients can be achieved by truncating the critical exponent to

$$\omega(d) = -(d - d_c) + \sum_{n=1}^{j}\frac{1}{N_f^n}\omega^{(n)}(d), \tag{3.187}$$

which corresponds to truncating $F^{(n)}$ to $F^{(j,n)}$ in $\mathcal{F}(x, N_f)$ in (3.184). The resulting function is denoted by $\mathcal{F}^{(j)}(x, N_f)$.

Let us now concentrate on the simplest case $j = 1$ correspoding to the $\mathcal{O}(1/N_f)$ critical epxonent $\omega^{(1)}$, where the truncation leads to the following differential equation for $\mathcal{F}^{(1)}$:

$$\partial_x \mathcal{F}^{(1)}(x, N_f) = \frac{1}{x^2}\omega^{(1)}\left(d_c - x\left(b + \frac{c + \mathcal{F}^{(1)}(x, N_f)}{N_f}\right)\right) , \tag{3.188}$$

where we have used (3.186). Notice that the brackets in $\omega^{(1)}(\dots)$ enclose the argument of $\omega^{(1)}$ as a function. If the critical exponent is known, this is a non-linear first-order differential equation for $\mathcal{F}^{(1)}$.

First, we notice that when neglecting the backreaction of $\mathcal{F}^{(1)}$ on the RHS of (3.188) the differential equation gives back the $\mathcal{O}(1/N_f)$ part of the β-function, namely $F^{(1)}$ only, that can be obtained analytically— it is in fact (3.180)— and is shown as the red solid line in Fig. 3.15 in the case of large-N_f QCD with $N_f = 50$. This of course coincides with the standard $\mathcal{O}(1/N_f)$ result for QCD [104] derived from (3.180) directly, and shows a putative UV fixed point at $x = 3$.

However, the advantage of our approach is that we can solve (3.188) as it is and only afterwards take the large-N_f limit [7]. This treatment encodes the fact that, if $F^{(1)}$ diverges around $x = 3$, the backreaction on the RHS of (3.188) is certainly not small. Equivalently, this amounts to resumming all the $F^{(1,n)}$'s, given explicitly in (3.181), that we know to be increasingly important near the singularity.

Equation (3.188) can be solved numerically, but let us first provide a simple asymptotic solution. The case we are interested in is when b (the large-N_f one-loop coefficient) and the sign of the singularity are of opposite sign, as it happens in large-N_f QED and QCD [8]. In this case, denoting by x_s the position of the would-be-singularity, we find that $\mathcal{F}^{(1)}$ approaches the form:

$$\mathcal{F}^{(1)}(x, N_f) = N_f\left(\frac{a}{x} - b\right) - c, \quad x \gtrsim x_s, \tag{3.189}$$

where a is typically $\mathcal{O}(1)$ and implicitly defined by

$$aN_f = -\omega^{(1)}(d_c - a), \tag{3.190}$$

where a and b need to have the same sign. This indicates that the alternating singularities in the $F_n^{(1)}$ can be resummed to yield a finite contribution. By using (3.189) and recalling that $x = gN_f$, the β function is found to be

$$\beta(g) = ag, \quad g \gtrsim g_s. \tag{3.191}$$

Including $\omega^{(2)}$ in the game yields the same conclusion, and similarly for any fixed-order truncation $\omega^{(j)}$.

We are now ready to evaluate the β-function for large-N_f QCD by solving (3.188) for a benchmark value $N_f = 50$. In our notation, $SU(3)$ corresponds to $b = 2/3$, $c = -11$.

[7] Note that, if the large-N_f expansion were under control, these two results should be approximately the same, as all the $F^{(1,n)}$ in (3.181) are formally higher orders. However, this will not be the case exactly because of the singularity.

[8] If b and the singularity in ω are of same sign, the higher-order terms would just enhance the original singularity and lead to a Landau pole as is the case of super-QED at $\mathcal{O}(1/N_f)$ [146] and in O(N) model at $\mathcal{O}(1/N^2)$ [147].

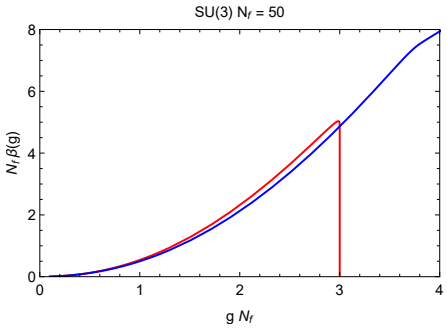

Figure 3.15: The β-function for $SU(3)$ for $N_f = 50$ computed according to (3.188). The red line shows the singular solution one encounters neglecting the back-reaction of $\mathcal{F}^{(1)}$ on the right-hand side of (3.188), whereas the blue line is the full numerical solution. As we can see, the two lines depart around $x = gN_f \approx 3$, where in fact the backreaction on the RHS of (3.188) becomes important.

The critical exponent is known up to $\mathcal{O}(1/N_f)$ and reads [103]:

$$\omega^{(1)}(2\mu) = \frac{\eta^{(1)}(2\mu)}{T_F}\left((2\mu-3)(\mu-3)C_F - \frac{(4\mu^4-18\mu^3+44\mu^2-45\mu+14)C_A}{4(2\mu-1)(\mu)}\right),$$

where $\mu = d/2$, $T_F = 1/2$ and $C_F = 4/3$ are the index and quadratic Casimir of the fermion representation, respectively, $C_A = 3$ is the Casimir of the adjoint representation, and $\eta^{(1)}$ reads

$$\eta^{(1)}(2\mu) = \frac{(2\mu-1)(\mu-2)\Gamma(2\mu)}{4\Gamma(\mu)^2\Gamma(\mu+1)\Gamma(2-\mu)}. \tag{3.192}$$

The asymptotic solution in (3.191) is given by $a_{\rm QCD} \approx 1.985$.

The blue line in Fig. 3.15 shows the numerical solution to Eq. (3.188) for $SU(3)$ with $N_f = 50$. The asymptotic solution is reached at $x = gN_f \lesssim 4$. As expected from the general analysis above, the singularity and the putative UV fixed points at $x = gN_f \approx 3$ have disappeared. This shows that the higher order contributions in (3.181) are actually important and the naked singularity in $F^{(1)}$ can in fact be resummed away.

We thus conclude that the singularities that have inspired speculations of UV fixed points can actually be resummed away when exploiting the structure of the higher-order functions coming from the critical exponents. No hint for a fixed point is thus found within this framework, as its existence relied entirely on the presence of a singularity. This is also in line with the first, although not yet conclusive, results from the lattice [148].

3.6 Summary

In this chapter we have investigated the β-functions for theories that exhibit a large flavor symmetry such as $SU(N_f)$ and thus contain a large number of degrees of freedom. Because of the large multiplicity N_f, the perturbative series is conveniently reorganized within the $1/N_f$ expansion, whose elements are resummed functions of the rescaled couplings that are all-order in the number of loops.

The novelty of our analysis with respect to previous studies was to consider the case in which a scalar field couples directly to a multiplicity of fermions through yukawa interactions, as inspired by UV completions of the Froggatt-Nielsen mechanism. We have then obtained the $\mathcal{O}(1/N_f)$ β-function for the pure yukawa theory in Sec. 3.2 and included the gauge counterpart in Sec. 3.3 by means of direct bubble resummation. These results provide new tools for analyzing the UV behavior of gauge–yukawa theories and are in fact relevant for investigating extensions of the SM with elementary scalars like possibly the Higgs itself, in which yukawa couplings should then be regarded as fundamental interactions.

In Sec. 3.4 we have taken a different perspective and discussed the connection between the large-N_f β-functions and the critical exponent ω related to the Wilson-Fisher fixed point in $d = 4-\epsilon$ dimensions for theories in the same universality class. In fact, these two quantities are related by the simple relation $\beta'(g_c) = \omega(d)$. Nonetheless, a systematic analysis of this correspondence was missing.

We found that for one-coupling models the knowledge of $\omega(d)$ obtained through the critical-point method is enough to fully reconstruct the β-function at the same order in the $1/N_f$ expansion, and we also provided the explicit dictionary connecting ω and β. We have then considered the Gross-Neveu model in $d = 2$ as a case of study for applying our procedure and investigated the possible appearence of an IR fixed point by using the β-function at $\mathcal{O}(1/N_f^2)$ obtained from the critical exponent. The putative fixed point turns out to be disfavored in agreement with previous studies employing different techniques.

For multi-coupling models the one-to-one relation between ω and the β-function no longer holds and the knowledge of the exponents can only constrain certain combinations of the resummed functions appearing in the β-functions. We have shown this explicitly for the Gross-Neveu-Yukawa model, where we have employed direct bubble resummation in order to calculate the full system of β-functions at $\mathcal{O}(1/N_f)$, while using the knowledge of the critical exponent ω to crosscheck our results.

Furthermore, we have commented on the possibility of extracting information regarding the QED$_3$-Gross-Neveu-Yukawa model which combines all types of interactions that have been discussed throughout this chapter (namely gauge, yukawa and scalar quartic) at the same time. Although the full system of β-functions could not be reconstructed combining the results of this chapter, it was nevertheless possible to obtain the $\mathcal{O}(1/N_f)$ critical exponents ω corresponding to the fixed point in $d = 4 - \epsilon$ for the first time. These results obtained in the large-N_f framework complement the ones in standard perturbation theory and may help the extrapolation to $d = 2 + 1$ where this theory is supposed to describe quantum phase transitions for fermionic systems on a lattice plane in a strongly-coupled regime.

Finally, our analysis also bears implications for asymptotic safety at large N_f. In fact, after asymptotic safety was proven in $d = 4$ both within perturbation theory and in the Veneziano limit, $N_f/N_c \to$ const., there has been some speculation about the appearence of the same behavior for gauge-yukawa theories in the complementary case of large N_f but fixed N_c. In addition to previous considerations about the (in)consistency of the correspoding conformal field theory, in Sec. 3.5 we have provided further evidence against the large-N_f fixed points by taking advantage of the connection with the critical exponent ω established in Sec. 3.4. We were in fact able to identify a class of formally higher-order contributions to the β-function which always comes together

with the original singularity that was supposed to drive the system to the fixed point. These contributions become increasingly important while approaching the singularity, and cannot be neglected. Remarkably, these terms can actually be resummed through the differential equation in (3.188) and the resulting β-function features no singularity. We thus conclude that no hint for a fixed point is found within the large-N_f limit alone, as this was entirely relying on the singular structure of the β-function.

Chapter 4

A Soft Composite Higgs

In the previous chapters we have discussed the interplay of an elementary Higgs with other aspects of physics beyond the SM, such as axions/flavor puzzle and the question of the UV fate for gauge–yukawa theories. These topics are intrinsically related to physics happening much above the scale of the electroweak interactions and our take regarding the Higgs hierarchy problem was to leave it aside favoring an agnostic point of view. This is certainly legit as fine-tuning is by no means an inconsistency of the theory and in the worst case it just represents a lack of understading. In fact, even though the mechanism that keeps the Higgs light is unknown, or even if there is no mechanism at all, one can still investigate the implications of a light and elementary Higgs, for instance trading fine-tuning for predictivity as in Chapter 2 or calculating the β-functions for yukawa couplings as in Chapter 3 motivated by new paradigms for the UV completion of the SM such as asymptotic safety.

Nevertheless, natural models for electroweak symmetry breaking still represent one of the most appealing scenarios for physics beyond the SM. In this class of models the Higgs is light due to the intrinsic properties of the underlying theory. A cornerstone solution is provided by Higgs compositeness, where the Higgs emerges as a bound state of a new strong dynamics that condenses not too far from the electroweak scale. The sensitivity of the Higgs mass to any new physics threshold above the condensation scale is automatically removed and so is the hierarchy problem. So far, all the scalar particles that we know in Nature have turned out to be bound states. Nonetheless, the agreement between a composite Higgs and the current results from the LHC is far from obvious. In fact, minimal models are under pressure because of the null-observation of light top partners, namely new colored fermions with the top quark quantum numbers that seem to be a necessary ingredient to ensure a light Higgs. The main source of fine-tuning in these models is thus dictated by the compliance with the LHC data and has long surpassed the minimal 10% tuning that was already implied by LEP.

In this chapter, we will present a new realization of Higgs compositeness that is based on one single assumption [VI]: the SM fermions and the composite resonances of the strong sector interact in a way that respects the global symmetry under which the Higgs is a (pseudo-)Nambu-Goldstone boson. As we shall see, this requires to introduce new vector-like fermions in the theory that complete the SM fermions to full representations of the global symmetry. The latter is in turn broken "softly" by the vector-like masses that make these states heavy to be compatible with current constraints and at the same time generate a viable Higgs potential. As we shall see, this is enough to release the

tension between a composite Higgs (CH) and the current LHC data. Moreover, when combined with other possible symmetries of the strong sector, soft-breaking leads to a model in which the Higgs is light, and all the new states are above 2 TeV with only 10% tuning [VII]. All the ingredients that we require in constructing our model turn out to have a very simple interpretation in the context of warped extra dimensions, that is the language in which the original minimal composite Higgs model (MCHM) was presented. In particular, soft breaking means universal boundary conditions for the 5D bulk fermions which are then modified dynamically due to the presence of brane-localized spinors. The resulting setup is as simple as the original holographic Higgs, but more successful phenomenologically.

This chapter is organized as follows. After reviewing the basic concepts behind a CH in Sec. 4.1 and the relevant experimental constrains in Sec. 4.2, we will introduce the idea of soft-breaking in Sec. 4.3, where we also provide a quantitative analysis in the context of phenomenological multi-site models according to [VI]. Sec. 4.4 is devoted to the combination of soft-breaking with maximal symmetry that turns out to be a perfect match in terms of tuning and compliance with the LHC bounds. The implementation of soft-breaking in the context of warped extra dimension is presented in Sec. 4.5. These last two sections are based on, [VII]. We summarize our findings in Sec. 4.6.

4.1 The standard picture

The mechanism underlying electroweak symmetry breaking is one of the major open questions in the SM. Quite generically, the dynamics responsible for it can be either weakly or strongly coupled. The former corresponds to the standard Higgs model, in which an elementary and weakly-interacting scalar field breaks the electroweak symmetry due to a non-zero condensate, $\langle h^\dagger h\rangle = v^2/2$. The scalar sector responsible for the condensate can be treated perturbatively, and the Higgs model is in fact very predictive. Moreover, due to an accidental global symmetry of the scalar potential the theory is endowed with an approximate $SU(2)$ custodial symmetry in the broken phase that makes it extremely successful in reproducing the experimental data. The second possibility still entails the formation of a condensate, but unlike the Higgs mechanism this occurs non-perturbatively in the strong-coupling regime of a new hidden sector. Probably the best known example of this kind of behavior is QCD: below the condensation scale of the color group, $\Lambda_{\rm QCD}$, quarks and anti-quarks form a condensate, $\langle\bar{q}q\rangle$, that breaks the $SU(2)_L \times SU(2)_R$ chiral symmetry of the up and down quarks down to the diagonal subgroup $SU(2)_V$. It is interesting to notice that in a Higg-less version of the SM this mechanism would actually provide a mass $\sim \Lambda_{\rm QCD}$ for the electroweak gauge bosons while ensuring custodial protection due to the unbroken $SU(2)_V$. In fact this shows that a simple scaled-up version of QCD with a condensation scale $\Lambda \sim v$ may be a good candidate for triggering electroweak symmetry breaking in the SM, and this class of models is generically called *technicolor* to stress the analogy with the QCD group [149–151].

From a phenomenological point of view, these two paradigms for electroweak symmetry breaking lead to very different predictions. In particular, due to the weakly-coupled nature of the Higgs model, the spectrum must contain a scalar particle which is *light* and *narrow*. As for technicolor models, they do predict scalar bound states in the theory (mesons), but these resonances are generically expected to be *heavy* and *broad*. The

discovery at the LHC of a light scalar with 125 GeV mass and a width of few MeV is certainly a milestone in the understanding of electroweak symmetry breaking as it shows the characteristic features of the Higgs model. Nonetheless, the very existence of a light and elementary scalar particle is certainly puzzling from a theoretical point of view, as we know that its mass is extremely sensitive to any new physics threshold between the electroweak and (possibly) the Planck scale. These thresholds are particularly probable given the open questions in the SM, such as strong CP problem and Grand Unified Theories. Thus, it is reasonable to regard the Higgs mechanism in the SM should as a very successful parameterization for physics at the electroweak scale, whereas a more fundamental description— also accounting for the shortcomings in the SM— is supposed to replace it at even higher scales. In this respect, it is curious to notice that if Nature had chosen technicolor as the mechanism behind electroweak symmetry breaking, the issue with the stability of the Fermi scale would have been automatically solved. The reason is what is called *dimensional transmutation*: a scale f is generated in QCD-like theories as the point in which a (marginal) gauge coupling leaves the perturbative regime as a result of its renormalization group evolution. The scale f has therefore a dynamical origin and is largely insensitive to new physics thresholds, as they introduce only a logarithmic dependence through the running.

Composite Higgs models arise as a synergy between the standard Higgs model and technicolor [23–25], see e.g. [152–156] for reviews. The main idea is to introduce a new strongly-coupled sector which confines at a certain scale $f \sim 1$ TeV that is generated via dimensional transmutation and is therefore stable under quantum corrections. Generically, the new strong dynamics can feature a global symmetry group G that undergoes spontaneous breaking to a subgroup H due to the formation of a condensate at the scale f. In order to obtain a viable model, one has to require that the full electroweak and color gauge groups are contained in the subgroup H such that the SM gauge symmetry is still unbroken at the scale f. By the Goldstone theorem, a certain number of light scalar particles corresponding to the G/H coset appear in the spectrum. The choice $G = SO(5) \times U(1)_X$ and $H = SO(4) \times U(1)_X$ [1] corresponds to the MCHM [157, 158], in which the spectrum of NG bosons just coincides with the SM Higgs, and the theory features the $SO(4)$ symmetry that will lead to the custodial protection. Realizing the Higgs as a pNGB makes it generically ligther than the other resonances which are usually above the scale f. Having a light scalar in the spectrum solves almost all the problems of technicolor constructions in terms of electroweak precision tests and is in agreement with the $h(125)$ discovery at the LHC. Moreover, as the Higgs is now a bound state, the corrections to its mass are anyway cutoff at the scale $f \sim 1$ TeV, thus solving the hierarchy problem.

If the global symmetry G were exact, the Higgs would be a true NG boson, and its potential would vanish identically. This means that one has to allow some explicit breaking of G such that a potential for the Higgs is generated beyond tree level. It is in fact this radiatively-induced potential that eventually triggers electroweak symmetry breaking similarly to the Higgs model at the scale $v \lesssim f$.

As the theory is strongly coupled below the condensation scale, a quantitative analysis of CH models is possible either by means of holography or within an effective-field-theory approach. In the following, we will follow the latter and postpone the extra-dimensional discussion to Sec. 4.5. The effective theory is based on the Goldstone

[1] The presence of the unbroken $SU(3)_c$ is understood.

matrix U:

$$U = \exp\left(i\frac{\sqrt{2}}{f}T^{\hat{a}}h^{\hat{a}}(x)\right) \tag{4.1}$$

where f is identified with the Higgs decay constant, and hatted indices $\hat{a} = 1, \ldots, 4$ correspond to the broken generators $T^{\hat{a}}$ after the $G \to H$ spontaneous breaking, see (A.2). The Goldstone matrix U has peculiar transformation properties under $SO(5)$:

$$U \to g\,U\,h^{\dagger}(h^{\hat{a}}, g), \quad g \in SO(5),\, h \in SO(4). \tag{4.2}$$

The simplest operator that accounts for the dynamics of the Goldstone degrees of freedom contains two derivatives and two insertions of U:

$$\mathcal{L}_{\partial^2} = \frac{f^2}{2}D_\mu\Phi D^\mu\Phi, \quad \Phi = U\cdot\Phi_0, \tag{4.3}$$

where $\Phi_0 = (0,0,0,0,1)^T$ stands for the $SO(4)$-preserving direction and D_μ is the standard covariant derivative that includes the electroweak gauging,

$$D_\mu = \partial_\mu - igW_\mu T^i_L - ig'Y_\mu T^3_R, \tag{4.4}$$

where we have used that the Goldstone matrix carries no X charge and the hypercharge is simply $Y = T^3_R$. The formulas for $T^3_{L,R}$ are given in (A.1).

A simpler description of the theory is obtained by choosing the unitary gauge such that the would-be-Goldstone modes within the Higgs doublet are removed. Setting the Higgs to its vev $\langle h\rangle$ in (4.3), one can read out the mass for the W and the Z bosons after electroweak symmetry breaking:

$$m_W^2 = \frac{g^2}{4}f^2\sin^2(\langle h\rangle/f), \quad m_Z^2 = \frac{g^2+g'^2}{4}f^2\sin^2(\langle h\rangle/f), \tag{4.5}$$

implying that the electroweak scale v is related to f as

$$v^2 = f^2\sin^2(\langle h\rangle/f). \tag{4.6}$$

It is thus convenient to define the misalignment ξ as

$$\xi \equiv \frac{v^2}{f^2} = \sin^2(\langle h\rangle/f), \tag{4.7}$$

in order to keep track of the relative size between v and f. The intuitive picture is that ξ measures the angle between the true vacuum and $SO(4)$-preserving direction, Φ_0, which would instead correspond to unbroken electroweak symmetry. Eq. (4.5) shows that the ρ parameter, defined as

$$\rho = \frac{m_W^2}{m_Z^2\cos^2\theta_W}, \tag{4.8}$$

is equal to one as long as the simplest operator in (4.3) is concerned. Actually, the custodial protection intrinsic of the $SO(5)/SO(4)$ setup ensures that $\rho = 1$ is preserved at tree-level at any order in the effective theory. In fact, the presence of an operator bringing a subleading correction $\sim v^2/f^2$ to ρ would already imply a very strong bound on the scale f of the order of $f \gtrsim 8$ TeV, see e.g. [154,159]. Such large hierarchy between

v and f will make the model unnatural, as we shall see, and in fact this is the reason why the more minimal coset $SU(3)/SU(2)\times U(1)$ without custodial protection is much less favourable. From (4.3), one can also determine the Higgs couplings to $V = W, Z$:

$$c_V \equiv \frac{g^{\rm CH}_{hVV}}{g^{\rm SM}_{hVV}} = \sqrt{1-\xi}, \quad \tilde{c}_V \equiv \frac{g^{\rm CH}_{hhVV}}{g^{\rm SM}_{hhVV}} = (1-2\xi), \tag{4.9}$$

which are in fact modified with respect to the SM at the $\mathcal{O}(\xi)$ level. By looking at (4.9), we can see that the CH approaches the SM Higgs boson whenever $\xi \to 0$, or equivalently $f \to \infty$. On the other hand, the case in which $\xi = 1$, or $v = f$, can be seen as the technicolor limit in which the electroweak symmetry is broken directly at the condensation scale of the new strong dynamics. CH models can then be seen as interpolating between these two limiting cases. As we shall see, agreement with current observation will require $\xi \lesssim 0.1$.

Let us now move to discuss the Higgs potential. Because of the pNGB nature, the Higgs can enter the theory only as trigonometric functions of argument h/f. The potential can then be written as

$$V(h) = \alpha \sin^2(h/f) + \beta \sin^4(h/f) + \dots \tag{4.10}$$

where the dots indicate higher powers of $\sin(h/f)$ which are subleading in determining the minimum as we already know that the misalignment will be small, $\xi \sim 0.1$. The potential in (4.10) is readily minimized with respect to h, yielding a possible position for the minimum at

$$\xi = \sin^2(\langle h\rangle/f) = -\frac{\alpha}{2\beta}. \tag{4.11}$$

The relation above implies that a non-trivial vacuum with $\xi \lesssim 0.1$ can appear at the price of a little tuning of the parameters. In fact, the trivial extrema would be $\langle h\rangle = 0$ or $\langle h\rangle = \pi f$ corresponding to no electroweak breaking and technicolor limit, respectively. Intuitively, the minimal tuning Δ corresponding to a certain misalignment ξ can be estimated as

$$\Delta \sim \frac{1}{\xi} = \frac{f^2}{v^2} \tag{4.12}$$

showing that configurations with smaller ξ becomes more and more disfavored in this respect. This statement can be made more precise by referring to an explicit measure for the tuning, as the one by Barbieri and Giudice [160], nonetheless (4.12) provides a good estimate. In particular, taking $\xi = 0.1$ already implies a tuning of order $\Delta^{-1} \sim 10\%$. The tolerable amount of tuning in a given theory certainly depends on taste, but few percent is generically considered a mild tuning for models that solve the hierarchy problem all the way up to the Planck scale.

One intriguing feature of CH models with a pNGB Higgs is that the potential is saturated in the low-energy and is in principle calculable as an expansion in the parameters that break the global $SO(5)$. In order to determine the structure of the Higgs potential, one can start by considering all the sources of this breaking. Since the electroweak group is only a subgroup of $SO(5)$, the SM gauge bosons break the global symmetry explicitly. The size of this contribution to the Higgs mass can be estimated by naive dimensional analysis:

$$\delta m_h^2 \sim \frac{g^2}{16\pi^2}\Lambda^2, \tag{4.13}$$

where $g^2/16\pi^2$ takes into account that this is a one-loop contribution proportional to the explicit breaking induced by the gauge coupling g and Λ is an effective UV cutoff. The appropriate value for Λ is given in CH models by the mass threshold of the composite states, as the new strong dynamics is indeed supposed to screen the Higgs potential from physics above the condensation scale. In case of the gauge contribution, these new states are spin-1 resonances, generically indicated by ρ, that have the right quantum numbers to mix with the W and Z boson. Therefore, one simply has $\Lambda \simeq m_\rho$ in (4.13), with typical values of m_ρ at the multi-TeV scale. Despite this contribution being sizeable, it turns out not to be enough to trigger electroweak symmetry breaking because the induced Higgs mass is always positive. In fact, as shown in Ref. [161], the gauge contribution in QCD-like gauge theories that confine always tries to align the vacuum such that the gauge symmetry is preserved.

However, one can find a simple way out by considering the fermionic sector. In fact, the SM fermions interact with the Higgs in a way that is only gauge-invariant and this generically breaks the $SO(5)$ global symmetry. This interaction needs to be there anyway in order to provide masses for the SM fermions after electroweak symmetry breaking. Among the different ways to realize this, there is a very intriguing possibility called *partial compositeness* [157, 158, 162, 163] which assumes that the SM fermions couple linearly to composite operators $\mathcal{O}_{L,R}$ of the strong sector:

$$\mathcal{L}_{\text{linear}} = \lambda_L\, \bar{q}_L(\Delta_L)\mathcal{O}_R + \lambda_R\, \bar{u}_R(\Delta_R)\mathcal{O}_L, \tag{4.14}$$

where we have just considered left-handed quarks, q_L, and right-handed up quarks, u_R, for simplicity, and $\Delta_{L,R}$ are the spurions that connect the $SU(2)_L \times U(1)_Y$ quantum numbers with the $SO(5)$ representation of $\mathcal{O}_{L,R}$, as will be explained below. The reason that makes partial compositeness preferable with respect to other realizations, as for instance bilinear couplings $\lambda\, \bar{q}\, q\, \mathcal{O}$, is flavor physics. In fact, models with bilinear terms struggle to achieve heavy-enough SM quarks and at the same time suppress dangerous flavor-violating couplings. This issue is so severe that in simple realizations one would need to raise the condensation scale f much above the electroweak scale thus introducing a large fine-tuning according to (4.12). Conversely, linear couplings comply more easily with flavor constraints and offer in addition a very elegant means to explain the flavor puzzle in the SM. In fact, a small difference in the quantum scaling of the operators $\mathcal{O}_i$ that couple to the different SM families can result in a large hierarchy for the effective yukawa couplings to the Higgs. This occurs naturally in case of a large separation between f and the scale at which the coupling $\lambda\, \bar{q}_i\, \mathcal{O}_i$ is generated, together with sizeable anomalous dimension for $\mathcal{O}_i$. Remarkably, these conditions can be satisfied by linear couplings without reintroducing the hierarchy problem and without running into formal inconcistencies for the underlying (nearly-)conformal field theory. This has a very simple interpretation in holographic Higgs models, as we shall see in Sec. 4.5 [2].

Let us now discuss the implications of partial compositeness from a low-energy perspective. To this end, we notice that below the condensation scale the operator $\mathcal{O}$ can excite a tower of massive fermion resonances from the vacuum. As the symmetry is now broken from $SO(5)$ to $SO(4)$, these resonances can be organized as $SO(4)$ multiplets.

[2] However, when considering purely four-dimensional theories of partial compositeness [164, 165], having a different operator for each SM flavor requires a large number of fermionic degrees of freedom in the fundamental theory above f. This generically conflicts with the requirement that the new strong dynamics confines in the IR. In these models, only third-family quarks are then partially composite.

For concreteness, let us consider the case in which the lowest resonances are $Q \sim \mathbf{4}$ and $\tilde{T} \sim \mathbf{1}$ of $SO(4)$. The effective Lagrangian is then

$$\begin{aligned}\mathcal{L}_{\text{mixing}} =& \lambda_L f\,(\bar{q}_L \Delta_L)_I \left(a_L\, U_{Ii}\, Q^i_R + b_L\, U_{I5}\, \tilde{T}_R\right) \\ &+ \lambda_R f\,(\bar{t}_R \Delta_R)_I \left(a_R\, U_{Ii}\, Q^i_L + b_R\, U_{I5}\, \tilde{T}_L\right) \\ &- m_Q \bar{Q}_L Q_R - \tilde{m}_T \bar{\tilde{T}}_L \tilde{T}_R + \text{h.c.},\end{aligned} \tag{4.15}$$

where $I = 1, \ldots 5$ and $i = 1, \ldots 4$ are $SO(5)$ and $SO(4)$ indices, respectively, and we have considered only the top quark as it gives the largest contribution to the Higgs potential. The size of the explicit breaking of $SO(5)$ is given by the dimensionless parameters $\lambda_{L,R}$, which need to be smaller than the typical interaction strength g_* among the composite states to treat the $SO(5)$ breaking perturbatively. The appearence of the U matrix is consistent with the Callan–Coleman–Wess–Zumino construction [166,167] and takes into account that the presence of the $SO(4)$ multiplets Q and $\tilde{T}$ is linked to the spontaneous (rather than explicit) breaking of $SO(5)$. In fact, when considering the transformation properties of the Goldstone matrix U in (4.2), one has that the combinations $U \cdot Q$ and $U \cdot \tilde{T}$ indeed transform linearly under $SO(5)$:

$$U \to g\, U\, h^\dagger, \quad Q \to h\, Q \quad \Rightarrow \quad U \cdot Q \to g\,(U \cdot Q), \tag{4.16}$$

and similarly for $\tilde{T}$.

One can see that the form of (4.15) actually describes a physical mixing between the SM quarks and the composite resonances. Before electroweak symmetry breaking, q_L mixes with the one doublet with the SM quantum numbers within the fourplet Q and t_R with $\tilde{T}$. The mixing angle $\theta_{L,R}$ is then related to the parameters in (4.15) as

$$\sin\theta_L \sim \frac{\lambda_L f}{m_Q}, \quad \sin\theta_R \sim \frac{\lambda_R f}{\tilde{m}_T}. \tag{4.17}$$

After electroweak symmetry breaking, this mixing induces a mass for the top quark that is given by

$$m_t \sim \sin\theta_L \sin\theta_R\, m_*\, \sin\left(\langle h \rangle / f\right), \tag{4.18}$$

where we have indicated by m_* the mass scale of the top partners. Thus, we can see that the more a SM field mixes with the composite states, the heavier it will be after electroweak symmetry breaking. More precisely, one finds [168]:

$$m_t \simeq \frac{\lambda_L \lambda_R f}{\sqrt{2} m_T} v, \tag{4.19}$$

where $m_T = \min(m_Q, \tilde{m}_T)$. With the Lagrangian (4.33), one can estimate the contribution to the Higgs potential from loops involving the top quark and the partners Q and $\tilde{T}$. Unlike the gauge sector, the sign of the fermion contribution is unconstrained, and the vacuum can actually be misaligned in the right way. The Higgs mass can then be evaluated from (4.10) as:

$$m_h^2 = \left.\frac{\partial^2 V}{\partial h^2}\right|_{\langle h \rangle} = \frac{8\beta}{f^2}(1-\xi)\xi. \tag{4.20}$$

The coefficient β was estimated in Ref. [168] according to (4.15) to be

$$\beta \simeq \frac{N_c}{16\pi^2} f^4 \lambda_L^2 \lambda_R^2, \tag{4.21}$$

where $N_c = 3$. Thus, combining (4.19) with (4.20) one obtains the following relation:

$$m_h \simeq \frac{\sqrt{3}}{\pi} m_t \frac{m_T}{f}. \tag{4.22}$$

As we can see, the relation above tightly connects the top mass, the Higgs mass and the mass of the top partners [158,168–171]. Eq. (4.22) is found to hold in minimal CH models with partial compositeness independently of the details of the concrete realization [3]. For $\xi = 0.1$ correspoding to $f \sim 800$ GeV one obtains $m_T \sim 1$ TeV in order to reproduce the correct Higgs mass. Such partner masses are actually rather odd as the mass m_* of a generic composite state is supposed to be parametrically larger than the scale f. In fact one usually has $m_* = g_* f$ with typical values $g_* \in (4, 8)$ assuming an underlying CFT with a number of colors $N_c \in (3, 10)$, see e.g. [173]. On the other hand, anomalously light top partners with $m_T \sim f$ seem to be a necessary ingredient in order to reproduce a light Higgs. This information is certainly crucial for the LHC searches of new colored states that can in fact be produced in this mass range, as we shall see in the next section.

4.2 Survey of experimental constraints

As discussed in the previous section, CH models generically predict new states at the TeV scale and modifications of the Higgs couplings to SM particles. This can result in potentially large modifications of the electroweak observables, precisely measured by LEP in the 90's. In particular, new physics contribution to the oblique Peskin-Takeuchi parameters S and T [174] is already severely constrained: too large corrections to the S parameter are in fact one of the main reasons to favor CH models with respect to technicolor. These parameters refer to tree-level or loop corrections to the propagators of the electroweak gauge bosons γ, Z and W. The term oblique is used as opposed to direct, the latter describing vertex and box corrections to a generic electroweak observable.

Let us now briefly review how CH models are supposed to contribute to S and T (see Refs [154,155] for a more complete discussion). The first class of corrections comes from the non-linear nature of the pNGB Higgs and is fully specified by the coset structure. It is therefore dubbed IR contribution, and is unavoidable in any CH realization. This correction involves loop diagrams as in Fig. 4.1, where capital and small letters stand for gauge bosons and Higgs degrees of freedom (including the electroweak Goldstones), respectively. These one-loop corrections occur in the SM as well, where the overall contribution turns out to be finite due to the renormalizability of the theory. However, in the effective theory describing a composite Higgs, a logarithmic sensitivity to the scale of the new resonances appears. Technically, this comes from the fact that different divergent contributions no longer cancel due to the modified Higgs couplings to vector bosons, see (4.9). These log-enhanced contributions are proportional to the misalignment

[3] An exception is given by the MCHM_{14}, where the SM fermions are embedded in the **14** of $SO(5)$. In this case the relation (4.22) can be violated, and a light Higgs can emerge at the price of *ad hoc* cancellations [172, 173].

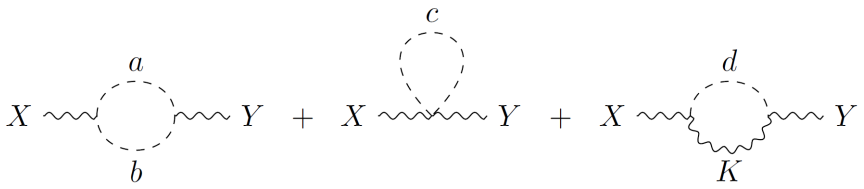

Figure 4.1: Loop contributions to $\hat{S}$ and $\hat{T}$ involving the Higgs doublet.

ξ that measures the non-linearity of the Higgs and its deviation from the SM expectation. For the $SO(5)/SO(4)$ coset one finds:

$$\begin{aligned}\Delta\hat{S}_h &= \frac{g^2}{192\pi^2}\xi\log\left(\frac{m_\rho^2}{m_h^2}\right) \simeq 1.4\times10^{-3}\xi,\\ \Delta\hat{T}_h &= -\frac{3g'^2}{64\pi^2}\xi\log\left(\frac{m_\rho^2}{m_h^2}\right) \simeq -3.8\times10^{-3}\xi,\end{aligned} \tag{4.23}$$

where Δ indicates that the SM contribution has been subtracted and the scale of the vector resonance ρ is set to $m_\rho = 3$ TeV for the numerical estimate. The hatted parameters are related to S and T as $\hat{S} = (\alpha/4\sin^2\theta_W)S$ and $\hat{T} = \alpha T$. Notice that the parameter $\hat{T}$ receives logarithmic corrections (rather than quadratic) because of the custodial symmetry of the $SO(5)/SO(4)$ coset.

Besides the IR contribution due to the modifed Higgs couplings to vector bosons, there are other two sources that affect $\hat{S}$ and $\hat{T}$, namely the contribution from the vector boson resonances ρ and the one from the fermion sector. As mentioned below (4.13), a vector boson ρ can have the right quantum numbers to mix with a Z or W boson. The vector resonances therefore affect the propagation of W and Z already at tree level and give the following contribution to $\hat{S}$:

$$\Delta\hat{S}_\rho = \frac{m_W^2}{m_\rho^2} \simeq 10^{-3} \tag{4.24}$$

with $m_\rho = 3\,\text{TeV}$. This potentially large tree-level effect is indeed the reason for taking ρ in the multi-TeV region. The contribution to the T parameter from the vector resonances turns out to be zero at tree-level again because of the custodial invariance. The radiative contribution is instead non-vanishing but lacks the logarithmic enhancement and is expected to be subleading with respect to $\Delta\hat{T}_h$ in (4.23).

The contribution of the fermionic sector can be similarly divided in IR contribution from loops involving the top quark and UV contribution by the fermionic resonances. Similarly to (4.23), the IR contribution is important as it can feature a logarithmic enhancement. The reason for this is the analogous modification of the top yukawa with respect to the SM value. The exact change depends on the coset structure and on the way the SM fermions are embedded in the theory. Nevertheless all changes are always $\mathcal{O}(\xi)$, and for the MCHM$_5$ one has

$$c_t = \frac{y_t^{\text{CH}}}{y_t^{\text{SM}}} = \frac{1-2\xi}{\sqrt{1-\xi}}. \tag{4.25}$$

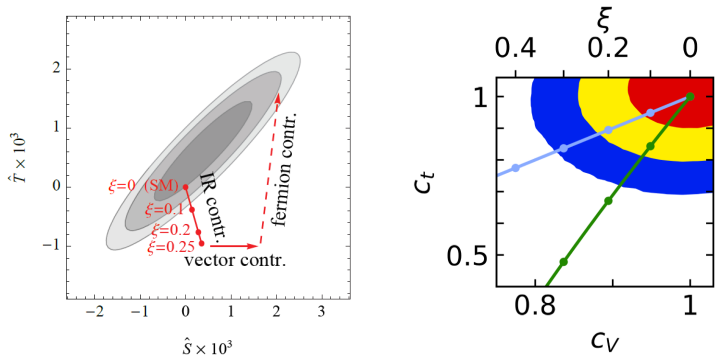

Figure 4.2: **Left:** Exclusion lines for $\hat{S}$ and $\hat{T}$ at 1,2,3σ CL from the electroweak precision tests [176]. CH models generically require cancellations among fermion and vector contributions to pass the electroweak precision tests. Larger values of the misalignment ξ correspond to larger cancellations. Plot taken from Ref. [177]. **Right:** Exclusion lines at 1,2,3σ CL for the misalignment ξ coming from the direct measurement of the Higgs couplings at the LHC. The green (light blue) line corresponds to the MCHM$_5$ (MCHM$_4$). Plot taken from Ref. [178].

The effect for the $\hat{T}$ parameter is estimated as [175]

$$\Delta\hat{T}_{\rm top} = \frac{3y_t^4}{16\pi^2 g_*^2}\xi\,\log\left(\frac{m_\Psi^2}{m_t^2}\right) \simeq 10^{-2}\xi, \tag{4.26}$$

where g_* is the coupling strength among the resonances, and we have taken $g_* = 3$ and $m_\Psi = 1.5\,\text{TeV}$ for the numerical estimate. The IR effect from the top quark on $\hat{S}$ is instead subleading with respect to the IR effect from the Higgs. Other contributions to $\hat{S}$ and $\hat{T}$ are found when considering the effect of the fermionic resonances, and can be as sizeable as (4.26), especially in case of anomalously light top partners, see e.g. [154].

The way the possible sources discussed so far act on the $(\hat{S},\hat{T})$ parameter space is shown in the left panel of Fig. 4.2. As we can see, $\mathcal{O}(1)$ values of ξ are strongly disfavored by the electroweak precision tests. However, a misalignment as large as $\xi \sim 0.25$ could become possible due to the interplay of the vector and fermion contributions as in (4.24) and (4.26), respectively. This possibility, however, relies on suitable cancellations and is therefore disfavored by fine-tuning arguments. For this reason, we shall always focus on the parameter space with $\xi \lesssim 0.1$ so that considering the IR-effect alone one is still close to the 3σ region. Of course, even with this choice of ξ the agreement with the electroweak precision tests is not a given and all contributions should be in principle evaluated in a specific model.

In any case, it is fair to say that the LEP data alone already imply that the deviations from the SM for the Higgs couplings must be rather small, and this translates into a constrain on the misalignment angle as strict as $\xi \lesssim 0.1$. According to our naive estimate in (4.12), this already bears a certain amount of fine-tuning in CH models of the order $\Delta^{-1} \sim 10\%$. Actually, with the rise of the LHC era, the parameter ξ can also be constrained directly by measuring the coupling of the Higgs boson to SM particles and looking for deviations as in (4.9) and (4.25). As we can see from the right panel of Fig. 4.2, these constraints are becoming more and more competitive and values of $\xi \gtrsim 0.2$ are highly disfavored in some benchmark models as the MCHM$_5$, further motivating the

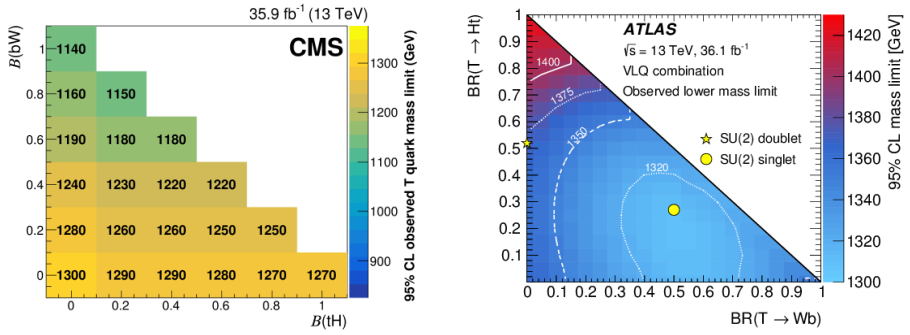

Figure 4.3: Results from a different combination of CMS (left) and ATLAS (right) searches for a vector-like quark $T_{2/3}$. Plots taken from [180].

.

choice of $\xi \lesssim 0.1$ [4].

Besides electroweak precision observables and Higgs couplings, CH models can be tested at the LHC by searching directly for fermion and vector resonances at the TeV scale. While vector bosons in the multi-TeV range are anyway favoured by electroweak precision tests, fermionic resonances are expected at the TeV scale or even lighter by consideration related to the top quark, as discussed below (4.22). If the top partners are not too heavy, they can be produced at the LHC either singly or in pairs. For top-partner masses around 1 TeV, pair production through strong coupling is the dominant mechanism [179]. For a T state with electromagnetic charge $2/3$, the main decay channels are $T \to ht, Wb, Zt$. The relative importance of these channels depends on whether T is a singlet or a doublet under $SU(2)_L$. A combination of different ATLAS and CMS searches for a vector-like quark $T_{2/3}$ is shown in Fig. 4.3. Both searches make use of 36 fb^{-1} data for collisions at center of mass energies of $\sqrt{s} = 13\,\text{TeV}$, These analyses cover the possible range for two relevant branching ratios, $B(ht)$ and $B(bW)$, whereas the third one $B(Zt)$ is easily deduced from the other two. As we can see, top partners with a mass $m_T < 1.3\,\text{TeV}$ are disfavored regardless of the details of the branching ratios. On the other hand, the region $m_T > 1.4\,\text{TeV}$ remains largely unconstrained.

When comparing these constraints with (4.22), one sees that minimal incarnations as the MCHM$_5$ with $\xi = 0.1$ are almost excluded as the light top partners should have already been seen at the LHC. Clearly, minimal models can be rescued by simply raising the decay constant f above the TeV scale or, equivalently, further decreasing ξ. In this sense, the lack of signals at the LHC represents a stronger constrain on ξ than the one from LEP. However, this way of resolving the tension has two immediate drawbacks: *(i)* increasing the Higgs decay constant f pushes the tuning of the model towards the percent level as it scales (at least) quadratically with f, see (4.12); *(ii)* a larger value for f explains the lack of signals in a very trivial way, as we already know that the limit of large decay constant is just the SM, and by doing so *all* signals of Higgs compositeness are simultaneously suppressed because of the non-observation of the top partners.

In the next section, we will introduce a new way of breaking the $SO(5)$ global symmetry such that the prediction of anomalously light top partners is avoided due to a

[4] The light-blue line in the right panel of Fig. 4.2 corresponds to embedding the SM fermions into spinorial representations **4** of $SO(5)$. This was in fact our choice for the axion-Higgs unification in Sec. 2.5. There, the misalignment ξ was realized as $\xi \ll 1$, and all bounds are easily avoided.

different parametric structure of the Higgs potential. As we shall see, this modifies the relation in (4.22) such that heavy top partners will become compatible with a light Higgs *without* the need of raising f.

4.3 Softening the explicit breaking

As discussed in Sec. 4.1, CH models are not only a means to address the stability of the electroweak scale: partial compositeness explains the hierarchy in the masses of the SM flavors as a result of relatively small differences among the quantum scaling dimensions of the composite operators they mix with, which are then spread throughout several orders of magnitude by RG running. Besides generating their masses, the mixing between SM fermions and composite operators is linked with the Higgs potential itself, as SM fields act as a source of explicit $SO(5)$ breaking. Loops containing SM fermions then contribute to the Higgs potential and can help misaligning the vacuum in the right way. Quantitatively, the top quark plays the major role as it features the largest interaction with the strong sector. As we have seen in (4.22), this very appealing construction brings along a sharp prediction that connects the top mass, the Higgs mass and the mass of the top partners. The latter is crucial for the searches of new colored particles, and the so-far null signals of new physics from the LHC around the TeV scale put the idea of Higgs compositeness under pressure.

The core assumption that leads to anomalously light top partners is the symmetry-breaking property of partial compositeness. There, the top yukawa is a hard source of explicit breaking and tries to push the Higgs mass above its observed value unless new particles come at a relatively low scale to rescue it.

In this section, we will mainly follow Ref. [VI] and present a novel way of tackling this issue based on a structural change of the way the elementary and composite sectors talk to each other. In particular, SM fermions will still couple linearly to composite operators not to spoil the nice features of partial compositeness. However, we shall assume that this mixing preserves the global symmetry $SO(5)$ such that the top yukawa is no longer a direct source of explicit breaking. This is possible by uplifting the SM fermions to complete representations of $SO(5)$, and a direct consequence of this is the appearence of new elementary fermions charged under the SM gauge group. The global $SO(5)$ still needs to be broken to misalign the vacuum: this is achieved by introducing vector-like masses for the new elementary fermions that provide the source of explicit breaking and at the same time account for the non-observation of light fermions other than the SM ones. In practice, the explicit breaking of $SO(5)$ has been moved from the interaction between the elementary and strong sector to the structure of the elementary sector itself. In particular, the microscopic interactions between the elementary fermions and the costituents of the strong sector no longer break the global symmetry. This is broken only by vector-like masses that are "soft" terms as opposed to "hard" dimensionless couplings [5].

Our immediate aim is to consider the low energy theory below the condensation scale f and investigate whether this new way of realizing the explicit $SO(5)$ breaking is of any help regarding the issue of light top partners. In doing so, the key parameter is going to be the mass scale of the new vector-like fermions, m_V. In fact, two relevant

[5] We envisage that this can have some implications also when investigating possible completions of the CH effective theory.

limits exist: when m_V exceeds the typical scale of the composite resonances, the new elementary states are effectively decoupled, and the soft-breaking assumption becomes indistinguishable from the standard partial compositeness. On the other hand, the whole Higgs potential becomes small in the limit of vanishing m_V, as the vector-like masses represent the only source of explicit breaking in the fermionic sector. Despite having no practical use, these two limits are conceptually helpful as we can understand the soft-breaking setup as smoothly interpolating between a scenario with no electroweak symmetry breaking at all, $m_V \ll f$, and conventional CH models with partial compositeness, $m_V \gg f$, the intermediate region being the target of our analysis.

4.3.1 Minimal realization

Our starting point is the effective Lagrangian in (4.15) correspoding to the MCHM$_5$, where the subscript refers to the emebedding of the SM fermions q_L and t_R as fundamental representations **5** of $SO(5)$ with $X = 2/3$. The hypercharge is as usual

$$Y = X + T^3_R. \tag{4.27}$$

The spurions $\Delta_{L,R}$ for this choice of the representations are explicitly given by [6]

$$\Delta_L = \frac{1}{\sqrt{2}} \begin{pmatrix} 0 & 0 & 1 & -i & 0 \\ 1 & i & 0 & 0 & 0 \end{pmatrix}, \quad \Delta_R = -i \begin{pmatrix} 0 & 0 & 0 & 0 & 1 \end{pmatrix}. \tag{4.28}$$

The presence of $\Delta_{L,R}$ in (4.15) signals that q_L and t_R act as an explicit source of $SO(5)$ breaking.

As mentioned above, we want to explore here a setup in which partial compositeness respects the global symmetry $SO(5)$. This implies that the SM fermions need to be completed to full $SO(5)$ representations, and new degrees of freedom exist in order to fill the gaps in (4.28). The set of new elementary fermions that can achieve this is not unique. For concreteness, we will now consider the setup that requires the least number of new states in the elementary sector that we shall refer to as soft MCHM$_5$ (sMCHM$_5$). It consists of three vector-like fermions: a singlet s and two doublets v and w that complete the SM fermions to full $SO(5)$ multiplets, ψ^t_L and ψ^t_R, as [VI]:

$$\psi^t_L = \Delta^\dagger_L\, q_L + \Delta^\dagger_w w_L + \Delta^\dagger_s s_L, \quad \psi^t_R = \Delta^\dagger_R t_R + \Delta^\dagger_w w_R + \Delta^\dagger_v v_R, \tag{4.29}$$

where $\Delta_s = \Delta_R$, $\Delta_v = \Delta_L$, and

$$\Delta_w = \frac{1}{\sqrt{2}} \begin{pmatrix} -1 & i & 0 & 0 & 0 \\ 0 & 0 & 1 & i & 0 \end{pmatrix}. \tag{4.30}$$

Notice that the Weyl spinors s_R and v_L are left out of the $\psi^t_{L,R}$ multiplets; their presence is however necessary in order to write down vector-like masses for s and v. In components, (4.29) amounts to

$$\Delta^\dagger_{q_L} q_L = \frac{1}{\sqrt{2}} \begin{pmatrix} b_L \\ -ib_L \\ t_L \\ it_L \\ 0 \end{pmatrix} \longrightarrow \psi^t_L = \frac{1}{\sqrt{2}} \begin{pmatrix} b_L - w^1_L \\ -ib_L - iw^1_L \\ t_L + w^2_L \\ it_L - iw^2_L \\ i\sqrt{2} s_L \end{pmatrix}, \tag{4.31}$$

[6] These new spurions for the fundamental **5** differ from the ones in (2.80) for the spinorial **4**, but we prefer to keep the same symbols throughout this chapter for simplicity.

	$SU(3)_c$	$SU(2)_L$	$U(1)_Y$
s	$\square$	$\mathbf{1}$	$2/3$
v	$\square$	$\square$	$1/6$
w	$\square$	$\square$	$7/6$

Table 4.1: New elementary vector-like fermions in the sMCHM$_5$ and their SM quantum numbers.

and

$$\Delta^\dagger_{t_R} t_R = \begin{pmatrix} 0 \\ 0 \\ 0 \\ 0 \\ -it_R \end{pmatrix} \longrightarrow \psi^t_R = \frac{1}{\sqrt{2}} \begin{pmatrix} v^2_R - w^1_R \\ -iv^2_R - iw^1_R \\ v^1_R + w^2_R \\ iv^1_R - iw^2_R \\ i\sqrt{2}t_R \end{pmatrix}. \tag{4.32}$$

The SM charges of s, v and w are given in Table 4.1. As we can see, v and s share the same quantum numbers of q_L and t_R, respectively, whereas w is an exotic quark. The partial compositeness Lagrangian now simply reads

$$\begin{aligned} \mathcal{L}_{\text{mixing}} =& \lambda_L f_\pi \bar{\psi}^t_{LI} \left(a_L U_{Ii} Q^i_R + b_L U_{I5} \tilde{T}_R \right) \\ &+ \lambda_R f_\pi \bar{\psi}^t_{RI} \left(a_R U_{Ii} Q^i_L + b_R U_{I5} \tilde{T}_L \right) \\ &- m_Q \bar{Q}_L Q_R - \tilde{m}_T \bar{\tilde{T}}_L \tilde{T}_R + \text{h.c.}, \end{aligned} \tag{4.33}$$

where the linear mixings in the first and second line are now truly $SO(5)$-invariant as opposed to (4.15). At this point, we still need to include mass terms for s, v and w together with possible mixings with q_L and t_R. This is done by considering all the terms in the elementary sector that are allowed by the SM gauge symmetries:

$$\begin{aligned} -\mathcal{L}_{\text{el}} =& m_s(\bar{s}_L s_R + \bar{s}_R s_L) + m_v(\bar{v}_L v_R + \bar{v}_R v_L) + m_w(\bar{w}_L w_R + \bar{w}_R w_L) \\ &+ (\delta_1 \, \bar{s}_L t_R + \delta_2 \, \bar{q}_L v_R + \text{h.c.}) \, . \end{aligned} \tag{4.34}$$

The elementary Lagrangian, $\mathcal{L}_{\text{el}}$, can be rewritten in terms of $\psi^t_{L,R}$, s_R and v_L as

$$-\mathcal{L}_{\text{el}} = m_s \bar{\psi}^t_L \Delta^\dagger_s \, s_R + m_v \bar{v}_L \, \Delta_v \psi^t_R + \bar{\psi}^t_L (m_w \Gamma_w + \delta_1 \Gamma_s + \delta_2 \Gamma_v) \psi^t_R + \text{h.c.} \tag{4.35}$$

where we have defined the matrices $(\Gamma_a)_{IJ} \equiv (\Delta^\dagger_a)_I (\Delta_a)_J$ for $a = s, v, w$. Eq.(4.35) accounts for the vector-like masses of the new elementary fermions and at the same time provides the explicit breaking of $SO(5)$, as it is now apparent due to the presence of the Δ and Γ spurions.

Because of the new way of breaking the global symmetry, the soft-breaking setup results in a parametrically different structure for the Higgs potential. In the MCHM$_5$, the linear mixings $\lambda_L \Delta_L$ and $\lambda_R \Delta_R$ always come together with the Goldstone matrix U. Therefore, a one-loop diagram with two propagators is already enough to provide a non-zero contribution to the Higgs potential, see the right panel of Fig. 4.4. In the sMCHM$_5$, however, the $SO(5)$ breaking is given by the vector-like masses in the elementary sector, and thus two extra steps are needed— from $\mathcal{L}_{\text{mixing}}$ to $\mathcal{L}_{\text{el}}$, and back— for the Goldstone matrix to enter the loop together with one of the spurions in (4.35) [7].

[7] At least one spurion should appear in the diagram to give a non-vanishing contribution.

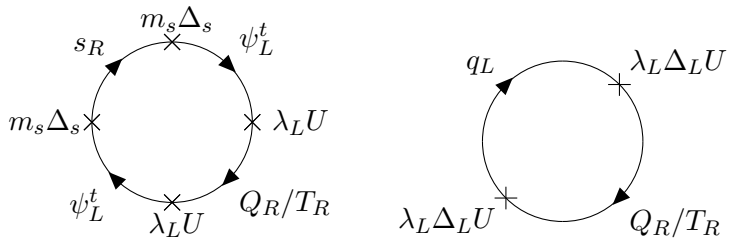

Figure 4.4: Typical contribution to the Higgs potential in the sMCHM$_5$ (left) from a s_R loop as compared to a q_L loop in the MCHM$_5$ (right). Two more propagators are needed in the sMCHM$_5$ to have the spurions Δ and the Goldstone matrix U appearing at the same time.

This is schematically shown in the left panel of Fig. 4.4. A larger number of propagators generically softens the UV behavior of a given diagram, thus further reducing the UV sensitivity of the Higgs potential.

In the next section, we will discuss the consequences of this in terms of divergences and renormalization in a class of phenomenological models for the CH called multi-site models.

4.3.2 Multi-site models: divergences and predictivity

Multi-site models are phenomenological incarnations of Higgs compositeness that allow for a calculable description of the low-energy effective theory [171, 181]. These are inspired by the extra-dimensional realization of the new strong dynamics based on the AdS/CFT correspondence [182]. As we shall see in Sec. 4.5, holographic models in 5D feature a Higgs potential that is always finite and thus captures the essential idea of the CH, namely that its potential is saturated by physics in the IR. This is indeed the core of the solution to the hierarchy problem, as the Higgs bound state disappears above the condensation scale.

It has been shown that the extra dimension can actually be discretized to a finite collection of sites, thus providing a purely 4D effective theory that reflects the key properties of the 5D construction. Physically, each site describes a new layer of composite resonances. The symmetry structure at the i-th site is based on a

$$SO(5)^{(i)}_R \times SO(5)^{(i+1)}_L / SO(5)^{(i)}_{L+R} \tag{4.36}$$

non-linear sigma model, and the Goldstone fields Ω_i are used to connect the sites forming a chain of nearest-neighbour interactions. All the Goldstone fields but one are eventually eaten as an iteration of the Higgs mechanism that provides the mass for the spin-1 resonances ρ_i. The remaining one is instead identified with the pNGB Higgs. At the left-most site of the chain the symmetry is just the SM gauge group, and this corresponds to the elementary sector, whereas at the right-most site one has the usual $SO(5)/SO(4)$ coset structure that mimics the spontaneous $SO(5) \to SO(4)$ breaking at the scale f. This setup is visualized in Fig. 4.5.

This class of models takes advantage from a property that is called *collective symmetry breaking*. The idea is that a contribution to the Higgs potential is generated only

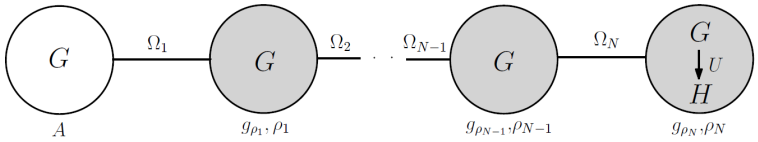

Figure 4.5: Graphical visualization of the structure of multi-site models. Figure taken from [183].

when several sources of explicit breaking come together at the same time. In this case, there are two sources of $SO(5)$ breaking: one is found at the elementary site at the one end of the chain, where the symmetry is only $SU(2)\times U(1)$; the second source is located at the other end of the chain which is only $SO(4)$-symmetric by construction. Since both these breakings need to appear at the same time, one needs to travel from one boundary to the other in order to obtain a non-vanishing contribution to the Higgs potential. Because of the nearest-neighbour interactions, this requires several propagators, and the loops become finite. Obtaining a calculable Higgs potential is then just a matter of considering a large-enough number of sites. This mechanism is closely related to the holographic description in 5D, where the ends of the chain are identified with the UV and IR brane. As we shall see in Sec. 4.5, the source of explicit breaking is there given by specific field boundary conditions on the branes and only loops that stretch from one boundary to the other can know about it. This cuts off any UV divergence yielding a potential that is proportional to the finite volume of the warped extra dimension.

Multi-site models are advantageous because of their transparency and calculability without having to rely on the full extra-dimensional picture. The simplest construction one can think of is in fact the two-site model. This includes the elementary SM fermions and only one layer of resonances, and is obtained by removing all the bulk sites from Fig. 4.5. This setup has been discussed for instance in Ref. [168] as a simple and powerful tool to derive quantitative relations for the spectrum of the top-partners. The Lagrangian of the two-site model is:

$$\mathcal{L}_{\text{two-site}} = \lambda_L \bar{q}_L^i\,(\Delta_L)_{iI}\tilde{\psi}_R^I + \lambda_R\,\bar{t}_R^i\,(\Delta_R)_I\tilde{\psi}_L^I - m_Q\bar{Q}Q - \tilde{m}_T\bar{\tilde{T}}\tilde{T}, \tag{4.37}$$

where $\tilde{\psi} = U(Q,\tilde{T})$. Comparing with (4.15), we see that the two-site Lagrangian simply corresponds to $a_L = b_L$ and $a_R = b_R$.

Let us now briefly discuss what kind of divergences are found within the conventional two-site model defined by (4.37). Referring to the parameterization of the Higgs potential in (4.10), one can check that α receives one-loop contributions from the right diagram in Fig. 4.4 and the analogous one with q_L replaced by t_R. The explicit calculation gives:

$$\alpha = \frac{3}{8\pi^2}(2\lambda_R^2 - \lambda_L^2)f^2\int_0^\Lambda p^3\,\mathrm{d}p\left(\frac{1}{p^2+\tilde{m}_T^2} - \frac{1}{p^2+m_Q^2}\right). \tag{4.38}$$

An interesting property of (4.38) is that the quadratic divergence $\propto \Lambda^2$ for α that one would naively guess from dimensional analysis is actually replaced by a logarithmic one $\sim \log\Lambda$. This is precisely because of collective symmetry breaking and shows that multi-site models are indeed effective in curing the divergences of the Higgs potential. This is even more apparent when looking at the coefficient β, which turns out to be finite already within the two-site model.

If one bulk site is added, thus switching to a three-site model, one finds that α becomes finite giving a fully calculable potential. This is simply understood as better reconstructing the fifth dimension. However, one can still keep the simplicity of the two-site model by employing standard renormalization techniques to get rid of the log-divergence in (4.38). The reasoning is as follows: it is sufficient to introduce a single counterterm in the Lagrangian (4.37) of the form $\delta_\alpha \sin^2(h/f)$ to keep $\alpha+\delta_\alpha$ finite order by order in perturbation theory. This means that the coefficient of $\sin^2(h/f)$ is not predictable in the two-site model, and the idea is to fix it once all the other parameters are given in order to reproduce the correct Higgs vev. However, the two-site model still predicts the crucial relation between the Higgs mass and the top partner mass through the coefficient β which is indeed always finite and related to the Higgs mass through the basic relation in (4.20). Indeed, the derivation of (4.22) did not require the calculation of α, and we thus conclude that the two-site model is still highly predictive.

Let us now move to discuss in detail the two-site model for the soft-breaking setup discussed in the previous section. The two-site Lagrangian is very similar to (4.37), with the crucial difference that q_L and t_R are completed to full multiplets $\psi^t_{L,R}$ [VI]:

$$\mathcal{L}^{\text{soft}}_{\text{two-site}} = \lambda_L f_\pi \bar{\psi}^t_L \tilde{\psi}_R + \lambda_R f_\pi \bar{\psi}^t_R \tilde{\psi}_L - m_Q \bar{Q} Q - m_T \bar{\tilde{T}} \tilde{T}, \tag{4.39}$$

together with $\mathcal{L}_{\text{el}}$ in (4.35). In principle, we could expect a different divergence structure because of the different number of propagators that are required to generate α, see again the left plot of Fig. 4.4. Indeed, it turns out that the first two terms in (4.35) proportional to m_s and m_v do provide a finite α; however, the remaining terms proportional to m_w, δ_1 and δ_2 give a log-divergent contribution making α not predictable within the soft two-site model either. In particular, one finds that w contributes to α as

$$\alpha = \cdots + \frac{3}{4\pi^2}\lambda_L \lambda_R f^2 \int_0^\Lambda p^3 \, \mathrm{d}\, p^3 \frac{m_w}{p^2+m_w^2}\left(\frac{m_Q}{p^2+m_Q^2} - \frac{\tilde{m}_T}{p^2+\tilde{m}_T^2}\right), \tag{4.40}$$

which is indeed log-divergent with Λ. Notice that decoupling the w state by giving it a large mass would be of no help, as the lack of these propagating degrees of freedom would reintroduce the log-divergence in the other terms. In Sec. 4.4.2 we will comment on the possibility to make the potential fully calculable in the soft two-site by choosing a slightly less minimal field content for the elementary vector-like fermions. In the following, we will stick to the minimal embedding in (4.29) and deal with this divergence similarly to what has been done for the standard two-site model in (4.37). In particular, when providing analytical estimates of the main relations in our model, it is sufficient to focus on β which is fully calculable. It can be derived from the Coleman-Weinberg potential,

$$V(h) = -\frac{2N_c}{8\pi^2}\int_0^\Lambda \mathrm{d}p\, p^3 \log\det\left[p^2 \mathbb{1} + m^\dagger m(h)\right], \tag{4.41}$$

where $m(h)$ is the field-dependent fermion mass matrix such that

$$\det\left[p^2\mathbb{1} + m^\dagger m(h)\right] = 1 + a(p^2)\sin^2(h/f) + b(p^2)\sin^4(h/f), \tag{4.42}$$

where $a(p^2)$ and $b(p^2)$ are functions of the fermion masses. Expanding the logarithm up to $\sin^4(h/f)$, one finds (4.10) where

$$\alpha = -\frac{2N_c}{8\pi^2}\int_0^\Lambda \mathrm{d}p\, p^3 a(p^2), \quad \beta = -\frac{2N_c}{8\pi^2}\int_0^\Lambda \mathrm{d}p\, p^3 \left(b(p^2) - \frac{a^2(p)}{2}\right). \tag{4.43}$$

Since α is log-divergent with Λ, we will assume that a counterterm δ_α has been introduced such that the Higgs gets the correct vev. As for β, the integral is convergent and the cutoff can be safely sent to infinity; we will then use the very expression in (4.43).

Instead, when performing numerical scans, we will refer to the renormalized version of the Coleman-Weinberg potential, where the freedom in the finite part of the counterterm δ_α translates to an arbitrary renormalization scale μ:

$$V(h) = -\frac{N_c}{16\pi^2}\sum_i m_i(h)^4\left[\log\left(\frac{m_i(h)^2}{\mu^2}\right) - \frac{3}{2}\right], \tag{4.44}$$

and $m_i(h)$ are the field-dependent fermion masses. The value of μ is determined, once all the other parameters are fixed in order to reproduce the correct Higgs vev. In particular, we require μ to be below the cutoff of the effective theory, $\Lambda \approx 4\pi f$, so that μ can actually be interpreted as an effective parameter capturing the effect of the heavier resonances, or, equivalently, of the additional sites.

As we have seen at the beginning of this chapter, another crucial quantity besides the Higgs potential in determining (4.22) is the mass of the top quark. In the two-site model, this evaluates to

$$m_t^2 = \frac{\lambda_L^2\lambda_R^2 f^2 (m_Q - \tilde{m}_T)^2}{2(m_Q^2 + \lambda_L f^2)(\tilde{m}_T^2 + \lambda_R f^2)} v^2, \tag{4.45}$$

which is in agreement with (4.19). A similar expression for m_t is found in the soft two-site model where however there are more states that can mix with the top, namely the singlet s and the doublet v. The explicit formula for m_t is therefore more involved although it brings no conceptual difficulty. For instance, setting $\delta_1 = \delta_2 = 0$ for simplicity, one has

$$m_t^2 = \frac{\lambda_L^2\lambda_R^2 f^2 m_s^2 m_v^2 (m_Q - \tilde{m}_T)^2}{2(m_Q^2 m_v^2 + \lambda_L^2 f^2 m_v^2 + \lambda_L^2\lambda_R^2 f^4)(\tilde{m}_T^2 m_s^2 + \lambda_R^2 f^2 m_s^2 + \lambda_L^2\lambda_R^2 f^4)} v^2. \tag{4.46}$$

In the limit of large m_s and m_v, one can check that the elementary fields effectively decouple and (4.46) approaches (4.45). In general, as long as $m_{s,v} \gtrsim \lambda_{L,R} f$, the new expression for m_t gives basically the same result as the standard one, namely the top mass is only mildly affected by promoting the SM fermions to complete $SO(5)$ multiplets.

The vector-like masses for the new elementary fermions, m_s, m_v and m_w, are *a priori* independent quantities, and their values could be predicted only in a more complete theory for the elementary sector. In the following, we will simply regard the vector-like masses as phenomenological parameters that can be arbitrarily varied with the aim of exploring which region of parameter space has the strongest impact, and refer to Sec. 4.5 for a possible rationale behind their actual values. In particular, we will retain the possibility that some mild hierarchies exist in the vector-like masses. Such hierarchies need not be extreme: whenever a state exceeds the typical scale of the composites $\sim 4\pi f$, it no longer contributes to the Higgs potential. Thus, we will consider two cases: First, we will assume that only the singlet s is active below the condensation scale. This drastically reduces the number of new free parameters with respect to the conventional two-site model and makes the analysis very simple and transparent. In the second case, all vector-like fermions participate to the dynamics, and we will then mainly rely on a scan over the parameter space.

4.3.3 Two-site model analysis

We present here the analysis within the soft two-site model introduced in the previous section considering the case of mild hierarchies among the elementary vector-like fermions as well as the general case in which all the new states are active below the condensation scale. What follows is based on Ref. [VI].

Singlet case

We start by considering the case in which v and w are heavier than s and reside above the condensation scale. We will thus remove these degrees of freedom from the model: this can be done either directly from (4.29) or by leaving (4.29) unchanged and eventually take the limit for $m_{v,w} \to \infty$. The only state that is possibly active is then the singlet state s. The full Lagrangian describing this setup is deduced from (4.35) and (4.39) and reads:

$$\begin{aligned}\mathcal{L}_{\text{singlet}} = \lambda_L f \bar{\psi}_L^t \tilde{\psi}_R + \lambda_R f\, \bar{\psi}_R^t \tilde{\psi}_L - m_s\, \bar{\psi}_L^t \Delta_s^\dagger\, s_R + \delta_1 \bar{\psi}_L^t \Gamma_s \psi_R^t \\ - m_Q \bar{Q}_L Q_R - \tilde{m}_T \bar{\tilde{T}}_L \tilde{T}_R + \text{h.c.},\end{aligned} \tag{4.47}$$

where we recall that $\tilde{\psi} = U(Q, \tilde{T})$, and w and v have been decoupled leaving only

$$\psi_L^t = \Delta_L^\dagger\, q_L + \Delta_s^\dagger s_L, \quad \psi_R^t = \Delta_R^\dagger t_R. \tag{4.48}$$

As we can see, there are two more parameters when comparing with the conventional two-site in (4.37), namely m_s and δ_1. In order to derive simple estimates for our model, we will set $\delta_1 = 0$ as the qualitative behavior is left unchanged (the case of a non-zero δ_1 will be considered when performing a numerical scan). Within this assumption, the top mass is given by:

$$m_t^2 = \frac{\lambda_L^2 \lambda_R^2 f^2 m_s^2 (m_Q - \tilde{m}_T)^2}{2 m_T'^2 [m_{\tilde{T}}^2 m_s^2 + \lambda_L^2 \lambda_R^2 f^4]} v^2 \tag{4.49}$$

where $m_T'^2 = m_Q^2 + \lambda_L^2 f^2$, $m_{\tilde{T}}^2 = \tilde{m}_T^2 + \lambda_R^2 f^2$. From (4.49) we can see that the expression for m_t is always slightly smaller than its counterpart in (4.45). By itself, this effect would imply even lighter the top partners. However, this is actually not the case when the more important modification in the Higgs potential is taken into account. To show this let us calculate β through (4.43). We find that $a^2(p^2)$ is always negliglible in this case, and β is given by

$$\beta \simeq \int_0^\infty \mathrm{d}p\, p^3 \frac{\lambda_L^2 \lambda_R^2 f^4 (m_Q - \tilde{m}_T)^2 \left[m_s^2 (p^2 + m_Q^2) - p^2 (p^2 + m_T'^2) \right]}{2 p^2 (p^2 + m_Q^2)(p^2 + m_T'^2)(\tilde{m}_T^2 (p^2 + m_s^2) + (p^2 + \lambda_R^2 f^2)(p^2 + m_s^2 + \lambda_L^2 f^2)}. \tag{4.50}$$

In the limit of $\lambda_{L,R} f$ much smaller than the mass of the vector-like fermions, one can approximate the top mass and β through analytical formulas. We will then introduce two dimensionless parameters, q and r, that will simplify our notation:

$$q \equiv m_Q / \tilde{m}_T, \quad r \equiv \tilde{m}_T / m_s. \tag{4.51}$$

In case of $q = 1$, the fourplet and singlet masses are exactly degenerate, thus removing the source of $SO(5)$ breaking at the right end of the chain in Fig. 4.5. From the discussion

in the previous section, this means that the potential generated in the fermionic sector will exactly vanish in this limit. Conversely, the parameter r controls the impact of the singlet state, s, on the potential. The case of $r \ll 1$ coincides with the singlet being fully decoupled, and the model will become indistinguishable from the conventional two-site. On the other hand, $r \gg 1$ means that s is much lighter than the composite resonances, thus introducing by hand a very light state in the theory. Therefore, the region of interest is $r \sim 1$. In the limit of $\lambda_{L,R} f \ll m_s, m_Q, \tilde{m}_T$ we can rewrite the top mass in terms of q as

$$m_t^2 \simeq \frac{\lambda_L^2 \lambda_R^2 f^2}{2 m_Q^2} (q-1)^2 v^2, \tag{4.52}$$

whereas the momentum integral in (4.50) can be performed analytically, giving

$$\beta(r^2) \simeq \frac{N_c}{16\pi^2} y_L^2 y_R^2 f^4 \frac{(1-q)^2}{1-q^2 r^2} \left[(r^2 + 1/q^2) F(q^2) - 2F(r^2) \right], \tag{4.53}$$

where we have defined

$$F(x^2) \equiv \frac{x^2}{1-x^2} \ln \frac{1}{x^2}. \tag{4.54}$$

It is interesting to see how β is modified for a non-zero value of r with respect to the standard case. In fact, one finds that

$$\beta(r^2) - \beta(0) = -C^2 \frac{F(q^2) - F(1/r^2)}{q^2 - 1/r^2} \leq 0, \tag{4.55}$$

where C^2 is a positive constant, and we have used $F(1/x^2) = F(x^2)/x^2$ together with the property that $F'(x) > 0$ for $x > 0$. The $\beta(0)$ term in (4.55) corresponds to the case in which the new singlet s is infinitely heavy and decouples. We have checked that it coincides with the conventional formula for β in the two-site MCHM$_5$, namely

$$\beta(0) \simeq \frac{N_c}{16\pi^2} \lambda_L^2 \lambda_R^2 f^4 \frac{(1-q)^2}{q^2} F(q^2). \tag{4.56}$$

The inequality in (4.55) is very important as it shows that including the singlet s always reduces the amount of explicit breaking leading to a lighter Higgs boson. Combining (4.52), (4.53) and the general form for the Higgs mass, (4.20), we find

$$m_Q^2 = \frac{1}{16} \lambda_L^2 \lambda_R^2 f^2 \frac{(1-q)^2}{\beta(r^2)} \left(\frac{m_h}{m_t} \right)^2, \tag{4.57}$$

which relates the Higgs mass to the spectrum of resonances. For concreteness, let us take $q = -1$ and evaluate (4.57) to see explicitly how (4.22) is modified in our setup. One finds:

$$m_h \simeq 0.6\, m_t \frac{\sqrt{1-r}}{1+r/3} \frac{m_Q}{f}. \tag{4.58}$$

For $r = 0$ we obtain the standard result, namely $m_Q \simeq 1.1$ TeV for $f = 800$ GeV ($\xi = 0.1$). However, when m_s is of the same order of m_Q, heavier top partners become compatible with a light Higgs. For instance, $m_s \approx 2 m_Q$ already gives $m_Q \simeq 1.8$ TeV without the need of raising f.

By inspecting (4.53), we notice that $\beta(r^2)$ actually vanishes for $q^2 r^4 = 1$ and it becomes negative for $q^2 r^4 > 1$, the latter case being in conflict with a viable electroweak

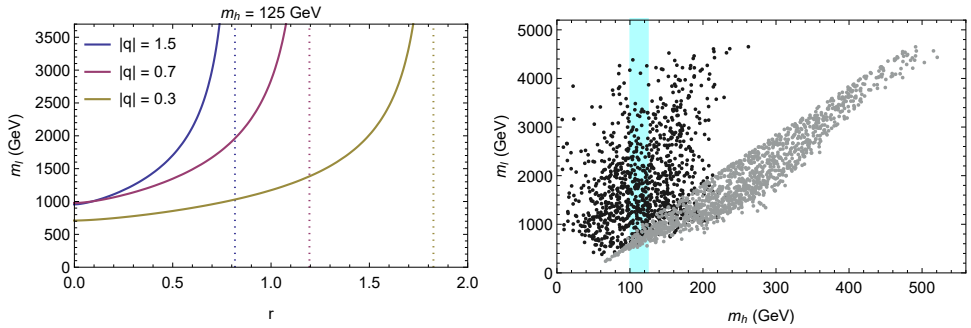

Figure 4.6: **Left**: The mass of the lightest state m_l for different values of $|q|$ as a function of $r = \tilde{m}_T/m_s$ for $m_h = 125\,\text{GeV}$. The dashed vertical lines indicate the value of r above which $\beta(r)$ turns negative. The plots are symmetric for $r \to -r$. **Right**: Scatter plot of (m_h, m_l) for $|r| \in (0.5, 2)$ (black points) and $r = 0$ (gray points). We scan in the range $|\lambda_{L,R}| \in (0.5, 2)$, $|\tilde{m}_T| \in (0.5, 4.5)$ TeV, $q \in (-2, -0.3)$ and $|\delta_1| \in (0, 2)$ TeV.

symmetry breaking. We will therefore restrain ourselves to the region $q^2 r^4 < 1$. As an estimate for the mass of the lightest eigenstate of the system, m_l, we take

$$m_l^2 \simeq \min\{m_Q^2, \tilde{m}_T^2, m_s^2\} = m_Q^2 \times \min\left\{1, \frac{1}{q^2}, \frac{1}{q^2 r^2}\right\} = m_Q^2 \times \min\left\{1, \frac{1}{q^2}\right\} \tag{4.59}$$

where m_Q^2 is given in (4.57). The estimate above is correct up to mixing terms $\sim \lambda_{L,R} f$. The last equality in (4.59) is derived as follows. By definition, m_s can be the lightest state only for $r^2 \geq 1$ and $r^2 \geq 1/q^2$. Moreover, r and q must satisfy $r^2 \leq r_0^2 = 1/|q|$, as discussed below (4.57). However, if $|q| > 1$ one immediately derives the contradiction $r^2 < 1$, while if $|q| < 1$ one has $r^2 \geq 1/q^2 = r_0^4 > r_0^2$, which is clearly not compatible with $r^2 \leq r_0^2$. In conclusion, the spectrum favors a configuration with the elementary singlet s not residing at the bottom. When s is about to become the lightest state, β flips sign, and the electroweak vacuum is no longer a minimum.

The value of m_l as predicted by (4.59) is shown in the left panel of Fig. 4.6 as a function of r for different values of q. We take $m_t \simeq 150\,\text{GeV}$ for the top mass at the scale f. The standard result is recovered for $r = 0$ and gives $m_l \lesssim 1$ TeV. As we can see, the mass of the lightest state always increases with r until it hits $q^2 r^4 = 1$ shown by the dotted vertical lines for each value of q. It is important to notice that m_l can be significantly heavier than in the standard case for values of r and q which are far from the vertical line. Thus, a heavier m_l does not correspond to fine tuning in the parameter space but rather to a general prediction of the soft-breaking hypothesis. This is confirmed by the results shown in the right panel of Fig. 4.6, where (m_h, m_l) are obtained as an output from a numerical scan using the general form of the Coleman-Weinberg one-loop potential given in (4.44). The window $m_h \in (100, 125)$ GeV visualized by the blue band is considered to take into account running effects on the actual value of the Higgs mass at the scale f. The value of r is scanned between $0.5 \leq |r| \leq 2$ (black points). Gray points correspond to the standard case, i.e. $r = 0$. The effect of the singlet s can be seen as effectively reducing the Higgs mass which is consistent with a certain value of m_l. For instance, $m_l = 3\,\text{TeV}$ is compatible with $m_h \sim 100\,\text{GeV}$ in our setup, whereas that would require $m_h > 300\,\text{GeV}$ in the conventional case. This is just an equivalent way of looking at (4.55), where the ratio $\beta(r^2)/\beta(0) = m_h^2(r^2)/m_h^2(0) < 1$ gives the correct

estimate for the softening of the Higgs mass.

General case

We present here the analysis for the case in which there are no hierarchies among the masses of the elementary vector-like fermions s, v and w. We then derive an expression for β following the same procedure that lead to (4.53), setting $m_v = m_w \equiv m_d$ for simplicity, which we will refer to as $\tilde{\beta}$ in the following[8]. The relative spread between the elementary states is parameterized by $x = m_d/m_s$, while $r = \tilde{m}_T/m_s$ relates the elementary state s to the composites as in (4.51). We notice that in this case the $a^2(p^2)$ term in (4.43) can actually be important and needs to be taken into account. The mass of the lightest state, m_l, is now estimated as

$$m_l^2 \simeq \min\{m_Q^2, \tilde{m}_T^2, m_s^2, m_d^2\} = m_Q^2 \times \min\left\{1, \frac{1}{q^2}, \frac{1}{q^2 r^2}, \frac{x^2}{q^2 r^2}\right\}, \tag{4.60}$$

while the top mass is still well approximated by (4.52). The quantity m_Q obeys (4.57), where β is now replaced by the new quartic $\tilde{\beta}$. We have checked that $\tilde{\beta}$ approaches zero for $r \gg 1$ corresponding to massless elementary fermions and thus restoring the $SO(5)$ global symmetry. In practice, such limit is not of much use because it would introduce very light states in the spectrum. However, its existence shows how drastically the Higgs potential can be modified with soft-breaking when compared to the conventional models.

When all the elementary fermions are kept in the spectrum, we identify three different regions depending on the value of $x = m_d/m_s$. First of all, the case of a large $|x|$ simply corresponds to the singlet case discussed in the previous section. Conversely, for $|x| \leq 2$ we find that the improvement in the top partner masses is not dramatic and m_l can be roughly as heavy as 2 TeV. Thus, we focus here on the intermediate case $2 \leq |x| \leq 4$ as it shows the main new effect. The analytical prediction based on $\tilde{\beta}$ is shown in the left panel of Fig. 4.7 for $x = 2.7$. For all the lines, the knee signals that the elementary singlet becomes the lightest state. This happens for r such that $r^2 \geq r_q^2 = \max(1, 1/q^2)$. Notice that this was not possible in the case in which the w and v doublets are infinitely heavy, since it would give a negative value of β, as discussed below (4.59). The dotted lines show the location of r such that $\tilde{\beta}$ formally vanishes. The values of r beyond the dotted lines actually lead to a viable m_l, its value being just too large to be shown in the plot. Although such high masses are cut off in a realistic scenario, this shows that the range of r leading to a viable electroweak symmetry breaking is enlarged with respect to the singlet case.

Since the largest possible m_l is typically found above the knee, a heavy top partner favors the case of the singlet s as the lightest particle, as opposed to the case in which v and w were decoupled. This also implies that a viable spectrum can be obtained without requiring the spin-1/2 resonances to lie much below the naive cutoff of the effective picture, as opposed to the conventional case in which the presence of anomalously light resonances is required to reproduce the correct Higgs mass. We explore this region of the parameter space in the right panel of Fig. 4.7, where (m_h, m_l) are obtained after a numerical scan according to (4.44). We assume $\tilde{m}_T$ to be in the range $(5, 10)$ TeV, where the latter coincides with the cutoff scale $4\pi f$ for $\xi = 0.1$. Moreover, we scan $1.5 \leq |r| \leq 5$,

[8] Although analogous to (4.53), the expression for $\tilde{\beta}$ is too involved to justify the inclusion of its explicit form.

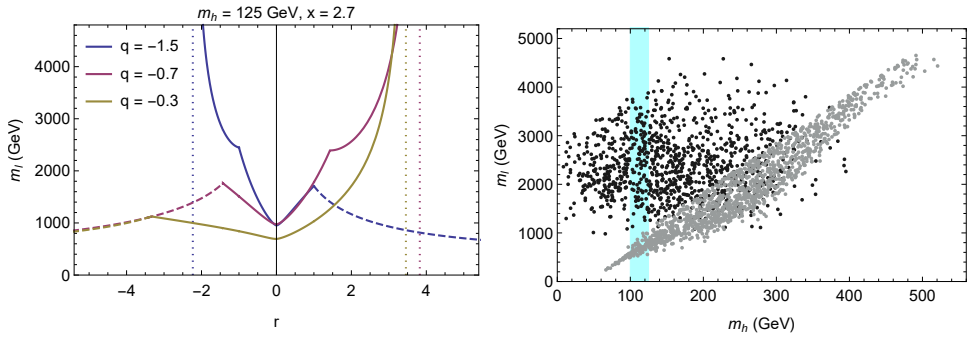

Figure 4.7: **Left**: The mass of the lightest state m_l for different values of q as a function of r with $m_h = 125\,\text{GeV}$ and $x = 2.7$. The vertical dotted lines indicate r such that $\tilde{\beta} = 0$. Dashed curves show configurations for which a decrease in m_l is driven by the lightness of the singlet s. **Right**: The mass of the lightest state m_l as a function of m_h in the sMCHM$_5$ (black points) and in the MCHM$_5$ (gray points). The scan for the sMCHM$_5$ assumes $|\lambda_{L,R}| \in (1,2)$, $q \in (-2,-0.3)$, $|\tilde{m}_T| \in (5,10)\,\text{TeV}$, $|r| \in (1.5,5)$ and $|\delta_{1,2}| \in (0,2)$ TeV. The doublet masses $m_{w,v}$ are scanned independently in the range $|m_{w,v}/m_s| \in (2,4)$.

while the doublet masses are independently scanned in the range $2 \leq |m_{v,w}/m_s| \leq 4$. To obtain the correct top mass, we consider $1 \leq |\lambda_{L,R}| \leq 2$. As we can see, the result is qualitatively the same as in Fig. 4.6 allowing for heavy top partners in the blue region compatible with the Higgs mass.

4.3.4 Remarks

Our analysis in Sec. 4.3.3 shows that heavy top partners become compatible with a light Higgs when implementing the soft-breaking idea. To show how the spectrum can look like, we choose two benchmark points, corresponding to the singlet and general case, respectively. For the former we take B_s as

$$B_s : \{\lambda_L = 1.4,\, \lambda_R = 1.3,\, \tilde{m}_T = 3\,\text{TeV},\, m_s = 3.8\,\text{TeV},\, \delta_1 = 0\}\,, \tag{4.61}$$

corresponding to $r = \tilde{m}_T/m_s \simeq 0.8$ and $q = -0.9$ and $m_t \simeq 140\,\text{GeV}$ in the notation of (4.51). The lightest eigenstate is the mainly composite singlet state $\tilde{T}_-$, with a mass $m_l \simeq 2.7\,\text{TeV}$ and electromagnetic charge $Q = 2/3$. The Higgs mass is found to be $m_h \simeq 110\,\text{GeV}$. The spectrum is shown in the left panel of Fig. 4.8. The states colored black correspond to mainly composite states, whereas the purple ones are mostly elementary. The composite resonances lie in the range $2.7 - 3.0$ TeV. The heaviest state is the mainly elementary singlet $\tilde{T}_+$ with a mass around 4 TeV.

For the general case we consider the following point

$$B_f : \{\lambda_L = 1.8, \lambda_R = 1.8,\, \tilde{m}_T = 9,\, m_s = 3.5,\, m_v = 9.8,\, m_w = 8.7,\, \delta_{1,2} = 0\}, \tag{4.62}$$

where dimensionful quantities are measured in TeV giving $q \simeq -0.4$ and $m_t \simeq 140\,\text{GeV}$. The lightest state is now the mostly elementary singlet $\tilde{T}_-$ with $m_l \simeq 3.4\,\text{TeV}$ and again electromagnetic charge $Q = 2/3$. The Higgs mass is $m_h \simeq 120\,\text{GeV}$. The spectrum is given in the right panel of Fig. 4.8, where the same color convention is used to distinguish

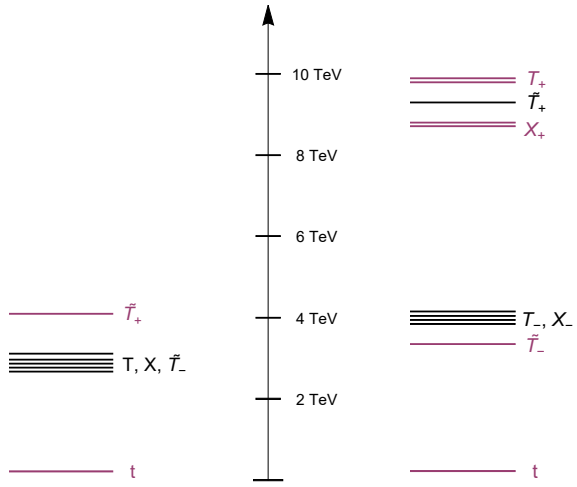

Figure 4.8: **Left**: The spectrum from the benchmark point B_s. The lightest particle mainly overlaps with the composite singlet $\tilde{T}$, with a mass $m_l \simeq 2.7\,\text{TeV}$. **Right**: The spectrum from the benchmark point B_f. The lightest particle is mainly the elementary singlet s, with a mass $m_l \simeq 3.4\,\text{TeV}$. For both spectra, states colored by black are mainly composites, whereas purple ones are mainly elementary.

the mostly elementary states from the mainly composites. The overall effect of bringing the doublets v and w down with respect to left panel (where they are instead decoupled) is to lift the lightest state which is now mostly elementary.

It is also quite interesting to see what happens if we perturb around our assumption of $SO(5)$-symmetric partial compositeness introduced in Sec. 4.3.1. In our setup, the new vector-like fermions are embedded together with the SM quarks to form complete $SO(5)$ multiplets and thus couple to the strong resonances in exactly the same way. The explicit breaking is then given only by the non-zero masses for the vector-like fermions. If we now relax this assumption and still think of adding some elementary vector-like fermions in the theory, their couplings to the strong sector no longer need to be the same as the SM fermions. In practice, we introduce a common "perturbation" κ acting on the couplings of s, v and w such that the case $\kappa = 1$ will reconstruct $SO(5)$ symmetric couplings and give the results of the previous section, whereas $\kappa = 0$ will decouple the new fermions from the composite resonances. We then recalculate the coefficient β in the Higgs potential that we refer to as β_κ. The ratio β_κ/β_0 thus measures the relative degree of explicit breaking between a setup with generic couplings and the conventional case in which only the SM fermions talk to the composites. This ratio is also directly related to the different predicitions for the Higgs mass through (4.20).

We show β_κ/β_0 via a contour plot in Fig. 4.9, where again $r = \tilde{m}_T/m_s$, $x = m_d/m_s$, with m_d the degenerate mass of the doublets v and w, for a reference value of $q = m_Q/\tilde{m}_T = -0.7$ and $x = 2.7$. At the bottom of the plot, β_κ/β_0 is trivially equal to one. For larger values of κ, the amount of explicit breaking is reduced up to the point $\kappa > 1.5$ beyond which it is actually monotonically enhanced (note that points with $r \approx 0$ give no change as the new states are too heavy). As we can see, the optimal region with the smallest amount of explicit breaking is around $\kappa \approx 1$, namely the $SO(5)$ symmetric point for partial compositeness which is automatically obtained within the soft-breaking setup. Thus, organizing the new elementary fermions (when possible) to complete full

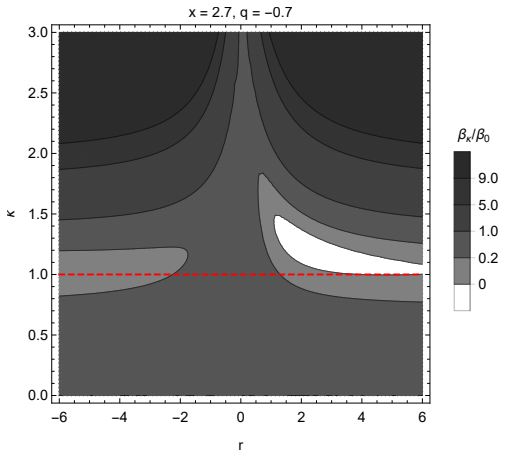

Figure 4.9: The ratio β_κ/β_0 as a contour plot in the (r, κ) plane for $x = 2.7$ and $q = -0.7$. The value of $\kappa = 1$ that yields an $SO(5)$-symmetric partial compositeness is highlighted by the red dashed line and corresponds to the smallest amount of explicit breaking. The plot is symmetric for $\kappa \to -\kappa$.

$SO(5)$ representations is not only motivated by symmetry arguments but it turns out to be in general the safest option to keep the Higgs light.

Let us now summarize our findings in this section. In Sec. 4.3.1 we have proposed a new way of breaking the global symmetry in CH models which controls the generation of a non-vanishing Higgs potential. Instead of breaking it in the conventional way due to the SM fermions not filling complete representations of the global symmetry— $SO(5)$ in our case— we break it "softly" via vector-like masses for the additional degrees of freedom that complete the SM fermions to full $SO(5)$ representations. In this way, the tight relation in (4.22) between the Higgs mass and anomalously light top partners that is in tension with the current LHC data is relaxed, allowing heavy top partners with a light Higgs already in minimal models such as the MCHM$_5$. We have provided quantitative evidence for this by performing a detailed analysis within the two-site realization of our setup, which is supposed to capture the main features of our model. While this is a necessary step to reconcile the CH idea with the so-far null signals of new physics at the LHC, another very important topic has not been tackled yet, namely how soft breaking impacts the fine-tuning that is needed to achieve the correct electroweak symmetry breaking. This will be discussed in Sec. 4.4.

4.4 Enhanced symmetries for a light Higgs

In the previous section we have introduced the idea of softening the explicit breaking of the global symmetry under which the CH is a pNGB, and provided a quantitative analysis based on the two-site model of the minimal sMCHM$_5$. Our main result was that anomalously light top partners can be successfully avoided without making the Higgs more and more elementary, as the conventional relations between the Higgs mass and the mass of the top partners are modified by the new symmetry structure. The two-site model discussed above had the major advantage of simplicity, but it also has the drawback of still yielding a divergent α. Besides the lack of a fully calculable potential,

which would be anyway desirable, this implies that evaluating the tuning in the model is not straightforward. Nonetheless, some considerations can be made.

In Sec. 4.1 we have seen that a misalignment ξ brings in a certain amount of intrinsic tuning of order $\Delta \sim 1/\xi$. On top of that, there can be actually other sources of tuning that depend on the details of the CH model, as for instance the embedding of the SM fermions. Our concrete example was based on the MCHM$_5$, where the fermions are embedded in the fundamental **5** of $SO(5)$, and it is therefore useful to review what is the actual tuning that is expected in the conventional picture. This can be estimated most easily using spurion analysis. Referring to (4.15), the embedding of the SM fermions into the **5** of $SO(5)$ is achieved through the matrices Δ_L and Δ_R that are the spurions characterizing the symmetry breaking due to the embedding of the SM fermions into $SO(5)$ representations, even though they do not form complete multiplets. The explicit form of these spurions is given in (4.28). Since they connect different groups, spurions have mixed indices: the columns transform under the elementary $SU(2)^0_L$ and the rows under $SO(5)$,

$$\Delta_L \sim \left[SU(2)^0_L \times U(1)^0_Y\right] \times SO(5), \quad \Delta_R \sim U(1)^0_Y \times SO(5), \tag{4.63}$$

whereas the $U(1)_Y$ appears as an arbitrary phase. These spurions fully encode the effects of the explicit breaking due to using incomplete multiplets, and can be used to obtain information on the possible structure of the Higgs potential. In practice, one first treats the spurions as dynamical fields and identifies the transformations that would formally restore $SO(5)$ as a true symmetry of the model. Physical quantities, such as the Higgs potential, need to be invariant when *all* the fields, including the spurions, are transformed. This requirement constrains the possible combinations of fields that can enter the Higgs potential. Once all the invariants are constructed, the spurions can be set to their actual form in (4.28) that can be regarded as the vacuum expectation value of the corresponding field.

The relevant symmetries here are the elementary $SU(2)^0_L \times U(1)^0_Y$ and the $SO(5)$ global symmetry. As the Higgs boson only transforms under $SO(5)$ [9], see (4.2), the spurions are forced to always appear in hermitian conjugated pairs with the SM indices (labeled by Greek letters) contracted among themselves, and complex conjugation ensuring $U(1)_Y$ invariance. This means that the spurions can enter the Higgs potential only through the following combinations [168]:

$$(\Gamma_L)_{IJ} \equiv (\Delta^*_L)^\alpha_I (\Delta_L)_{\alpha J}, \quad (\Gamma_R)_{IJ} \equiv (\Delta^*_R)_I (\Delta_R)_J, \tag{4.64}$$

with $\alpha = 1, 2$ being the $SU(2)^0_L$ indices, while $I, J = 1, \ldots, 5$ are $SO(5)$ indices. As the latter are the only free indices left, the $\Gamma_{L,R}$ spurions only transform under $SO(5)$:

$$\Gamma_{L,R} \to g\, \Gamma_{L,R}\, g^\dagger, \quad g \in SO(5). \tag{4.65}$$

Because of its NG nature, the Higgs belongs to the $SO(5)/SO(4)$ coset and always appears through the Goldstone matrix U in (4.1). Actually, for symmetric cosets as $SO(5)$, there exists an automorphism V with $VT^AV^\dagger = s_A T^A$, where $s_A = +/-$ for

[9] The electroweak group in fact corresponds to the gauged diagonal $SU(2)_L \times U(1)_Y$ subgroup of the elementary and composite global symmetries, and we omit an additional $U(1)_X$ factor that is not crucial here [154, 171].

the unbroken/broken generators $A = a/\hat{a}$, that can be used to define a new Goldstone matrix, Σ [10], with linear transformation properties:

$$\Sigma = U^2\, V \to g\, \Sigma\, g^\dagger, \quad g \in SO(5). \tag{4.66}$$

This is explained in detail in Appendix C.1. The $\Gamma_{L,R}$ spurions and the linear Goldstone matrix Σ defined in (4.64) and (4.66), respectively, are the ingredients needed to investigate the fermion contribution to the Higgs potential. As already mentioned, higher orders in perturbation theory correspond to larger number of insertions of the couplings that explicitly break the global symmetry. In this case, this corresponds to more insertions of the Γ spurions (keeping the same order in the loop expansion). The leading order for the potential thus corresponds to one spurion insertion. One finds that at this order there are only two different invariants:

$$V_{\rm LO}(h) = c_L \mathrm{Tr}\left(\Sigma\, \Gamma_L\right) + c_R \mathrm{Tr}\left(\Sigma\, \Gamma_R\right) = (2c_R - c_L)\sin^2(h/f), \tag{4.67}$$

where the coefficients $c_{L,R}$ can only be fixed in an explicit calculation. The issue with (4.67) is that it does not allow for extrema besides the trivial ones at $h = 0, \pi f$. Therefore, one needs to balance next-to-leading order contributions to the potential with the leading order in (4.67) in order to obtain a non-trivial vacuum with $v \lesssim f$. Intuitively, this means that the tuning in the MCHM$_5$ is actually worse than the naive estimate $\Delta \sim 1/\xi$ because of the particular structure of the Higgs potential. As higher orders are supposed to come with higher powers of $\lambda_{L,R}/g_*$, the tuning in order to obtain the 125 GeV Higgs in the MCHM$_5$ was estimated in Ref. [172] as

$$\Delta_{\mathbf{5}} \simeq \frac{1}{\xi}\left(\frac{\alpha}{2\beta}\right) \simeq \frac{1}{\xi} \times g_*^2 = \frac{f^2}{v^2} \times 10, \tag{4.68}$$

where $(\alpha/2\beta)$ is understood as the natural size of these parameters (namely, before tuning), and we have taken $g_* \sim 3$ as a typical value. As we can see, on top of the irreducible tuning f^2/v^2 there is an extra factor ~ 10, that is referred to as *double tuning*. This additional amount of tuning could be avoided by choosing *ad hoc* representations; however, as we shall see in Sec. 4.4.1, there exists a symmetry of the strong sector called maximal symmetry [184, 185] that can remove the double tuning without the need of changing the fermion representation.

For our purposes, it is interesting to see how the tuning in the MCHM$_5$ depends on the mass of the lightest top partner. This can be done straightforwardly by trading the scale f for m_T in the standard relation (4.22). One finds

$$\Delta_{\mathbf{5}} \simeq 100\, \left(\frac{m_T}{1\,\mathrm{TeV}}\right)^2, \tag{4.69}$$

where the quadratic growth simply follows from the fact that one can raise the top partner masses only by raising f, and the large prefactor is due to the double tuning. As we can see, the tuning is already at the 1% level even with light partner masses.

We can try to estimate the tuning in the sMCHM$_5$ along the same lines of (4.68):

$$\Delta_{\mathbf{5}}^{\rm soft} \simeq \frac{1}{\xi} \times \left(\frac{\alpha_s}{2\beta_s}\right), \tag{4.70}$$

[10] This Goldstone matrix Σ is a new object and should not be confused with the multiplet defined in (2.77) for the axiflavon-Higgs unification.

where α_s, β_s are the natural values in our model with soft breaking. The main difference between these two setups is the modified relation between the Higgs mass and m_T. In particular we have shown that β_s can be naturally smaller than in the standard MCHM$_5$, thus modifying (4.22) to

$$m_h = 130\sqrt{\beta_s/\beta}\frac{m_T}{1.4f}\,\text{GeV}. \tag{4.71}$$

By solving (4.71) with $m_h = 125$ GeV, we find $\beta_s \simeq (1.3f/m_T)^2\beta$, while α_s will remain unchanged, $\alpha_s \sim \alpha$ [11]. Therefore, one has

$$\Delta_{\mathbf{5}}^{\text{soft}} \simeq \left(\frac{m_T}{1.3f}\right)^2 \times \frac{1}{\xi}\left(\frac{\alpha}{2\beta}\right). \tag{4.72}$$

The last two factors are now related to the standard MCHM$_5$, where they are indeed the only source of tuning and must coincide with the expression in (4.68). We then take $\alpha/2\beta \sim 10$ by comparison and finally get

$$\Delta_{\mathbf{5}}^{\text{soft}} \simeq \left(\frac{m_T}{1\,\text{TeV}}\right)^2 \times 100, \tag{4.73}$$

where we have taken $f \simeq 800\,\text{GeV}$ or equivalently $\xi \simeq 0.1$. As we can see, the overall tuning is practically unchanged with respect to the conventional case. In fact, even though it is possible to raise the top partner masses without increasing the decay constant, f, the fact that β is reduced while α is unchanged worsens the tuning to obtain the correct misalignment angle. Eventually, the tuning in the MCHM$_5$ and sMCHM$_5$ is estimated to be of the same order, see (4.69) and (4.73).

The main point, however, is that the leading source of tuning in the soft-breaking setup is not irreducible, as it does not come from an increasingly small misalignment ξ, and thus can be largely cut down whenever other ingredients are added to model. As we shall see shortly in Sec. 4.4.1, a perfect match is obtained when combining soft-breaking with maximal symmetry.

4.4.1 What is maximal symmetry?

The Higgs potential of the MCHM$_5$, (4.67) contains only one trigonometric function at the leading order in the explicit breaking parameters. Since this cannot lead to successful electroweak symmetry breaking, one needs additional tuning such that next-to-leading terms can allow for the correct minimum. This fact introduces an extra degree of tuning on top of the irreducible one $\sim 1/\xi$ readily pushing the overall tuning to the percent level also with light top partners.

In this section, we will review what maximal symmetry [184, 185] is, and how it can eliminate double tuning following the spurion analysis presented in Ref. [VII]. To this end, let us focus on the composite fermionic resonances that will appear in the spectrum below the condensation scale. In general, these states do not need to fill complete $SO(5)$ representations (but they always have to obey the unbroken $SO(4)$ global symmetry). The assumption leading to maximal symmetry is that such resonances nevertheless still come in complete $SO(5)$ multiplets. For generic values of the resonance

[11] We envisage that α may also be softened in the sMCHM$_5$ similarly to what happens for β. However, this cannot be seen at the level of the estimate and could be supported only through explicit computation; we therefore conservatively assume $\alpha_s \sim \alpha$.

masses, the residual symmetry is still only $SO(4)$. However, if we neglect these masses for a moment we see that the original $SO(5)$ would be actually doubled to the chiral group $SO(5)_L \times SO(5)_R$, meaning that each chirality can transform indipendently under "its own" $SO(5)$ group. Interestingly, there exists a value of resonance masses that exhibits a residual symmetry larger than $SO(4)$, which is referred to as maximal symmetry. This can in fact be defined as the largest group that can be preserved by turning on non-zero masses for the composite states that still gives a non-vanishing Higgs potential. In practice, maximal symmetry turns out to be the $SO(5)'$ subgroup of $SO(5)_L \times SO(5)_R$ that satisfies

$$g_L V g_R^\dagger = V, \quad g_L \in SO(5)_L, \quad g_R \in SO(5)_R, \tag{4.74}$$

where $V = \mathrm{diag}(1,1,1,\sigma_3)$ is the automorphism introduced above (4.66). Another possibility would be the diagonal subgroup defined by $g_L \mathbb{1} g_R^\dagger = \mathbb{1}$, which however would make the Higgs an exact NG boson as long as the fermion sector is concerned.

Let us now go back to the estimate of the potential in the MCHM$_5$ and see how maximal symmetry solves the double tuning. As discussed above, maximal symmetry is a symmetry of the composite resonances. These are supposed to appear as full $SO(5)$ multiplets, and their masses are such that the residual symmetry is $SO(5)'$ defined in (4.74). Referring to the conventional partial-compositeness Lagrangian in (4.15), this means that maximal symmetry forces $a_L = b_L$ and $a_R = b_R$ such that full multiplets $\Psi = (Q, \tilde{T})$ are reconstructed, and the mass of the composite resonances need to satisfy $m_Q = -\tilde{m}_T = M$ for the $SO(5)'$ group to be a symmetry. The linear mixing in (4.15) then becomes

$$-\mathcal{L}_{\rm mass} = \lambda_L f\, \bar{q}_L \Delta_L\, U\, \Psi_R + \lambda_R f\, \bar{t}_R \Delta_R\, U\, \Psi_L + M \bar{\Psi}_L V \Psi_R + \text{h.c.} \tag{4.75}$$

The key quantities to estimate the Higgs potential are still represented by the $\Gamma_{L,R}$ spurions in (4.64) and the Goldstone matrix Σ in (4.66). However, when $SO(5)'$ is promoted to a symmetry of the theory, more insertions of the spurions are needed in order to generate a potential. Indeed, possible contributions are now more constrained as they need to be invariant not only under $SU(2)^0_L \times U(1)^0_Y$ and $SO(5)$ as before, but also under $SO(5)'$. To see this explicitly we first have to identify the transformation properties of $\Gamma_{L,R}$ under $SO(5)'$. The starting point is to perform a transformation on the chiral components of Ψ:

$$U\Psi_L \to g_L\,(U\Psi_L), \quad U\Psi_R \to g_R\,(U\Psi_R). \tag{4.76}$$

The invariance of (4.75) requires the spurions Δ_L and Δ_R to transform as

$$\Delta_L \to \Delta_L\, g_R^\dagger, \quad \Delta_R \to \Delta_R\, g_L^\dagger. \tag{4.77}$$

At the level of the $\Gamma_{L,R}$ spurions in (4.64), this implies that the transformation under $SO(5)'$ is a simple "chiral" generalization of (4.65):

$$\Gamma_L \to g_R\, \Gamma_L\, g_R^\dagger, \quad \Gamma_R \to g_L\, \Gamma_R\, g_L^\dagger. \tag{4.78}$$

The only twist is that due to partial compositeness q_L couples to the right-handed composites that by definition transform with $SO(5)_R$, and similarly for t_R. As for the Goldstone matrix Σ, we can define the action of $SO(5)'$ as [184]

$$\Sigma \to g_L \Sigma\, g_R^\dagger = \Sigma. \tag{4.79}$$

	$SO(5)$	$SO(5)'$
Γ_L	$\Gamma_L \to g\,\Gamma_L\,g^\dagger$	$\Gamma_L \to g_R\,\Gamma_L\,g_R^\dagger$
Γ_R	$\Gamma_R \to g\,\Gamma_R\,g^\dagger$	$\Gamma_R \to g_L\,\Gamma_R\,g_L^\dagger$
Σ	$\Sigma \to g\,\Sigma\,g^\dagger$	$\Sigma \to g_L\,\Sigma\,g_R^\dagger$

Table 4.2: Transformation properties of the spurions $\Gamma_{L,R}$ defined in (4.64) and the linear Goldstone matrix Σ under the global symmetry group, $SO(5)$, and maximal symmetry, $SO(5)'$.

It is now apparent that both the terms in (4.67) are forbidden by maximal symmetry, as they are not invariant under (4.78) and (4.79). The leading contribution to the potential actually requires at least two spurions to appear simultaneously, i.e.,

$$V_{\rm LO}(h) = c_{\rm LR}\mathrm{Tr}(\Sigma\,\Gamma_L\,\Sigma^\dagger\,\Gamma_R) = 2\,c_{\rm LR}\sin^2(h/f)\cos^2(h/f). \tag{4.80}$$

A summary of the transformation properties that we have used to derive (4.67) and (4.80) can be found in Table 4.2. The main difference compared to (4.67) is that now a non-trivial minimum occurs already at the leading order, thus solving the double-tuning problem. However, we can actually see that this minimum is still rather special, as it corresponds to $\alpha = -\beta$ and thus implies

$$\xi = \sin^2(\langle h\rangle/f) = 0.5 \tag{4.81}$$

independently of any choice of the parameters! Such a value of ξ is by now excluded experimentally— but in principle the gauge sector can come to rescue since it contributes to the Higgs potential as well and, with a small degree of accidental cancellation, can help misaligning the vacuum in the right way. The reason of this sharp prediction for ξ is the appearance of a discrete exchange symmetry

$$\sin(h/f) \leftrightarrow -\cos(h/f). \tag{4.82}$$

For a symmetric coset, this trigonometric parity is always a symmetry related to the existence of the automorphism V. Requiring maximal symmetry practically ensures that it remains a symmetry of the whole theory. Trigonometric parity in fact plays a crucial role in forbidding the linear terms in (4.67) and hence reduces the corrections to the Higgs mass, similarly to what happens in Twin Higgs constructions [186].

As the maximally symmetric version of the MCHM$_5$ is free from double tuning one simply has $\Delta \sim 1/\xi$, mainly coming from the cancellation between fermion and gauge sectors. However, the relation between the Higgs mass and the top partner mass m_T is still unchanged. This leads to a quadratic sensitivity of the tuning on m_T similarly to (4.69):

$$\Delta_{\mathbf{5}}^{\text{max sym}} \simeq 9\left(\frac{m_T}{1\,\text{TeV}}\right)^2. \tag{4.83}$$

Despite the model with maximal symmetry being certainly more natural with respect to (4.69), we can still identify two ways of further improvement. In fact, *(i)* it would be nice to get rid of the unwanted prediction of $\xi = 0.5$ within the fermion sector while still removing the double tuning, so that the cancellation against the gauge sector is no longer necessary to obtain a viable ξ. Moreover, the soft-breaking setup can accommodate for

heavier top partners without raising the scale f due to a parametric reduction of the coefficient β. However, the estimate for α is unchanged with respect to the conventional MCHM$_5$ and the overall tuning turns out to be of the same order, see (4.73) and below. Thus, *(ii)* if maximal symmetry and soft breaking could be combined the coefficients α and β would be related via trigonometric parity ensuring a fully softened Higgs potential and consequently a natural spectrum of resonances above the current LHC bounds. As we shall see, both options are possible and explained in detail in the next sections.

4.4.2 Combining soft-breaking and maximal symmetry

Our aim here is to investigate whether the soft-breaking setup is compatible with maximal symmetry. This is motivated by the search of a CH model that can provide a natural spectrum of top partners that is compatible with the current LHC bounds. First, let us notice that maximal symmetry and soft-breaking are actually rather similar concepts: the former forces the composite states to fill out complete $SO(5)$ multiplets, whereas the latter is based on completing the SM fermions to full $SO(5)$ multiplets as well. Therefore, it feels quite natural to try to combine them. The most naive way of doing so is discussed in the following preliminaries, and, as we shall see, it does not work. Yet, it is important for deriving the conditions that lead to a successful combination, which is then presented at the end of this section. What follows is based on Ref. [VII].

Preliminaries

Let us try to implement soft breaking in the maximally symmetric Lagrangian (4.75) in the most naive way, namely by promoting q_L and t_R to full $SO(5)$ multiplets according to the minimal embedding (4.29),

$$-\mathcal{L}_{\text{mass}} = \lambda_L f\, \bar{\psi}^t_L\, U\, \Psi_R + \lambda_R f\, \bar{\psi}^t_R\, U\, \Psi_L + M \bar{\Psi}_L V \Psi_R + \text{h.c.}\,, \tag{4.84}$$

and by introducing the elementary Lagrangian (4.35) containing the explicit breaking unchanged. As always, the contributions to the Higgs potential must be proportional to the terms that explicitly break the $SO(5)$. In the soft-breaking setup these are given in (4.35). For the moment, let us focus on the contribution from the term proportional to m_w,

$$\Delta\mathcal{L} = m_w \bar{\psi}^t_L \Gamma_w \psi^t_R + \text{h.c.}, \tag{4.85}$$

where the explicit form of Γ_w is given by

$$\Gamma_w = \frac{1}{2}\,\text{diag}\,(\mathbb{1}_{2\times2} + \sigma_2, \mathbb{1}_{2\times2} - \sigma_2, 0)\,. \tag{4.86}$$

In order to predict the contribution to the Higgs potential, we need to derive the transformation properties of the spurion Γ_w under maximal symmetry. To this end, we recall that the chiral components of Ψ transform under $SO(5)'$ as in (4.76), and in turn this implies that the elementary multiplets $\psi^t_{L,R}$ transform as

$$\psi^t_L \to g_R\, \psi^t_L, \quad \psi^t_R \to g_L\, \psi^t_R \tag{4.87}$$

to make the linear mixing in (4.84) invariant. Thus, we see that (4.85) is formally invariant if the spurion Γ_w transforms as

$$\Gamma_w \to g_R \Gamma_w g_L^\dagger\,. \tag{4.88}$$

The problem with (4.88) is that the following term is allowed in the Higgs potential:

$$V_{\rm LO}(h) = c_w \mathrm{Tr}\left(\Sigma\,\Gamma_w\right) \propto m_w \sin^2(h/f), \tag{4.89}$$

which contains only one Σ insertion and whose explicit form is actually rather similar to what we have calculated in (4.40) just with $m_Q = -\tilde{m}_T$. The leading-order potential in (4.89) does not allow for non-trivial minima, and similarly to what we concluded below (4.67) the double tuning is reintroduced despite our attempt of employing maximal symmetry. This is a consequence of trigonometric parity being badly broken by the spurion Γ_w. The same conclusion holds when considering the $\delta_{1,2}$ terms in (4.35). In general, whenever ψ^t_L and ψ^t_R have a direct interaction term as in (4.85), one finds that trigonometric parity is badly broken and double tuning is reintroduced [12].

We conclude that the simplest realization of soft-breaking in the MCHM$_5$ specified by the new vector-like fermions in (4.29) is not directly compatible with maximal symmetry. However, we will see shortly that a slight change in the embedding (4.29) allows us to successfully combine maximal symmetry and soft breaking. This will lead to an increase in the mass of the top partners with minimal tuning, and also to the disappearence of the unwanted prediction for the misalignment angle.

The model

We are now ready to introduce our simple model in which maximal symmetry and soft breaking are successfully combined resulting in a composite resonance spectrum naturally above the LHC bounds. The obstacle for this turned out to be the mass of the vector-like fermion w which reintroduced the double tuning. We will now show that there is a simple way to avoid this. All we need to do is to further split the vector-like fermion w into two: rather than marrying up w_L appearing in ψ^t_L directly with w_R appearing in ψ^t_R, we introduce separate partners for these two w's. Hence our embedding in (4.29) will be modifed as

$$\psi^t_L = \Delta^\dagger_{q_L} q_L + \Delta^\dagger_{w_1} w_{1L} + \Delta^\dagger_s s_L, \quad \psi^t_R = \Delta^\dagger_{t_R} t_R + \Delta^\dagger_{w_2} w_{2R} + \Delta^\dagger_v v_R, \tag{4.90}$$

where $\Delta_{w_1} = \Delta_{w_2} = \Delta_w$, the last given in (4.30). For the mass terms of the elementary fields, we will take a simple modification of (4.34) [13]:

$$\begin{aligned} -\mathcal{L}_{\rm el} =& m_{w_1}(\bar{w}_{1L} w_{1R} + \bar{w}_{1R} w_{1L}) + m_{w_2}(\bar{w}_{2L} w_{2R} + \bar{w}_{2R} w_{2L}) \\ &+ m_v(\bar{v}_L v_R + \bar{v}_R v_L) + m_s(\bar{s}_L s_R + \bar{s}_R s_L)\ . \end{aligned} \tag{4.91}$$

Note that there are additional mixing terms that would be allowed by the SM gauge symmetries and are not included in the Lagrangian above. We will discuss these below in (4.95).

It is convenient to collect the chiralities that do not enter either of $\psi^t_{L,R}$ in two multiplets

$$\eta_R \equiv (w_{1R}, s_R), \quad \xi_L \equiv (w_{2L}, v_L). \tag{4.92}$$

[12] Clearly, trigonometric parity is restored if s, v, w become infinitely heavy, since the maximally symmetric MCHM$_5$ is effectively recovered.

[13] We notice that by choosing this less minimal embedding the correspoding two-site model would provide a fully calculable Higgs potential even without maximal symmetry, as mentioned in Sec. 4.3.2.

The full Lagrangian of our model in terms of these fields is then

$$-\mathcal{L} = \bar{\psi}^t_L\, M^\dagger_R\, \eta_R + \bar{\psi}^t_R\, M^\dagger_L\, \xi_L + \lambda_L f \bar{\psi}^t_L U \Psi_R + \lambda_R f \bar{\psi}^t_R U \Psi_L + M \bar{\Psi}_L V \Psi_R + \text{h.c.}, \quad (4.93)$$

where V is the usual automorphism, $V = \text{diag}\,(1,1,1,\sigma_3)$. The first two terms correspond to a compact way of writing (4.91) via matrices accounting for the masses of the elementary vector-like fermions:

$$M^\dagger_R = \frac{1}{\sqrt{2}} \begin{pmatrix} m_{w_1} & 0 & 0 \\ i m_{w_1} & 0 & 0 \\ 0 & m_{w_1} & 0 \\ 0 & -i m_{w_1} & 0 \\ 0 & 0 & i m_s \end{pmatrix}, \quad M^\dagger_L = \frac{1}{\sqrt{2}} \begin{pmatrix} m_{w_2} & 0 & 0 & m_v \\ i m_{w_2} & 0 & 0 & -i m_v \\ 0 & m_{w_2} & m_v & 0 \\ 0 & -i m_{w_2} & i m_v & 0 \\ 0 & 0 & 0 & 0 \end{pmatrix}, \quad (4.94)$$

where the columns correspond to the $SO(5)$ indices and the shape of the matrices reflects the dimensionality of η_R (triplet) and ξ_L (fourplet).

As we mentioned above, there are three more mixing terms between the elementary fields that would be allowed in (4.91) which are given by

$$\begin{aligned} -\mathcal{L}_{\text{odd}} &= \delta_1 \bar{s}_L t_R + \delta_2 \bar{q}_L v_R + \delta_{12} \bar{w}_1 w_2 + \text{h.c.} \\ &\equiv \bar{\psi}^t_L \Delta(\delta_1, \delta_2) \psi^t_R + \bar{\xi}_L \Delta'(\delta_{12}) \eta_R + \text{h.c.}, \end{aligned} \quad (4.95)$$

where the last line defines the spurions $\Delta(\delta_1, \delta_2)$ and $\Delta'(\delta_{12})$. Based on the discussion in the previous section, it is clear that a non-zero value for any of the δ's in (4.95) would be incompatible with maximal symmetry and reintroduce the double tuning; we thus require $\delta_1 = \delta_2 = \delta_{12} = 0$. This can be easily achieved by introducing a Z_2 symmetry under which the parities of ψ^t_L and η_R are opposite to the parities of ψ^t_R and ξ_L, for example $\psi^t_L, \eta_R : +$ and $\psi^t_R, \xi_L : -$. When considering the whole Lagrangian in (4.93), the Z_2 is actually broken softly by the the composite mass M. In the 5D picture (see Sec. 4.5.3) this corresponds to a Z_2 symmetry that is only broken on the IR brane.

Let us now investigate the key properties of our main model defined in (4.93) regarding double tuning and trigonometric parity by using spurion analysis. For this we need to derive the transformation properties of the $M_{R,L}$ spurions in (4.94). First, as long as the electroweak gauge interactions are neglected, and $M_{R,L} = 0$, the fields η_R and ξ_L are "free" and exhibit a large symmetry of their kinetic terms, i.e. $U(3)^0 \times U(4)^0$ (notice that η_R is a triplet and ξ_L a fourplet). This large symmetry extends the $SU(2)^0_L \times U(1)^0_Y$, see the discussion above Eq. (4.64), and similarly implies that $M_{L,R}$ enter the potential only through quadratic combinations

$$\Gamma_R \equiv M^\dagger_R M_R, \quad \Gamma_L \equiv M^\dagger_L M_L, \quad (4.96)$$

which transform under $SO(5)'$ similarly to (4.78) (except with $L \leftrightarrow R$):

$$\Gamma_R \to g_R\, \Gamma_R\, g^\dagger_R, \quad \Gamma_L \to g_L\, \Gamma_L\, g^\dagger_L. \quad (4.97)$$

The explicit forms of Γ_L and Γ_R read

$$\Gamma_L = \begin{pmatrix} m_v^2 + m_{w2}^2 & i(m_v^2 - m_{w2}^2) & 0 & 0 & 0 \\ -i(m_v^2 - m_{w2}^2) & m_v^2 + m_{w2}^2 & 0 & 0 & 0 \\ 0 & 0 & m_v^2 + m_{w2}^2 & -i(m_v^2 - m_{w2}^2) & 0 \\ 0 & 0 & i(m_v^2 - m_{w2}^2) & m_v^2 + m_{w2}^2 & 0 \\ 0 & 0 & 0 & 0 & 0 \end{pmatrix} \quad (4.98)$$

and

$$\Gamma_R = \begin{pmatrix} m_{w1}^2 & -im_{w1}^2 & 0 & 0 & 0 \\ im_{w1}^2 & m_{w1}^2 & 0 & 0 & 0 \\ 0 & 0 & m_{w1}^2 & im_{w1}^2 & 0 \\ 0 & 0 & -im_{w1}^2 & m_{w1}^2 & 0 \\ 0 & 0 & 0 & 0 & m_s^2 \end{pmatrix} \tag{4.99}$$

which can also be rewritten in terms of the Pauli matrices similarly to (4.86). We notice that, unlike in the conventional case, higher orders in the expansion parameter $\lambda_{L,R}/g_*$ do not correspond to more insertions of the spurions $\Gamma_{L,R}$, which in fact only depend on the vector-like masses. The leading-order Higgs potential is rather determined by the least number of Σ insertions, since the Higgs only enters through the Goldstone matrix that always appears together with $\lambda_{L,R}$ in (4.93). Due to (4.97), the leading contribution requires two Σ's to appear simultaneously, and its structure is fixed as:

$$V_{\rm LO}(h) = c_{LR} \sum_{i,j=1}^{\infty} a_{ij}\, {\rm Tr}(\Sigma^\dagger \Gamma_L^i \Sigma\, \Gamma_R^j), \tag{4.100}$$

where i, j are arbitrary powers for the $\Gamma_{L,R}$ matrices, for which (4.100) is still formally invariant under $SO(5)'$, and the coefficients can be determined from explicit calculation. Next-to-leading terms in the potential correspond to more insertions of Σ. On the other hand, since the elementary vector-like masses are not necessarily small, all powers of $\Gamma_{L,R}$ contribute. Anyway, in order to have a feeling of the structure in (4.100), we can evaluate the first term corresponding to $i = j = 1$:

$$\begin{aligned} V_{\rm LO}^{(1,1)}(h) \propto &\left(m_s^2 m_v^2 + m_s^2 m_{w2}^2 - 2m_{w1}^2 m_{w2}^2\right) \sin^2(h/f) \\ &+ (m_v^2 m_{w1}^2 - m_s^2 m_v^2 + m_{w1}^2 m_{w2}^2 - m_s^2 m_{w2}^2) \sin^4(h/f), \end{aligned} \tag{4.101}$$

which would give $\xi = 0.1$ for instance for $m_s = 2.4$ TeV, $m_{w1} = 3$ TeV, $m_{w2} = 4$ TeV and $m_v = 5$ TeV (although the actual value of ξ can change when including the terms with $i, j > 1$). An actual calculation of ξ within our model that takes into account all powers of $\Gamma_{L,R}$ is shown in Fig. 4.10 as a function of m_v, fixing the other parameters such that the Higgs mass and the top mass are correctly reproduced at the point $\xi = 0.1$. As we can see, ξ is slowly varying with m_v implying that reproducing $\xi = 0.1$ does not require significant tuning.

We thus conclude that the soft MCHM$_5$ with maximal symmetry specified in (4.93) is free from double tuning, because the structure in the potential is rich enough to provide a non-trivial minimum for electroweak symmetry breaking at the leading order. Moreover, we notice that ξ is not constrained to be $\xi = 0.5$ as it was found for the leading-order potential in (4.80). As we have seen, this implication for the misalignment ξ is controlled by trigonometric parity and we can ask ourselves what is its fate in the soft-breaking setup. While a detailed analysis is presented in Sec. C.2, here we just give the result, which is that trigonometric parity is always broken in the soft-breaking setup already within the fermion sector, unless the masses of the new vector-like fermions are given very particular values:

$$s_h \leftrightarrow -c_h \text{ is unbroken} \quad \Leftrightarrow \quad \xi = 0.5 \quad \Leftrightarrow \quad (m_v^2 - m_{w_2}^2) m_{w_1}^2 = 0. \tag{4.102}$$

We then conclude that, for generic values of the vector-like masses, the unwanted prediction $\xi = 0.5$ can be avoided in our setup already within the fermion sector *without*

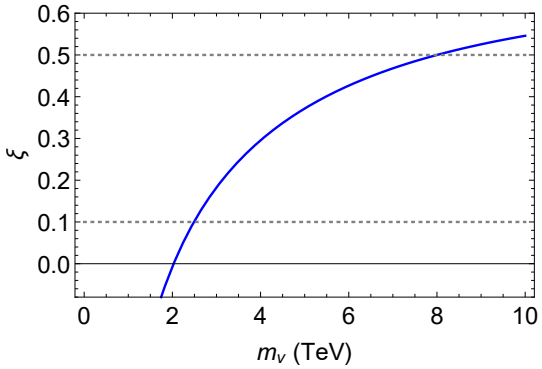

Figure 4.10: The value of $\xi \equiv \sin^2(\langle h \rangle / f) = -\alpha/2\beta$ as a function of m_v for $M = 2.6$ TeV, $m_{w_1} = m_{w_2} = 8$ TeV, $m_s = 2.4$ TeV.

reintroducing the double tuning, as trigonometric parity is broken in a controlled way by the vector-like masses (besides very particular points).

In the next section, we will provide a quantitative analysis of the potential in (4.100) and calculate the tuning in our model, which will turn out to be natural also with top partner masses above 2 TeV.

4.4.3 Heavy top partners with minimal tuning

We present here the quantitative results for our model and calculate the amount of tuning needed to achieve correct electroweak symmetry breaking together with heavy top partners above the LHC bounds. Using the standard parametrization of the potential (4.10), we find at leading order in $\lambda_{L,R}$

$$\alpha + \beta = -C \int_0^\infty p^3 \, \mathrm{d}p \frac{M^2 m_{w_1}^2 (m_v^2 - m_{w_2}^2)}{(M^2 + p^2)^2 (m_{w_1}^2 + p^2)(m_{w_2}^2 + p^2)(m_v^2 + p^2)} \,, \tag{4.103}$$

and

$$\beta = C \int_0^\infty p^3 \mathrm{d}p \frac{M^2 (2 m_v^2 m_{w_2}^2 + (m_v^2 + m_{w_2}^2) p^2)(m_s^2 (m_{w_1}^2 + 2p^2) - m_{w_1}^2 p^2)}{p^2 (p^2 + M^2)^2 (p^2 + m_s^2)(p^2 + m_v)^2 (p^2 + m_{w_1}^2)(p^2 + m_{w_2}^2)} , \tag{4.104}$$

where

$$C = \frac{2 N_c}{8\pi^2} \lambda_L^2 \lambda_R^2 f^4 . \tag{4.105}$$

In particular, since $\xi = -\alpha/(2\beta)$, the point corresponding to unbroken trigonometric parity $\xi = 0.5$ is realized if the integrand in (4.103) vanishes. This happens when $m_{w_1}^2 (m_v^2 - m_{w_2}^2) = 0$, in agreement with (4.102), and can be checked explicitly by looking again at Fig. 4.10.

In addition to the terms from the top sector, the potential also contains a contribution from the gauge sector. It mainly affects α, and we will take this into account by adding the following term [187]:

$$\alpha_g = \frac{9}{64\pi^2} g^2 f^2 m_\rho^2 , \tag{4.106}$$

where m_ρ is the mass of the spin-1 vector resonance ρ.

In order to quantitatively estimate the tuning of the theory Δ, we adopt the Barbieri-Giudice measure [160, 172]:

$$\Delta = \max\{|\Delta_i|\}, \quad \Delta_i = \frac{2x_i c_h^2}{s_h m_h^2 f^2} \frac{\partial^2 V}{\partial x_i \partial s_h}, \tag{4.107}$$

where $s_h \equiv \sin(h/f)$ and similarly for c_h, and the independent variables x_i are

$$x_i = \{\lambda_L, \lambda_R, f, m_\rho, M, m_s, m_v, m_{w_1}, m_{w_2}\}. \tag{4.108}$$

Before moving to an actual calcuation using (4.107), let us estimate the tuning in our model (4.93) where maximal symmetry and soft breaking are successfully combined. To this end we recall that the maximally symmetric version of the MCHM$_5$ is free from double tuning and the estimate is simply $\Delta \sim 1/\xi$. With maximal symmetry alone, however, heavier top partners can be achieved only at the price of decreasing ξ yielding the quadratic growth in (4.83). Crucially, this is not the case when maximal symmetry and soft breaking are married as heavier top partners are now compatible with a light Higgs without raising the scale f. Moreover, since α and β are now related via trigonometric parity the reasoning that lead to (4.73) is not applicable and the quadratic growth with m_T is avoided. We can then estimate the tuning in our model where maximal symmetry and soft breaking are successfully combined to be, as a first approximation, independent of the top-partner masses and equal to the minimal tuning as in Ref. [184] with $\xi = 0.1$ and $m_\rho > 2\,\text{TeV}$:

$$\Delta \simeq \frac{1}{\xi} - 2 = 8. \tag{4.109}$$

This is in fact the essence of combining soft breaking and maximal symmetry: the former allows to raise the top partner masses without raising f and the latter provides the connection $\alpha \approx \beta$ via trigonometric parity ensuring a fully softened potential. As we shall see, (4.109) is in fact a good approximation of the tuning for top partner masses satisfying $m_T \lesssim 2\,\text{TeV}$: up to this value, obtaining a light Higgs will require no additional tuning; for larger masses, however, fixing the Higgs mass to 125 GeV implies a certain amount of extra cancellations in the potential and the overall tuning will deviate from the minimal one in (4.109).

The tuning in the various models discussed in this section as a function of the top partner mass, m_T, is presented in Fig. 4.11. Solid lines correspond to the simple analytic estimates given in Eqs (4.69) and (4.73) (blue), (4.83) (red) and (4.109) (green), while the dots to numerical calculations using the expression of the one-loop Higgs potential as well as the measure in (4.107). As we can see, for the soft maximal symmetry case (green color) the tuning is in fact independent of m_T in the low-mass region and coincides with the estimate in (4.109); on the other hand, for $m_T \gtrsim 2\,\text{TeV}$ the tuning is driven by the requirement of a light Higgs and the result deviates from (4.109). The model turns out to be nonetheless rather natural also for heavier m_T and ρ masses: we actually find $\Delta \simeq 20$ for $m_T \simeq 2.5$ TeV, whereas taking a more stringent cut on the ρ mass, $m_\rho > 3$ Tev, will change the m_T-independent estimate in (4.109) from 8 to 16.

We can then clearly see that the sMCHM$_5$ with maximal symmetry allows for minimal tuning, at the level of $\Delta^{-1} \lesssim 10\%$, while avoiding the anomalously light top partners disfavored by the LHC. In particular, the region in which the tuning increases due to

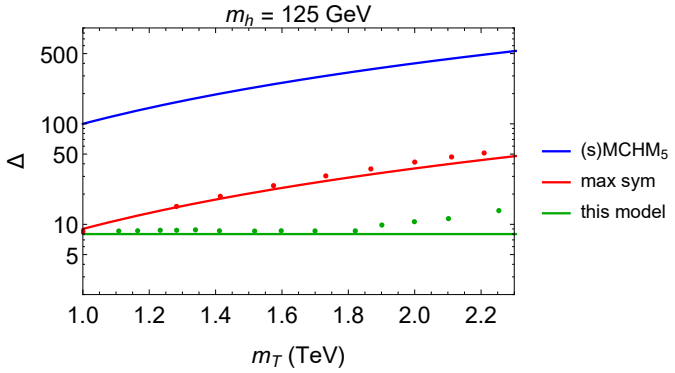

Figure 4.11: Comparison of the tuning Δ in several models as a function of the mass of the lightest top partner m_T. Solid lines correspond to the analytical estimates and dots to a numerical calculation according to Eq. (4.107). The mass of the spin-1 vector-resonance, ρ, is taken $m_\rho > 2$ TeV.

the non-observation of the top partners is postponed in our model to $m_T \gtrsim 2\,\text{TeV}$. Thus, in contrast to other minimal realizations, this natural CH is only just about to be tested now, at the HL-LHC, or FCC [188–191]. In fact, even before turning on the LHC, electroweak precision tests told us that $\xi \lesssim 0.1$ and therefore the tuning for a CH was to be expected at the 10% level, see again the discussion in Sec. 4.2. However, for the conventional MCHM$_5$ and also for its maximally symmetric version, the tuning is actually driven by the non-observation of light top partners that is already cutting values of ξ previously unconstrained by LEP. On the contrary, Fig. 4.11 confirms that the LHC limit on top partners is not driving the tuning in our model, bringing us back to the pre-LHC era.

4.5 Warped 5D implementation

In this section, we will discuss CH models from the perspective of extra-dimensional theories, where all the ingredients that we have introduced in the 4D relization of our model presented in Sec. 4.4.2 will turn out to have a very simple interpretation [VII].

The link between Higgs compositeness and extra dimensions is provided by the AdS/CFT correspondence [182], which relates d-dimensional conformal field theories to $d+1$ models in anti-de Sitter (AdS) space-time. The reason why this is convenient boils down to the fact that the strongly coupled regime of the CFT corresponds to weak coupling in the extra-dimensional model ensuring calculability. This is clearly advantageous for studying CH models, as the Higgs emerges as a bound state of a new strong dynamics which is close to conformality until it condenses generating the scale f. This said, it is certainly true that, as explored in the previous sections, phenomenological models in 4D already provide an excellent tool to make a quantitative analysis of the low-energy theory.

There are however two good reasons to look at our new model from the extra-dimensional perspective. The first one is *(i)* investigating the origin of the soft-breaking setup itself. As we shall see, this has to do with the fact that the elementary multiplets that we have completed to full $SO(5)$ representations by adding the new elementary

fermions are actually the fundamental objects to start with in the 5D model. Also, the appearance of discrete symmetries as the Z_2 parity that forbids the terms in (4.95) is more easily understood in 5D as an interplay of different symmetries at the boundaries of AdS. The second reason is *(ii)* to provide a rationale behind the mass scale of the elementary vector-like fermions that has been so-far considered as a phenomenological free parameter. In fact, the new fermions can impact the Higgs potential only if they are light enough to be active below the condensation scale, thus having a mass comparable to the composite resonances. This can be viewed as a sort of "coincidence" problem. In fact, even if the Planck scale is the only scale in the game, it is easy to accommodate a TeV-scale composite resonance by dimensional transmutation. This mechanism is clearly not at work for elementary fermions, and a bare mass which is much smaller than $M_{\rm Pl}$ is rather *ad hoc*. On the other hand, fermion masses are technically natural due to chiral symmetry and thus this does not represent a real fine-tuning problem. Anyway, besides any naturalness issue, the generation of elementary vector-like masses at the TeV scale is certainly worth investigating and, as we shall see, the 5D picture can easily provide a mechanism for this.

Let us get started by introducing the five-dimensional space-time that we are going to use throughout this section, see e.g. [152, 192, 193] for reviews. It consists of a slice of AdS space, delimited by two 4D branes that are connected along the extra dimension z. The UV brane is located at $z = R$ and the IR brane at $z = R'$ with $R' > R$. The conformally-flat AdS_5 metric is

$$\mathrm{d}s^2 = a(z)^2(\eta_{\mu\nu}\mathrm{d}x^\mu \mathrm{d}x^\nu - \mathrm{d}z^2), \tag{4.110}$$

where $\eta_{\mu\nu}$ describes the standard Minkowski space time with $\mu, \nu = 0, \ldots, 3$ and the fifth coordinate z can vary as $z \in [R, R']$. The warping factor $a(z)$ reads

$$a(z) = \frac{R}{z}. \tag{4.111}$$

Notice that $a(R') < 1$, meaning that energy scales are warped down on the IR brane with respect to the UV brane, and hence their names. The position R of the UV brane is related to the smallest distance at which the theory can be trusted, and thus it is usually set to the Planck scale: $R^{-1} \sim M_{\rm Pl}$. Conversely, the IR brane represents the scale at which the strong sector of the dual 4D theory loses conformality (see e.g. [194]) and thus provides an IR cutoff, namely the condensation scale. Since we expect the Higgs decay constant f to be around 1 TeV, one takes $R'^{-1} \sim 1\,\mathrm{TeV}$.

As for the field content and symmetries, we will assume that the bulk of AdS_5 (namely, everywhere between the branes) possesses an $SO(5) \times U(1)_X$ gauge symmetry. This is because gauge symmetries in the extra dimension are known to correspond to global symmetries in the 4D dual. There are then exactly 10+1 gauge bosons $A^\alpha_M(x, z)$, where $M = \mu, 5$ ($\mu = 0, \ldots, 3$) is a space-time index according to the five-dimensional Lorentz group $SO(4, 1)$, and $\alpha = 1, \ldots, 11$ counts the dimensionality of the adjoint of $SO(5) \times U(1)_X$.

From the perspective of a 4D observer the symmetry of the space-time is the standard $SO(3, 1)$, and thus each gauge boson decomposes as a vector A^α_μ and a scalar field A^α_5 with respect to the standard Lorentz group:

$$A^\alpha_M(x, z) = \begin{pmatrix} A^\alpha_\mu(x, z) \\ A^\alpha_5(x, z) \end{pmatrix}. \tag{4.112}$$

Since space-time has boundaries along the fifth dimension, a crucial role is played by the boundary conditions that are assigned to a given field. In particular, the boundary conditions for the gauge fields are chosen to reproduce the following symmetry reduction on the branes:

- $SO(5) \times U(1)_X \to SO(4) \times U(1)_X$ on the IR brane at $z = R'$. This mimics the $SO(5)/SO(4)$ breaking due to condensation of the new strong dynamics.
- $SO(5) \times U(1)_X \to SU(2)_L \times U(1)_Y$ on the UV brane at $z = R$. This implements the fact that the elementary fields only respect the SM gauge symmetry.

From general arguments, we know that the pNGB Higgs is associated with the broken generators of $SO(5)/SO(4)$. This remains true also in the 5D model, where the Higgs degrees of freedom are identified as the fifth components of the $SO(5)$ gauge bosons $A_5^{\hat{a}}$, $\hat{a} = 1, \ldots, 4$, corresponding to these broken directions. These degrees of freedom are indeed Lorentz scalars, as discussed above (4.112). As the Higgs is embedded within an extra-dimensional gauge field, this setup realizes what is also called gauge-Higgs unification, and the tree-level Higgs mass is now forbidden by gauge symmetry. However, the gauge symmetry is broken by the presence of the UV and IR branes, and thus a potential for the Higgs will be generated radiatively, as in the usual pNGB picture.

Let us now move to discuss how matter fields, including the SM fermions, are included. First of all, let us note that standard dimensional analysis implies that the canonical dimension of a fermion field Ψ in $d = 5$ is:

$$[\Psi] = \frac{d-1}{2} = 2. \tag{4.113}$$

In $d = 4$, spin-1/2 irreducible representations of the Lorentz group are known to be chiral Weyl fermions. However, the smallest representation of the Lorentz group for spin-1/2 particles in 5D contains both chiralities and is instead a Dirac fermion:

$$\Psi(x, z) = \begin{pmatrix} \chi_\alpha(x, z) \\ \bar{\psi}^{\dot{\alpha}}(x, z) \end{pmatrix}, \tag{4.114}$$

where we are using two-component spinor notation, $\alpha, \dot{\alpha} = 1, 2$. This clearly poses an issue when trying to identify the SM fermions within these 5D multiplets, as we know that they are fully chiral under the SM gauge symmetry. However, the two chiralities within Ψ can be actually "separated" by assigning them different boundary conditions on the branes. This procedure is called *orbifolding* and has been shown to be successful in reproducing a chiral spectrum of fermions at low energy. The choice of the boundary conditions for Ψ impacts the Higgs potential as well, as they will also break the 5D gauge symmetry and contribute to it similarly to the gauge bosons.

In the next section, we will discuss the role of boundary conditions on a slice of AdS and discuss the physical interpretation of this from the perspective of a 4D observer.

4.5.1 Boundary conditions and Kaluza-Klein modes

Let us here focus on the 5D fermionic sector as we find there the crucial new element of our soft-breaking setup.

As a first step, we need to write down a 5D action for the fermions from which we can derive the classical equations of motion (eom). Neglecting for the moment the

$SO(5)\times U(1)_X$ gauge interaction, the free Lagrangian for 5D fermions in curved space-time is, see e.g. [195],

$$S=\int \mathrm{d}^4x\int_R^{R'}\mathrm{d}z\ \sqrt{g}\left(\frac{\mathrm{i}}{2}(\bar\Psi e_a^M\gamma^a D_M\Psi - D_M\bar\Psi e_a^M\gamma^a\Psi)-m_\Psi\bar\Psi\Psi\right), \tag{4.115}$$

where $e_a^M=(z/R)\delta_a^M$ is the fünfbein and $\gamma^{a\prime}s$ are Dirac matrices. By D_M, we indicate the covariant derivative on the curved space-time, $D_\mu\Psi=(\partial_\mu+\gamma_\mu\gamma_5/4z)$, $D_5\Psi=\partial_5\Psi$. The action in (4.115) can be expanded in terms of the chiral components in (4.114) as

$$S=\int \mathrm{d}^4x\int_R^{R'}\mathrm{d}z\left(\frac{R}{z}\right)^4\left\{-\imath\bar\chi\bar\sigma^\mu\partial_\mu\chi-\imath\psi\sigma^\mu\partial_\mu\bar\psi+\frac{1}{2}(\psi\overleftrightarrow{\partial_5}\chi-\bar\chi\overleftrightarrow{\partial_5}\bar\psi)+\frac{c}{z}(\psi\chi+\bar\chi\bar\psi)\right\}, \tag{4.116}$$

where we have rewritten the fermion mass in units of R, $m_\Psi=c/R$, and $\overleftrightarrow{\partial_5}=\overrightarrow{\partial_5}-\overleftarrow{\partial_5}$. The symbols σ^μ, $\bar\sigma^\mu$ are related to the Pauli matrices, σ^i, as $\sigma^\mu_{\alpha\dot\alpha}=(-\mathbb{1},\sigma^i)$ and $\bar\sigma^{\mu\,\dot\alpha\alpha}=(-\mathbb{1},-\sigma^i)$ [196].

The Euler-Lagrange eom are obtained in the standard way by varying the action with respect to the fields:

$$\delta S=\int \mathrm{d}^4x\int_R^{R'}\mathrm{d}z\left\{\left(\frac{\delta\mathcal{L}}{\delta\phi^a}-\partial_M\frac{\delta\mathcal{L}}{\delta\partial_M\phi^a}\right)\delta\phi^a+\partial_M\left(\frac{\delta\mathcal{L}}{\delta\partial_M\phi^a}\delta\phi^a\right)\right\}=0. \tag{4.117}$$

Notice that the second term, that is a total derivative, does not necessarily vanish as the 5D space-time has boundaries. Requiring the first term to vanish enforces the following eom in the bulk— recall that $\mathcal{L}$ here contains also the $(R/z)^4$ prefactor:

$$\begin{aligned}\frac{\delta\mathcal{L}}{\delta\bar\chi}-\partial_M\frac{\delta\mathcal{L}}{\delta\partial_M\bar\chi}&=\left(\frac{R}{z}\right)^4\left(-\imath\bar\sigma^\mu\partial_\mu\chi-\frac{1}{2}\partial_z\bar\psi+\frac{c}{z}\bar\psi\right)-\partial_z\left[\left(\frac{R}{z}\right)^4\frac{1}{2}\bar\psi\right]\\&=\left(\frac{R}{z}\right)^4\left(-\imath\bar\sigma^\mu\partial_\mu\chi-\partial_z\bar\psi+\frac{c+2}{z}\bar\psi\right),\end{aligned} \tag{4.118}$$

and similarly

$$\frac{\delta\mathcal{L}}{\delta\psi}-\partial_M\frac{\delta\mathcal{L}}{\delta\partial_M\psi}=\left(\frac{R}{z}\right)^4\left(-\imath\sigma^\mu\partial_\mu\bar\psi+\partial_z\chi+\frac{c-2}{z}\chi\right). \tag{4.119}$$

As for the total derivative in (4.117), the standard 4D space-time components can be neglected as there is no boundary. The term with $M=5$ however gives the following contribution:

$$\frac{1}{2}\int \mathrm{d}^4x\left[\left(\frac{R}{z}\right)^4(\delta\bar\chi\,\bar\psi+\psi\,\delta\chi-\delta\bar\psi\,\bar\chi-\chi\,\delta\psi)\right]_{z=R}^{z=R'}. \tag{4.120}$$

We see that (4.120) is generically non-zero unless suitable boundary conditions are chosen for the fields. At each boundary $\tilde z=R,R'$ there are exactly two possibilities: either

$$\chi(x,\tilde z)=0\,(\delta\chi=0)\ \Rightarrow\ \partial_z\bar\psi(x,\tilde z)=\frac{2+c}{z}\bar\psi(x,\tilde z) \tag{4.121}$$

where the implication follows by using the bulk eom in (4.118), or

$$\psi(x,\tilde z)=0\,(\delta\psi=0)\ \Rightarrow\ \partial_z\chi(x,\tilde z)=\frac{2-c}{z}\chi(x,\tilde z) \tag{4.122}$$

where we have used (4.119). Either way, we can see that the boundary conditions at $z = R, R'$ for the two chiralities χ and ψ are not independent, as they are connected through the eom. The condition $\phi(x, \tilde{z}) = 0$ is denoted as Dirichlet, and it implies a condition on the opposite chirality which for $c = 0$ and flat space-time reduces to Neumann boundary condition, $\partial_z \phi(x, \tilde{z}) = 0$.

Going back to the Dirac fermion Ψ, we will denote by $\Psi[+]$ a Dirichlet boundary condition for its right-handed component, namely $\psi = 0$ as in (4.122), and by $\Psi[-]$ a Dirichlet boundary condition on the left-handed component, $\chi = 0$ as in (4.121). In the actual case of two boundaries, we will use $\Psi[a, b]$ ($a, b = +$ or -) where a and b refer to the UV and IR branes, respectively.

Let us now move to discuss the relevance of the Kaluza-Klein (KK) decomposition for fields that live on a compact space. This applies to our discussion because the fifth dimension is limited by the UV and IR branes. The idea is to decompose each 5D field as an infinite sum of pure 4D fields, the weight of each given by a profile function that only depends on the coordinate in the extra dimension z. For fermions, we shall use the following decomposition:

$$\chi(x, z) = \sum_n g_n(z)\chi_n(x), \quad \bar{\psi}(x, z) = \sum_n f_n(z)\bar{\psi}_n(x, z). \tag{4.123}$$

Each 4D spinor then satisfies the 4D Dirac equation with mass m_n:

$$\begin{cases} -\imath\bar{\sigma}^\mu \partial_\mu \chi_n + m_n \bar{\psi}_n = 0 \\ -\imath\sigma^\mu \partial_\mu \bar{\psi}_n + m_n \chi_n = 0 \end{cases} . \tag{4.124}$$

By plugging the ansatz (4.123) in the bulk eom, (4.118) and (4.119), and using the 4D eom (4.124), one finds the following equations for the profiles:

$$\begin{cases} g_n' - m_n f_n + \frac{c-2}{z} g_n = 0 \\ f_n' + m_n g_n - \frac{c+2}{z} f_n = 0 \end{cases} . \tag{4.125}$$

Moreover, the various 4D modes need to satisfy orthonormalization conditions of the kinetic terms that are given by

$$\int_R^{R'} a(z)^4 g_n(z) g_m(z)\, \mathrm{d}z = \int_R^{R'} a(z)^4 f_n(z) f_m(z)\, \mathrm{d}z = \delta_{n,m}. \tag{4.126}$$

It is extremely relevant for the low-energy phenomenology whether massless fermions can appear in the spectrum. Let us then set $m_0 = 0$ in (4.125) and solve the consequently two uncoupled equations. One simply finds

$$g_0 = A_0 \left(\frac{z}{R}\right)^{2-c}, \quad f_0 = B_0 \left(\frac{z}{R}\right)^{c+2}, \tag{4.127}$$

where A_0 and B_0 are two independent constants. We see that a zero-mode can appear only if the boundary conditions $\Psi[a, b]$ are such that $a = b$. In particular,

$$\begin{aligned} &\Psi[+,+] \Rightarrow B_0 = 0 \text{ and } g_0 = A_0 \left(\frac{z}{R}\right)^{2-c} && \text{LH zero mode,} \\ &\Psi[-,-] \Rightarrow A_0 = 0 \text{ and } f_0 = B_0 \left(\frac{z}{R}\right)^{2+c} && \text{RH zero mode.} \end{aligned} \tag{4.128}$$

It is also important to understand the qualitative behavior of the zero-mode profiles along the extra dimension. In particular, it is crucial to determine where a given zero mode has the largest wave function in order to understand its properties. As we shall see, this is how the SM flavor puzzle is solved in the 5D dual of partial compositeness that we referred to in Sec. 4.1. Generically one identifies two possibilities: either UV localization or IR localization. This property is however not straightforward by just looking at the profile functions in (4.128). The best way to see this is to look at the profiles in a covariant way, namely including the fact that the extra dimension is warped. Let us then calculate the normalization condition in (4.126) for a LH zero mode:

$$\int_R^{R'} a^4(z) g_0^2(z)\,\mathrm{d}z = A_0^2 R^{2c} \int_R^{R'} z^{-2c}\,\mathrm{d}z = 1. \tag{4.129}$$

In order to understand where this zero mode is localized, we can now consider the limit in which either brane is removed, namely $R \to 0$ or $R' \to \infty$. If the mode remains normalizable, namely the integral is finite, it means that it is localized on the other brane. It is now easy to see that for a LH mode $c > 1/2$ implies UV localization, whereas the mode is IR localized for $c < 1/2$. The same relations hold for a RH zero-mode but with $c \to -c$: $c < -1/2$ implies UV localization and $c > -1/2$ gives IR localization. As mentioned before, this very simple fact provides the solution to the SM flavor puzzle, and will also be relevant for the mass scale of the elementary vector-like fermions in our model of soft breaking.

Let us now move to discuss massive modes, which are truly called KK excitations. One can rewrite (4.125) increasing the order in the derivatives but disentangling the g_n and f_n profiles as

$$\begin{cases} g_n'' - \frac{4}{z} g_n' + \left(m_n^2 - \frac{c^2+c-6}{z^2}\right) g_n = 0 \\ f_n'' - \frac{4}{z} f_n' + \left(m_n^2 - \frac{c^2-c-6}{z^2}\right) f_n = 0 \end{cases} . \tag{4.130}$$

The two equations are the same modulo $c \to -c$, so we can just focus on the first one. As it is a second-order differential equation, there exist two independent solutions, that are customarily indicated as warped sine $S(z, m, c)$ and warped cosine $C(z, m, c)$, see e.g. [197,198], that are defined in the Sec. C.3. The generic solution to both (4.125) and (4.130) is:

$$\begin{aligned} g_n(z) &= \left(\frac{R}{z}\right)^{c-2} \left[b_n S(z, m_n, c) - a_n C(z, m_n, c)\right], \\ f_n(z) &= \left(\frac{R}{z}\right)^{-c-2} \left[a_n S(z, m_n, -c) + b_n C(z, m_n, -c)\right], \end{aligned} \tag{4.131}$$

where a_n, b_n are arbitrary coefficients that are fixed by imposing boundary and normalization conditions, and the masses m_n are obtained by quantization conditions as we shall see. The warped trigonometric functions satisfy useful equalities

$$C(R, m, c) = 1, \quad S(R, m, c) = 0, \tag{4.132}$$

which make them ideal to impose Dirichlet boundary conditions at $z = R$, together with the Wronskian relation

$$C(z, m, c) C(z, m, -c) + S(z, m, c) S(z, m, -c) = 1 \tag{4.133}$$

that generalizes $\cos^2\theta + \sin^2\theta = 1$.

Let us now discuss how the masses m_n of the various KK excitations are obtained. For each Dirac state $(\chi_n, \bar{\psi}_n)$ there are two arbitrary constants a_n and b_n. However, there are two boundary conditions that need to be satisfied together with ortho-normalization requirements for the 4D kinetic terms, (4.126). As the system is over-constrained, all requirements can be met only if the two boundary conditions are actually *linearly dependent*. This happens only for suitable (discrete) values of the masses m_n, which are indeed determined this way.

To see how this works, let us take for example a fermion with boundary conditions $\Psi[-,+]$. Referring to the profile solution in (4.131), one has $g_n(R) = f_n(R') = 0$ which implies $a_n = 0$ together with

$$C(R', m_n, -c) = 0, \tag{4.134}$$

where the latter condition actually gives all the possible values of m_n. For instance, $c = -0.3$ and $R' = 1$ TeV^{-1} gives $m_1 \sim 2$ TeV. For each m_n, the last parameter b_n is then fixed by the normalization of the kinetic terms, (4.126)

$$b_n^2 \int_R^{R'} \mathrm{d}z \left(\frac{R}{z}\right)^{2c} S^2(z, m_n, c) = 1, \tag{4.135}$$

and all the other normalization conditions are automatically satisfied.

The KK decomposition of gauge bosons can be carried out in a similar way. There one finds that imposing a Dirichlet boundary condition for the vector part A_μ^α implies Neumann for the scalar component A_5^α, and vice versa. This has the same implication in terms of KK decomposition and zero modes as for the fermions. In particular, the broken gauge bosons of $SO(5)$, $A_\mu^{\hat{a}}$, need to have Dirichlet boundary conditions on both branes to allow for the zero modes within $A_5^{\hat{a}}$ corresponding to the pNGB Higgs degrees of freedom. Conversely, the three SM gauge bosons corresponding to $SU(2)_L$ emerge for instance as zero modes of A_μ^i, $i = 1, 2, 3$ once Dirichlet boundary conditions are set for A_5^i on both branes.

4.5.2 The holographic Higgs

We discuss here the 5D setup that represents the holographic dual of the conventional MCHM$_5$, which is in fact the way this model was first introduced in Ref. [157]. The symmetry structure is the same as always, namely a $SO(5) \times U(1)_X$ gauge symmetry in the bulk which is reduced to $SU(2)_L \times U(1)_Y$ and $SO(4) \times U(1)_X$ on the UV and IR branes, respectively. The values for R and R' are fixed by phenomenological considerations. As mentioned already, the position R of the UV brane is given by the smallest distance at which the theory can be trusted, and thus it is usually set at the Planck scale: $R = 1/M_{\rm Pl}$. Conversely, the IR brane represents the IR cutoff of the theory and needs to be identified with the scale at which the strong sector of the dual 4D theory loses conformality, and thus coincides with the condensation scale. Since we expect the Higgs decay constant to be around 1 TeV, one assumes $R' \sim 1\,\mathrm{TeV}$. The choice of embedding the quark doublet q_L and the singlet t_R as $\mathbf{5}$ of $SO(5)$ corresponds here to introducing two different 5D fermion fields Ψ_q and Ψ_t in the $\mathbf{5}_{2/3}$ representation of $SO(5) \times U(1)_X$:

$$\Psi_q = \begin{pmatrix} w_u[-,+] & t[+,+] \\ w_d[-,+] & b[+,+] \end{pmatrix} \oplus s[-,+], \quad \Psi_t = \begin{pmatrix} w'_u[+,-] & v_u[+,-] \\ w'_d[+,-] & v_d[+,-] \end{pmatrix} \oplus t'[-,-]. \tag{4.136}$$

The fields have been presented according to $\mathbf{4}\oplus\mathbf{1}$ representations of $SO(4)$. The boundary conditions for (t,b) are such their LH components allow for a zero mode, which is then identified with the SM quark doublet q_L. Similarly, the boundary conditions for t' allow for a RH zero mode correspoding to t_R. The other fields instead only have opposite boundary conditions on the UV/IR branes and thus only give massive KK excitations, that correspond to the resonances of the strong sector. This choice is dictated by avoiding light zero modes for exotic quarks. The notation introduced for s, v, w and w' makes contact with the fields that we have been using throughout this chapter. As we can see, the boundary conditions on the UV brane in (4.136) are only $SU(2)_L$ symmetric. In the partial compositeness picture, this corresponds to incomplete multiplets as in (4.15) where the null entries of the spurions in (4.28) are here interpreted as the lack of zero-modes for the corresponding 5D fields.

The action for Ψ_q and Ψ_t has exactly the same form of (4.115), with the only difference that gauge fields are included in the covariant derivatives:

$$D_\mu = \partial_\mu + \frac{1}{4z}\gamma_\mu\gamma_5 + ig_5 T^\alpha A^\alpha_\mu + \imath g_X X_\mu, \quad D_5 = \partial_5 + ig_5 T^\alpha A^\alpha_5 + \imath g_X X_5, \tag{4.137}$$

where g_5 and g_X are the gauge couplings correspoding to $SO(5)$ and $U(1)_X$ respectively, and have mass dimension $[g_{5,X}] = -1/2$. The interaction with the Higgs is found by looking at the fifth component of the $SO(5)/SO(4)$ broken generators, $\alpha = \hat{a}$:

$$\Delta\mathcal{L} = \sum_{k=q,t} \bar{\Psi}_k(x,z)\gamma^5 T^{\hat{a}}\Psi_k(x,z)\; g_5\, A^{\hat{a}}_5(x,z) + \text{ h.c.}, \tag{4.138}$$

In the unitary gauge, only $\hat{a} = 4$ will describe the physical interaction with the Higgs. Thus, performing KK decomposition on A^4_5

$$A^5_5(x,z) = f_h(z)h(x) + \sum_n f_n(z)h_n(x), \tag{4.139}$$

and keeping only the $h(x)$ zero mode, we find

$$\Delta\mathcal{L} \supset \sum_{k=q,t} g_5\, f_h(z)\, \bar{\Psi}_k(x,z)\gamma^5\, T^4\, \Psi_k(x,z)\, h(x) + \text{ h.c.} \tag{4.140}$$

Although the interaction above has the structure of a yukawa coupling, the Higgs mediates no link between q_L and t_R as there is no cross-interaction between Ψ_q and Ψ_t. Thus, in order to give a mass to SM fermions after electroweak symmetry breaking one needs to add at least a localized action that lives in the IR brane:

$$S_{\text{IR}} = \int \mathrm{d}^4x \left(\frac{R}{R'}\right)^4 \left(\mu_4 \bar{\Psi}^{\mathbf{4}}_q(x,R')\Psi^{\mathbf{4}}_t(x,R') + \mu_1 \bar{\Psi}^{\mathbf{1}}_q(x,R')\Psi^{\mathbf{1}}_t(x,R') + \text{ h.c.}\right), \tag{4.141}$$

where $\mathbf{4}$ and $\mathbf{1}$ refer to the decomposition in fourplet and singlet in (4.136) and $\mu_{4,1}$ are dimensionless parameters.

At this point, we should also notice that (4.131) gives the solution to the bulk eom only for a free 5D fermion. However, the Higgs couples to the fermions through the covariant derivative in the bulk as we have just seen, and this interaction cannot be neglected if one wants to investigate the generated Higgs potential. This leads to coupled differential equations among the different $SO(5)$ components of the $\Psi_{q,t}$ fields

considerably complicating their eom which also pick a dependence on the Higgs vev. The new KK decomposition for a Weyl spinor $\chi(x,z)$ taking this into account becomes

$$\chi(x,z) = \sum_n g_n(z,\langle h\rangle)\,\chi_n(x), \quad \bar\psi(x,z) = \sum_n f_n(z,\langle h\rangle)\,\bar\psi_n(x), \tag{4.142}$$

which gives back (4.123) for $\langle h\rangle = 0$.

Fortunately, there exists a gauge transformation that allows to remove the Higgs vev from the bulk. It is called *holographic gauge* and reads [199]

$$\Psi_f(x,z) \to \Omega(z)\Psi_f(x,z), \tag{4.143}$$

where $f = q,t$ together with

$$T^\alpha A_M^\alpha(x,z) \to \Omega(z)\,T^\alpha A_M^\alpha(x,z)\,\Omega(z)^T - (i/g_5)\,\partial_M\Omega(z)\,\Omega(z)^T, \tag{4.144}$$

and $\Omega(z)$ is the Wilson line defined as

$$\Omega(z) = \exp\left(-\imath g_5 T^4\langle h\rangle \int_R^z \mathrm{d}\tilde z\, f_h(\tilde z)\right). \tag{4.145}$$

After applying $\Omega(z)$ the dependence on the Higgs vev from all bulk profiles drops out, and one can relate $g_n(z,\langle h\rangle)$ to $g_n(z,0)$ simply by

$$g_n^a(z,\langle h\rangle) = \Omega(z)^{ab}\,g_n^b(z,0), \quad f_n^a(z,\langle h\rangle) = \Omega(z)^{ab}\,f_n^b(z,0), \tag{4.146}$$

where $a,b = 1,\dots,5$ are $SO(5)$ indices. Hence, the boundary conditions that are originally defined for $g_n(z,\langle h\rangle)$ and $f_n(z,\langle h\rangle)$ can be easily related to the free profiles via (4.146). Notice that, as $\Omega(R) = 1$, both profiles coincide on the UV brane and thus have the same boundary conditions.

The actual picture, however, is modified by the presence of brane-localized terms. To see this, we refer explicitly to the IR-localized that was given in (4.141) by simply taking the value of the 5D fields at $z = R'$. Introducing such boundary terms, however, requires a more careful treatment in order to comply with the variational principle and we will here follow the procedure outlined in Ref. [195]. According to the notation in (4.114), we will indicate by $\chi_{q,t}$ and $\bar\psi_{q,t}$ the LH and RH component of $\Psi_{q,t}$, respectively. Moreover, each Weyl component comes with $SO(4)$ indices representing either the **4** or the **1** of $SO(4)$. With this notation, (4.141) can be expanded in terms of the χ and ψ fields as

$$\begin{aligned} S_{\rm IR} = \int \mathrm{d}^4x \left(\frac{R}{R'}\right)^4 \Big[&\mu_4\left(\psi_q^{\mathbf{4}}(x,R')\chi_t^{\mathbf{4}}(x,R') + \bar\chi_q^{\mathbf{4}}(x,R')\bar\psi_t^{\mathbf{4}}(x,R')\right) \\ &\mu_1\left(\psi_q^{\mathbf{1}}(x,R')\chi_t^{\mathbf{1}}(x,R') + \bar\chi_q^{\mathbf{1}}(x,R')\bar\psi_t^{\mathbf{1}}(x,R')\right) + \text{h.c.}\Big]. \end{aligned} \tag{4.147}$$

Moreover, we will simplify the expression above by using directly the boundary conditions in (4.136), $\psi_q^{\mathbf{4},\mathbf{1}}(x,R') = 0$ and $\chi_t^{\mathbf{4},\mathbf{1}}(x,R') = 0$. This leads to

$$S_{\rm IR} = \int \mathrm{d}^4x \left(\frac{R}{R'}\right)^4 \left[\mu_4\,\bar\chi_q^{\mathbf{4}}(x,R')\bar\psi_t^{\mathbf{4}}(x,R') + \mu_1\,\bar\chi_q^{\mathbf{1}}(x,R')\bar\psi_t^{\mathbf{1}}(x,R') + \text{h.c.}\right] \tag{4.148}$$

However, recalculating the Euler-Lagrange eom from the bulk action together with $S_{\rm IR}$, we will find that the boundary terms will no longer vanish with the standard set of Dirichlet conditions as in (4.136) exactly because of the new terms in (4.148). In order to have a consistent variational principle, one needs to rely on a certain prescription when introducing a boundary action. We will follow the one that first moves all the terms in (4.148) away from the IR brane by $\epsilon > 0$, yielding

$$S_{\rm IR} = \int \mathrm{d}^4x \int \mathrm{d}\, z \left(\frac{R}{z}\right)^4 \left[\mu_4\, \bar{\chi}_q^{\mathbf{4}}(x,z)\bar{\psi}_t^{\mathbf{4}}(x,z) + \mu_1\, \bar{\chi}_q^{\mathbf{1}}(x,z)\bar{\psi}_t^{\mathbf{1}}(x,z) + \text{h.c.}\right]\delta(z - R' + \epsilon), \tag{4.149}$$

where $\delta(x)$ is the Dirac delta-function. The eom now give:

$$\begin{aligned} &-\imath\bar{\sigma}^\mu\partial_\mu\chi_q^{\mathbf{r}} - \partial_z\bar{\psi}_q^{\mathbf{r}} + \frac{c_q+2}{z}\bar{\psi}_q^{\mathbf{r}} + \mu_r\,\bar{\psi}_t^{\mathbf{r}}\,\delta(z-R'+\epsilon) = 0, \\ &-\imath\sigma^\mu\partial_\mu\bar{\psi}_t^{\mathbf{r}} + \partial_z\chi_t^{\mathbf{r}} + \frac{c_t-2}{z}\chi_t^{\mathbf{r}} + \mu_r\,\chi_q^{\mathbf{r}}\,\delta(z-R'+\epsilon) = 0, \end{aligned} \tag{4.150}$$

where we have introduced $\mathbf{r} = \mathbf{4}, \mathbf{1}$ to keep the notation compact. The idea is now to integrate the eom in (4.150) around the δ-functions from $z = R' - \epsilon$ to $z = R'$ and obtain a new set of boundary conditions. One can see that the wave functions that enter the modified eom with ∂_z will undergo a *jump* at $z = R' - \epsilon$, whereas all the other profiles will receive modifications that vanish when $\epsilon \to 0$. Performing the integral, one finds:

$$\begin{aligned} &\bar{\psi}_q^{\mathbf{r}}(x,R'-\epsilon) - \cancel{\bar{\psi}_q^{\mathbf{r}}(x,R')} + \mu_r\,\bar{\psi}_t^{\mathbf{r}}(x,R'-\epsilon) + \mathcal{O}(\epsilon) = 0, \\ &\cancel{\chi_t^{\mathbf{r}}(x,R')} - \chi_t^{\mathbf{r}}(x,R'-\epsilon) + \mu_r\,\chi_q^{\mathbf{r}}(x,R'-\epsilon) + \mathcal{O}(\epsilon) = 0, \end{aligned} \tag{4.151}$$

where we have used the original boundary conditions at $z = R$ to simplify the expression. The new boundary conditions are then defined by taking the $\epsilon \to 0$ limit in (4.151)

$$\begin{cases} f_q^{\mathbf{r}}(R',\langle h\rangle) = 0 \\ g_t^{\mathbf{r}}(R',\langle h\rangle) = 0 \end{cases} \longrightarrow \begin{cases} f_q^{\mathbf{r}}(R',\langle h\rangle) + \mu_r\, f_t^{\mathbf{r}}(R',\langle h\rangle) = 0 \\ g_t^{\mathbf{r}}(R',\langle h\rangle) - \mu_r\, g_q^{\mathbf{r}}(R',\langle h\rangle) = 0 \end{cases}, \tag{4.152}$$

which fully capture the effect of having the IR-localized action in (4.148). In the equation above we stressed that these new conditions actually hold for the Higgs-dependent profiles. However, using (4.146) we can obtain the final sets of the IR boundary conditions in terms of the free profiles, whose general solution is given in (4.131), as:

$$\begin{cases} f_q(R') + \Omega^{-1}(R')\, M\, \Omega(R') f_t(R') = 0, \\ g_t(R') - \Omega^{-1}(R')\, M\, \Omega(R') g_q(R') = 0, \end{cases} \tag{4.153}$$

where $M = \mathrm{diag}\,(\mu_4,\mu_4,\mu_4,\mu_4,\mu_1)$, and f, g are expressed as $SO(5)$ vectors. Notice that in the particular case $\mu_4 = \mu_1$, we have $M \propto \mathbb{1}_{5\times5}$ and the Higgs vev is removed from the theory (namely, it is unphysical) showing that the Higgs would be an exact NG boson as long as the fermion sector is concerned. This has to do with the "collective breaking" of the multi-site models discussed in Sec. 4.3.2, which indeed take inspiration from the 5D models. In fact, it is not only necessary to break $SO(5)$ on the UV brane (or the elementary site in the dual picture) but also on the IR brane.

While referring to Ref. [157] for the actual details, let us note here that the new boundary conditions in (4.153) make apparent that the mass of the SM fermions, which

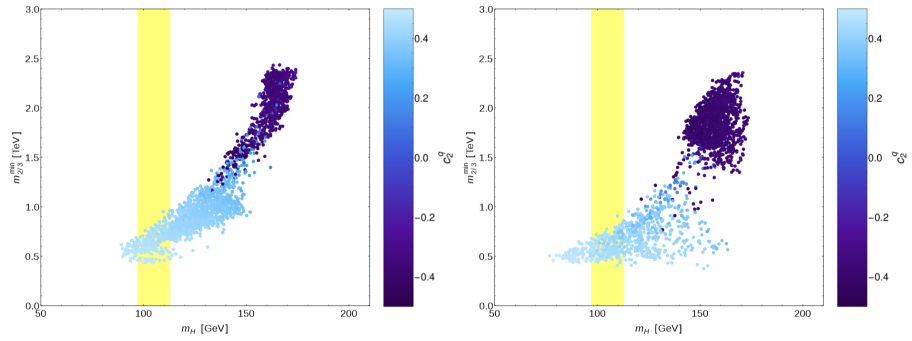

Figure 4.12: Scatter plot of the (m_h, m_T) parameter space as obtained from the holographic MCHM$_5$. As we can see, reproducing the correct Higgs mass generically requires top parterns below 1 TeV. The left and right panels correspond to different choices of the IR-brane masses μ_4 and μ_1. Plot taken from [173].

is linked to the Higgs vev and thus to $\Omega(R')$, will strongly depend on the behavior of the corresponding zero modes around the IR brane. As discussed in Sec. 4.5.1, this can be understood in terms of their localizations: when a zero mode is UV localized, its overlap with the IR brane will be highly suppressed, whereas an IR-localized mode will be largely affected by the Higgs vev. Thus, it is clear that one can reproduce the SM spectrum by UV localizing the light generations, whereas the third generation will feature IR localization. This automatically gets rid of the large hierarchies of the yukawa couplings in the SM, as completely different masses are here obtained simply depending on whether $c > 1/2$ or $c < 1/2$, see again the discussion below (4.129).

On similar grounds, one can show that the largest contribution to the Higgs potential is given by the zero modes that are the most IR localized, which simply correspond to the SM fermions that have the largest yukawa to the Higgs. Similarly to what happens in purely 4D models, one then finds a very tight relation between the top mass, the Higgs mass and the mass of the partners, which is qualitatively the same as (4.22) and actually hints for even lighter top partners. These are here interpreted as anomalously light KK modes, whose natural scale would be set instead by geometrical consideration as $\sim \pi/R' \sim 3\,\text{TeV}$. This is shown in Fig. 4.12 for the holographic dual of the MCHM$_5$ defined in (4.136). We thus conclude that the 5D models describing a holographic Higgs are (even more) in tension with the LHC. Again, one could solve this by simply raising the Higgs decay constant, f, (which in the 5D picture is given as $f = 2R^{1/2}/g_5 R'$, see e.g. [173]) whose drawbacks have already been discussed at the end of Sec. 4.2.

In the next section, we will discuss how to implement the soft breaking in the holographic picture. As we shall see, the idea behind our setup becomes even more transparent in the 5D approach where all its features can be interpreted in a very simple way.

4.5.3 Universal boundary conditions for a light Higgs

We present here a realization of the soft-breaking idea using the warped 5D setup, where we will see that every ingredient of the 4D models have a very natural implementation [VII]. The resulting 5D model is in fact quite simple and natural, and in no way more contrived than the original [157] holographic MCHM$_5$, but phenomenologically more

successful.

The implementation of soft breaking is very simple and natural in 5D. All one needs to do is impose $SO(5)$-*universal* boundary conditions on the bulk fields $\Psi_{q,t}$ that the SM fermions are embedded into. This means all $SO(5)$ components of the fields have the same boundary conditions, and (4.136) simply becomes

$$\Psi_q[+,+], \quad \Psi_t[-,-]. \tag{4.154}$$

With no further ingredient, such universal boundary conditions would produce a full $SO(5)$ multiplet of zero modes for every bulk fermion, which is clearly not viable phenomenologically. This can however be avoided by including a brane-localized action similar to (4.141), but this time at the UV boundary so that the zero modes can be lifted due to the presence of 4D spinors, s_R, v_L, w_{1R} and w_{2L}, which can mix with the bulk fermions on the UV brane. To obtain the same mixing pattern as in our 4D setup in which maximal symmetry and soft breaking can be successfully combined, the Lagrangian for the localized fields is chosen as

$$S_{\rm UV} = \int \mathrm{d}^4x \Big\{ -i\eta_R\sigma^\mu\partial_\mu\bar\eta_R - i\bar\xi_L\bar\sigma^\mu\partial_\mu\xi_L + \frac{1}{\sqrt{R}}\chi_q(R)\, M_R^\dagger\,\eta_R + \frac{1}{\sqrt{R}}\psi_t(R)\, M_L^\dagger\,\xi_L + \text{h.c.}\Big\}, \tag{4.155}$$

where χ_q (ψ_t) is the LH (RH) chirality of the $SO(5)$ multiplet Ψ_q (Ψ_t) as in (4.114). The 4D spinors η_R, ξ_L are the same fields as in (4.92) and $M_{R,L}$ are the the dimensionless mass matrices analogous to (4.94), where the masses are now measured in units of $R \sim 1/M_{\rm Pl}$ and are replaced by the dimensionless coefficients $\mu_i = m_i R$ (the presence of the $1/\sqrt{R}$ factor is due to the difference mass dimension of 4D and 5D fermions). The expression above is tailored to the model in (4.93). It is however straightforward to write down the 5D dual also for the minimal model of soft breaking with the elementary Lagrangian given in (4.35): in this case, the mass for w would correspond to a direct yukawa interaction between χ_q and ψ_t, which is formally the same as the one in the IR-localized action. In the following, we will stick to the setup in (4.155) as we have seen that the combination with maximal symmetry is very important to reduce the tuning.

Note that in (4.155) we are again forbidding couplings of the type $\eta_R - \xi_L$ and $\chi_q - \psi_t$ in order to avoid reintroducing the double tuning, as discussed below (4.95). In the 5D version this can be enforced by introducing a Z_2 symmetry under which the entire Dirac multiplet in the bulk, Ψ_q, (both χ_q and ψ_t) as well as η_R have negative parity, while the other fields have positive parity. This Z_2 symmetry will only be broken on the IR brane, where the $\chi_q - \psi_t$ terms in (4.148) are necessary to give masses to the SM quarks. This is quite natural in the 5D approach, as we have seen that the symmetry content of the two branes has different meanings, namely symmetry of the elementary fields vs. symmetry of the strong sector. In this respect, implementing maximal symmetry is straightforward: as this is a symmetry of the strong sector, one simply needs to require that the IR action in (4.148) possesses the $SO(5)'$ symmetry defined in (4.74). This simply amounts to setting $\mu_4 = -\mu_1$ in (4.153).

In complete analogy to the 4D model, the explicit breaking of the Higgs shift symmetry is fully encoded in the dimensionless matrices $M_{R,L}$ with elements μ_i. Actually, brane localized fields analogous to η_R and ξ_L were already considered in [200] as classical Lagrangian multipliers to enforce the desired boundary conditions in the holographic approach: soft breaking can thus be seen as making those fields dynamical and controlling their impact through their masses μ_i. In the limit of $\mu_i \gg 1$, η_R and ξ_L become

in fact true Lagrange multipliers enforcing opposite boundary conditions for the $SO(5)$ components not corresponding to SM fermions. In this limit, all results from conventional holographic CH models are recovered. However, as long as the brane fields are dynamical they will contribute to the Higgs potential and realize the 5D analogy of soft breaking. In practice, one can now interpolate between true zero modes for the new vector-like quarks ($\mu_i = 0$) and pure KK excitations ($\mu_i \gg 1$) by dialing μ_i. For intermediate values, partially elementary KK states appear in the low energy spectrum, and the model is expected to modify the Higgs potential similarly to its 4D dual.

How large values of μ_i should we choose to get a realistic model reproducing the success of the 4D picture? The most naive answer would be that $\mu_i \sim \text{TeV}/M_{\text{Pl}}$ and hence unnaturally small. However it is known that in 5D an effective TeV state can arise from a Planckian mass due to wave-function suppression or, equivalently, renormalization-group running in presence of large anomalous dimension for the corresponding operator [201, 202]. To see how this works, we need to investigate how the original boundary conditions on the UV brane are modified by the presence of the UV action. This can be done similarly to the case of S_{IR}: first we impose the conditions (4.154) in S_{UV} and then recalculate the eom including the bulk action with the UV action moved ϵ-away from the brane:

$$S_{\text{UV}} = \int \mathrm{d}^4x \int_R^{R'} \mathrm{d}z \left(\frac{R}{z}\right)^4 \delta(z - R - \epsilon)\, \mathcal{L}_{\text{UV}}(x, z), \tag{4.156}$$

where $\mathcal{L}_{\text{UV}}$ is deduced from (4.155). We find the following new equations of motion:

$$\begin{aligned}
&- i\sigma^\mu \partial_\mu \bar{\eta}_R(x) + \frac{1}{\sqrt{R}} \chi_q(x, R+\epsilon) M_R^\dagger = 0, \;\; -i\bar{\sigma}^\mu \partial_\mu \xi_L(x) + \frac{1}{\sqrt{R}} M_L \bar{\psi}_t(x, R+\epsilon) = 0, \\
&- i\sigma^\mu \partial_\mu \bar{\psi}_t(x, z) + \partial_z \chi_t(x, z) + \frac{c_t - 2}{z} \chi_t(x, z) + \delta(z - R - \epsilon) \frac{1}{\sqrt{R}} M_L^\dagger \xi_L(x) = 0, \\
&- i\bar{\sigma}^\mu \partial_\mu \chi_q(x, z) - \partial_z \bar{\psi}_q(x, z) + \frac{c_q + 2}{z} \bar{\psi}_q(x, z) + \delta(z - R - \epsilon) \frac{1}{\sqrt{R}} \bar{\eta}_R(x) M_R = 0.
\end{aligned} \tag{4.157}$$

Integrating the last two equations around the δ-function one obtains:

$$\begin{aligned}
&\chi_t(x, R+\epsilon) - \cancel{\chi_t(x, R)} + \frac{1}{\sqrt{R}} M_L^\dagger \xi_L(x) + \mathcal{O}(\epsilon) = 0, \\
&\cancel{\bar{\psi}_q(x, R)} - \bar{\psi}_q(x, R+\epsilon) + \frac{1}{\sqrt{R}} \bar{\eta}_R(x) M_R + \mathcal{O}(\epsilon) = 0.
\end{aligned} \tag{4.158}$$

Applying the $-i\bar{\sigma}^\mu \partial_\mu$ ($-i\sigma^\mu \partial_\mu$) operator to the first (second) equation in (4.158), and substituting the expression for η_R and ξ_L in the first line of (4.157), we obtain the final set of boundary conditions for the 5D fields that describes our soft-breaking setup:

$$\begin{cases} \psi_q(x, R) = 0 \\ \chi_t(x, R) = 0 \end{cases} \longrightarrow \begin{cases} -i\sigma^\mu \partial_\mu \bar{\psi}_q(x, R) + \frac{1}{R} \chi_q(x, R) \Gamma_R = 0 \\ -i\bar{\sigma}^\mu \partial_\mu \chi_t(x, R) - \frac{1}{R} \Gamma_L \bar{\psi}_t(x, R) = 0 \end{cases} \tag{4.159}$$

where $\Gamma_{L,R}$ are exactly the dimensionless equivalent of the spurions in (4.96). As we can see, the effect of the brane localized spinors η and ξ can be recasted as a set of relations involving the 5D fields only. In particular, one can check that in the limit of very large

brane terms, $\Gamma_{L,R}$, this set of boundary conditions gives back the standard assignments in (4.136) for the different $SO(5)$ components.

However, the new UV boundary conditions contain derivative operators and it is not obvious how to interpret them at first sight. In order to gain some understanding, we will explicitly investigate the KK spectrum for the simplified case in which only the UV-localized singlet spinor $s_R(x) \in \eta_R(x)$ is dynamical. This actually corresponds to the 5D dual of the singlet case discussed in Sec. 4.3.3. We then consider the $SO(4)$-singlet component of Ψ_q consisting of two Weyl spinors, $s_L \in \chi_q$ and $\sigma_R \in \psi_q$, that are KK decomposed as:

$$s_L(x,z) = \sum_n g_n(z)\chi_n(x), \quad \bar{\sigma}_R(x,z) = \sum_n f_n(z)\bar{\psi}_n(x), \tag{4.160}$$

where $\chi_n(x)$ and $\psi_n(x)$ solve the 4D Dirac equation with mass m_n, (4.124), and $g_n(z), f_n(z)$ are the bulk profiles. One also needs to expand the brane-localized field, $s_R \in \eta_R$, in the same basis in order to account for the mixing in (4.155) with the 5D field:

$$\bar{s}_R(x) = \sum_n e_n \bar{\psi}_n(x). \tag{4.161}$$

The boundary conditions for $s_L(x,z)$ and $s_R(x,z)$ can be read out from (4.159) by picking the $SO(4)$ singlet component in $\bar{\psi}_q$ and χ_q, namely $\bar{\sigma}_R$ and s_L, respectively. The derivative operator can be simplified by plugging in the KK decomposition in (4.160) and using the 4D eom. The new UV boundary condition is then

$$f_n(R) - \frac{\mu_s^2}{m_n R} g_n(R) = 0 \quad \Rightarrow \quad b_n + \frac{\mu_s^2}{m_n R} a_n = 0 \tag{4.162}$$

whereas $f_n(R') = 0$ is unaffected (we are for the moment neglecting all effects from the IR brane) and implies

$$a_n S(R', m_n, -c_q) + b_n C(R', m_n, -c) = 0, \tag{4.163}$$

where we have used the explicit form of the free profiles in (4.131). Notice that the condition above reduces to $[+,+]$ in case $\mu_s = 0$, implying an additional zero mode, and to $[-,+]$ if $\mu_s \gg 1$ implying that the lightest state is a pure KK excitation, as mentioned above. As we shall see, for intermediate values of μ_s a partially elementary state can instead appear in the spectrum. The modified boundary condition can be rewritten by requiring (4.162) and (4.163) to be linearly dependent. One finds:

$$S(R', m_n, -c_q) - \frac{\mu_s^2}{m_n R} C(R', m_n, -c_q) = 0. \tag{4.164}$$

Moreover, the orthonormalization of the profiles requires:

$$e_n^2 + \int_R^{R'} a(z)^4 g_n^2(z) = 1, \quad \int_R^{R'} a(z)^4 f_n^2(z) = 1, \tag{4.165}$$

which differ from the standard (4.126) because we have to take into account the presence of the brane component, e_n. The warped sine and cosine can actually be expanded for small masses, $mz \lesssim 1$:

$$S(z,m,c) = (mR)\, Z_{\rm S}(z,c) + \mathcal{O}(m^3 z^3), \quad C(z,m,c) = 1 - (mR)^2 Z_{\rm C}(z,c) + \mathcal{O}(m^4 z^4) \tag{4.166}$$

where

$$Z_{\rm S}(z,c) = \frac{1}{1+2c}\left[\left(\frac{z}{R}\right)^{1+2c} - 1\right] \tag{4.167}$$

and

$$Z_{\rm C}(z,c) = \frac{1}{2(1-4c^2)}\left[1-2c+(1+2c)\left(\frac{z}{R}\right)^2 - 2\left(\frac{z}{R}\right)^{1+2c}\right]. \tag{4.168}$$

One then obtains from (4.164) that the lightest state, m_1, has a mass given by:

$$m_1^2 = \frac{\mu_s^2 R^{-2}}{Z_{\rm S}(R',-c_q) + \mu_s^2 Z_{\rm C}(R',-c_q)}. \tag{4.169}$$

For small μ_s, one can actually neglect the $Z_{\rm C}$ term and obtain

$$m_1^2 \sim \begin{cases} (2c_q-1)\mu_s^2 R^{-2} & c_q > 1/2 \Rightarrow \text{UV} \\ (1-2c_q)\mu_s^2 R'^{-2}\left(\frac{R}{R'}\right)^{-1-2c_q} & c_q < 1/2 \Rightarrow \text{IR} \end{cases}. \tag{4.170}$$

The dependence of m_1 on the various parameters as μ_s and c_q can be understood as follows. First, when $\mu_s \to 0$ the lightest state becomes massless due to the emergence of the $[+,+]$ boundary condition that implies a LH zero mode. Instead, for $\mu_s \neq 0$ the mass of m_1 strongly depends on the localization of the would-be zero mode. In case of UV localization corresponding to $c_q > 1/2$, the mass of this state is indeed simply given by the mass term on the UV brane, which is exactly $\mu_s R^{-1}$ (remember that μ_s was measured in units of Planck mass). Thus, unless μ_s is tuned tiny, $\mu_s \sim 10^{-16}$, the UV-localized spinor s_R decouples from the low-energy theory, and the state with mass m_1 would be indistinguishable from a standard KK mode coming from an effective $[-,+]$ boundary condition.

However, what is interesting about (4.170) is that a TeV-scale state with a sizable overlap with the elementary spinor s_R and mass $m_1 \sim R'^{-1}$ can now emerge from a Planckian mass, $\mu_s \lesssim 1$, in case of deep IR localization, $c_q \approx -1/2$, due to the effect of the wave-function suppression given by the factor $(R/R')^{1-2c_q}$. The picture is simply that a large Planckian mass on the UV brane can be diluted to much smaller values due to the fact that one mode has very little overlap with the UV brane itself. Moreover, we notice that, since the occurrence of such a partially elementary state is linked to the presence of IR-localized zero modes, it is relevant only for the third generation fermions, which are exactly those that contribute the most to the Higgs potential and usually require light partners. Hence the issue of light partners is getting naturally resolved in this setup, and no additional tweaking of the model is needed.

To investigate this in a more quantitative way, let us evaluate what is the degree of "elementariness" of the state with mass m_1 as a function of the UV-brane mass μ_s. To this end, we will obtain the mass of the lightest state directly from the exact condition (4.164) and calculate the value of e_n according to (4.165). The point is that, as long as e_n is sizeable, the lightest state has a large elementary component, and the effect of the soft breaking can be important. Conversely, if e_n is very small the top partner looks effectively as a standard KK excitation.

The comparison between the approximate formula (4.170) shown in orange and the true numerical result shown in blue is displayed in Fig. 4.13 for $c_q = -0.3$ (left) and $c_q = -0.4$ (right), where $R' = 1/3\,\text{TeV}^{-1}$. The two lines depart at values of μ_s such that the $Z_{\rm C}$ term becomes important. The green lines in Fig. 4.13 show the elementary

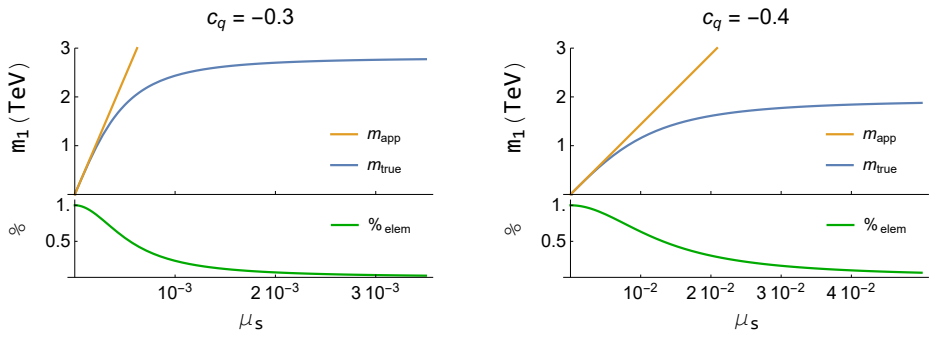

Figure 4.13: The mass of the lightest state, m_1, as a function of μ_s for $c_q = -0.3$ (left) and $c_q = -0.4$ (right). The blue line is the true numerical value, that is compared with the approximate formula (4.170) in orange. The two lines depart for values of μ_s for which the Z_C term becomes important. The green line reprents the overlap of this state with the UV-localized spinor, s_R, and 1 means 100%. When such overlap becomes negligible, the $[-,+]$ boundary condition is effectively recovered and there is no elementary state in the spectrum at low energy.

content of the lightest state with mass m_1, corresponding to the numerical value of e_1^2 in (4.161) after canonically normalizing $\chi_1(x)$. As expected it is almost completely elementary in the $\mu_s \to 0$ limit and becomes mostly composite for large values of μ_s, approaching the limit of the $[-,+]$ boundary condition. We notice that the closer c_q is to -0.5, the more natural the value of μ_s can be: for $c_q = -0.4$ a largely elementary state with $\sim 1\,\text{TeV}$ mass is realized for $\mu_s \sim 0.01$, whereas $c_q = -0.3$ requires $\mu_s \sim 0.001$, but allows for $m_1 \gtrsim 2\,\text{TeV}$. In fact, for larger values of μ_s, the elementary state "migrates" towards higher KK excitations and decouples from the low-energy theory. Slightly smaller values of μ_s show instead a sizable elementary component of the lightest excitation, thus realizing the 4D low-energy theory discussed in the previous section. Notice that due to the almost complete IR localization, the mass of this state is very similar to the mass of a light custodian from a $[-,+]$ boundary condition to which it asymptotes, $m_1 \lesssim m_{\text{cust}}$ [158]. Of course, even though the mass is similar, this state is substantially different from a light custodian due to its degree of "elementariness" and correspondingly different impact on the Higgs potential. If one wants to keep $\mu_s \in (0.001, 0.01)$ and therefore $c_q \in (-0.4, -0.3)$, we need to raise R' to compensate the suppression typical of a light custodian, if we want to realize $m_1 \gtrsim 2\,\text{TeV}$. This is the reason behind the choice of $R' = 1/3\,\text{TeV}^{-1}$ in Fig. 4.13. With $f = 800\,\text{GeV}$, such value of R' implies $g_* \sim 7.5$ and thus $N_{\text{CFT}} \sim 3$ [14].

Let us finally move to consider the more realistic setup in which an IR action is included to provide a mass for the top after electroweak symmetry breaking. We thus implement the IR boundary conditions in (4.153) where the Higgs appears through the Wilson line $\Omega(R')$. Our aim is to calculate the top mass together with the mass of the partially elementary KK state as in (4.170). This can be regarded as a first step in providing a full 5D calculation of the singlet setup. Our findings are shown in Fig. 4.14 as a function of μ_s assuming that all the other brane localized fields are decoupled and thus replaced by the corresponding static boundary conditions. We have chosen the

[14] Allowing for (technically natural) smaller μ_s makes it possible to keep $R' = 1\text{TeV}^{-1}$.

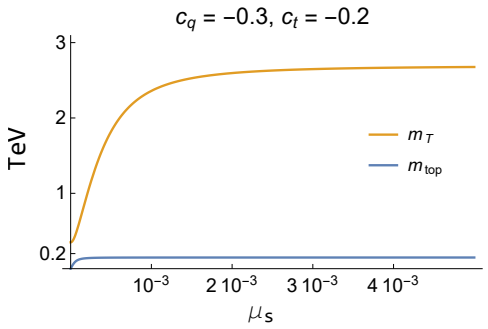

Figure 4.14: The top mass and the top-partner mass as a function of μ_s for $c_q = -0.3$, $c_t = -0.2$, $\mu_4 = -\mu_1 = 0.12$ and $R' = 1/3$ TeV^{-1}. As its mass is largely varying with μ_s, the top partner shows a sizeable elementary component in the region where the top mass is correctly reproduced, showing that soft breaking in 5D is phenomenologically viable.

localization for Ψ_q and Ψ_t as $c_q = -0.3$ and $c_t = -0.2$, whereas the IR-localized mass terms in (4.148) are $\mu_4 = -\mu_1 \simeq 0.12$, $R' = 1/3$ TeV^{-1} and $R = 1/M_{\rm Pl}$. As we can see, the top mass is reproduced correctly as $m_{\rm top} \sim 150$ GeV almost independently of μ_s, confiming the findings in Sec. 4.3.3 where the top mass was found to be almost insensitive to the singlet mass m_s. As for the top partner, we can see that the mass m_T is still varying with μ_s in a region where the top mass is already at its correct value. The change with μ_s implies that this state has a sizeable elementary component, as shown explicitly in Fig. 4.13, meaning that partially elementary KK states are compatible with reproducing the correct top mass.

The calculation of the Higgs potential follows from the set of boundary conditions derived in this section. This study, together with a detailed phenomenology of the 5D setup, is however left for future work.

4.6 Summary

Higgs compositeness is arguably one of the most appealing solutions to the hierarchy problem. Minimal models, however, are in tension with the null signals of new physics from the LHC. In particular, the prediction of light top partners that seem to be a necessary ingredient to ensure a light Higgs is clashing with the experimental bounds that force these new colored states to be as heavy as $m_T \gtrsim 1.4$ TeV. The simplest way of dealing with this is by raising the Higgs decay constant f as much as necessary to meet the present constraints. Physically, this corresponds to make the Higgs more and more SM-like, thus generically suppressing all possible signals of new physics. Moreover, raising f worsens the tuning required to reproduce the correct electroweak symmetry breaking, pushing the minimal models towards the percent-level.

Instead, we have proposed a new way of realizing a CH that removes the sharp prediction for the light top partners. This is so because of a structural change in the way the explicit breaking is realized in our model. In particular, the couplings responsible for partial compositeness are assumed to respect the global symmetry of the theory ($SO(5)$ for the minimal realizations). This is possible by completing the SM fermions to full representations introducing new elementary fermions. These are vector-like under the

SM gauge symmetry and their masses account both for the soft breaking of $SO(5)$ and their non-observation.

In Sec. 4.3, we have shown how the Higgs mass and the top-partner mass can be disentangled in this setup avoiding the prediction of light partners without the need of raising f. This represents a first and necessary step in releasing the tension between CH models and the current LHC data. The effect of soft breaking on the tuning has been investigated in Sec. 4.4. There, we have found that the tuning can generically be tamed in minimal models with the help of soft breaking. In particular, we have explored the possibility of combining the soft breaking with an additional symmetry of the strong sector, called maximal symmetry, which similarly requires the composite fermions to fill out complete $SO(5)$ representations and enhances the symmetry of the theory. These two approaches turn out to be a perfect match: maximal symmetry removes the double tuning while soft breaking raises the top partners allowing a complete natural model to emerge. In fact, top partners as heavy as 2 TeV are now compatible with the minimal 10% tuning already implied by LEP. This means that, contrary to other realizations in which the tuning is driven by the lack of signals at the LHC, our model becomes testable only now at the HL-LHC or FCC.

In Sec. 4.5 we have shown how all the ingredients that we have employed in the 4D models can be naturally realized in the context of warped extra dimensions. In particular, soft breaking corresponds to a simple modification of the conventional holographic Higgs in which the UV boundary conditions are universal for all the $SO(5)$ components of the bulk fields. On top of this, brane-localized spinors are included in order to lift the resulting full multiplet of would-be zero modes ensuring a viable phenomenology and a non-vanishing Higgs potential. This can be seen as replacing the static boundary conditions of the conventional models by dynamical fields. Moreover, the coincidence problem of having elementary vector-like fermions at the same scale as the composite states is solved in the 5D picture due to the large wave-function suppression which is in fact automatically there for the third-generation quarks.

Moving towards a detailed analysis of the 5D model, we have also shown that the top mass can be successfully reproduced in presence of partially-elementary Kaluza-Klein states. The calculation of the Higgs potential in the 5D setup and a phenomenological analysis of other possible effects connected to soft breaking are left for future work.

Chapter 5

Conclusion

The discovery of the Higgs boson at the LHC and the measurement of its properties represent a giant step in understanding the electroweak symmetry breaking. Nonetheless, the remarkable confirmation of the SM as the effective theory describing the physics below the TeV scale leaves many aspects unexplained. The hierarchy problem stands amongst them as the immediate drawback of the minimal Higgs model featuring an elementary scalar field in the theory. The other shortcomings only make the hierarchy problem worse: whenever a new high-scale mechanism is proposed, as for instance the axion solution to the strong CP problem, the stability of the weak scale is threatened and fine-tuning is automatically introduced in the theory. We can identify two possible ways to deal with this when exploring new physics beyond the SM. The first one is to leave the hierarchy problem aside by focussing on the other open questions. After all, fine-tuning is not an inconsistency of the theory, and there are more concrete issues that beg for an explanation as for instance the nature of dark matter. In fact, the hierarchy problem may not be a problem at all, or its resolution can simply rely on something that cannot be captured by effective-field-theory considerations. This is the case for solutions that involve a selection of our vacuum for anthropic or dynamical reasons in the early Universe, such as relaxation. The second approach is the exact opposite. It is based on the belief that uncovering the mechanism behind the generation of the electroweak scale will also bring along new insights for the other puzzles in the SM. As a matter of fact, natural models of electroweak symmetry breaking as supersymmetry or Higgs compositeness can also address the open questions at the cosmological level such as dark matter and matter-antimatter asymmetry. In doing so, one still needs to accept a certain fine-tuning in the theory, say 10%, that may be however a fair price for solving the hierarchy problem once and for all above a certain scale f. However, this class of models is currently under pressure due to the null signals of new physics at the LHC which is questioning naturalness as a paradigm, and the fine-tuning is in practice much worse than that motivating the search of alternative realizations.

The work presented in this thesis is inspired by the interplay of the Higgs boson with the open questions in the SM. In particular, both the approaches regarding the hierarchy problem outlined above have been discussed throughout our work. In Chapter 2, our focus has been on the axion solution to the strong CP problem and dark matter. As recently pointed out, the flavor puzzle in the SM can also be addressed in a unified framework by identifying the Peccei-Quinn symmetry as a flavor symmetry itself, namely the $U(1)$ charge characteristic of the Froggatt-Nielsen mechanism. The axion and the

flavon, which represent the main actors in this framework, belong now to the same complex scalar field (the axiflavon) such that both angular and radial components play a crucial role. This model provides a benchmark for testing axion physics by searching for rare processes in the SM such as flavor and lepton number violation. In fact, the axion couplings to matter are fixed by the observed pattern of SM fermion masses and mixings. Therefore, flavor transitions such as $d \to s$ are only suppressed by the Cabibbo angle and hence sizeable, making this axion model within the reach of future flavor experiments.

Our new element was to take into account a non-trivial interplay between the axiflavon field and the Higgs in the spirit of the first approach to the hierarchy problem mentioned above. In particular, we have investigated a UV completion of this setup based on the idea that all the scalar degrees of freedom may be unified at high energies. It is then reasonable to realize both the axion and the Higgs as pseudo-Nambu-Goldstone bosons in order to provide a rationale for their lightness with respect to the flavon, thus providing an example of (flavored)axion-Higgs unification. The hierarchy problem is not addressed in this setup as the natural size of the Higgs mass is still close to the axion scale f_a. However, the assumption of unification and the dynamical origin of electroweak symmetry breaking allow us to grasp more information about the model than simply regarding the Higgs and the axiflavon as independent fields. In fact, the requirement of reproducing the correct Higgs mass turns out to be powerful enough to constrain the scale f_a of the axion physics to be around the point in which the Higgs quartic coupling turns negative according to its running within the SM. This is interestingly close to the natural scale for the axion to be dark matter, and due to the properties of this flavored axion will be fully tested at forthcoming flavor experiments. Thus, while the origin of the Fermi scale is still unsolved, the interplay of an elementary Higgs with shortcomings of the SM other than the hierarchy problem has allowed us to trade fine-tuning for increased predictivity.

There is however another relevant implication of having an elementary Higgs in the theory: the yukawa couplings between fermions and scalars should now be regarded as fundamental interactions, as opposed to their "original" purpose of describing the effective theory of nucleons and pions. This clears the path to other paradigms for the high-energy completion of the SM such as asymptotic safety. The general idea is that the SM should be extended in such a way that the renormalization-group flow of the new theory is connected to an interacting fixed point in the UV, which in turn defines a consistent quantum field theory valid at arbitrarily short distances. Besides this being very attractive on its own, asymptotic safety can also be seen as a common framework in which the SM and quantum gravity could be married. A crucial role in uncovering this kind of UV behavior is played by the β-functions which govern the flow of the relevant interactions in the theory. Interestingly, it has been shown that yukawa couplings are a necessary ingredient for interacting fixed points to emerge in perturbation theory, thereby providing a completely independent *raison d'être* for the Higgs (and other elementary scalars) besides breaking the electroweak symmetry. Moreover, additional examples of four-dimensional asymptotically safe quantum field theories have been found by looking at systems with many degrees of freedom that are organized according to a large flavor symmetry, $SU(N_f)$, and a large color group, $SU(N_c)$, in the Veneziano limit. Driven by the search of asymptotically safe extensions of the SM, the exploration has been recently moved further to discuss the complementary case in which N_f is large but

N_c is small, such as large-N_f QED or QCD, with $N_c = 1$ and $N_c = 3$, respectively.

Motivated by the aforementioned considerations about yukawa couplings, and by the large multiplicity of fermions coupled this way in generic UV completions of the Froggatt-Nielsen mechanism, our contribution to this field was to first consider the case of a pure yukawa theory at large N_f which was still unexplored. We have bridged this gap in the literature by calculating the corresponding large-N_f β-functions in combination with abelian gauge interactions, thus providing new ingredients for the investigation of gauge-yukawa theories at high energies.

The calculation of the β-functions at large N_f involves resummation techniques that account for the appearence of the multiplicity N_f at all orders in perturbation theory. There is however another perspective on this that has opened for us another interesting line of research at the interface with condensed matter. In fact, the β-functions at large N_f turn out to be tightly connected to the Wilson-Fisher-type of fixed points for the same theory in $d = 4 - \epsilon$ dimensions that emerge as a balance between the classical and the quantum scaling of the correspoding interactions. The critical coupling is related to the dimensionality and in particular is controlled by ϵ: this is in fact reminiscent of what happens in the last step of the large-N_f resummation, when the ϵ introduced in the context of dimensional regularization is eventually replaced by the coupling. By taking advantage of the conformal (and universal) properties of the theory at the Wilson-Fisher fixed point, one can calculate the critical exponents that characterize the correspoding phase transition within the $1/N_f$ expansion. In particular, the exponent ω describing the subleading scaling of the correlation length in the vicinity of the fixed point is related to the slope of the β-function at criticality, $\beta'(g_c) = \omega$.

Although it was known that the large-N_f β-functions could be obtained from ω without having to rely on direct resummation, a systematic analysis of this connection was still missing. In this respect, we have found that explicit resummation and critical-point method are equivalent only for one-coupling models, in which the knowledge of ω is in fact enough to reconstruct the β-function. By taking advantage of this, we have extended previous studies on the possible appearance of an IR fixed point for the Gross-Neveu model in $d = 2$, and found it to be disfavoured confirming earlier results. Beyond one-coupling, this one-to-one correspondence is broken and ω can constrain only few combinations of the resummed functions entering the β-functions. We have specialized our analysis to the Gross-Neveu-Yukawa model in $d = 4$ where we have shown this explicitly by providing the full system of β-functions through explicit calculation, and using the information from ω as a non-trivial crosscheck.

The new insights that we have acquired by investigating the connection between β-functions and critical exponents have led us to a different perspective on asymptotic safety and gauge β-functions at large N_f. In fact, it turns out that the singular structure that has originally inspired the speculation of a UV fixed point for non-abelian gauge theories at large-N_f can be resummed away when employing the whole information stemming from the critical exponents. The resulting β-function features no singularity, and we thus find no hint for asymptotic safety within the $1/N_f$ expansion for this class of theories.

Besides gaining information on the structure of the β-functions from the knowledge of the critical exponents, it was eventually possible to reverse the logic and learn something about the critical exponent ω for the QED$_3$-Gross-Neveu-Yukawa model by combining all our results for the β-functions in Chapter 3. This is presented in Sec. 3.4.3 for the

first time and represents a new result with respect to the original papers on which this thesis is based. The QED_3-Gross-Neveu-Yukawa model is relevant in condensed-matter theory as it is supposed to describe quantum phase transitions among fermions on a two-dimensional lattice such as graphene. In fact, the transition of interest takes place in $d = 2 + 1$ and our result in $d = 4 - \epsilon$ is not directly applicable. However, the fixed point in $d = 3$ is strongly coupled and a direct calculation is still lacking. For this reason, there have been attempts to calculate the critical exponents in $d = 4 - \epsilon$ in standard perturbation theory by exploiting that the fixed point is weakly coupled for small ϵ, and then extrapolate to $\epsilon = 1$ with the help of other techniques. Our result provides complementary information stemming from the large-N_f perspective and may improve the quality of this extrapolation to lower dimension.

After discussing the possible implications of an elementary Higgs boson, in Chapter 4 we have started our exploration of physics beyond the SM by focussing directly on the Higgs and the electroweak symmetry breaking as the portal to new physics. The guiding principle is naturalness as a solution to the hierarchy problem based on quantum-field-theory arguments. A cornerstone solution is represented by Higgs compositeness in which the Higgs emerges as a bound state of a new strong dynamics that condenses at a scale f not much above the electroweak scale. The Higgs mass becomes insensitive to new physics thresholds as its fundamental constituents are resolved at short distances. From a phenomenological point of view, the appearence of a new strong dynamics close to the electroweak scale has plenty of implications for colliders and cosmology. The minimal model that describes the Higgs as a composite Nambu-Goldstone boson requires the new strong dynamics to have a global $SO(5)$ symmetry that is broken down to the subgroup $SO(4)$ at the condensation scale. This is the minimal coset that ensures custodial protection and contains no additional light scalars besides the Higgs. It is worth mentioning that the strong dynamics that is responsible for this group structure does not have a clear interpretation in terms of a four-dimensional quantum field theory, and the best realization of this model is by means of holography. Of course, this does not mean that the model cannot be realized in four dimensions, but just that the correspoding field theory is something completely different than those we have discovered so far. Besides solving the hierarchy problem, this model provides a very elegant means to explain the flavor puzzle in the SM as a result of renormalization-group evolution in presence of strong dynamics, which is referred to as partial compositeness. However, minimal models for a composite Higgs are under pressure due to the non-observation of new physics at the LHC, and in particular due to the lack of light colored states, called top partners, that seem to be a necessary ingredient to keep the Higgs light.

Our work in Chapter 4 was devoted to present a new idea in composite-Higgs models that keeps the appealing features of partial compositeness but removes the unwanted prediction of light top partners. This is based on the single assumption that partial compositeness respects the global symmetry of the strong sector, $SO(5)$ in the minimal models. This immediately implies that there exist new elementary fermions that complete the SM multiplets to full $SO(5)$ representations. The explicit breaking of the Higgs shift symmetry is no longer directly related to the largest yukawa coupling as in the conventional models, but rather to the "soft" vector-like masses of the new fermions that are introduced along with the SM quarks. These masses make the new states relatively heavy and account for their non-observation at the electroweak scale; at the same time, these mass terms provide the explicit breaking of $SO(5)$ that is required to gen-

erate a viable Higgs potential. In practice, the explicit breaking has been moved from the interaction between the elementary fields and the new strong sector to the structure of the elementary sector itself. In Sec. 4.3, we have shown that the soft-breaking assumption gets rid of the tight correlation between the Higgs mass and the top-partner mass allowing for a light Higgs without light partners and releasing the tension with the current results from the LHC without making the Higgs more elementary. This means that the fine-tuning in a composite-Higgs model with soft breaking can be drastically reduced with respect to conventional realizations.

The implications for the fine-tuning have been explored in Sec. 4.4, where we have investigated the combination of soft breaking with maximal symmetry, the latter being an additional global symmetry of the strong sector which borrows ideas from Twin-Higgs models such as trigonometric parity. What we have shown is that enhancing the symmetries on both the elementary side (with soft breaking) and the composite side (with maximal symmetry) leads to a model in which the tuning coincides with the minimal amount already implied by LEP, while accommodating gauge and fermion resonances above the LHC bounds. In this sense, we challenge the common lore that the so-far null signals of new physics at the LHC are disfavoring naturalness, as our natural minimal model becomes testable only now at the HL-LHC or at the FCC.

These results were derived within a four-dimensional effective-theory approach for the strong dynamics below the condensation scale. The only minor drawbacks that we could identify were the motivation for completing the SM quarks to full $SO(5)$ representations in the first place, and the "coincidence problem" of having elementary vector-like fermions in the theory with a mass comparable to the composite states. In Sec. 4.5 we have shown that both these requirements can be naturally understood from the corresponding warped 5D implementation. In fact, our complete representations are the fundamental objects one starts with in 5D as the global $SO(5)$ is there promoted to a gauge symmetry. Moreover, the implementation of soft breaking simply amounts to replace the static and specific boundary conditions of the conventional realizations with new boundary conditions that are universal and dynamical due the presence of UV-localized (and hence elementary) spinors. The bare masses of these spinors are not yet to be identified with the vector-like masses that we have considered in the phenomenological models. Indeed, as these fields are stuck on the UV brane whose position corresponds to $R^{-1} \sim M_{\rm Pl}$, their bare mass is also expected to be of order $M_{\rm Pl}$. Nevertheless, we have shown that the UV-localized spinors do not decouple from the low-energy theory even in presence of a Planckian mass as partially-elementary TeV-scale states can arise due to the wave-function suppression that is automatically at work for third-generation quarks. This means that the 5D implementation can straightforwardly reproduce all the main features of our four-dimensional model thus corroborating this new way of realizing a natural composite Higgs in the light of the LHC data.

Chapter 6

Acknowledgments

I want to start by thanking my supervisor Dr. Florian Goertz. First of all, I would like to express my graditude again for accepting me as part of your group at the MPIK. After our first skypes I was sure that this was a great opportunity for me, not only for the absolute matching of scientific interest, but also for your kindness. This positive feeling has not changed one bit during my years in Heidelberg. Thanks to you I had the possibility to learn lots of new topics and share them with other researchers around the world. I would also like to thank you for the way you have lead your group: the reassuring feeling that I have always experienced in relation to you as supervisor and with the other members of the group has greatly helped in setting the right stage to carry out our research. Thanks for all the support and encouragement that I have received during these years, including the postdoc applications and while completing this thesis.

The second person I want to thank is Dr. Tommi Alanne. Your role has gone far beyond the formal supervision: since my first days in the new group I have felt that I could rely on you for everything than spans from physics to daily life. Listing the reasons for which I am deeply in debt with you Tommi would probably take an entire section of this thesis. Let me here just express my gratitude for the precious collaboration regarding the papers that we wrote together and those that we didn't, the careful reading of the present manuscript, the relentless support during postdoc applications and in general any time that I had an issue of any kind. I am glad that we could meet.

My gratitude also goes to Prof. Dr. Dr. h.c. Manfred Lindner for the great expertise that he constantly shares with the members of his division at the MPIK, and for the efforts that make it possible to conduct research in such a stimulating environment. I would like to thank Prof. Dr. Csaba Csáki for the hospitality that he granted me during my visit at Cornell University: even though for just few weeks, that was a great opportunity to make contact with new interesting ideas and initiate a project that now constitutes an important part of this thesis. In addition, I would like to thank Prof. Dr. John Gracey for the useful discussions on the large-N_f ideas. I also want to thank Prof. Dr. Jörg Jäckel, Prof. Dr. André Schöning, Prof. Dr. Jörg Evers for agreeing on being part of my PhD committee: thank you very much for your time.

An important thank you goes to Anja Berneiser and Britta Schwarz for the valuable help with the administration at the MPIK, and also the HGSFP for the support and the opportunities offered to the graduate students.

I am very happy to thank all the other collaborators that shared their expertise with me during my PhD: Dr. Nicola Andrea Dondi, Dr. Kai Schmitz, Dr. Vedran Brdar. It

was fun to work with all of you! I would also like to thank Dr. Anders Ellen Thomsen and Dr. Ofri Telem for the valuable discussions that have played an important role in finalizing the corresponding projects. A special thanks goes to Julian Bollig for the nice collaboration from which this work has benefited.

Doing a PhD is an experience that certainly leaves an important mark in your life but it becomes really valuable if you have the possibility to share your time with great people: one of them is Valentin Tenorth. Besides the holy coffee (and its hypster variant), *pallo* and so on and so forth [1], I want to thank you for the empathy that we have soon developed and for the feeling that we could always back each other up, no matter what. Without any doubt this has made a difference in the way I will remember my time in Heidelberg. I hope having me around was not so annoying, even though I never stop talking. Also, I want to thank your for the countless times in which you patiently helped me with some form/table to fill and for all the German translations, including the abstract of this thesis. My Italian lessons were probably not as valuable, but at least now you can use some *non capisco*.

I also want to thank all the people that I had the pleasure to meet during these years. Amongst the MPIK guys, I want to explicitly mention Dr. Lukáš Gráf for your kindness and friendship, Karla Tame Narvaez and Dr. Ulises J. Saldaña-Salazar for always being nice with me, and Andreas Bally for pretty challenging table-soccer games with your weird rules that add tension (and indeed they do). I also want to acknowledge the ping-pong club and the table-soccer crowd for the good time that I have spent with them. Moreover, I want to thank all the friends that I have met during winter and summer schools: forming these bonds constitutes the biggest success of these events. In particular, I want to thank Cristina Mondino and Gabriele Rigo whose hospitality during my trip in the USA I won't forget. I also want to thank Davide Rindori, a true master of LaTeX and beauty in general, for creating the cover page of this thesis.

A distinguished thank you goes to Janet: your patience in relieving my heavy heart and the happiness that we have shared together mean a lot to me.

Finally, I want to thank my parents for making my whole academic path possible: they did it with their unconditional love, especially now that I am far and they cannot see me as often as before. My eternal gratitude goes to my grandparents as well: they deserve credit for any good thing that I will ever do.

[1] Tommi also involved.

Appendix A

$SO(5)$ generators and spinorial representation

We provide here the explicit form of the $SO(5)$ generators in the fundamental representation, **5**, and in the spinorial, **4**, as well as the expression for the Γ^α matrices that connect them. The convention we are using follows closely Ref. [152].

In general, the $SO(5)$ generators can be divided in two sets: the first set consists of six elements, $T^a_{L,R}$ with $a = 1, 2, 3$, that generate the $SO(4) \simeq SU(2)_L \times SU(2)_R$ subgroup, whereas the second set contains four elements, $T^{\hat{a}}$, $\hat{a} = 1, \ldots, 4$, which do not form a subgroup and coincide with the broken generators of the $SO(5)/SO(4)$ coset. We will use the same symbols, $T^a_{L,R}$ and $T^{\hat{a}}$, for both representations, as it is always clear from the context which representation they refer to.

For the fundamental **5**, the generators are 5×5 matrices. The generators defining the $SU(2)_L \times SU(2)_R$ subgroup are given by:

$$\left(T^a_{L,R}\right)_{ij} = -\frac{i}{2}\left[\frac{1}{2}\epsilon^{abc}(\delta^b_i\delta^c_j - \delta^c_i\delta^b_j) \pm (\delta^a_i\delta^4_j - \delta^a_j\delta^4_i)\right], \quad i,j = 1,\ldots,5, \tag{A.1}$$

whereas the broken generators read

$$T^{\hat{a}}_{ij} = -\frac{i}{\sqrt{2}}\left[\delta^{\hat{a}}_i\delta^5_j - \delta^{\hat{a}}_j\delta^5_i\right], \quad i,j = 1,\ldots,5. \tag{A.2}$$

As for the spinorial **4**, the generators are 4×4 matrices. They are given by

$$T^a_L = \frac{1}{2}\begin{pmatrix}\sigma^a & 0\\ 0 & 0\end{pmatrix}, \quad T^a_R = \frac{1}{2}\begin{pmatrix}0 & 0\\ 0 & \sigma^a\end{pmatrix}, \tag{A.3}$$

and

$$T^{\hat{a}} = \frac{i}{2\sqrt{2}}\begin{pmatrix}0 & \sigma^{\hat{a}}\\ -\sigma^{\hat{a}\,\dagger} & 0\end{pmatrix}, \quad \sigma^{\hat{a}} = (\sigma^i, -i\,\mathbb{1}_{2\times2}), \tag{A.4}$$

where σ^i are the Pauli matrices.

The **5** and the **4** can be connected through a set of Γ^α matrices, $\alpha = 1, \ldots, 5$, that are given by

$$\Gamma^{\hat{a}} = \begin{pmatrix}0 & \sigma^{\hat{a}}\\ \sigma^{\hat{a}\,\dagger} & 0\end{pmatrix}, \quad \Gamma^5 = \begin{pmatrix}\mathbb{1}_{2\times2} & 0\\ 0 & -\mathbb{1}_{2\times2}\end{pmatrix}, \tag{A.5}$$

where $\hat{a} = 1, \ldots, 4$ and $\sigma^{\hat{a}}$ are those in (A.4). The properties of the Γ^{α} are such that given two multiplets, ξ_j and ξ_{j+1}, transforming as two spinorial representations **4**, the following combination

$$\bar{\xi}_{j+1}\Gamma^{\alpha}\xi_j \tag{A.6}$$

transforms as the fundamental **5**. Thus, the "current" in (A.6) can be coupled to a field $\Sigma_{\alpha} \sim \mathbf{5}$ in a $SO(5)$-invariant manner as in (2.81). This is analogous to what happens for the Lorentz group and spin-1/2 representations, where $\bar{\psi}\gamma^{\mu}\psi$ can in fact couple to a Lorentz vector, A_{μ}.

Appendix B

Loop integrals and large-N_f perturbative results

In this Appendix we present supplementary material related to the β-functions at large N_f discussed in Chapter 3.

B.1 Loop integrals

The basic object for our calculations is the one-loop function $G(n_1, n_2)$ related to the following momentum integral:

$$\int \frac{d^d k}{(2\pi)^d} \frac{1}{D_1^{n_1} D_2^{n_2}} = i \frac{1}{(4\pi)^{d/2}} (-p^2)^{d/2-n_1-n_2} (-1)^{n_1+n_2} G(n_1, n_2), \tag{B.1}$$

where $D_1 = (k+p)^2$ and $D_2 = k^2$, and is explicitly given by [203]:

$$G(n_1, n_2) = \frac{\Gamma(-d/2 + n_1 + n_2)\Gamma(d/2 - n_1)\Gamma(d/2 - n_2)}{\Gamma(n_1)\Gamma(n_2)\Gamma(d - n_1 - n_2)}. \tag{B.2}$$

This function is particularly suitable for our purpose because it is valid for arbitrary values of n_1 and n_2, including non-integer values that often arise when dealing with large-N_f resummation. In fact, we have seen that the basic effect of having a bubble chain is to replace the simple propagtor $1/q^2$ to a more complicated power as in (3.3).

The calculation of the pure yukawa β-function carried out in Sec. 3.2 has required the calculation of the three renormalization constants related to vertex correction, fermion self-energy and scalar self-enegy. The loop integrals correspoding to the vertex correction and fermion self-energy correspond to basic one-loop topologies and only involve the function $G(n_1, n_2)$ in (B.2); their explicit expression have been already evaluated in (3.32) and (3.41).

The case of the scalar self-energy is however more complicated, as the basic topologies are two-loop diagrams and one needs to go beyond (B.2). The correspoding n-loop

contribution, indicated by $S_K^{(n)}$ is given by the following integral ($n \geq 2$):

$$\begin{aligned} p^2 S_K^{(n)}(p^2,\epsilon) = &-(4\pi^2)^2(-1)^n \left(\frac{1}{(4\pi)^{d/2-2}}\frac{G(1,1)}{2}\right)^{n-2}(-1)^\alpha \int \frac{d^dk_1}{(2\pi)^d}\int\frac{d^dk_2}{(2\pi)^d} \\ &\left\{\frac{6}{(p+k_1)^2k_2^2((k_1-k_2)^2)^{1-\alpha}} - \frac{2}{k_1^2(p+k_1)^2k_2^2((k_1-k_2)^2)^{-\alpha}}\right. \\ &-\frac{2p^2}{k_1^2(p+k_1)^2k_2^2((k_1-k_2)^2)^{1-\alpha}} + \frac{2p^2}{k_1^4(p+k_1)^2k_2^2((k_1-k_2)^2)^{-\alpha}} \\ &\left.-\frac{2p^2}{k_1^2(k_1+p)^2(k_2+p)^2k_2^2((k_1-k_2)^2)^{-\alpha}}\right\}, \end{aligned} \tag{B.3}$$

where $\alpha = (n-2)(d/2-2) = -(n-2)\epsilon/2$. Evaluating (B.3) requires two-loop integrals which can be performed according to the formula in Ref. [203]:

$$\int \frac{d^dk_1}{(2\pi)^d}\int\frac{d^dk_2}{(2\pi)^d}\frac{1}{D_1^{n_1}D_2^{n_2}D_3^{n_3}D_4^{n_4}D_5^{n_5}} = (-1)^{1+\sum n_i}\frac{\pi^d(-p^2)^{d-\sum n_i}}{(2\pi)^{2d}}G(n_1,n_2,n_3,n_4,n_5), \tag{B.4}$$

where $D_1 = (k_1+p)^2$, $D_2 = (k_2+p)^2$, $D_3 = k_1^2$, $D_4 = k_2^2$, $D_5 = (k_1-k_2)^2$. The functions $G(n_1,n_2,n_3,n_4,n_5)$ are symmetric with respect to the index exchanges $(1 \leftrightarrow 2, 3 \leftrightarrow 4)$ and $(1 \leftrightarrow 3, 2 \leftrightarrow 4)$. Moreover, they reduce to a product of $G(n_1,n_2)$ if at least one of the entries is zero:

$$G(n_1,n_2,n_3,n_4,0) = G(n_1,n_3)G(n_2,n_4), \tag{B.5}$$

$$G(0,n_2,n_3,n_4,n_5) = G(n_3,n_5)G(n_2,n_3+n_4+n_5-d/2). \tag{B.6}$$

It turns out that the first four integrals in (B.3) can always be written in terms of $G(n_1,n_2)$ making use of (B.5) and (B.6). However, the last integral in (B.3) involves $G(1,1,1,1,(n-2)\epsilon/2)$ and, for $n>2$, its expression can be obtained in terms of hypergeometric functions ${}_3F_2$ by means of the Gegenbauer technique [204]. We have evaluated the function $G(1,1,1,1,(n-2)\epsilon/2)$ recursively according to Eqs (2.19) and (2.21) in Ref. [203].

The other loop integrals that we have encountered for the calculations in Chapter 3 can be carried out with the help of $G(n_1,n_2)$ and $G(n_1,n_2,n_3,n_4,n_5)$, as the basic topologies before the dressing of the gauge or scalar propagators with bubble chains are either one-loop or two-loop. The only three-loop basic topology we have encountered is the one in Fig. 3.13 for the Gross-Neveu-Yukawa model that can however be splitted as two distinct two-loop and one-loop diagrams.

All the formulas for the loop integrals that one encounters in the large-N_f renormalization of the pure yukawa theory are given explicitly in (3.32), (3.41) and (B.3). The analogous formulas for the gauge contributions in Sec. 3.3 and the ones for the Gross-Neveu-Yukawa model in Sec. 3.4.2 are too cumbersome to justify their inclusion in this thesis.

B.2 Perturbative results

We present here the expansions of the $\mathcal{O}(1/N_f)$ β-functions that we have calculated in a closed form in Chapter 3 to make contact with standard perturbation theory, thereby checking the validity of our results while predicting new coefficients.

B.2.1 Gauge-yukawa

Let us start with the couple system of β-functions corresponding to the gauge-yukawa theory discussed in Sec. 3.3.2. Expanding the β-function, for the rescaled yukawa coupling, β_K in (3.70), and for the rescaled gauged coupling, β_E in (3.71), around $K=0$ and $E=0$ we find:

$$\begin{aligned}\beta_E =&\frac{2}{3}E^2+\frac{1}{2N_f}E^3-\frac{1}{4N_f}E^2K-\frac{11}{72N_f}E^4+\frac{7}{32N_f}E^2K^2\\&-\frac{77}{1944N_f}E^5-\frac{3}{64N_f}E^2K^3\\&\underbrace{+\frac{107+144\zeta_3}{15552N_f}E^6-\frac{9+16\zeta_3}{1024N_f}E^2K^4}_{\text{five-loop prediction}}+\dots\end{aligned}\tag{B.7}$$

$$\begin{aligned}\beta_K =&\left(1+\frac{3}{2N_f}\right)K^2-\frac{3}{N_f}EK-\frac{3}{2N_f}K^3+\frac{5}{4N_f}EK^2+\frac{5}{6N_f}E^2K\\&+\frac{7}{16N_f}K^4-\frac{1}{2N_f}E^2K^2+\frac{35}{108N_f}E^3K\\&+\frac{11}{96N_f}K^5+\frac{1}{3888N_f}\left(-1625+1296\zeta_3\right)E^3K^2+\frac{1}{648N_f}(83-144\zeta_3)E^4K\\&\underbrace{+\frac{19-48\zeta_3}{512N_f}K^6-\frac{8125-144\pi^4+3600\zeta_3}{77760N_f}K^2E^4+\frac{325-8\pi^4+400\zeta_3}{6480N_f}KE^5}_{\text{five-loop prediction}}+\dots\end{aligned}\tag{B.8}$$

We have checked that our expansions agree with the four-loop results [97, 110–113] in the leading order in N_f.

B.2.2 Gross-Neveu-Yukawa

We provide here the expansion of the functions $\varphi^{(1)}_{1-4}$ appearing in the $\mathcal{O}(1/N_f)$ system of β-functions, (3.118) and (3.119), of the Gross-Neveu-Yukawa model analyzed in Sec. 3.4.2. We will therefore check against the known perturbative results and predict the $\mathcal{O}(1/N_f)$ terms that would appear up to six-loop order.

First, for the yukawa β-function in (3.118), we have

$$\begin{aligned}y^2\varphi^{(1)}_1(yN_f) =&-6y^3N_f+\frac{7}{2}y^4N_f^2+\frac{11}{6}y^5N_f^3\\&+\underbrace{\left(\frac{19}{16}-3\zeta_3\right)}_{\text{five-loop prediction}}y^6N_f^4+\underbrace{\left(\frac{7}{8}+\frac{14}{5}\zeta_3-\frac{18}{5}\zeta_4\right)}_{\text{six-loop prediction}}y^7N_f^5+\dots\end{aligned}\tag{B.9}$$

As for the quartic-coupling β-function, (3.119), one can predict the coefficients based on $\varphi_2^{(1)}$, $\varphi_3^{(1)}$ and $\varphi_4^{(1)}$. Their contribution to the β-function is:

$$y^2\varphi_2^{(1)}(yN_f) = 4y^3N_f - \frac{157}{8}y^4N_f^2 + \left(42\zeta_3 - \frac{193}{6}\right)y^5N_f^3 + \underbrace{\left(-\frac{2623}{64} - \frac{157}{4}\zeta_3 + 90\zeta_4\right)}_{\text{five-loop prediction}}y^6N_f^4 + \underbrace{\left(-\frac{3993}{80} - \frac{491}{5}\zeta_3 - \frac{426}{5}\zeta_4 + 234\zeta_5\right)}_{\text{six-loop prediction}}y^7N_f^5 + \dots \tag{B.10}$$

$$\lambda^2\varphi_3^{(1)}(yN_f) = -72y\lambda^2N_f - 108y^2\lambda^2N_f^2 + 144(2\zeta_3 - 1)\lambda^2y^3N_f^3 \underbrace{-180(1 + 2\zeta_3 - 3\zeta_4)}_{\text{five-loop prediction}}\lambda^2y^4N_f^4 \underbrace{-216(1 + 2\zeta_3 + 3\zeta_4 - 6\zeta_5)}_{\text{six-loop prediction}}\lambda^2y^5N_f^5 + \dots \tag{B.11}$$

$$y\lambda\varphi_4^{(1)}(yN_f) = 7\lambda y^2N_f + \frac{217}{2}\lambda y^3N_f^2 + \left(\frac{1685}{12} - 228\zeta_3\right)\lambda y^4N_f^3 + \underbrace{\left(\frac{699}{4} + 248\zeta_3 - 450\zeta_4\right)}_{\text{five-loop prediction}}\lambda y^5N_f^4 + \underbrace{\left(\frac{3359}{16} + \frac{2123}{5}\zeta_3 + \frac{2409}{5}\zeta_4 - 1116\zeta_5\right)}_{\text{six-loop prediction}}\lambda y^6N_f^5 + \dots \tag{B.12}$$

We have checked that the expansions up to $\mathcal{O}(N_f^3)$ agree with the known leading-N_f four-loop perturbative result [108]. The $\mathcal{O}(N_f^4)$ and $\mathcal{O}(N_f^5)$ terms are the leading-N_f prediction for the five- and six-loop terms, respectively.

Appendix C

Additional material for a soft composite Higgs

In this Appendix we collect additional material that is relevant for the discussion in Chapter 4.

C.1 Symmetric coset and linear Goldstone matrix

In Sec. 4.4 we have used the fact that $SO(5)/SO(4)$ is a symmetric coset and defined a Goldstone matrix, Σ, with linear transformation properties under $g \in SO(5)$, (4.66). We detail here what this actually means and how Σ is related to the "standard" Goldstone matrix, U, in (4.1).

As mentioned, the first ingredient is the presence of a symmetry coset G/H. Denoting by T^A the generators of the G algebra, where $A = a, \hat{a}$ for the unbroken/broken generators after the $G \to H$ spontaneous breaking, one generically has

$$[T^a, T^b] = \imath f_c^{ab} T^c, \quad [T^a, T^{\hat{a}}] = \imath f_{\hat{c}}^{a\hat{b}} T^{\hat{c}} \tag{C.1}$$

and

$$[T^{\hat{a}}, T^{\hat{b}}] = \imath f_c^{\hat{a}b} T^c + \imath f_{\hat{c}}^{\hat{a}\hat{b}} T^{\hat{c}}. \tag{C.2}$$

The first two equalities are general and follow from the property of H being a subgroup. Conversely, (C.2) takes a special form for symmetric cosets, which are defined by the property

$$f_{\hat{c}}^{\hat{a}\hat{b}} \equiv 0. \tag{C.3}$$

It follows that $[T^{\hat{a}}, T^{\hat{b}}] \sim T^c$, and this allows for the presence of a discrete symmetry V acting on the generators as

$$T^a \to V T^a V^\dagger = T^a, \quad T^{\hat{a}} \to V T^{\hat{a}} V^\dagger = -T^{\hat{a}}. \tag{C.4}$$

Notice that the transformations in (C.4) leave (C.2) invariant only for symmetric cosets.

As mentioned above (4.66), the existence of V allows to define a linear representation for the standard Goldstone matrix in (4.1). The first step is to introduce a new matrix $\tilde{U}$ as

$$\tilde{U} = VUV = \exp\left(\imath \frac{\sqrt{2}}{f_\pi} h^{\hat{a}} V T^{\hat{a}} V\right) = \exp\left(-\imath \frac{\sqrt{2}}{f_\pi} h^{\hat{a}} T^{\hat{a}}\right) = U^\dagger. \tag{C.5}$$

Under $g \in SO(5)$, the matrix $\tilde{U}$ transforms as

$$\tilde{U} \to V\,(gUh^\dagger)\,V = VgV(VUV)Vh^\dagger V = VgV\tilde{U}h^\dagger, \tag{C.6}$$

where we have used that $V^2 = \mathbb{1}$, and for the last equality we have used that $h \in H$ and thus $Vh^\dagger V = h^\dagger$.

With $\tilde{U}$ at hand, one can define the new Goldstone matrix Σ as

$$\Sigma = U\tilde{U}^\dagger V = U^2 V. \tag{C.7}$$

Under a transformation $g \in G$, one finds:

$$\boxed{\Sigma \to (gUh^\dagger)(h\,\tilde{U}^\dagger V g^\dagger V)V = g(U\,\tilde{U}^\dagger V)g^\dagger = g\Sigma g^\dagger,} \tag{C.8}$$

namely that Σ transforms linearly with $g \in G$. In our basis for the $SO(5)$ generators, one has that $V = \mathrm{diag}\,(1,1,1,1,-1)$ and in the unitary gauge Σ is given by

$$\Sigma = \begin{pmatrix} \mathbb{1}_{3\times 3} & 0 & 0 \\ 0 & \cos(2h/f) & -\sin(2h/f) \\ 0 & -\sin(2h/f) & -\cos(2h/f) \end{pmatrix} \tag{C.9}$$

C.2 Trigonometric parity and soft breaking

In this section we discuss the fate of trigonometric parity in the soft-breaking setup defined by the Lagrangian in (4.93).

To this end, we recall that the trigonometric parity $\sin(h/f) \leftrightarrow -\cos(h/f)$ can be defined as the following discrete symmetry [184]:

$$\Sigma \to V\,\Sigma\,P', \quad \Psi_L \to P\Psi_L, \quad \Psi_R \to VPV\,\Psi_R, \quad \psi_L \to V\psi_L, \quad \psi_R \to P'\,\psi_R, \tag{C.10}$$

where $P = \mathrm{diag}\,(1,1,1,\sigma_1)$, $P' = \mathrm{diag}\,(1,1,1,-\sigma_3)$.

The transformation (C.10) would be a symmetry of the Lagrangian (4.93) if $M_{L,R}$ were to transform as

$$M_R \to V\,M_R, \quad M_L \to P'\,M_L \;\Rightarrow\; \Gamma_R \to V\,\Gamma_R\,V, \quad \Gamma_L \to P'\,\Gamma_L P', \tag{C.11}$$

where $\Gamma_{L,R}$ are defined in (4.96).

Whether trigonometric parity is eventually preserved or not depends on the spurion vacuum expectation values, namely on their explicit form in (4.96). The parity-conserving vacuum is found by solving

$$\Gamma_R = V\,\Gamma_R\,V \quad \text{and} \quad \Gamma_L = P'\,\Gamma_L\,P'. \tag{C.12}$$

The first condition is always trivially satisfied; while the second one implies

$$(m_v - m_{w_2})(m_v + m_{w_2}) = 0. \tag{C.13}$$

Moreover, we notice that there is another way to implement trigonometric parity in addition to (C.10), namely interchanging the left and right chiralities in (C.10):

$$\Sigma \to V\,\Sigma\,P', \quad \Psi_L \to VPV\,\Psi_L, \quad \Psi_R \to P\Psi_R, \quad \psi_L \to P'\psi_L, \quad \psi_R \to V\,\psi_R, \tag{C.14}$$

Similar arguments then imply the following spurion transformations:

$$\Gamma_R \to P' \Gamma_R P', \quad \Gamma_L \to V \Gamma_L V, \tag{C.15}$$

so that another parity-preserving vacuum exists if

$$\Gamma_R = P' \Gamma_R P' \quad \text{and} \quad \Gamma_L = V \Gamma_L V. \tag{C.16}$$

The second condition is satisfied identically, whereas the first one requires:

$$m_{w_1}^2 = 0. \tag{C.17}$$

Combining (C.13) and (C.17), we conclude that trigonometric parity is a true symmetry of the theory if and only if

$$\boxed{(m_v^2 - m_{w_2}^2) m_{w_1}^2 = 0.} \tag{C.18}$$

Thus, we see that $\xi = 0.5$ can be avoided in our setup within the fermion sector besides very particular values of the fermion masses. Moreover, this way of breaking trigonometric parity still ensures that double tuning is avoided, see discussion below (4.100).

C.3 Warped Sine and Cosine

We give here the explicit form of the warped sine and cosine used in the warped 5D implementation in Sec. 4.5. Let us first consider the following differential equation

$$y'' - \frac{4}{z} y' + \left(m^2 - \frac{c^2 + c - 6}{z^2} \right) y = 0 \tag{C.19}$$

and look for two solutions, $y_1(z)$ and $y_2(z)$, that satisfy the following boundary conditions at $z = R$:

$$y_1(R) = 1, \quad y_2(R) = 0. \tag{C.20}$$

These two solutions are in fact given in terms of the warped sine and cosine as

$$y_1(z) = \left(\frac{R}{z} \right)^{c-2} C(z, m, c), \quad y_2(z) = \left(\frac{R}{z} \right)^{c-2} S(z, m, c), \tag{C.21}$$

where (see also Ref. [170])

$$\begin{aligned} S(z,m,c) &= \frac{\pi}{2} mR \left(\frac{z}{R} \right)^{1/2+c} \left[J_{1/2+c}(mR) Y_{1/2+c}(mz) - J_{1/2+c}(mz) Y_{1/2+c}(mR) \right], \\ C(z,m,c) &= \frac{\pi mR}{2 \cos(c\pi)} \left(\frac{z}{R} \right)^{1/2+c} \left[J_{-1/2+c}(mR) J_{-1/2-c}(mz) + J_{1/2+c}(mz) J_{1/2-c}(mR) \right]. \end{aligned} \tag{C.22}$$

The funcions $J_\nu(x)$ and $Y_\nu(x)$ are the Bessel functions of the first and second kind, respectively. The S and C functios satisfy the basic properties at $z = R$

$$C(R, m, c) \equiv 1, \quad S(R, m, c) \equiv 0, \tag{C.23}$$

and also

$$C'(R, m, c) = 0, \quad S'(R, m, c) = m, \tag{C.24}$$

where the derivative has been taken with respect to the first argument, z.

References

[I] T. Alanne, S. Blasi and F. Goertz, *"Common source for scalars: Flavored axion-Higgs unification,"* Phys. Rev. D **99** (2019) no.1, 015028, [arXiv:1807.10156]

[II] T. Alanne and S. Blasi, *"The β-function for Yukawa theory at large N_f,"* JHEP **08** (2018), 081, [arXiv:1806.06954]

[III] T. Alanne and S. Blasi, *"Abelian gauge-Yukawa β-functions at large N_f,"* Phys. Rev. D **98** (2018) no.11, 116004, [arXiv:1808.03252]

[IV] T. Alanne, S. Blasi and N. A. Dondi, *"Bubble-resummation and critical-point methods for β-functions at large N,"* Eur. Phys. J. C **79** (2019) no.8, 689, [arXiv:1904.05751]

[V] T. Alanne, S. Blasi and N. A. Dondi, *"Critical look at β-function singularities at large N,"* Phys. Rev. Lett. **123** (2019) no.13, 131602, [arXiv:1905.08709]

[VI] S. Blasi and F. Goertz, *"Softened symmetry breaking in Composite Higgs models,"* Phys. Rev. Lett. **123** (2019) no.22, 221801, [arXiv:1903.06146]

[VII] S. Blasi, C. Csaki and F. Goertz, *"A natural Composite Higgs via universal boundary conditions,"* [arXiv:2004.06120]

[VIII] S. Blasi, V. Brdar and K. Schmitz, *"Fingerprint of low-scale leptogenesis in the primordial gravitational-wave spectrum,"* [arXiv:2004.02889]

[1] H. Georgi and S. L. Glashow, *Unity of all elementary-particle forces*, *Phys. Rev. Lett.* **32** (Feb, 1974) 438–441.

[2] J. C. Pati and A. Salam, *Lepton number as the fourth "color"*, *Phys. Rev. D* **10** (Jul, 1974) 275–289.

[3] R. N. Mohapatra and R. E. Marshak, *Local B-L symmetry of electroweak interactions, majorana neutrinos, and neutron oscillations*, *Phys. Rev. Lett.* **44** (May, 1980) 1316–1319.

[4] S. Weinberg, *Baryon- and Lepton- nonconserving processes*, *Phys. Rev. Lett.* **43** (Nov, 1979) 1566–1570.

[5] R. Barbieri, *Electroweak theory after the first Large Hadron Collider phase*, *Phys. Scripta T* **158** (2013) 014006, [arXiv:1309.3473].

[6] G. Isidori, G. Ridolfi, and A. Strumia, *On the metastability of the standard model vacuum*, *Nucl. Phys.* **B609** (2001) 387–409, [hep-ph/0104016].

[7] G. D'Ambrosio, G. Giudice, G. Isidori, and A. Strumia, *Minimal flavor violation: An Effective field theory approach*, *Nucl. Phys. B* **645** (2002) 155–187, [hep-ph/0207036].

[8] **Planck** Collaboration, N. Aghanim et al., *Planck 2018 results. VI. Cosmological parameters*, arXiv:1807.06209.

[9] H. Velten, R. vom Marttens, and W. Zimdahl, *Aspects of the cosmological "coincidence problem"*, *Eur. Phys. J. C* **74** (2014), no. 11 3160, [arXiv:1410.2509].

[10] P. W. Graham, D. E. Kaplan, and S. Rajendran, *Cosmological Relaxation of the Electroweak Scale*, *Phys. Rev. Lett.* **115** (2015), no. 22 221801, [arXiv:1504.07551].

[11] R. D. Peccei and H. R. Quinn, *CP conservation in the presence of pseudoparticles*, *Phys. Rev. Lett.* **38** (Jun, 1977) 1440–1443.

[12] R. D. Peccei and H. R. Quinn, *Constraints imposed by CP conservation in the presence of pseudoparticles*, *Phys. Rev. D* **16** (Sep, 1977) 1791–1797.

[13] **XENON** Collaboration, E. Aprile et al., *First Dark Matter Search Results from the XENON1T Experiment*, *Phys. Rev. Lett.* **119** (2017), no. 18 181301, [arXiv:1705.06655].

[14] C. D. Froggatt and H. B. Nielsen, *Hierarchy of Quark Masses, Cabibbo Angles and CP Violation*, *Nucl. Phys.* **B147** (1979) 277–298.

[15] L. Calibbi, F. Goertz, D. Redigolo, R. Ziegler, and J. Zupan, *Minimal axion model from flavor*, *Phys. Rev.* **D95** (2017), no. 9 095009, [arXiv:1612.08040].

[16] Y. Ema, K. Hamaguchi, T. Moroi, and K. Nakayama, *Flaxion: a minimal extension to solve puzzles in the standard model*, *JHEP* **01** (2017) 096, [arXiv:1612.05492].

[17] S. Weinberg. In Hawking, S.W., Israel, W.: General Relativity, 790-831 (Cambridge University Press, Cambridge, 1980).

[18] J. Braun, H. Gies, and D. D. Scherer, *Asymptotic safety: a simple example*, *Phys. Rev. D* **83** (2011) 085012, [arXiv:1011.1456].

[19] A. Eichhorn, *An asymptotically safe guide to quantum gravity and matter*, *Front. Astron. Space Sci.* **5** (2019) 47, [arXiv:1810.07615].

[20] A. D. Bond and D. F. Litim, *Theorems for Asymptotic Safety of Gauge Theories*, *Eur. Phys. J.* **C77** (2017), no. 6 429, [arXiv:1608.00519]. [Erratum: Eur. Phys. J.C77,no.8,525(2017)].

[21] G. M. Pelaggi, F. Sannino, A. Strumia, and E. Vigiani, *Naturalness of asymptotically safe Higgs*, *Front. in Phys.* **5** (2017) 49, [arXiv:1701.01453].

[22] D. F. Litim and F. Sannino, *Asymptotic safety guaranteed*, *JHEP* **12** (2014) 178, [arXiv:1406.2337].

[23] D. B. Kaplan and H. Georgi, *SU(2) x U(1) Breaking by Vacuum Misalignment*, *Phys. Lett.* **136B** (1984) 183–186.

[24] D. B. Kaplan, H. Georgi, and S. Dimopoulos, *Composite Higgs Scalars*, *Phys. Lett.* **136B** (1984) 187–190.

[25] M. J. Dugan, H. Georgi, and D. B. Kaplan, *Anatomy of a Composite Higgs Model*, *Nucl. Phys.* **B254** (1985) 299–326.

[26] S. Bruggisser, B. Von Harling, O. Matsedonskyi, and G. Servant, *Electroweak Phase Transition and Baryogenesis in Composite Higgs Models*, *JHEP* **12** (2018) 099, [arXiv:1804.07314].

[27] M. Redi and A. Strumia, *Axion-Higgs Unification*, *JHEP* **11** (2012) 103, [arXiv:1208.6013].

[28] I. Brivio, M. B. Gavela, S. Pascoli, R. del Rey, and S. Saa, *The Axion and the Goldstone Higgs*, arXiv:1710.07715.

[29] C. G. Callan, Jr., R. F. Dashen, and D. J. Gross, *The Structure of the Gauge Theory Vacuum*, *Phys. Lett.* **63B** (1976) 334–340.

[30] R. D. Peccei, *QCD, strong CP and axions*, *J. Korean Phys. Soc.* **29** (1996) S199–S208, [hep-ph/9606475].

[31] D. J. E. Marsh, *Axion Cosmology*, *Phys. Rept.* **643** (2016) 1–79, [arXiv:1510.07633].

[32] C. G. Callan, R. Dashen, and D. J. Gross, *Toward a theory of the strong interactions*, *Phys. Rev. D* **17** (May, 1978) 2717–2763.

[33] C. A. Baker, D. D. Doyle, P. Geltenbort, K. Green, M. G. D. van der Grinten, P. G. Harris, P. Iaydjiev, S. N. Ivanov, D. J. R. May, J. M. Pendlebury, J. D. Richardson, D. Shiers, and K. F. Smith, *Improved experimental limit on the electric dipole moment of the neutron*, *Phys. Rev. Lett.* **97** (Sep, 2006) 131801.

[34] M. Kobayashi and T. Maskawa, *CP Violation in the Renormalizable Theory of Weak Interaction*, *Prog. Theor. Phys.* **49** (1973) 652–657.

[35] Y. H. Ahn, H.-Y. Cheng, and S. Oh, *Wolfenstein Parametrization at Higher Order: Seeming Discrepancies and Their Resolution*, *Phys. Lett.* **B703** (2011) 571–575, [arXiv:1106.0935].

[36] M. Dine, *TASI lectures on the strong CP problem*, in *Flavor physics for the millennium. TASI 2000*, pp. 349–369, 2000. hep-ph/0011376.

[37] P. Fileviez Perez and H. H. Patel, *The Electroweak Vacuum Angle*, *Phys. Lett.* **B732** (2014) 241–243, [arXiv:1402.6340].

[38] **Fermilab Lattice, MILC, TUMQCD** Collaboration, A. Bazavov et al., *Up-, down-, strange-, charm-, and bottom-quark masses from four-flavor lattice QCD*, *Phys. Rev.* **D98** (2018), no. 5 054517, [arXiv:1802.04248].

[39] W. A. Bardeen, *Instanton Triggered Chiral Symmetry Breaking, the U(1) Problem and a Possible Solution to the Strong CP Problem*, *Submitted to: Phys. Rev. Lett.* (2018) [arXiv:1812.06041].

[40] A. E. Nelson, *Naturally Weak CP Violation*, *Phys. Lett.* **136B** (1984) 387–391.

[41] S. M. Barr, *Solving the Strong CP Problem Without the Peccei-Quinn Symmetry*, *Phys. Rev. Lett.* **53** (1984) 329.

[42] S. M. Barr, *Natural class of non-Peccei-Quinn models*, *Phys. Rev. D* **30** (Oct, 1984) 1805–1811.

[43] H. Georgi, D. B. Kaplan, and L. Randall, *Manifesting the Invisible Axion at Low-energies*, *Phys. Lett.* **169B** (1986) 73–78.

[44] G. Grilli di Cortona, E. Hardy, J. Pardo Vega, and G. Villadoro, *The QCD axion, precisely*, *JHEP* **01** (2016) 034, [arXiv:1511.02867].

[45] M. Dine, W. Fischler, and M. Srednicki, *A simple solution to the strong CP problem with a harmless axion*, *Physics Letters B* **104** (1981), no. 3 199 – 202.

[46] A. R. Zhitnitsky, *On Possible Suppression of the Axion Hadron Interactions. (In Russian)*, *Sov. J. Nucl. Phys.* **31** (1980) 260. [Yad. Fiz.31,497(1980)].

[47] J. E. Kim, *Weak-interaction singlet and strong CP invariance*, *Phys. Rev. Lett.* **43** (Jul, 1979) 103–107.

[48] M. Shifman, A. Vainshtein, and V. Zakharov, *Can confinement ensure natural CP invariance of strong interactions?*, *Nuclear Physics B* **166** (1980), no. 3 493 – 506.

[49] F. Wilczek, *Problem of strong P and T invariance in the presence of instantons*, *Phys. Rev. Lett.* **40** (Jan, 1978) 279–282.

[50] S. Weinberg, *A new light boson?*, *Phys. Rev. Lett.* **40** (Jan, 1978) 223–226.

[51] J. Preskill, M. B. Wise, and F. Wilczek, *Cosmology of the Invisible Axion*, *Phys. Lett.* **B120** (1983) 127–132.

[52] L. F. Abbott and P. Sikivie, *A Cosmological Bound on the Invisible Axion*, *Phys. Lett.* **B120** (1983) 133–136.

[53] M. Dine and W. Fischler, *The Not So Harmless Axion*, *Phys. Lett.* **B120** (1983) 137–141.

[54] F. D'Eramo, L. J. Hall, and D. Pappadopulo, *Multiverse Dark Matter: SUSY or Axions*, *JHEP* **11** (2014) 108, [arXiv:1409.5123].

[55] S. J. Asztalos, G. Carosi, C. Hagmann, D. Kinion, K. van Bibber, M. Hotz, L. J. Rosenberg, G. Rybka, J. Hoskins, J. Hwang, P. Sikivie, D. B. Tanner, R. Bradley, and J. Clarke, *Squid-based microwave cavity search for dark-matter axions*, *Phys. Rev. Lett.* **104** (Jan, 2010) 041301.

[56] T. M. Shokair et al., *Future Directions in the Microwave Cavity Search for Dark Matter Axions*, *Int. J. Mod. Phys.* **A29** (2014) 1443004, [arXiv:1405.3685].

[57] D. Budker, P. W. Graham, M. Ledbetter, S. Rajendran, and A. Sushkov, *Proposal for a Cosmic Axion Spin Precession Experiment (CASPEr)*, *Phys. Rev.* **X4** (2014), no. 2 021030, [arXiv:1306.6089].

[58] **MADMAX Working Group** Collaboration, A. Caldwell, G. Dvali, B. Majorovits, A. Millar, G. Raffelt, J. Redondo, O. Reimann, F. Simon, and F. Steffen, *Dielectric Haloscopes: A New Way to Detect Axion Dark Matter*, *Phys. Rev. Lett.* **118** (2017), no. 9 091801, [arXiv:1611.05865].

[59] Y. Kahn, B. R. Safdi, and J. Thaler, *Broadband and Resonant Approaches to Axion Dark Matter Detection*, *Phys. Rev. Lett.* **117** (2016), no. 14 141801, [arXiv:1602.01086].

[60] R. Daido, F. Takahashi, and N. Yokozaki, *Enhanced axion photon coupling in GUT with hidden photon*, *Physics Letters B* **780** (2018) 538 – 542.

[61] K. Olive, *Review of particle physics*, *Chinese Physics C* **40** (2016), no. 10 100001.

[62] L. Di Luzio, F. Mescia, and E. Nardi, *Redefining the Axion Window*, *Phys. Rev. Lett.* **118** (2017), no. 3 031801, [arXiv:1610.07593].

[63] A. Ayala, I. Dominguez, M. Giannotti, A. Mirizzi, and O. Straniero, *Revisiting the bound on axion-photon coupling from Globular Clusters*, *Phys. Rev. Lett.* **113** (2014), no. 19 191302, [arXiv:1406.6053].

[64] E. Masso and R. Toldra, *On a light spinless particle coupled to photons*, *Phys. Rev.* **D52** (1995) 1755–1763, [hep-ph/9503293].

[65] M. M. Miller Bertolami, B. E. Melendez, L. G. Althaus, and J. Isern, *Revisiting the axion bounds from the Galactic white dwarf luminosity function*, *JCAP* **1410** (2014), no. 10 069, [arXiv:1406.7712].

[66] W. Keil, H.-T. Janka, D. N. Schramm, G. Sigl, M. S. Turner, and J. R. Ellis, *A Fresh look at axions and SN-1987A*, *Phys. Rev.* **D56** (1997) 2419–2432, [astro-ph/9612222].

[67] H. Primakoff, *Photo-production of neutral mesons in nuclear electric fields and the mean life of the neutral meson*, *Phys. Rev.* **81** (Mar, 1951) 899–899.

[68] A. Payez, C. Evoli, T. Fischer, M. Giannotti, A. Mirizzi, and A. Ringwald, *Revisiting the SN1987A gamma-ray limit on ultralight axion-like particles*, *JCAP* **1502** (2015), no. 02 006, [arXiv:1410.3747].

[69] **CAST** Collaboration, V. Anastassopoulos et al., *New CAST Limit on the Axion-Photon Interaction*, *Nature Phys.* **13** (2017) 584–590, [arXiv:1705.02290].

[70] **IAXO** Collaboration, E. Armengaud et al., *Physics potential of the International Axion Observatory (IAXO)*, *JCAP* **1906** (2019), no. 06 047, [arXiv:1904.09155].

[71] K. Ehret et al., *New ALPS Results on Hidden-Sector Lightweights*, *Phys. Lett.* **B689** (2010) 149–155, [arXiv:1004.1313].

[72] R. Baehre et al., *Any light particle search II, Technical Design Report*, *JINST* **8** (2013) T09001, [arXiv:1302.5647].

[73] F. Bjorkeroth, E. J. Chun, and S. F. King, *Flavourful Axion Phenomenology*, *JHEP* **08** (2018) 117, [arXiv:1806.00660].

[74] **E949, E787** Collaboration, S. Adler et al., *Measurement of the K+ -> pi+ nu nu branching ratio*, *Phys. Rev.* **D77** (2008) 052003, [arXiv:0709.1000].

[75] **NA62** Collaboration, R. Fantechi, *The NA62 experiment at CERN: status and perspectives*, in *12th Conference on Flavor Physics and CP Violation (FPCP 2014) Marseille, France, May 26-30, 2014*, 2014. arXiv:1407.8213.

[76] A. Jodidio, B. Balke, J. Carr, G. Gidal, K. A. Shinsky, H. M. Steiner, D. P. Stoker, M. Strovink, R. D. Tripp, B. Gobbi, and C. J. Oram, *Search for right-handed currents in muon decay*, *Phys. Rev. D* **34** (Oct, 1986) 1967–1990.

[77] **TWIST** Collaboration, R. Bayes et al., *Search for two body muon decay signals*, *Phys. Rev.* **D91** (2015), no. 5 052020, [arXiv:1409.0638].

[78] A. Blondel et al., *Research Proposal for an Experiment to Search for the Decay $\mu \to eee$*, arXiv:1301.6113.

[79] **MEG II** Collaboration, A. M. Baldini et al., *The design of the MEG II experiment*, *Eur. Phys. J.* **C78** (2018), no. 5 380, [arXiv:1801.04688].

[80] R. Ziegler, *Flavored Axions*, *PoS* **CORFU2018** (2019) 035, [arXiv:1905.01084].

[81] F. Wilczek, *Axions and family symmetry breaking*, *Phys. Rev. Lett.* **49** (Nov, 1982) 1549–1552.

[82] T. Alanne, H. Gertov, F. Sannino, and K. Tuominen, *Elementary Goldstone Higgs boson and dark matter*, *Phys. Rev.* **D91** (2015), no. 9 095021, [arXiv:1411.6132].

[83] T. Alanne, A. Meroni, F. Sannino, and K. Tuominen, *Radiatively induced Fermi scale and unification*, *Phys. Rev.* **D93** (2016), no. 9 091701, [arXiv:1511.01910].

[84] S. Coleman and E. Weinberg, *Radiative corrections as the origin of spontaneous symmetry breaking*, *Phys. Rev. D* **7** (Mar, 1973) 1888–1910.

[85] P. Minkowski, *$\mu \to e\gamma$ at a Rate of One Out of 10^9 Muon Decays?*, *Phys. Lett.* **67B** (1977) 421–428.

[86] M. Gell-Mann, P. Ramond, and R. Slansky, *Supergravity*. North Holland, Amsterdam, 1979.

[87] T. Yanagida, "Proc. of the Workshop on Unified Theories and the Baryon Number of the Universe." KEK, Japan, 1979.

[88] R. N. Mohapatra and G. Senjanovic, *Neutrino Mass and Spontaneous Parity Violation*, *Phys. Rev. Lett.* **44** (1980) 912.

[89] J. Schechter and J. W. F. Valle, *Neutrino Masses in SU(2) x U(1) Theories*, *Phys. Rev.* **D22** (1980) 2227.

[90] J. Schechter and J. W. F. Valle, *Neutrino Decay and Spontaneous Violation of Lepton Number*, *Phys. Rev.* **D25** (1982) 774.

[91] T. Gherghetta, N. Nagata, and M. Shifman, *A Visible QCD Axion from an Enlarged Color Group*, *Phys. Rev.* **D93** (2016), no. 11 115010, [arXiv:1604.01127].

[92] M. K. Gaillard, M. B. Gavela, R. Houtz, P. Quilez, and R. Del Rey, *Color Unifed Dynamical Axion*, arXiv:1805.06465.

[93] **ADMX** Collaboration, S. J. Asztalos et al., *A SQUID-based microwave cavity search for dark-matter axions*, *Phys. Rev. Lett.* **104** (2010) 041301, [arXiv:0910.5914].

[94] **ADMX** Collaboration, N. Du et al., *A Search for Invisible Axion Dark Matter with the Axion Dark Matter Experiment*, *Phys. Rev. Lett.* **120** (2018), no. 15 151301, [arXiv:1804.05750].

[95] T. Alanne, S. Blasi, and F. Goertz, *Axiflavon-Higgs Unification*, in *54th Rencontres de Moriond on Electroweak Interactions and Unified Theories*, 5, 2019. arXiv:1905.07285.

[96] L. Janssen and Y.-C. He, *Critical behavior of the qed3-gross-neveu model: Duality and deconfined criticality*, *Phys. Rev. B* **96** (Nov, 2017) 205113.

[97] N. Zerf, P. Marquard, R. Boyack, and J. Maciejko, *Critical behavior of the QED_3-Gross-Neveu-Yukawa model at four loops*, *Phys. Rev.* **B98** (2018), no. 16 165125, [arXiv:1808.00549].

[98] R. Mann, J. Meffe, F. Sannino, T. Steele, Z.-W. Wang, and C. Zhang, *Asymptotically Safe Standard Model via Vectorlike Fermions*, *Phys. Rev. Lett.* **119** (2017), no. 26 261802, [arXiv:1707.02942].

[99] G. M. Pelaggi, A. D. Plascencia, A. Salvio, F. Sannino, J. Smirnov, and A. Strumia, *Asymptotically Safe Standard Model Extensions?*, *Phys. Rev.* **D97** (2018), no. 9 095013, [arXiv:1708.00437].

[100] O. Antipin and F. Sannino, *Conformal Window 2.0: The large N_f safe story*, *Phys. Rev.* **D97** (2018), no. 11 116007, [arXiv:1709.02354].

[101] D. Espriu, A. Palanques-Mestre, P. Pascual, and R. Tarrach, *The γ Function in the $1/N_f$ Expansion*, *Z. Phys.* **C13** (1982) 153.

[102] A. Palanques-Mestre and P. Pascual, *The $1/N_{\rm F}$ Expansion of the γ and Beta Functions in QED*, *Commun. Math. Phys.* **95** (1984) 277.

[103] J. A. Gracey, *The QCD β-function at $O(1/N_f)$*, *Phys. Lett.* **B373** (1996) 178–184, [hep-ph/9602214].

[104] B. Holdom, *Large N flavor beta-functions: a recap*, *Phys. Lett.* **B694** (2011) 74–79, [arXiv:1006.2119].

[105] R. Shrock, *Study of Possible Ultraviolet Zero of the Beta Function in Gauge Theories with Many Fermions*, *Phys. Rev.* **D89** (2014), no. 4 045019, [arXiv:1311.5268].

[106] K. Kowalska and E. M. Sessolo, *Gauge contribution to the $1/N_F$ expansion of the Yukawa coupling beta function*, *JHEP* **04** (2018) 027, [arXiv:1712.06859].

[107] O. Antipin, N. A. Dondi, F. Sannino, A. E. Thomsen, and Z.-W. Wang, *Gauge-Yukawa theories: Beta functions at large N_f*, arXiv:1803.09770.

[108] N. Zerf, L. N. Mihaila, P. Marquard, I. F. Herbut, and M. M. Scherer, *Four-loop critical exponents for the Gross-Neveu-Yukawa models*, *Phys. Rev.* **D96** (2017), no. 9 096010, [arXiv:1709.05057].

[109] J. A. Gracey, *Critical exponent ω in the Gross-Neveu-Yukawa model at $O(1/N)$*, *Phys. Rev.* **D96** (2017), no. 6 065015, [arXiv:1707.05275].

[110] M. E. Machacek and M. T. Vaughn, *Two Loop Renormalization Group Equations in a General Quantum Field Theory. 1. Wave Function Renormalization*, *Nucl. Phys.* **B222** (1983) 83–103.

[111] M. E. Machacek and M. T. Vaughn, *Two Loop Renormalization Group Equations in a General Quantum Field Theory. 2. Yukawa Couplings*, *Nucl. Phys.* **B236** (1984) 221–232.

[112] A. G. M. Pickering, J. A. Gracey, and D. R. T. Jones, *Three loop gauge beta function for the most general single gauge coupling theory*, *Phys. Lett.* **B510** (2001) 347–354, [hep-ph/0104247]. [Erratum: Phys. Lett.B535,377(2002)].

[113] K. G. Chetyrkin and M. F. Zoller, *Three-loop β-functions for top-Yukawa and the Higgs self-interaction in the Standard Model*, *JHEP* **06** (2012) 033, [arXiv:1205.2892].

[114] A. N. Vasiliev, Yu. M. Pismak, and Yu. R. Khonkonen, *Simple Method of Calculating the Critical Indices in the 1/N Expansion*, *Theor. Math. Phys.* **46** (1981) 104–113.

[115] A. N. Vasiliev, Yu. M. Pismak, and Yu. R. Khonkonen, *1/N Expansion: Calculation of the Exponents η and Nu in the Order $1/N^2$ for Arbitrary Number of Dimensions*, *Theor. Math. Phys.* **47** (1981) 465–475.

[116] A. N. Vasiliev, Yu. M. Pismak, and Yu. R. Khonkonen, *1/N expansion: Calculation of the exponent eta in the order 1/N**3 by the conformal bootstrap method*, *Theor. Math. Phys.* **50** (1982) 127–134. [Teor. Mat. Fiz.50,195(1982)].

[117] J. A. Gracey, *Quark, gluon and ghost anomalous dimensions at O(1/N) in quantum chromodynamics*, *Phys. Lett.* **B318** (1993) 177–183, [hep-th/9310063].

[118] M. Ciuchini, S. E. Derkachov, J. A. Gracey, and A. N. Manashov, *Computation of quark mass anomalous dimension at $O(1/N^2)$ in quantum chromodynamics*, *Nucl. Phys.* **B579** (2000) 56–100, [hep-ph/9912221].

[119] J. A. Gracey, *Calculation of exponent eta to O(1/N**2) in the O(N) Gross-Neveu model*, *Int. J. Mod. Phys.* **A6** (1991) 395–408. [Erratum: Int. J. Mod. Phys.A6,2755(1991)].

[120] J. A. Gracey, *Anomalous mass dimension at O(1/N**2) in the O(N) Gross-Neveu model*, *Phys. Lett.* **B297** (1992) 293–297.

[121] S. E. Derkachov, N. A. Kivel, A. S. Stepanenko, and A. N. Vasiliev, *On calculation in 1/n expansions of critical exponents in the Gross-Neveu model with the conformal technique*, hep-th/9302034.

[122] A. N. Vasiliev, S. E. Derkachov, N. A. Kivel, and A. S. Stepanenko, *The 1/n expansion in the Gross-Neveu model: Conformal bootstrap calculation of the index eta in order 1/n**3*, *Theor. Math. Phys.* **94** (1993) 127–136.

[123] A. N. Vasiliev and A. S. Stepanenko, *The 1/n expansion in the Gross-Neveu model: Conformal bootstrap calculation of the exponent 1/nu to the order 1/n**2*, *Theor. Math. Phys.* **97** (1993) 1349–1354.

[124] J. A. Gracey, *Computation of Beta-prime (g(c)) at O(1/N**2) in the O(N) Gross-Neveu model in arbitrary dimensions*, *Int. J. Mod. Phys.* **A9** (1994) 567–590, [hep-th/9306106].

[125] J. A. Gracey, *Computation of critical exponent eta at O(1/N**3) in the four Fermi model in arbitrary dimensions*, *Int. J. Mod. Phys.* **A9** (1994) 727–744, [hep-th/9306107].

[126] A. N. Manashov and M. Strohmaier, *Correction exponents in the Gross Neveu Yukawa model at $1/n^2$*, *Eur. Phys. J.* **C78** (2018), no. 6 454, [arXiv:1711.02493].

[127] J. A. Gracey, *Large N_f quantum field theory*, *Int. J. Mod. Phys.* **A33** (2019), no. 35 1830032, [arXiv:1812.05368].

[128] D. J. Gross and A. Neveu, *Dynamical symmetry breaking in asymptotically free field theories*, *Phys. Rev. D* **10** (Nov, 1974) 3235–3253.

[129] G. Choi, T. A. Ryttov, and R. Shrock, *Question of a Possible Infrared Zero in the Beta Function of the Finite- N Gross-Neveu Model*, *Phys. Rev.* **D95** (2017), no. 2 025012, [arXiv:1612.05580].

[130] J. A. Gracey, T. Luthe, and Y. Schroder, *Four loop renormalization of the Gross-Neveu model*, *Phys. Rev.* **D94** (2016), no. 12 125028, [arXiv:1609.05071].

[131] J. F. Schonfeld, *Higher Orders in Inverse n in the Gross-Neveu Model*, *Nucl. Phys.* **B95** (1975) 148–172.

[132] W. E. Thirring, *A Soluble relativistic field theory?*, *Annals Phys.* **3** (1958) 91–112.

[133] A. H. Mueller and T. L. Trueman, *Anomalous short-distance behavior of quantum field theory - a massive thirring model*, *Phys. Rev.* **D4** (1971) 1635–1652.

[134] M. Gomes and J. H. Lowenstein, *Asymptotic scale invariance in a massive thirring model*, *Nucl. Phys.* **B45** (1972) 252–266.

[135] J. Zinn-Justin, *Four fermion interaction near four-dimensions*, *Nucl. Phys. B* **367** (1991) 105–122.

[136] L. N. Mihaila, N. Zerf, B. Ihrig, I. F. Herbut, and M. M. Scherer, *Gross-Neveu-Yukawa model at three loops and Ising critical behavior of Dirac systems*, *Phys. Rev.* **B96** (2017), no. 16 165133, [arXiv:1703.08801].

[137] A. Codello, M. Safari, G. P. Vacca, and O. Zanusso, *Leading CFT constraints on multi-critical models in $d > 2$*, *JHEP* **04** (2017) 127, [arXiv:1703.04830].

[138] A. Codello, M. Safari, G. P. Vacca, and O. Zanusso, *Functional perturbative RG and CFT data in the ϵ-expansion*, *Eur. Phys. J.* **C78** (2018), no. 1 30, [arXiv:1705.05558].

[139] A. Codello, M. Safari, G. P. Vacca, and O. Zanusso, *Leading order CFT analysis of multi-scalar theories in $d>2$*, *Eur. Phys. J.* **C79** (2019), no. 4 331, [arXiv:1809.05071].

[140] A. Codello, M. Safari, G. P. Vacca, and O. Zanusso, *Multi-critical multi-field models: a CFT approach to the leading order*, 2019. arXiv:1905.01086.

[141] E. Molinaro, F. Sannino, and Z. W. Wang, *Asymptotically safe Pati-Salam theory*, *Phys. Rev.* **D98** (2018), no. 11 115007, [arXiv:1807.03669].

[142] G. Cacciapaglia, S. Vatani, T. Ma, and Y. Wu, *Towards a fundamental safe theory of composite Higgs and Dark Matter*, arXiv:1812.04005.

[143] F. Sannino, J. Smirnov, and Z.-W. Wang, *Safe Clockwork*, arXiv:1902.05958.

[144] C. Cai and H.-H. Zhang, *Minimal asymptotically safe dark matter*, *Phys. Lett.* **B798** (2019) 134947, [arXiv:1905.04227].

[145] T. A. Ryttov and K. Tuominen, *Safe Glueballs and Baryons*, arXiv:1903.09089.

[146] P. M. Ferreira, I. Jack, D. R. T. Jones, and C. G. North, *Beta functions in large N(f) supersymmetric gauge theories*, *Nucl. Phys.* **B504** (1997) 108–126, [hep-ph/9705328].

[147] J. A. Gracey, *Progress with large N_f beta functions*, *Nucl. Instrum. Meth.* **A389** (1997) 361–364, [hep-ph/9609409].

[148] V. Leino, T. Rindlisbacher, K. Rummukainen, F. Sannino, and K. Tuominen, *Safety versus triviality on the lattice*, arXiv:1908.04605.

[149] S. Weinberg, *Implications of dynamical symmetry breaking*, *Phys. Rev. D* **13** (Feb, 1976) 974–996.

[150] S. Weinberg, *Implications of dynamical symmetry breaking: An addendum*, *Phys. Rev. D* **19** (Feb, 1979) 1277–1280.

[151] L. Susskind, *Dynamics of spontaneous symmetry breaking in the weinberg-salam theory*, *Phys. Rev. D* **20** (Nov, 1979) 2619–2625.

[152] R. Contino, *The Higgs as a Composite Nambu-Goldstone Boson*, in *Physics of the large and the small, TASI 09*, pp. 235–306, 2011. arXiv:1005.4269.

[153] B. Bellazzini, C. Csaki, and J. Serra, *Composite Higgses*, *Eur. Phys. J.* **C74** (2014), no. 5 2766, [arXiv:1401.2457].

[154] G. Panico and A. Wulzer, *The Composite Nambu-Goldstone Higgs*, *Lect. Notes Phys.* **913** (2016) pp.1–316, [arXiv:1506.01961].

[155] F. Goertz, *Composite Higgs theory*, *PoS* **ALPS2018** (2018) 012.

[156] C. Csaki, S. Lombardo, and O. Telem, *TASI Lectures on Non-supersymmetric BSM Models*, pp. 501–570. WSP, 2018. arXiv:1811.04279.

[157] K. Agashe, R. Contino, and A. Pomarol, *The Minimal composite Higgs model*, *Nucl. Phys.* **B719** (2005) 165–187, [hep-ph/0412089].

[158] R. Contino, L. Da Rold, and A. Pomarol, *Light custodians in natural composite Higgs models*, *Phys. Rev.* **D75** (2007) 055014, [hep-ph/0612048].

[159] R. Barbieri, A. Pomarol, R. Rattazzi, and A. Strumia, *Electroweak symmetry breaking after LEP-1 and LEP-2*, *Nucl. Phys. B* **703** (2004) 127–146, [hep-ph/0405040].

[160] R. Barbieri and G. F. Giudice, *Upper Bounds on Supersymmetric Particle Masses*, *Nucl. Phys.* **B306** (1988) 63–76.

[161] E. Witten, *Some inequalities among hadron masses*, *Phys. Rev. Lett.* **51** (Dec, 1983) 2351–2354.

[162] D. B. Kaplan, *Flavor at SSC energies: A New mechanism for dynamically generated fermion masses*, *Nucl. Phys.* **B365** (1991) 259–278.

[163] R. Contino, Y. Nomura, and A. Pomarol, *Higgs as a holographic pseudoGoldstone boson*, *Nucl. Phys.* **B671** (2003) 148–174, [hep-ph/0306259].

[164] G. Ferretti and D. Karateev, *Fermionic UV completions of Composite Higgs models*, *JHEP* **03** (2014) 077, [arXiv:1312.5330].

[165] G. Ferretti, *Gauge theories of Partial Compositeness: Scenarios for Run-II of the LHC*, *JHEP* **06** (2016) 107, [arXiv:1604.06467].

[166] S. Coleman, J. Wess, and B. Zumino, *Structure of phenomenological lagrangians. I*, *Phys. Rev.* **177** (Jan, 1969) 2239–2247.

[167] C. G. Callan, S. Coleman, J. Wess, and B. Zumino, *Structure of phenomenological lagrangians. II*, *Phys. Rev.* **177** (Jan, 1969) 2247–2250.

[168] O. Matsedonskyi, G. Panico, and A. Wulzer, *Light Top Partners for a Light Composite Higgs*, *JHEP* **01** (2013) 164, [arXiv:1204.6333].

[169] A. Pomarol and F. Riva, *The Composite Higgs and Light Resonance Connection*, *JHEP* **08** (2012) 135, [arXiv:1205.6434].

[170] C. Csaki, A. Falkowski, and A. Weiler, *The Flavor of the Composite Pseudo-Goldstone Higgs*, *JHEP* **09** (2008) 008, [arXiv:0804.1954].

[171] S. De Curtis, M. Redi, and A. Tesi, *The 4D Composite Higgs*, *JHEP* **04** (2012) 042, [arXiv:1110.1613].

[172] G. Panico, M. Redi, A. Tesi, and A. Wulzer, *On the Tuning and the Mass of the Composite Higgs*, *JHEP* **03** (2013) 051, [arXiv:1210.7114].

[173] A. Carmona and F. Goertz, *A naturally light Higgs without light Top Partners*, *JHEP* **05** (2015) 002, [arXiv:1410.8555].

[174] M. E. Peskin and T. Takeuchi, *Estimation of oblique electroweak corrections*, *Phys. Rev. D* **46** (Jul, 1992) 381–409.

[175] A. Azatov, R. Contino, A. Di Iura, and J. Galloway, *New Prospects for Higgs Compositeness in $h \to Z\gamma$*, *Phys. Rev.* **D88** (2013), no. 7 075019, [arXiv:1308.2676].

[176] M. Baak, M. Goebel, J. Haller, A. Hoecker, D. Kennedy, R. Kogler, K. Moenig, M. Schott, and J. Stelzer, *The Electroweak Fit of the Standard Model after the Discovery of a New Boson at the LHC*, *Eur. Phys. J. C* **72** (2012) 2205, [arXiv:1209.2716].

[177] C. Grojean, O. Matsedonskyi, and G. Panico, *Light top partners and precision physics*, *JHEP* **10** (2013) 160, [arXiv:1306.4655].

[178] J. de Blas, O. Eberhardt, and C. Krause, *Current and Future Constraints on Higgs Couplings in the Nonlinear Effective Theory*, *JHEP* **07** (2018) 048, [arXiv:1803.00939].

[179] A. De Simone, O. Matsedonskyi, R. Rattazzi, and A. Wulzer, *A First Top Partner Hunter's Guide*, *JHEP* **04** (2013) 004, [arXiv:1211.5663].

[180] **ATLAS, CMS** Collaboration, L. Serkin, *Top quarks and exotics at ATLAS and CMS*, in *11th International Workshop on Top Quark Physics (TOP2018) Bad Neuenahr, Germany, September 16-21, 2018*, 2019. arXiv:1901.01765.

[181] G. Panico and A. Wulzer, *The Discrete Composite Higgs Model*, *JHEP* **09** (2011) 135, [arXiv:1106.2719].

[182] J. M. Maldacena, *The Large N limit of superconformal field theories and supergravity*, *Int. J. Theor. Phys.* **38** (1999) 1113–1133, [hep-th/9711200].

[183] E. Vigiani, *Effective model with higgs pseudo goldstone boson: analysis of non minimal terms*, *Master thesis in collaboration with S. de Curtis and M. Redi.* (2011/12).

[184] C. Csaki, T. Ma, and J. Shu, *Maximally Symmetric Composite Higgs Models*, *Phys. Rev. Lett.* **119** (2017), no. 13 131803, [arXiv:1702.00405].

[185] C. Csáki, T. Ma, J. Shu, and J.-H. Yu, *Emergence of Maximal Symmetry*, arXiv:1810.07704.

[186] C. Csaki, T. Ma, and J. Shu, *Trigonometric Parity for Composite Higgs Models*, *Phys. Rev. Lett.* **121** (2018), no. 23 231801, [arXiv:1709.08636].

[187] D. Marzocca, M. Serone, and J. Shu, *General Composite Higgs Models*, *JHEP* **08** (2012) 013, [arXiv:1205.0770].

[188] A. Thamm, R. Torre, and A. Wulzer, *Future tests of Higgs compositeness: direct vs indirect*, *JHEP* **07** (2015) 100, [arXiv:1502.01701].

[189] O. Matsedonskyi, G. Panico, and A. Wulzer, *On the Interpretation of Top Partners Searches*, *JHEP* **12** (2014) 097, [arXiv:1409.0100].

[190] T. Golling et al., *Physics at a 100 TeV pp collider: beyond the Standard Model phenomena*, *CERN Yellow Rep.* (2017), no. 3 441–634, [arXiv:1606.00947].

[191] **FCC** Collaboration, A. Abada et al., *FCC Physics Opportunities*, *Eur. Phys. J.* **C79** (2019), no. 6 474.

[192] C. Csaki, *TASI lectures on extra dimensions and branes*, pp. 605–698, 4, 2004. hep-ph/0404096.

[193] T. Gherghetta, *A Holographic View of Beyond the Standard Model Physics*, in *TASI lectures*, pp. 165–232, 2011. arXiv:1008.2570.

[194] N. Arkani-Hamed, M. Porrati, and L. Randall, *Holography and phenomenology*, *JHEP* **08** (2001) 017, [hep-th/0012148].

[195] C. Csaki, C. Grojean, J. Hubisz, Y. Shirman, and J. Terning, *Fermions on an interval: Quark and lepton masses without a Higgs*, *Phys. Rev.* **D70** (2004) 015012, [hep-ph/0310355].

[196] J. A. Bagger, *Weak scale supersymmetry: Theory and practice*, in *TASI 95*, pp. 109–162, 4, 1996. hep-ph/9604232.

[197] A. Falkowski, *About the holographic pseudo-Goldstone boson*, *Phys. Rev. D* **75** (2007) 025017, [hep-ph/0610336].

[198] A. Falkowski, *Pseudo-goldstone higgs from five dimensions*, in *15th International Conference on Supersymmetry and the Unification of Fundamental Interactions (SUSY07)*, pp. 658–661, 10, 2007. arXiv:0710.4050.

[199] Y. Hosotani and M. Mabe, *Higgs boson mass and electroweak-gravity hierarchy from dynamical gauge-Higgs unification in the warped spacetime*, *Phys. Lett. B* **615** (2005) 257–265, [hep-ph/0503020].

[200] R. Contino and A. Pomarol, *Holography for fermions*, *JHEP* **11** (2004) 058, [hep-th/0406257].

[201] N. Arkani-Hamed and M. Schmaltz, *Hierarchies without symmetries from extra dimensions*, *Phys. Rev.* **D61** (2000) 033005, [hep-ph/9903417].

[202] A. E. Nelson and M. J. Strassler, *Suppressing flavor anarchy*, *JHEP* **09** (2000) 030, [hep-ph/0006251].

[203] A. G. Grozin, *Lectures on multiloop calculations*, *Int. J. Mod. Phys.* **A19** (2004) 473–520, [hep-ph/0307297].

[204] A. V. Kotikov, *The Gegenbauer polynomial technique: The Evaluation of a class of Feynman diagrams*, *Phys. Lett.* **B375** (1996) 240–248, [hep-ph/9512270].